FATIGUE AND FRACTURE FROM NOTCHES IN CAST STEELS

by

T. I. AL-ZAIDI

B.Sc. (M.E.) M.Sc. (Mat.Enging.)

A Thesis Submitted to the
University of Aston in Birmingham
for the degree of
Doctor of Philosophy

SEPTEMBER 1977

FATIGUE AND FRACTURE FROM NOTCHES IN CAST STEEL

by

T. I. AL-ZAIDI

A Thesis submitted to the

University of Aston in Birmingham

for the degree of

Doctor of Philosophy

SUMMARY

Two types of carbon-manganese cast steels (BS1456A and BS1458A) containing 0.07% and 0.28% of molybdenum respectively were tested in fatigue at five different temperatures, room temperature, +50°C, +100°C, -50°C and -100°C. All fatigue tests were completed in bending. Notches machined in specimens were of 0.127 mm, 12.7 mm and 25.4 mm root radii.

A good correlation was found between the number of cycles to produce a detectable fatigue crack and the range of stress intensity factor divided by the square root of the notch root radius raised to the power of (-m) for both materials $|N i \alpha (\Delta K/\rho^{\frac{1}{2}})^{-m}|$. The results indicate that the mechanical properties could be a good prediction to the crack initiation behaviour. Fatigue crack propagation rates were also predicted and results showed that the rate is high for the first 1.2 mm in length. Results also showed that the addition percentage of molybdenum made no significant effect on fatigue properties.

The acoustic emission technique was also used when notched specimens were tested at room temperature. The results are encouraging for further work for a prediction of a detectable fatigue crack. The total acoustic emission counts were found to be higher for blunt notches and lower for sharper notches.

Fracture toughness tests were also carried out at five different temperatures for both steels, and results showed that the K_C value for both steels was about 146.0 MN $m^{-3/2}$. This value increased by 20% at higher temperatures and dropped to an average value of 40.0 Mn $m^{-3/2}$ and 20.0 MN $m^{-3/2}$ at temperatures of -50°C and -100°C respectively. Toughness, K_C, values obtained by the linear elastic fracture mechanics (L.E.F.M.) method, and by the J-integral method, were in agreement at room temperature. K_C values at lower and higher temperatures were obtained using the L.E.F.M. method only.

Both fatigue and fracture toughness results provided a useful engineering measure for design against fatigue failure from a wide range of stresses.

Key words:

Fatigue, fracture, cast steels, notches, acoustic emission.

CONTENTS

CHAPTER 1

INTRODUCTION

This work was planned to compare the fatigue and fracture properties of two cast steel materials, BS 1458A and BS 1456A, at five different temperatures, namely room temperature (≃ 20°C), +50°C, +100°C, -50°C and -100°C.

In order to improve fracture and fatigue properties of steels at sub-zero temperature, the composition is normally altered by the addition of a small percentage of nickel. This adversely affects castability and has not therefore been a practice with cast steels. There is evidence that increasing molybdenum content from 0.05% to about 0.30% in cast steels improves low temperature properties. The major difference between the two specifications chosen is their molybdenum content. Even if the extra molybdenum does not markedly change the fracture and fatigue resistance the data of these properties should be valuable, since no information at present exists for either of these steels on fatigue crack initiation and fatigue crack propagation rates. The behaviour of both steels under cyclic loading is particularly important due to the fact that fatigue may account for about 80% of all service failures[80].

In addition to the fact that materials differing in composition were used, the project covers a variation in geometry. Notches of various root radii have been tested in order to simulate typical engineering stress concentrators. In all cases a three point bend test was used for testing since this is the test recommended by both American and British Standards.

The fatigue behaviour of most materials is expressed in the form of S-N curves which are of a limited use. They do not indicate the fatigue behaviour of defects, which in materials such as cast steels, may be casting discontinuities or stress concentrations due to local machining. Very few components or structural members of metallic materials are of uniform cross-section. Most contain some form of change in cross-section resulting from a discontinuity such as, for example, a fillet, a hole, or an external groove or notch. For convenience, any of these discontinuities is generally referred to as a notch irrespective of its geometric shape. Examination of components which have failed in service as a consequence of cyclic loadings reveals that, in many cases the cause of failure has been the initiation of a fatigue crack at some point on the boundary of a notch. A crack forms here because the cyclic stresses at and near the notch boundary are higher than the nominal cyclic stresses remote from the notch.

The crack growth rate of fatigue cracks has been shown to be a function of the stress intensity factor range, Frost et al.(1974), and for this approach to be useful, the calibration curve used to calculate the stress intensity factor has to be known, for the particular component

defect geometry under investigation. This analysis ignores the initiation of fatigue cracks, assumes that the growth of cracks can be described by a simple equation which applies to the whole of the growth rate curve and assumes that other effects are unimportant.

A major problem facing the designer is the selection of the right materials from which to manufacture a particular design of component or structure. The material properties must ensure that it carries out the duties for which it was designed without breaking within a guaranteed life, and yet must enable it to be sold at a price which a customer is prepared to pay.

The acoustic emission and J-integral techniques were also planned to be used in this work. Previous theories[70,157,163,71] defined the acoustic emission as a stress wave generated in a material due to the energy released by mechanisms that govern its deformation and fracture behaviour. Audible sounds are produced due to energy conversion into elastic waves in the material. In most materials, however, sufficient energy is not released for the acoustic emission to be audible. In such cases, the low intensity stress waves can be detected at the surface of the material with high sensitivity transducers. This technique is a dynamic one as opposed to the "post mortem" type of static microscopic observation of fracture[71], slip-line structure and dislocation density and distribution by optical and electron metallography.

Theories of acoustic emission from metals were based on concepts of small, sharp yield drops in the flow stress arising from dislocation motion.

Later work showed that the total emission was proportional to the extent of plastic behaviour from the crack tip[123]. Though these and other theories are concerning the relation between the acoustic emission from a sharp notch preceding crack propagation from its tip[163], there is no information on the acoustic emission from blunt notches under similar conditions. There is a possibility that the acoustic emission is likely to relate to the extent of yielding from the notch, and to the area of a yielded zone at the notch tip. Acoustic emission is likely to arise due to plastic enclave formation and to decrease as this plastic enclave enlarges to a region of general yield across a net section, or as the enclave initiates a macrocrack which rapidly crosses the net section. It is therefore of importance to establish the pattern of acoustic emission preceding failure from a blunt notch by the spread of plasticity or by the initiation of a macrocrack.

Relating these concepts to the experimental work carried out on fatigue it seems important to extend these concepts to failure by fatigue from a notch. This will contain the problem of acoustic emission arising before the initiation of a fatigue crack, and the pattern of acoustic emission arising as the fatigue crack nucleus grows into an extensive fatigue crack.

It was thought that a range of four notch root radii was sufficient to establish acoustic emission patterns. The range should demonstrate the major type of change in behaviour arising from change in notch geometry. The most influential factor is likely to be the change in shape and size of the initial plastic enclave emanating from the notch.

The material for such experiments is cast steel which conforms to BS 1456B, pearlitic steel. This material is relatively brittle and design information on events preceding fracture are therefore particularly valuable.

This project is based on using currently available techniques, namely linear elastic fracture mechanics (LEFM) (7), acoustic emission[157,71], and J-integral Techniques (8), all were used conjointly. In order to detect crack initiation directly the potential drop technique was used[60].

A designer is continually endeavouring to achieve more economical design. To obtain this, he must increase his allowable design stress; metallurgists have responded nobly with increases in tensile strength of all classes of materials. However, designers soon discovered that factors of safety appropriate to a particular type of mild steel component or structure when applied to the new stronger steels (or other materials) did not necessarily lead to a satisfactory service performance. Success in traditional design was due largely to the avoidance of past errors and to the use of familiar materials in familiar situations.

However with the development of the steam engine and mechanical transport and the more extensive use of mechanical devices, the failure of moving parts that carried a repeatedly applied load were beginning to become a common occurrence. Failures were found to occur at low nominal stresses but in situations where the load was repeatedly changing and were usually located at a change in section in the component or structure.

That these failures were starting to worry engineers over a hundred years ago is illustrated by the fact that in 1830 Albert[2] repeatedly proof-loaded welded nine hoist chains, continuing some tests up to 10^5 cycles. Between 1850 and 1865 both Hodgkinson[79] and Fairbairn[42] carried out repeated bending tests on beams, Fairbairn using a mechanism actuated by a water wheel to repeatedly apply a load to the centre of a 6.7 m long wrought iron built-up girder; the beam broke statically under a central load of 120 kN, but Fairbairn found repeated loads of only 30 kN would eventually cause failure. The general opinion developed that the material had tired of carrying the load or that the continual re-application of a load had in some way exhausted the ability of the material to carry the load because these failures occurred in a part that had functioned satisfactorily for a certain time. Thus the word "fatigue" was coined to describe such failure, and the name has survived to this day. With the increasing demand for more efficient and economic components and structures (for example, higher operating speeds and minimum weight design) the number of failures by fatigue has continued to increase until today it is by far the commonest cause of failure of load-carrying metallic parts operating at or close to room temperature as well as at elevated and sub-zero temperature.

CHAPTER 2

LITERATURE SURVEY OF FATIGUE PROCESS

2.1 Early Work of Fatigue

The reasons for the failure of materials under the continued application of a stress, which, if applied once would not cause failure, have engaged the engineer and metallurgist for a long time. Accounts of this early work have been given by Gough[62], Moore and Kommers[116] and Mann[102]. It was of interest to note that it is now over a hundred years since Wohler[174] published the results of his classical experiments on fatigue. He constructed various types of fatigue testing machines and carried out the first fatigue tests on metallic specimens in which strict attention was paid to the magnitude of the applied loads. He concluded from tests on iron and steel specimens that the range of applied stress rather than the maximum tensile stress in the loading cycle determined the life of a specimen, and that a limiting lower stress range existed below which a specimen did not break no matter how many times the stress cycles were applied. Since Wohler's work, the fatigue properties of different materials tested under various conditions of loading and environment have been studied intensively. In addition, fatigue tests have been carried out on both components and structures, often subjecting them to loading cycles comparable with those to which it is expected they will be subjected in service. However, despite the fact that most engineers and

designers are aware of fatigue, and that a vast body of experimental data has been accumulated, many important breakdowns of plant and machinery still occur today. All too often, plant or equipment whose overall functional demands have been adequately met with break down in service because of the fatigue failure of a detail apparently not immediately concerned with the functional requirements of the complete unit. Thus, lack of attention to some aspects of detail in design is a major factor responsible for fatigue failures. There is nothing as effective as a failure in service for making an engineering designer concerned about details in design. When a failure in service does occur, whether it be of a dramatic or spectacular nature such as the Comet aircraft or the Queen Elizabeth II turbine blade, or on a more humble level such as a vehicle stub-axle, there is usually no lack of expert opinion as to why it happened. Some reasons for failure appear too obvious after failure has occurred that it is difficult to appreciate why it was not so before the event happened[44]. There are three factors contributing to this state of affairs: Firstly, exact information for a particular set of circumstances is not always available and a designer must estimate fatigue performance from whatever data is to hand: Secondly, only rarely do the fatigue properties of a material bear any general relationship to component performance in service: Thirdly, precise service loading is unknown either through ignorance or accidental overloading or because the service requirements have been altered after the part has been manufactured.

A further factor is that traditional design assumed a material to be a flawless continuum. However, it is known today that rational design and material assessment need an understanding of the presence of cracks

in the continuum. Many materials, components and structures contain either flaws or defects inherently, as part of the manufacturing procedure, or develop them at some stage of their life. An understanding of how a cracked body behaves under loading is essential to an understanding of any fatigue problem.

Because much of the information on fatigue from both laboratory tests and service behaviour was obtained and interpreted before the study of cracked material behaviour was established, there was no underlying central theme to correlate the data. Thus, isolated sets of data became almost fatigue folklore, and their relationship to other sets of data was not obvious.

Until recent years little effort had been devoted to the experimental determination of the laws governing the growth of a fatigue crack. In fact, no accurate quantitative experimental data had been published prior to 1953, the year Head[72] published his theoretically derived relationship between crack length and number of stress cycles. This may have been due to the fact that the assessment of design stresses, in those cases where it was considered necessary to give due regard to the fatigue properties of a material, had been almost always based on the plain fatigue limit or strength of the material, as obtained from smooth laboratory specimens. Naturally the purpose of these design stresses was to prevent the initiation of any cracks under the working loads by keeping all cyclic stresses below some critical value. However, it is only possible to do this when the components or structural members are of a

relatively simple shape and the magnitude of the working loads precisely known. The need to produce components or members of complex shape, which are not uneconomic in their use of material, to operate under service conditions which are not precisely defined, has led to the possibility of cracks forming even at relatively low nominal cyclic loads, usually as a consequence of fretting or in the locally highly stressed material around some discontinuity. This implies that some components and structural members, particularly those designed to have a limited life must operate successfully even though they do contain fatigue cracks. It is worth mentioning that, to obtain a macrocrack in a specimen at a stress level less than the plain fatigue limit of a material, some form of notch must be introduced into the specimen so that the effective length of a crack formed at the notch root is increased to a value sufficient to grow directly as a macrocrack at the applied nominal stress level. In some cases modern inspection procedures have enabled small cracks to be detected in certain components at an early stage in their expected life. However, it has been stated[22] that a crack roughly 5.15 mm long is about the smallest flaw that can be readily detected during routine service inspection. In addition, the necessity to assume the existence of cracked members in engineering structures despite the efforts of designers to design fatigue resistant structures is now generally accepted. Whether these cracks will grow and, if they do, the rate at which they grow will depend on material and the values of the applied nominal mean and alternating stresses. The selection of a material from those which fulfil other necessary design considerations, giving the slowest rate of crack growth for a given external loading will lead to an increased margin of safety between routine inspections. Thus, a knowledge of the

growth rate characteristics of a material, together with regular inspections, may enable a cracked component to have a long useful life before having to be replaced. A fail-safe design[67] (that is, a structure so designed that, should cracks form, they will not cause catastrophic failure under the working loads until one of them reaches a known length) implies that a limiting crack length can be established which must be detected by inspection if the crack is not to extend to cause failure before the next inspection. Therefore, designers should use all possible means to achieve the ideals of a low rate of crack propagation and a high residual static strength in the presence of a crack. Probably the best way of assessing the merits of a fail-safe design is by the length of inspection periods which it allows in relation to the weight involved.

Numerous, apparently different "laws" of fatigue crack growth shall be described in the coming literature[23] and by making various plausible assumptions some of them can be derived theoretically. All the laws can be regarded as valid in the sense that they describe a particular set of fatigue crack growth data, and they can be used to predict crack growth rates in situations similar to those used to collect the data. It is sometimes possible to fit the same set of data to apparently contradictory laws; in such cases it is not possible to decide which law is the most 'correct'.

Since the end of World War II, the problem of brittle fracture has been studied extensively. It has been found that such low stress (compared to the yield stress of the material) fractures always originate

at flaws or cracks of various types. The fracture mechanics approach to residual static strength in the presence of a crack makes use of the stress intensity factor K_I concept to describe the stress field at a crack tip. When K_I reaches a critical value K_C the crack extends, usually catastrophically. Values of K_I are known for a wide range of crack configurations[15, 18, 39, 40, 139, 149 & 144] and the fracture mechanics approach has proved useful in problems of material development, design, and failure analysis. In view of its success in dealing with static fracture problems, it is logical to use a similar general approach to analyse fatigue crack growth data. The availability of a master curve for a particular material relating fatigue crack growth rate and range of stress intensity factor enables a designer to predict growth rates for any cracked body configuration, and he is not limited to situations similar to those pertaining to the cracked specimen geometry used to generate the original data.

2.2 Fatigue Crack Formation

A fatigue crack can form in a component or a structural member, usually at a point of stress concentration or at a joint or in an area of fretting, or from some inherent defect, at relatively low nominal alternating stresses. If the magnitude of the nominal cyclic stress is sufficient, the crack will grow until the cross-sectional area of the component or member is so reduced that it can no longer support the maximum tensile stress due to both the imposed static and cyclic loads and catastrophic failure occurs. Catastrophic failure can occur either before or after the average net area tensile stress reaches the yield stress of the material. In the later case, fracture will occur in a ductile manner; in the former case, the fracture will occur in a brittle manner (that is, with no visible signs of gross plastic deformation).

Whether a metal fails in a ductile or brittle manner depends on certain conditions such as chemical composition, metallurgical treatments, shape of specimen (including notch configuration), the values of the stresses around the notch, temperature, and the rate of deformation. Factors which delay the onset of plasticity, for example, low temperature, plane strain conditions, and increased rate of loading, make the material more susceptible in brittle fracture.

Slip-line development on the surface of a fatigue specimen has been studied by many workers since the turn of the century. As early as 1903, Euring and Humphrey[41] tested specimens of Swedish iron in rotating bending at stress levels above their fatigue limit a test being stopped

at frequent intervals and the specimen surface polished and etched. They observed few slip lines initially, but as a test proceeded, new slip lines formed close to existing ones producing bands of slip. Although these bands grew wider and more dense, there were areas between the bands where no slip was observed. Fatigue cracks formed eventually in the broadened bands, but it was not possible to define precisely when this happened. Numerous slip bands were found to contain cracks at the end of the test, especially when a specimen had a long life.

Successive workers using other ductile polycrystals and more sophisticated metallographic techniques have added more detail which, in general, has confirmed the sequence of events described by Ewing and Humphrey. For example, some fifty years later Thompson, Wadsworth and Louat[160] tested annealed electropolished, polycrystalline high-purity copper specimens in reversed direct stress (zero mean load). A specimen being removed from the fatigue machine periodically and examined metallurgically. Slip bands appeared early in a test and became more numerous as the test progressed. Electropolishing removed the roughness associated with a slip band, and most of them became invisible. A few, however, became accentuated and were termed 'persistent slip bands', fatigue cracks grew eventually from these bands. If the electropolishing was continued until the persistent bands were removed, it was found that, on retesting, the slip band reformed and again became persistent. In many cases the pattern of the new bands reproduced in some detail that which had been removed, implying that slip was still active on the same planes. No new markings were ever uncovered during the electropolishing, showing that the origin of cracking was associated with the free surface. Persistent slip

bands were observed in some tests after only 5 per cent of the total life, but they did not in general extend far down into the metal; for example, some were found to be more than 30 μm deep after 24 per cent of life. Similar observations were made in polycrystalline nickel specimens, the main difference from the copper observations being the absence of slip bands other than those directly associated with cracks.

As well as leading to the formation of crevices or intrusions, intensive slip can give rise to the complementary process of extrusion. This was first reported by Forsyth[50, 51] who studied the surface characteristics of many pure metals and alloys, at various temperatures, using specimens about 0.6 mm thick, tested in reversed plane bending at relatively large strain amplitudes. He found that, whereas cyclic deformation in annealed aluminium consisted of coarse slip situated in bands with fine slip markings spread widely across the grains between the coarse bands, cracks appearing first in these coarse bands, in an age-hardened 4½% Cu-Al alloy the coarse slip bands were absent; instead a fine dispersion of slip-line markings was observed after cyclic stressing. Some of these became accentuated and clearly defined on the surface, cracks appearing from irregular markings associated with the accentuated slip lines. These irregular markings were found, under higher magnification, to be ribbon extrusions, not thicker than 0.1 μm and about 10 μm long.

Many workers have observed both intrusions and extrusions occurring at slip bands in polycrystalline ductile metals (for example, low carbon steel alloy and alloy steels[97, 24]), over a wide range of temperatures.

To study extrusion formation in more detail, Forsyth[50] tested transparent single and polycrystal silver chloride specimens and found that profuse slip and extrusions phenomena occurred. He observed that extrusions did not create internal voids, instead, complementary surface crevices or intrusions, of about the same size as extrusions, formed. Cottrell and Hull[28] also found from reversed direct stress fatigue tests on copper that both intrusions, and extrusions occurred in comparable abundance and with similar dimensions along slip bands and that this was so at temperatures down to -250°C.

Further work[83] showed that extrusions and intrusions could form in slip bands even when the temperature of the specimen was lowered to that of liquid helium, intrusions being detected on some specimens after only 1 per cent of their life. This suggested that their formation was by purely mechanical movement of atoms and was not dependent on diffusion processes. Intrusions have also been shown to act as crack nuclei on specimens subjected to a wholly compressive loading cycle[24].

Slip-band cracking can occur in ductile metal polycrystals, which does not necessarily lead to complete failure of the test-piece. For example, [76,77] 0.09% C steel strip specimens tested in reversed plane bending, cyclically stressed 33 per cent above the fatigue limit, showed slip lines formed in a few grains after 1.0 per cent of the life, the lines growing longer and broader as a test continued until they formed bands. Although slip-band cracking has been widely observed in many ductile metals tested at room temperature and stress levels not too far removed from the fatigue limit, altering the conditions of test or adding certain alloying constituents can lead to grain boundary cracking.

Raising the temperature is a technique which has been used by many workers to change the mode of cracking from transcrystalline to intercrystalline. For example, reversed direct stress tests on 4 mm diameter magnesium specimens were carried out at both room temperature and 250°C[106]. It was found that at room temperature, all cracks were transcrystalline, being initiated in either slip bands or twin boundaries. On the other hand, at 250°C all cracks were intergranular. It was suggested that this was a consequence of grain boundary sliding. At sub-zero and room temperature cracks in pure aluminium developed in persistent slip bands[68, 69] but at elevated temperatures they were initiated mainly at grain boundaries. Both slip band and grain boundary cracking were found to occur after less than 5 per cent of the expected life. Grain boundary cracking occurred generally in those boundaries lying close to the maximum shear stress direction and also in those boundaries separating grains which had a large difference in orientation, so that the slip from one grain could not be transmitted to the neighbouring one.

The behaviour of slip lines on the surface of both cold-worked and annealed high-purity aluminium single crystals subjected to alternate tensile and compressive loads has been studied[33], the magnitude of the applied loads being such that the strain during any half-cycle was less than few tenths of a per cent. It was found that there was no obvious relationship between the slip lines formed during tension and those formed during the subsequent compression loading. A slip line was unaffected, in general, by a reversal of load up to a value of twice the initial load. This would seem to imply that fatigue cracking is due to the geometric surface effects caused by extrusions and intrusions and not due to some internal damage process along a particular slip plane.

In addition to the surface observations described, many workers have studied the changes in mechanical properties and metallurgical structure that occur in a cyclically loaded specimen. The measurements taken generally recorded a change in strain range response to a given stress range (after detected by a change in the shape of the hysteresis loop generated), a hardening or softening of the material, a change in temperature, enhanced diffusion characteristics, or a change in X-ray diffraction pattern. All these results are grouped nicely by Frost W.E. et al.[55].

2.3 Fatigue Crack Initiation

Early theories of fatigue generally fall into two categories; those based on repeated slip leading to some form of damage along a preferred slip plane and hence eventually to a crack (for example, the attrition theory of Ewing and Humphrey[41]) and those based on the repeated work-hardening of a soft element, surrounded by an elastic matrix (or of a grain surrounded by grains having different elastic limits and strain hardening characteristics, the work-hardened element (or grain) either reaching a stable state not leading to fracture or work-hardening until it reaches its fracture stress (for example, Afanasev[1], Dehlinger[30], and Orowan[121]. Even as late as 1965, theories (for example, Yoshikawa[175]) based on a critical amount of plastic strain being accumulated were being postulated. It is worth emphasizing at the outset that

(1) fatigue failure is a consequence of the initiation of a crack and the subsequent growth of this crack,

(2) in homogeneous metals cracks initiate at a free surface and no damage is done to metal away from this surface by the cyclic stressing,

(3) the initiation of a slip-band crack is only possible in ductile metals,

(4) other materials may exhibit fatigue characteristics but this is due to the propagation of a crack from some initial defect or flaw.

In ductile metals cyclic stressing can be regarded as a very sensitive technique for detecting the onset of plastic deformation or slip in

a particular surface grain. It is not necessary for the bulk of the grains in a piece of metal to deform plastically for it to fail by fatigue. Continuing cyclic plastic deformation in one localized surface region is sufficient. It is this fact that fatigue failure is a consequence of an extremely localized surface occurrence that distinguishes it from other modes of mechanical failure.

The general and basic features of fatigue failure are the initiation of surface microcracks and their subsequent extension across and penetration into the body of the metal. The increased life resulting from the removal of a surface layer at frequent intervals throughout the test, irrespective of whether the life is many millions or only a few thousand cycles[135] demonstrates that crack initiation is confined to the surface grains. The direction of development of surface microcracks is initially that of the operative slip planes. It remains so until a microcrack is of such a size that the amount it opens and closes, under resolved cyclic stresses acting normal to the crack faces, is sufficient to affect a large enough volume of material along its edge for it to grow as in a continuum.

This is because the initiation and development of surface microcracks are associated with localized surface regions of cyclic plastic strain. For this reason, the initiation and development of microcracks by to-and-fro slip along crystallographic planes will be influenced by local differences in microstructure (the more complex the microstructure, the more pronounced the effect) and the time taken, at a given nominal stress

level, for a microcrack to reach the macrocrack stage may therefore vary in different specimens of nominally similar material. However, having reached the macrocrack stage local changes in microstructure generally have little effect on the growth rate (as will be seen in the next section) and thus the scatter in lines of nominally identical specimens subjected to the same nominal stress level is associated with the effect of microstructure on the initiation and rate of development of microcracks.

Because slip-band intrusions (microcracks) have been found to occur at liquid helium temperature it has been argued that their formation is by a purely mechanical movement of atoms. Wood[173] suggested that slip caused pronounced changes in local surface contours and the formation of surface microcracks was primarily a simple geometric consequence of to-and-fro slip movements within broad slip bands as shown in figure 1. Cottrell and Hull[28] proposed a model for forming extrusions and intrusions on the surface based purely on the mechanical movement of atoms by supposing that two intersecting slip bands as shown in figure 2 operating sequentially during both the tension and compression halves of the stress cycle.

Other dislocation models leading to surface cracking have been proposed, [for example, Fujita[58] and Mott[117]] and these are summarized by Kennedy[96]. They essentially lead to a geometric cause of damage or to damage on the slip plane itself[96, 141]. Damage on the slip plane itself entails slip occurring on the same plane and progressively

unbonding atoms each cycle. If this were so it might be expected that environment may affect crack initiation. For example, a film of oxide or absorbed gas may form on the exposed slip step and be drawn down the plane in successive cycles. Thus forming a surface microcrack.

The evidence would suggest that the major role played by slip is to cause a geometric change to the surface profile rather than to cause damage leading to a crack along the slip plane itself.

Assuming this geometric consequence as slip, May[106] considered that the disturbance of a surface by to-and-fro slip movements in the slip bands might be due to dislocations in transit between limits of the oscillatory trajectory along paths which were shifted in a random fashion with respect to previous paths, the shifts being comparable to the width of the slip bands. Such a random distribution of slip would roughen the surface, leading to a redistribution of stress, so that in later cycles slip would tend to be concentrated in the valleys already formed. Subsequent surface movement would make some valleys less deep but others would become deeper and in these more slip would be concentrated. To see whether such a model led to cracks forming after a reasonable time, he assumed that after t cycles, the fraction f of the valleys of width w which had depth between z and z+dz was

$$f = F_{exp}\ [-\{\sqrt{z+w} - \sqrt{w}\}^2/b\epsilon t] \qquad (1)$$

where F was a slowly varying function of z, w and t. The slip vector b and the plastic strain range ϵ in the slip band were assumed constant for

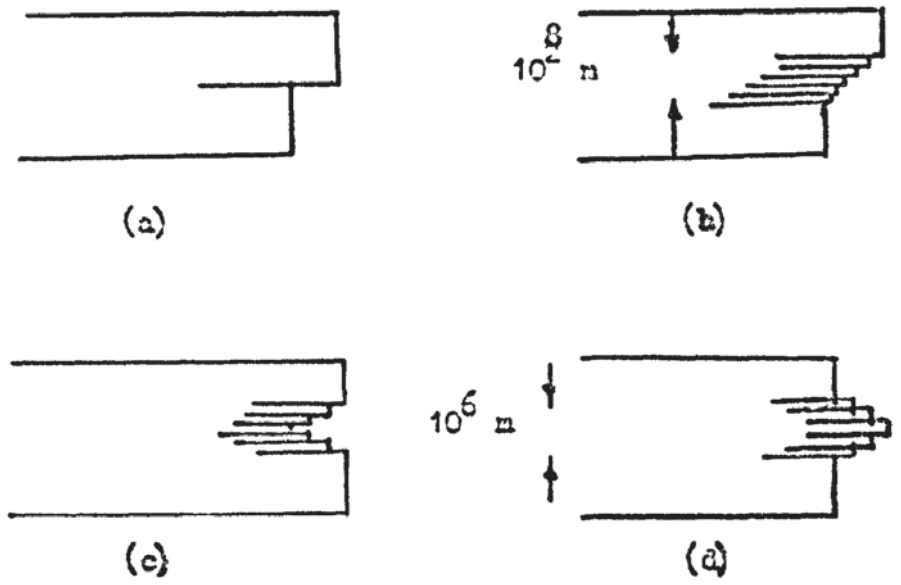

Figure 1 Formation of surface cracks by slip. Static slip forms unidirectional steps: (a) Optical microscope. (b) Electron microscope. Fatigue slip by to and fro movements in slip band may form notch (c) or peak (d).

Frost (1974)

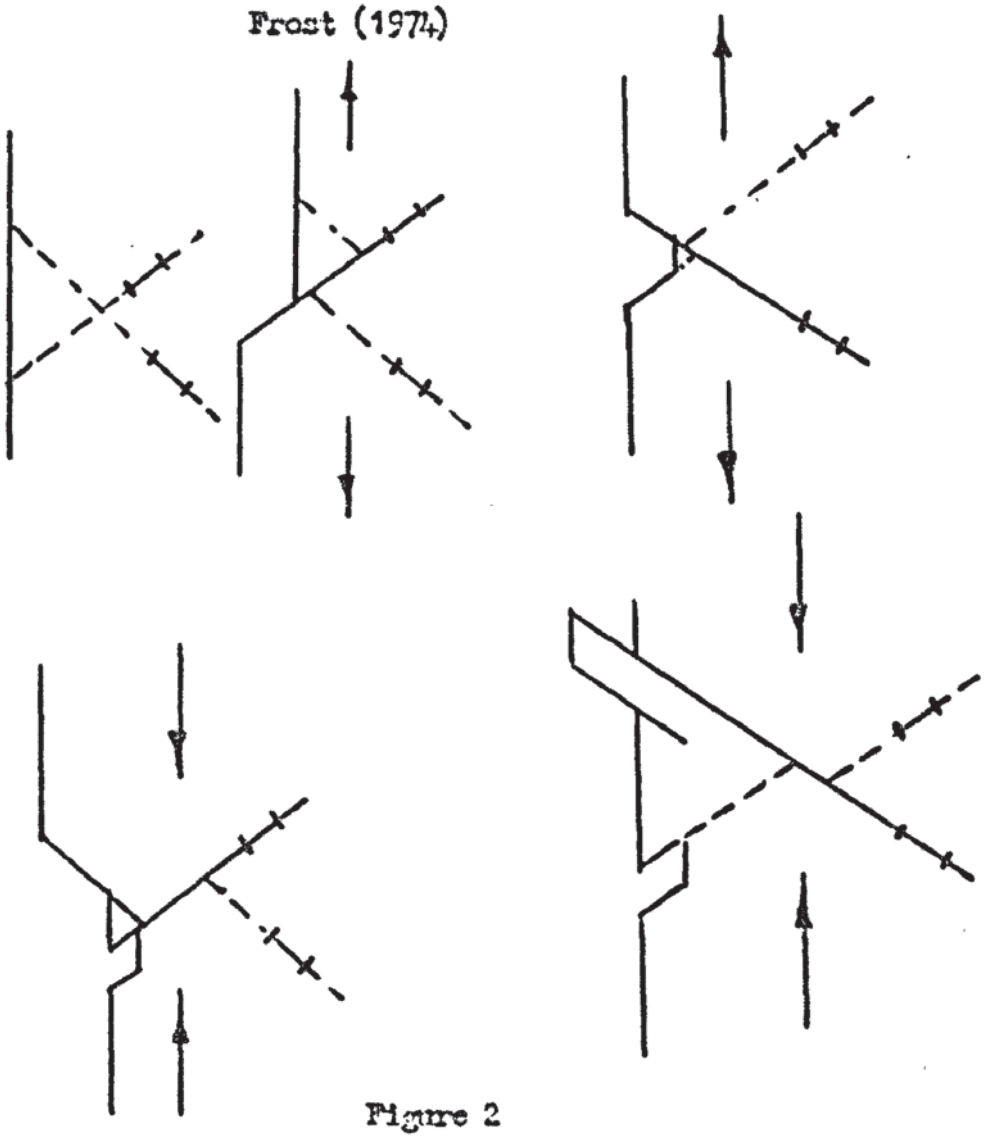

Figure 2

Cottrell and Hull proposed model for forming extrusions and intrusions

a given test. He then assumed that at some large value of z (say Z) a valley was deep enough to be considered a crack. Thus $z/b\varepsilon$ was regarded as a time constant T, controlling the rate at which valleys attained the depth z. When cracks reached this depth their subsequent growth rate was considered to be rapid so that T could be regarded as the life of the specimen. May assumed that a valley whose depth was ten times its width was a true crack (macrocrack), that is $Z = 10w$ which for $w = 10^{-3}$mm $b = 5 \times 10^{-6}$mm, and $\varepsilon = 10^{-3}$ gave a value of $T(=Z/b\varepsilon)$ of 2×10^{6} cycles, from this he concluded that his model could predict lines of the right order.

The fatigue strength of many metals increases with decreasing grain size although results have been reported on other metals (Zinc [43] and Niobium[38] whose fatigue strength was insensitive to grain size. Generally a material's resistance to plastic deformation (yield stress and hardness) increased as the grain size decreased, and thus the cyclic stress to cause continuing slip might also be expected to increase in qualitatively the same way. Whether or not this is so, for a particular material, the grain size may also affect the cyclic stress necessary for a microcrack to develop beyond the grain in which it is formed. If this were the case, then the fatigue strength would decrease with increasing grain size, because with a small grain size, a microcrack may not be able to penetrate to a sufficient depth for it to grow as a macrocrack before encountering a grain boundary, whereas it may be able to do so in a larger grain. If the metal is such that microcracks change into macrocracks at smaller size, any change in grain size above this has no effect on the subsequent fatigue strength.

It is worth emphasizing that, if a specimen is so loaded that it eventually breaks, changes in surface topography occur from the first stress cycle applied, and in this sense it is irrelevant to divide the life into the number of cycles to initiate a crack and the number of cycles to propagate it across the specimen. It is probably more correct to consider the number of cycles spent in developing a microcrack to the macrocrack stage and the number of cycles spent in propagating the macrocrack[55].

The experimental data suggest that only those metals and alloys which strain-age have their fatigue strength increased by coaxing procedures[55] and rest periods, and exhibit S/N curves having sharp knees and definite fatigue limit. There is also evidence that microcracks are present in slip bands in strain-ageing metals at stress levels corresponding to, or just below, their fatigue limit. This implies that before a microcrack has reached the necessary size for it to be able to grow as a macrocrack, strain ageing, by locally increasing the flow stress, inhibits the to-and-fro slip process responsible for its development. The fatigue limit thus corresponds to the maximum cyclic stress that will just not cause the microcrack to continue developing rather than that necessary to just initiate continuing to-and-fro cyclic slip. These arguments are supported by the fact that, although strain-ageing increases the fatigue limit of mild steel, the sharpness of the knee of the S/N curve is dependent on grain size, and the smaller the grain size the sharper the knee[176]. Thus, microcracks formed in small grains will not have reached the necessary size to grow as

macrocracks before they reach the grain boundaries. If their development is held up by the grain boundary (because operative slip planes are at different orientations in adjacent grains) the fatigue limit, that is the stress level necessary to force the crack to pass the grain boundary is greater the smaller the grain size. If the grains are large, microcracks can reach the macrocrack stage before they reach the boundaries; the boundaries do not now retard the growth of a macrocrack, and the knee in the S/N curve becomes less definite. The fact that the stress level at the fatigue limit of a strain-ageing material, such as mild steel, is greater than that required to cause continuing plastic deformation of the bulk of the material explains why it exhibits a hysteresis loop at and just below the fatigue limit stress.

Although non-strain-ageing materials do not exhibit an S/N curve having a sharp knee and a definite fatigue limit, the slopes of their S/N curves usually become very shallow at about 10^8 cycles, and provided the specimen surface is not attacked chemically by the atmosphere, the curve must ultimately become asymptotic to the maximum shear level that will be marginally below the level that causes continuous to-and-fro slip. If the atmosphere does attack the surface, then the fatigue strength decreases continuously with increasing endurance.

The assumption of a linear accumulation of damage, in the form of plastic opening displacement, with the number of cycles, lead to a theoretical prediction of the number of cycles No required to accumulate damage to the point of crack initiation. Theory predicts[6]:

$$N_o \propto 1/\Delta K^2 \qquad (2)$$

2.4 Fatigue Crack Propagation (Growth)

It has been mentioned in Section 3 that, if the cyclic stress level is sufficiently high, a surface microcrack will spread across the surface and penetrate into the body of a material by continuing to-and-fro slip processes until it has reached such a size that it is able to grow as a macrocrack; that is, its growth behaviour will depend on the amount it opens and closes under normal cyclic stress across its faces. To obtain a macrocrack in a specimen at a stress level less than the plain fatigue limit of a material, some form of notch must be introduced into the specimen so that the effective length of a crack formed at the notch root is increased to a value sufficient to grow directly as a macrocrack at the applied nominal stress level. This section discusses the speed at which a macrocrack grows and unless stated otherwise, it is implicit in any reference to fatigue crack growth that the crack has reached the macrocrack stage.

Until recent years, little effort had been devoted to the experimental determination of the laws governing the rate of growth of a fatigue crack; in fact, no accurate quantitative experimental data had been published prior to 1953, the year Head[72] published his theoretically derived relationship between crack length and number of stress cycles. This may have been due to the fact that the assessment of design stresses in those cases where it was considered necessary to give due regard to the fatigue properties of a material, had been almost always based on the plain fatigue limit or strength of the material as obtained from smooth laboratory specimens. Naturally, the purpose of

these design stresses was to prevent the initiation of any cracks under the working loads by keeping all cyclic stresses below some critical values. However, it is only possible to do this when the components or structural members are of a relatively simple shape and the magnitude of the working loads precisely known. The need to produce components of members of complex shape, which are not uneconomic in their use of material, to operate under service conditions which are not precisely defined, has led to the possibility of cracks forming, even at relatively low nominal cycled loads, usually as a consequence of fretting or in the locally highly stressed material around some discontinuity. This implies that some components and structural members, particularly those designed to have a limit life, must operate successfully even though they do not contain fatigue cracks.

In some cases, modern inspection procedures have enabled cracks to be detected in certain components at an early stage in their expected life. However, it has been stated[22] that a crack roughly 5-15 mm long is about the smallest flaw that can be readily detected during routine service inspection. In addition, the necessity to assume the existence members in engineering structures despite the efforts of designers to design fatigue-resistant structures is now generally accepted. Whether these cracks will grow will depend on material and the values of the applied nominal mean and alternating stresses. The selection of a material, from those which fulfill other necessary design considerations, giving the slowest rate of crack growth for a given external loading will lead to an increased margin of safety between routine inspections. Thus, a knowledge of the growth rate character-

istics of a material, together with regular inspections, may enable a cracked component to have a long useful life before having to be replaced. A fail-safe design[67] (that is, a structure so designed that, should cracks form, they will not cause catastrophic failure under the working loads until one of them reaches a known length) implies that a limiting crack length can be established which must be detected by inspection if the crack is not to extend to cause failure before the next inspection. Therefore, designers should use all possible means to achieve the ideals of a low rate of crack propagation and a high residual static strength in the presence of a crack. Probably the best way of assessing the merits of a fail-safe design is by the length of inspection periods which it allows in relation to the weight involved.

Numerous, apparently different 'Laws' of fatigue crack growth have been described in the literature[23] and by making various plausible assumptions. Some of them can be derived theoretically. All the laws can be regarded as valid in the sense that they describe a particular set of fatigue crack growth data, and they can be used to predict crack growth rates in situations similar to those used to collect the data. It is sometimes possible to fit the same set of data to apparently contradictory laws; in such cases it is not possible to decide which law is the most 'Correct".

Since the end of World War II, the problem of brittle fracture has been studied extensively. It has been found that such low stress (compared to the yield stress of the material) fractures always originates at flaws or cracks of various types. The fracture mechanics approach to

residual static strength in the presence of a crack makes use of the stress intensity factor K_I concept to describe the stress field at a crack tip; when K_I reached a critical value K_C the crack extends, usually catastrophically. Values of K_I are known for a wide range of crack configurations, [124, 18, 39, 139, 115, 170] and the fracture mechanics approach has proved useful in problems of material development design, and failure analysis. In view of its success in dealing with static fracture problems, it is logical to use a similar general approach to analyse fatigue crack growth data. The availability of a master curve for a particular material relating fatigue crack growth rate and range of stress intensity factor enables a designer to predict growth rates for any cracked body configuration, and he is not limited to situations similar to those pertaining to the cracked specimen geometry used to generate the original data.

2.4.1 Modes of fatigue crack growth

There are three basic modes of crack surface displacement[111] which can cause crack growth; these are shown in Fig. 3.

I. The opening mode. The crack surfaces move directly apart.

II. The edge sliding mode. The crack surfaces move normal to the crack front and remain in the crack plane.

III. The shear mode. The crack surface moves parallel to the crack front and remain in the crack plane.

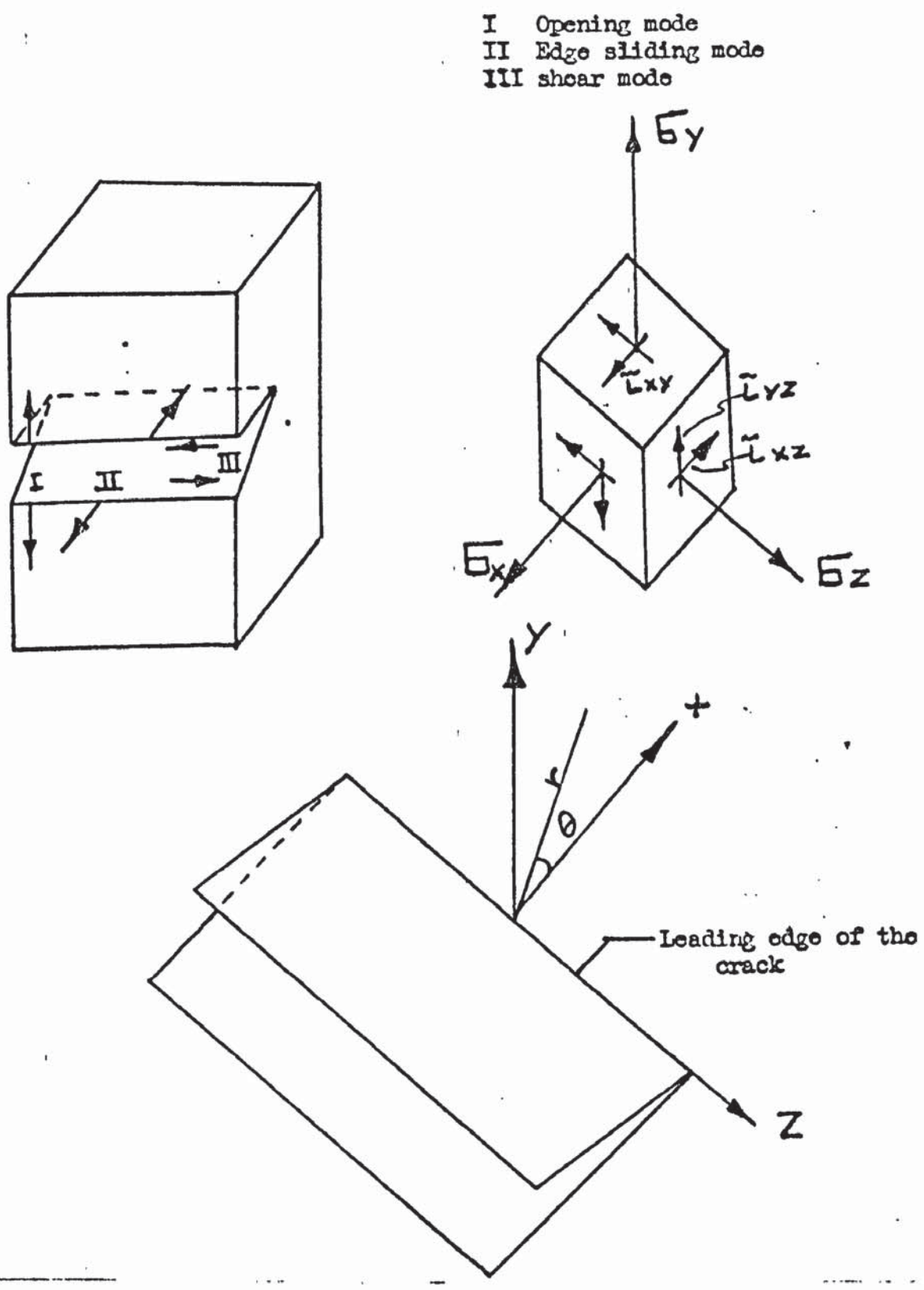

Figure 3. Basic modes of crack surface displacement, coordinates measured from the leading edge of a crack and the stress components in the crack tip stress field (Frost).

The superimposition of these three modes is sufficient to describe the most general case of crack surface displacement. It is conventional to add the Roman numbers I, II, III, as subscripts to various symbols to indicate the mode.

In fracture mechanics only the macroscopic mode of crack growth is considered. Crack growth on 45° planes, often referred to as 'shear fracture', is a combination of Modes I and III, but is usually treated in calculations as if it were Mode I.

For strictly two-dimensional cases and thin-shell problems, only Modes I and III can exist. However, 'two-dimensional' is often taken to include examples of plates of finite (constant) thickness. Mode II displacements can only exist at internal or mathematically deep external cracks.

2.4.2 Stress Intensity Factor

Crack surfaces are stress-free boundaries adjacent to the crack tip and therefore dominate the distribution of stresses in that area[124]. Remote boundaries and loading forces affect only the intensity of the stress field at the crack tip. These fields can be divided into three types corresponding to the three basic modes of crack surface displacement, and are conveniently characterized by the stress intensity factor K (with subscripts I, II, III, to denote the mode). K has the dimension S (stress), X (length)$^{\frac{1}{2}}$, and is a function of the specimen dimensions and loading conditions. In general, it is proportional to

(gross stress) X (crack length)$^{\frac{1}{2}}$. Conventionally, K is expressed in MN m$^{-3/2}$.

In general, the opening mode intensity factor is given by

$$K_I = \sigma(\pi a)^{\frac{1}{2}}\alpha \qquad (3)$$

where σ is the gross tensile stress perpendicular to the crack (compressive stresses simply close the crack), a is the crack length and α is a factor, of the order of unity, which depends on geometry and loading conditions; for engineering purposes α can often be taken as 1. The value of K_I for a crack at a sharp notch, in general is equal to that for a crack of the same total length provided that the notch profile lies within an envelope having an included angle of 30° drawn from the crack tip[126].

When K is known, stresses and displacements near the crack tip can be calculated using standard equations[124]. Thus, for example, in Mode I, referring to Fig. 3 for notation (where U, V, W are displacements in the X, Y, Z directions, these can be given for plane strain as

$$\sigma_x = \frac{K_I}{(2\pi r)^{\frac{1}{2}}} \operatorname{Cos}\frac{\theta}{2}\left(1 - \operatorname{Sin}\frac{\theta}{2}\operatorname{Sin}\frac{3\theta}{2}\right)$$

$$\sigma_y = \frac{K_I}{(2\pi r)^{\frac{1}{2}}} \operatorname{Cos}\frac{\theta}{2}\left(1 + \operatorname{Sin}\frac{\theta}{2}\operatorname{Sin}\frac{3\theta}{2}\right)$$

$$\tau_{xy} = \frac{K_I}{(2\pi r)^{\frac{1}{2}}} \operatorname{Sin}\frac{\theta}{2}\operatorname{Cos}\frac{\theta}{2}\operatorname{Cos}\frac{3\theta}{2} \qquad (4)$$

$$\sigma_z = \nu(\sigma_x + \alpha y)$$

$$\tau_{xz} = \tau_{yz} = 0$$

$$U = \frac{K_I}{G} \left(\frac{r}{2\pi}\right)^{\frac{1}{2}} \text{Cos}\ \frac{\theta}{2} \left(1 - 2\nu + \text{Sin}^2\ \frac{\theta}{2}\right)$$

$$V = \frac{K_I}{G} \left(\frac{r}{2\pi}\right)^{\frac{1}{2}} \text{Sin}\ \frac{\theta}{2} \left(2 - 2\nu - \text{Cos}^2\ \frac{\theta}{2}\right)$$

$$W = 0$$

where G is the shear modulus and ν is Poisson's ratio.

Elastic stresses are inversely proportional to the square root of the distance from the crack tip, and become infinite at the crack tip. Provided that only one mode is present, the stress intensity factors due to different loadings can be superimposed by algebraic additions if more than one mode is present, the individual stress components and displacements can be similarly superimposed.

Small scale non-linear effects, such as those due to yielding, micro structural irregularities, internal stress, local irregularities in the crack surfaces, and 45° crack growth in thin sheets do not affect the general character of the stress field and can be regarded as being within the crack tip stress field[118]. Similarly, the actual fracture process can be regarded as taking place within the stress field at the crack tip. The concept of stress intensity factor therefore provides a convenient mathematical framework for the study of fracture processes.

The representation of a crack tip stress field by a stress intensity factor is a basic concept in fracture mechanics. The term should not be confused with the 'stress concentration factor' or 'stress intensification factor' which are terms used to describe the ratio between the maximum

and nominal stress at a disconitnuity.

It is found that, under increasing load, a crack will start to grow (provided that general yielding does not intervene) when K_I reaches a critical value (K_C) and will continue to grow as long as the loading conditions are such that $K_I > K_C$.

2.4.3 Crack direction

The expected direction of crack growth in a uniaxially loaded sheet specimen is normal to the loading direction with the machine face on a plane through the thickness of 90° to the plane of the specimen (termed 90° growth: Mode I); in some materials, zinc and titanium, this is what occurs. However, in other materials, such as steels, copper alloys, and aluminium alloys[23, 126, 148], a transition to growth on a plane through the thickness inclined at approximately 45° to the plane of specimen (termed 45° growth; a combination of Modes I and III) usually takes place after an initial period of 90° crack growth. As theoretical and experimental results show that crack growth on a 45° plane is faster than on 90° planes, 45° planes are therefore energetically more favourable[56]. However, rotation of the crack surfaces to 45° planes can only take place if a suitable mechanism is available. Growth on 45° plane only occurs in those materials in which the static tensile fracture of a piece of material of the same thickness as the crack growth specimen occurs on a 45° plane through the thickness. If the static fracture occurs on a 90° plane (as it does with zinc and titanium), a fatigue crack grows on a 90° plane throughout.

2.4.4 Microscopic appearance of fatigue crack

Since 1950[177] a great deal of effort has been devoted to the microscopic examination of fatigue fracture surfaces, particularly since the advent of the electron microscope[37], and various collections of electron micrographs showing the details of the fracture faces created by a growing fatigue crack have been published[93, 37, 131, 108]. The most prominent features of fatigue fracture surfaces (particularly those created by cracks growing on 90° planes) are distinct fine markings, parallel to each other and normal to the direction of crack growth. These are generally called striations; each striation corresponds to one load cycle. In general, striations are more clearly defined in ductile than brittle materials, for instance, in the stronger steels[130], striations are short and discontinuous and their successive positions not clearly defined.

The presence of striations on a fracture surface is proof that failure was caused by fatigue[52], but they cannot always be found on all fatigue fracture surfaces, often because the microscope used has sufficient resolution. Striations varying in spacing from about 2.5 mm to less than 7.5×10^{-5} mm have been observed on various materials.

On a microscopic scale, fatigue growth is often an irregular process. Examination of the fracture surfaces of some particular material using a stereoscan microscope showed that the main fracture surface was irregular with numerous interconnected cracks intersecting the main cracks[112]. Some of these cracks were at nearly 90° to the main fracture. Much earlier a study of the shape of the front of a

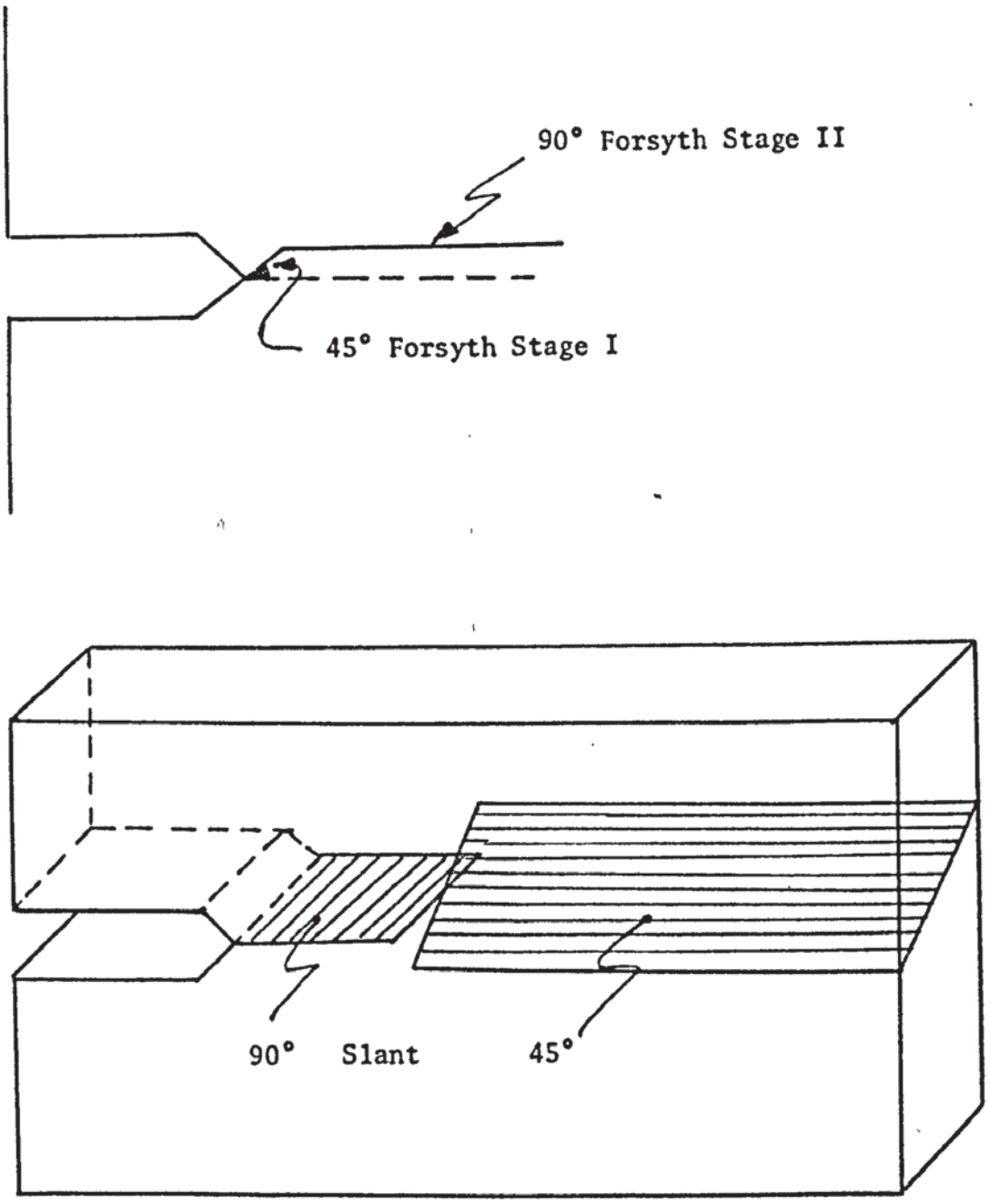

Figure 4.

crack growing in a 3.2 mm thick mild steel sheet was made by examining sections of planes normal to the direction of crack growth so as to eventually intersect the crack front. This showed that the crack front bows forward slightly so that a section can be made with the leading part of the crack in the middle of the sheet thickness. In the region of the crack front, numerous apparently independent cracks were found. These cracks may be similar to those found in the aluminium alloy.

The other equipment which is available for use to study the fractured surfaces is the scanning electron microscope (SEN). It is a combination of electron-optical, vacuum, and electron control devices for impinging a beam of electrons on a pinpointed spot on the surface of a target specimen and collecting and displaying the signals given off from that target. The SEM was developed initially to obtain information about surface topography and was thought of as complementing the capabilities of the light microscope and the transmission electron microscope.

For each fractograph the crack depth, the overall direction of crack propagation, and the overall shape of the crack front should be determined. Then, if the stress-intensity factor is known from a fracture-mechanics test, the size of the plastic zone that existed at the crack tip can be estimated. In all photographs, whether they are of a cleavage fracture or of a ductile fracture, the size of the features observed should be related to the dimension of the plastic zone to which they were associated during fracture.

To simplify identification in the fractograph of crack-propagation direction, it is usually convenient to orient a specimen so that propagation is from the lower part to the upper part of the photograph and to view the fracture at an angle of 30° to 45°. It is more important to maintain the overall direction of crack propagation along the short dimension of the photograph than to maintain a constant tilt angle. Very often, to get better contrast of a given region on a rough fracture surface, the tilt angle may have to be as much as 60°. Finally, it is important that an SEM fractograph be viewed right side up. If the effect of shadowing is inverted features can be quite misleading and the fracture may thereby be completely misunderstood. The greatest change in appearance when an SEM fractograph is inverted, is that dimples look like projections rather than depressions.

2.4.5 Some Fatigue Crack Growth Theories

Although crack growth data can be presented simply as a series of curves of crack length plotted against a number of cycles for different mean tensile and alternating stresses, it is more convenient to handle if presented as a mathematical relationship including crack length, number of stress cycles, tensile mean stress, alternating stress, and a material constant. Several attempts have been made to derive such a relationship theoretically by treating the material as a continuum. All relate crack length and number of cycles. Some offer a prediction of the stress dependence of the growth rate but in general, do not predict the material constant, which must be determined experimentally.

All the theories discussed assume that crack growth is in Mode I, usually considering a central transverse crack length 2a, in an infinite sheet subjected to a remotely applied uniaxial stress σ. Examination of the fracture faces created by a moving crack shows that a fatigue crack moves forward each stress cycle. In view of this, any theory of crack growth based on the assumption that a crack remains stationary for a certain number of cycles of stress, while the material ahead of the tip is conditioned in some way prior to fracture, is invalid.

Head's theory

Head's[72] theory was developed before treatments of plasticity near cracks were available and was based on various simplifying assumptions. A cracked body was regarded as consisting of a composite array of three types of continua. Taking infinitesimal elements of each three types, material directly ahead of the crack was viewed as an array of independent, rigid-plastic tensile bar, each hardening linearly from a yield stress σ_y to a maximum tensile stress σ_f at a modulus E_w, but without any Bauschinger effect[72]. The material above and below the crack and rigid plastic bar array was regarded as an array of independent elastic tensile bars of modulus E, each carrying the remotely applied stress, which transmitted the load to the rigid plastic bars both directly and through a third array of elements transmitting the load by shear. The properties of the shear elements and lengths of the elastic bars were selected so that the model gave the correct elastic opening at the centre of the crack. He considered the history of a small volume of material in line with the advancing crack and argued that as the crack tip approached it would begin to deform plastically, work-hardening progressively, until its ductility was exhausted, at which point it would fracture and become part of the main crack.

a) This model gave for an applied stress $\pm \sigma$, when $\sigma < \sigma_y$

$$\frac{da}{dN} = \frac{2E_w \sigma^3 a^{3/2}}{3E(\sigma_f - \sigma_y)(\sigma_y - \sigma)2h^{\frac{1}{2}}} \qquad (5)$$

where 2h is the height of the rigid plastic elements infront of the crack.

Because $\sigma_y > \sigma$ equation (5) is equivalent to

$$\frac{da}{dN} \alpha K_1^3$$

b) For a remotely applied stress greater than the yield stress $\sigma > \sigma_y$ this theory gave

$$\frac{da}{dN} = \frac{2E_w \sigma^3 a^{3/2}}{E\sigma_f(\sigma_f^2 - \sigma^2)h^{\frac{1}{2}}} \qquad (6)$$

Thus in a given test in which gross stresses are kept constant, $a^{-\frac{1}{2}}$ can be plotted linearly against the number of cycles; h must be obtained from the experimental data.

The geometrical similarity hypothesis

This is based[57] upon consideration of a small idealized transverse slit, in a perfectly elastic sheet of infinite extract, subject to plane stress and loaded in uniaxial tension. If a unit diagram is prepared in which dimensions are scaled by taking the slit length as unity, elastic theory shows that at any point defined by a vector drawn from the origin, the stress or displacement is the same regardless of the actual slit length, dimensional analysis of all the parameters that have a bearing on the problem always gives the same result.

The same argument can be applied to a finite sheet, provided that the sheet width is large compared with the slit length, because stresses in the vicinity of the crack will only be slightly affected. Briefly, this theory thus leads to the growth law:

$$\frac{da}{dN} = Da \tag{7}$$

that is,

$$\ell n(\frac{a}{a_o}) = DN \tag{8}$$

where a_o is the initial crack length.

Thus, in a given crack growth test on a sheet of finite width, in which the gross stresses are kept constant, $\ell n(a)$ should vary linearly with the corresponding number of cycles N, until the crack reached such a length that it can no longer be regarded as growing in an infinitively wide sheet. The coefficient D depends on both the mean and alteranting stresses and on the material; it cannot be predicted, but must be obtained from analysis of experimental data.

Net area stress theories

Weibull developed a theory[166, 167] based upon consideration of a central transverse crack growing in a thin sheet of finite width subjected to a zero to tensile loading cycle. He argued that, as the crack length/sheet width ratio increased, the effective stress at the crack tip would also increase so that the rate of growth at a given crack length/sheet width ratio would depend only on the instantaneous value of the effective stress at the crack tip, that is:

$$\frac{d}{dN}\left(\frac{2a}{W}\right) = F\sigma_t^{\beta} \tag{9}$$

where F and β are constants,

2a is the overall crack length

σ is the effective crack tip stress

W is the sheet width

N is the number of cycles.

He assumed that the effective crack tip stress depended only on the maximum nominal stress acting on the net uncracked area of the sheet. His final equation after several steps of substitutions emerged as

$$\frac{d\ (2a)}{dN} = CW\sigma_N^{\ n} \tag{10}$$

where

$$C = FA^{\beta} \qquad \text{and } n = m\beta$$

If a crack growth test is carried out in which the external loads are continually reduced as the crack grows so that the nominal net cyclic stress σ_N is maintained at a constant value throughout, equation (10) can be iterpreted to give

$$2a = CW\sigma_N^{\ n}N \tag{11}$$

Thus, in a constant net area stress crack propagatiom test on a sheet of finite width, the crack length should vary linearly with the number of cycles, irrespective on crack length. The material constant and stress dependence are not predicted and must be obtained from experimental data. However, for sheets of different width, the slope of the a versus N plots, at a given σ_N should be directly proportional to the width W.

Weibull's net area stress relationship can be deduced using fracture mechanics[150]. The stress intensity factor for a finite width sheet under uniaxial tension can be written as[124]

$$K_I = \sigma_N(1 - \frac{2a}{W})(\pi a)^{\frac{1}{2}}(\frac{W}{\pi a}\tan\frac{\pi a}{W})^{\frac{1}{2}} \qquad (12)$$

McEvilly and Illg [111, 66] also proposed a net area stress theory based on the assumption that the effective stress at the tip of a crack was given by the expression $K_N\sigma_{Na}$, where σ_{Na} was the alternating stress on the net uncracked area and K_N the effective stress concentration factor for the crack. Provided $K_N\sigma_{Na}$ was greater than the plain fatigue limit of the material, they postulated that a crack would grow at a rate which was a function of the current values of $K_N\sigma_{Na}$, that is

$$\frac{da}{dN} = f(K_N\sigma_{Na}) \qquad (12a)$$

The stress also could be written, after deriving K_N from Neuber's equation for zero flank angle which gives

$$K_N = 1 + \frac{1}{2}(K_H - 1)(\frac{a}{A})^{\frac{1}{2}} \qquad (13)$$

where S is a material constant of the dimensions of length and K_H is the elastic stress concentration factor for a hole of radius C in a sheet of the same width and K_N in equation (13) is for a crack of length a equal to c.

Accumulated strain hypothesis

Various hypotheses based on an element of material ahead of the crack tip fracturing when it has accumulated some critical amount of plastic deformation have been put forward. As an example[91] consider the case of a central crack transverse to the loading direction in a thin sheet subjected to a zero to maximum loading cycle, and assume that an elementary length of material ε ahead of the crack fractures as an entity when the average repeated tensile strain accumulated by the element reaches some critical value. Assuming that the average strain across the element is not appreciably different from that obtained by considering the material as wholly elastic, the rate of growth is given by

$$\frac{da}{dN} = \frac{\varepsilon^{1-n/2}}{C} \left(\frac{A\sigma}{E}\right)^{n} a^{n/2} \qquad (14)$$

where

ε is a strain,

C is a material constant,

E is Young's modulus, and

n is obtained from constant strain amplitude data of plain specimens of the same material.

For a given test of particular material, the growth rate is therefore proportional to $a^{n/2}$. At different stress levels the rate will be proportional to $(\sigma\, a^{\frac{1}{2}})^{n}$ that is, proportional to some function of the stress intensity factor.

The functional relationship between growth rate and $K_N\sigma_{Na}$ and incidentally, A, could only be obtained from analysis of experimental data. This concept is equivalent to the use of stress intensity factor.

Dislocation theories

In the case of a crack loaded in anti-plane strain (Mode III), the plastic zone and its tip can be conveniently represented by a continuously distributed array of infinitesimal dislocations on the crack plane. Theories based on dislocation arrays assume that crack growth will start when the accumulated plastic strain distributed at a crack tip exceeds a critical value, and the plastic strain continued at this value is exceeded at successive points ahead of the original crack tip. At some point in a theory, it is assumed that the behaviour in Mode I is similar to behaviour in Mode III. In general[73], such theories predict that the rate of crack growth is proportional to K_I^4, which could predict the Model in the following form:

$$\frac{da}{dN} \alpha K_I^4 \qquad (15)$$

where $K_I = \sigma_{max} (\pi a)^{\frac{1}{2}}$.

Energy theories

The energy associated with the plastic zone at crack tip is proportional to K_I^4, so that theories based on the energy required to operate the fracture mechanism in general, will predict that the rate of crack growth is proportional to K_I^4, in agreement with dislocation theories.

For instance, a theory can be based[138] on a rigid plastic strip model where the cracked body becomes two elastic half planes joined

together along a strip of rigid plastic material, with a void in the strip to simulate the crack. Tracing the deformation history of a particular point ahead of the crack tip, from when the plastic zone first reaches it to the time it is reached by the crack tip, it is assumed that the separation occurs when the total absorbed hypothesis energy U per newly created surface area equals a postulated critical value U_c. Letting ΔU_y (x,0) be the plastic displacements of the discrete surface of tensile yielding per load reversal when the crack tip is set at x = 0, and assuming then that the growth rate is constant while crossing a zone W of reversed deformation, after several mathematical steps, the crack growth rate is given by

$$\frac{da}{dN} \quad \alpha(\Delta K)^4 \qquad (16)$$

Frost and Dixon's theory

Frost and Dixon [56] argued that the absence of evidence to support internal cracking ahead of the crack tip in a homogeneous material (internal cracking may occur in a material in which inclusions or other non-homogeneities give rise to elements of part fracture occurring in the growth process), together with the fact that crack growth cannot be considered merely as a consequence of the slip process which lead to the initiation of a surface microcrack, lead to the conclusion that a crack grows because its tip profile is successively blunted and re-sharpened each stress cycle. The unloading half of the stress cycle is essential to the growth process for, unless the crack tip is re-sharpened each cycle, fresh surfaces cannot be created during the process of crack tip blunting when the load is re-applied. It is not necessary

for the material to be unloaded to zero in order for the crack tip to resharpen, because compressive residual stresses of the order of the yield stress of the material will be induced at the crack tip as soon as an increment of load is removed from the maximum load applied. These compressive residual stresses will tend to sharpen the crack tip. Thus the profile of a crack in a ductile material loaded from 0 to σ_1, will be different from that loaded from 0 to σ_2, unless $\sigma_2 > \sigma_1$ and then unloaded to σ_1, because in the former case the compressive residual stresses induced during the unloading from σ_2 to σ_1 will tend to sharpen the crack tip. The next model was constructed for a crack growth.

$$\frac{da}{dN} = \frac{8}{\pi} \left(\frac{\Delta K}{E}\right)^2 \quad \text{or} \quad \frac{da}{dN} \; \alpha(\Delta K)^2 \tag{17}$$

Linear elastic fracture-mechanics crack growth theory

Frost and Dixon's theory can be re-expressed in fracture-mechanic terms with equation (30) defined directly from the stress and displacement fields around cracks and sharp notches. These predict that the crack opens up into a parabola. Following the original theory, consider the stress at the periphery of a parabolic notch having the same profile as the parabola. Unlike the original theory for an elliptic shaped crack, peripheral stresses fall to zero at infinity. Thus, to formulate a growth law, a different fracture criterion is required. This is achieved by assuming that the part of the crack profile subjected to a tensile stress greater than the yield stress retains its length on unloading. For typical values of $E/\sigma y$ this leads to

$$\frac{da}{dN} = \frac{9}{\pi} \left(\frac{K_I}{E}\right)^2$$
$$\frac{da}{dN} = \frac{7}{\pi} \left(\frac{K_I}{E}\right)^2 \tag{18}$$

By assuming the von Mises yield criterion, the theory can be extended to Mode III on a combination of Modes I and III, but cannot be applied to Mode II. In Mode II, stresses and displacements are anti-symmetrical about the crack plane, hence an increase in profile length on one crack surface is balanced by a decrease on the opposite surface. Crack growth on 45° planes can be treated by making some simplifying assumptions leading to

$$\frac{da}{dN} \simeq \frac{13}{\pi} \left(\frac{K}{E}\right)^2 \qquad (19)$$

which implies a faster rate of growth than equation (18).

As with Frost and Dixon's theory, the final equation (18) implies that any value of ΔK, no matter how low, will result in a positive value of da/dN. It has been shown experimentally that a minimum value of ΔK_C of ΔK is necessary for crack growth to occur, and that it appears to be associated with the minimum possible fatigue crack growth rate of one lattice spacing per cycle. Continuum mechanics provides only a rough guide to behaviour at crack growth rates of this order. Nevertheless, for the zero to tension loading case ΔK_C can be estimated by substituting the lattice spacing into equation (18). The resulting values are between one-forth and one half of those obtained experimentally.

Experimental assessment of the validity of a fatigue crack growth theory is difficult, since data can usually be found in the literature to either support or vitiate any particular theory. Thus, the fact that experimental evidence is cited in support of a theory does not guarantee its validity. In addition, the theories mostly relate to a zero to

tensile strain loading cycle, whereas much data, especially on sheet specimens, are obtained under the stress cycle $\sigma_m \pm \sigma_a$ where $\sigma_m > \sigma_a$. None of the theories predict the effect of a mean tensile stress. Barnby[6] used the law of crack growth rate and agreed that it obeys the following relationship

$$N_{(a)} \alpha \frac{1}{\Delta K^n} \tag{20}$$

The latest model for fatigue crack propagation proposed[142] where they assumed that the crack advanced ℓ unit in ΔN cycles according to Manson-Coffin equation

$$4\Delta N(\bar{\varepsilon}_\rho/\varepsilon_f)^{1/\beta} = 1 \tag{21}$$

where $\bar{\varepsilon}_\rho$ = average plastic strain range in process zone

ε_f = monotonic fracture strain

ΔN = cycles to propagate units

β = Coffin-Manson Exponent

The final expression for a fatigue crack growth rate was:

$$\frac{1}{N} = \frac{da}{dN} = 4\left(\frac{0.7\alpha}{E\sigma_{ys}^{1+s}\varepsilon_f}\right)^{1/\beta}\left(\frac{1}{\ell^{1/\beta-1}}\right)(\Delta K)^{(2+s)/\beta} \tag{22}$$

This last result is in agreement with Paris's empirical equation

$$\frac{da}{dN} = R(\Delta K)^n \tag{23}$$

2.5 Factors Affecting Fatigue

2.5.1 Stress Concentrations around a Notch

The elastic stress distribution around a notch is determined by the form of the notch, and the most important feature is the elevation of stresses in the vicinity of the notch root. If the maximum elastic boundary stress created by a given notch in a uniaxially longitudinally loaded specimen is known, the ratio of the maximum longitudinal elastic stress at the notch root σ_{max}, to the nominal elastic stress σ applied to the specimen, that is, σ_{max}/σ, is commonly denoted by K_t where K_t is called the geometric elastic stress concentration factor. Similarly, values of K_t can be obtained for notched specimens loaded in torsion, K_t now being the ratio of the maximum elastic shear stress at the notch root or boundary to the nominal shear stress applied to the specimen. Values of K_t for a wide variety of notch profiles due to either tension, bending or torsion loads are available [65, 20, 29] the data usually being presented in graphical form. The value of K_t depends on whether the nominal stress is based either on the area of two minimum cross sections of the specimen (that is, net area) or on the overall cross section of the specimen, ignoring the presence of the notch (that is, gross area). In practice, nominal stresses are usually based on net area and consequently K_t is generally expressed in terms of net area. Stress concentration factors provide a convenient single parameter description of the stress condition at a notch root, but their utility is limited because they do not give information on the stress distribution around the notch. The localised nature of the high stress in the vicinity of a notch is illustrated by the elastic distribution around a circular hole in thin rectangular sheet whose boundaries are an infinite distance away from the centre of the hole.

In the case of a circumferentially notched cylindrical specimen subjected to tension or bending, the stress distribution is dominated by the notch root radius δ. Provided that the notch depth is at least equal to δ and the minimum specimen diameter is at least 10.

The life of a broken notched specimen is the sum of the number of stress cycles required to initiate a surface crack with those to develop it through the highly stressed material at and around the notch rest, and those required to propagate this crack across the remainder of the specimen cross-section which is subjected only to the applied cyclic stresses. The ratio of the number of cycles in these two stages will vary with the material, notch geometry, specimen size and stress level. Cracks may form quickly at the root of sharp notches, even at low stress levels, and their propagation across the specimen may occupy the major part of the life. Indeed, if the notch is very sharp and the nominal stress range sufficiently small (or if the loading cycle is wholly compressive), cracks may form at the notch root which do not continue to grow across the specimen cross-section.

2.5.2 Temperature Variations

In some practical applications, components are required to operate at temperatures either above or below room temperature, the former being the more common requirement. This is reflected in the fact that there are much more experimental data available on the fatigue strengths of materials at temperatures above room temperature than at temperatures below it. A further reason for this may be that the fatigue

strength of a material decreases as the temperature decreases, for example, the ratio of the fatigue limit at liquid air temperature to that at room temperature is in the range 1.5 - 2.5 for most metallic alloys[47]. Softer materials generally give higher values of this ratio than harder materials. Thus, a design based on room temperature fatigue data will be safe for use at lower temperatures, although of course, any increased susceptibility to brittle fracture under the applied loadings must be taken into account. Materials for use at elevated temperatures, in addition to possessing adequate static and fatigue properties, must be resistant to corrosive attack by the atmosphere at the operating temperature. Special alloys possessing these properties have been developed for components such as the blades and discs in a gas-turbine engine. At elevated temperatures, factors which have no significant effect at room (and lower) temperatures become important, for example, metallurgical changes in microstructures due to prolonged soaking at the operative temperature and chemical attack of the specimen surface by the atmosphere.

Because these effects become more pronounced the longer the specimen is kept at the elevated temperature, surface damage may occur which is not solely dependent on the amplitude of the stress cycle and the number of times it is applied. The best way of seeing that, for the two different temperatures, is to tabulate the early results by several authors (Table 1),(Table 2) by Forrest[47] and (Table 3)[20].

Material	Reference	Fatigue Strength ($MN\ m^{-2}$)					
		20°C	-40°C	-78°C	-188°C	-253°C	-269°C
Copper‡‡	120	±100	-	-	±145	±240	±260
Brass ‖	121	±175	±185	-	-	-	-
Cast Iron ‖	121	± 60	± 75	-	-	-	-
Mild steel+	122	±185	-	±255	570	-	-
Carbon Steel+	117	±230	-	±290	625	-	-
Ni-Chromium alloy steel+	117	±540	-	±580	765	-	-
Duralumin ‖	121	±115	±145	-	-	-	-
Aluminium 2014T6		±100	-	-	±170	±310	-
Alloys § 2020T6	123	±125	-	-	±155	±280	-
7075T6		± 85	-	-	±140	±240	-

+ fatigue limit

‡‡ fatigue strength, 10^6 cycles.

§ fatigue strength, 10^7 cycles.

‖ fatigue strength, 5×10^7 cycles.

TABLE 1

Alloys	Ratio: Fatigue strength (10^6 cycles) at given temperature / Fatigue strength (10^6 cycles) at room temperature		
	-40°C	-78°C	-188°C
Carbon Steels	1.2	1.3	2.6
Alloy Steels	1.05	1.1	1.6
Stainless Steels	1.15	1.2	1.5
Aluminium Alloys	1.15	1.2	1.7
Titanium Alloys	-	1.1	1.4

TABLE 2

Steel	Fatigue strength, 10^8 cycles (MNm^{-2})		
	20°C	70°C	100°C
0.6%C, 0.7%Mn	±430	±370	-
0.24%C, 3.9%Ni, 1.0%Cr.	±490	±430	-
0.2%C, 4.7%Ni, 1.4%Cr, 0.6%Mo	±570	-	±450

TABLE 3

2.5.3 Notch Configuration (Root radius affecting Fatigue Life)

Allery[3] has done some work considering the effect of notch root radius on the fatigue crack initiation and propagation process. The deleterious effect of notches and other stress raisers has been appreciated from the time when fatigue was first recognized as a problem associated with repeated loading. Other less obvious stress raisers exist which may be classed as metallurgical defects. There are features such as cavities, blowholes, slag or oxide particles and defects due to metallurgical processes such as casting, rolling or welding. In engineering practice the common notches or stress raisers are holes, screw threads, splines, keyways and changes in section, and it is clear that whilst such features cannot be eliminated, their effects can be minimised with good design practice.

The strength reducing effects of notches are of obvious importance in design and life prediction and a large amount of data exists which compare the strength of notched fatigue specimens with that of plain specimens. The ratio of the plain to notched fatigue strength is called the strength reduction factor and is denoted K_f. The presence of a notch of small root radius does not reduce the fatigue strength to the extent expected from a consideration of the magnitude of the theoretical stress concentration factor K_t. The experimental fatigue sensibility, δ , can be expressed as:

$$\delta = \frac{K_f - 1}{K_t - 1} \qquad (24)$$

The value of δ is a function of both the material tested and the radius of the notch root ρ. To account for the size effect, Neuber[121]

proposed that the effective stress concentration factor, K_N be expressed in terms of the theoretical factor K_t modified in the following manner:

$$K_N = 1 + \frac{K_t - 1}{1+\sqrt{\rho'/\rho}} \tag{25}$$

where the material constant ρ', is across which is stress gradient cannot exist (further called Neuber constant). As ρ approaches zero, K_N approaches a constant value for a given material and notch depth. In the analysis of notch fatigue results it has been assumed[98] that K_f can be similarly modified to give

$$K_f = 1 + \frac{K_t - 1}{1+\sqrt{\rho'/\rho}} \tag{25a}$$

Allery's work was based on a single edge-notch specimen. Variations in notch root, radius produced marked changes in the cycles required to initiate fatigue crack at the root of a notch. It was also proved that increasing notch root radius causes a marked increase in the number of cycles to initiation.

The variation in the number of cycles to initiate a fatigue crack with notch root radius is due to the progressively decreasing stress concentration factor with increasing notch root radius. Hence, although the net section stress conditions are identical in tests with varying notch root radii, the notch tip stress will decrease as the notch root radius increases. Assuming elastic conditions, the laternating stress distribution under the notch is given by the expression

$$\sigma_a = K_t \sigma_N \tag{26}$$

where σ_a is the effective alternating stress and σ_N is the nominal applied alternating stress. Another factor was also stated[3] that is as the notch root radius increases, the extent of the zone under the notch influence by the stress field of the notch will increase.

2.6 Fatigue of Notched and Plain Specimens

In general[12], the results of short endurance constant nominal stress amplitude tests on notched specimens give an S/N curve of similar form to that for the plain specimen, except that it is displaced to the left and can cross over that for plain specimens at very short endurance. The fact that the nominal stress amplitude required to cause fracture in a given short endurance may be higher for a notched than for plain specimens in a consequence of the triaxial stress system generated across the minimum section of the former specimen. This reduces the plastic deformation and the onset of necking in this region, thus leading to an increased tensile strength (based on original net area) compared to that obtained on a plain specimen of the same minimum cross-sectional area. The initial flat portion of the S/N curve for notched specimens may also be much shorter than for plain specimens, probably because the material at the notch of the root is restrained by the bulk of the specimen and tends to undergo constant strain amplitude cycling even though the specimen as a whole is subjected to a nominal constant stress amplitude loading cycle. Several users[169] have found that the constant nominal stress amplitude S/N curves for notched specimens may cross that for smooth specimens somewhere in the region of 100-1000 cycles.

In the case of sharp notches, cracks form quickly at high stress levels and the life of a specimen is spent wholly in crack propagation; the life of a specimen or component therefore bears little relationship to the K_t value of the notch. It depends on the distance the crack must traverse to cause complete failure. The rate of growth of a crack at these high stress (or strain) levels cannot be predicted using the

crackgrowth relationship discussed earlier because they are applicable only as long as the bulk of the specimen remote from the crack tip is deforming elastically. A rough estimate can be made in the case of a crack growing under a constant strain amplitude by converting the strain to an equivalent elastic stress, and using one of the crack growth relationships discussed earlier. (In the case of notched specimens, the initial crack length must be taken as the notch depth and the crack length subsequently measured from the free surface.) This approach is equivalent to assuming that the strain distribution is the same above and below general yielding, and has been used to predict static failure[172]. It is more likely to be successful when the crack length is small compared with other dimensions. Fatigue crack growth data in the fully plastic region has been successfully correlated using displacements calculated from slip fields[28], and with measurements of the crack opening displacement (C.O.D.) at the crack tip.

Morrow and his co-workers[162, 171] have developed an analysis of notched fatigue behaviour in the low-endurance region by considering the local stress-strain response at the notch. Changes in nominal stress ΔS and nominal strain Δe are related to corresponding changes in local stress $\Delta\sigma$ and local strain $\Delta\varepsilon$ by the relationship

$$K_t(\Delta S \Delta e E)^{\frac{1}{2}} = (\Delta\sigma\Delta\varepsilon E)^{\frac{1}{2}} \qquad (27)$$

They claim that life predictions for notched members may be made by this analysis from smooth specimen data, but this can presumably only apply if the whole life of a specimen is spent in initiating and developing a microcrack. When this is so, the Morrow approach would seem to be

merely a quantitative alternative to obtaining the endurance from a smooth specimen plastic strain endurance curve. Hence the life of a mildly notched specimen ($K_t \simeq 2$ or 3) can be obtained from this curve using the appropriately factored plastic strain. It must be emphasized that this approach applies only to specimens with smooth well prepared surfaces. Although a component with an as-forged finish would display the same stress strain response as a polished component, the life of the as-forged component would be spent wholly in propagating a macrocrack and therefore should be estimated by fracture mechanics methods.

The experimental results suggest that the life of a plain specimen tested in low-endurance fatigue is given by $\varepsilon N^m = c$, where ε is the strain range and m and c are constants for a particular material and testing conditions. When ε is expressed as the plastic strain range εp and the number of cycles to failure N defined by the presence of visible surface cracks, then we have a value of about ½ for all materials. The value of N over which this relationship is valid depends on material, and it should be argued that it corresponds to the number of cycles required to develop a surface crack to the stage where it can spread rapidly. Indeed May [107] showed that his model of surface cracking when modified to apply to a specimen subjected to a constant plastic strain amplitude tends to an $\varepsilon pN^m = c$ relationship.

On the other hand, the fracture faces of short endurances, high strain amplitude specimens exhibit striations immediately adjacent to the point of crack initiation , suggesting that a crack commences as a

macrocrack at a very early stage in its life [133]. The general relationship $N^m\varepsilon = c$, that would be expected if low endurance fatigue failure under a given strain amplitude is essentially a crack propagation problem. Since the growth rate of a crack is a function of its length and the nominal strain range is the bulk of the material, this could be taken as

$$\frac{da}{dN} = A\varepsilon^b a^c \tag{28}$$

If c is considered to be equal to one, then $\ell n(a_f/a_o) = A\varepsilon^b N$, where a_f is the crack length at final fracture and a_o the length at which a surface crack can be first considered a macrocrack. For a given series of tests $\ell n(a_f/a_o)$ will be sensibly constant and thus

$$\varepsilon^b N = \text{Constant}$$

or

$$\varepsilon N^m = \text{Constant} \tag{29}$$

The relationship would not be expected to hold below the plastic strain range at which the number of cycles spent in developing a microcrack to the macrocrack stage becomes a significant proportion of the total life.

It has been suggested that a relationship of the form $N^{\frac{1}{2}}\varepsilon p = C$, could be obtained [104] by equating the total plastic work at fracture absorbed in a fatigue specimen to the plastic work absorbed by a tensile specimen up to the point of fracture. However, any arguments that a specimen subjected to a given plastic strain range fractures when it has absorbed some critical amount of work in invalidated at least for fatigue failure, by the fact that the life of a specimen is

increased by machining a thin layer from the surface and in these circumstances is determined only by its original size and the frequency and depth of surface machining, irrespective of the work done in deforming it plastically each cycle.

It must be borne in mind that few engineering components behave like plain polished specimens, so that data applicable only to such specimens are of limited use. In finite life design situations, cracks will be present in notched components long before complete failure occurs. For sharply notched components and constant amplitude stress levels such that the net area maximum nominal stress is less than 80 per cent of the yield stress, life should be calculated from crack growth data. At higher stress levels estimates of expected life may be made along the lines indicated at the beginning of this section. For components containing less severe stress concentrations and for variable amplitude loading conditions, the only certain way of determining the crack life is to carry out a fatigue test on the component itself, simulating service loadings as closely as possible.

2.7 Plasticity and Plastic Zone Size

2.7.1 The Mathematical Theory of Plasticity

The need to understand and consider explicitly the behaviour of structures and machines in the inelastic range is fully recognised now in both the practice and the teaching of engineering analysis and design. For quite some time, a philosophic objection was raised to plastic analysis and design on the grounds that the computed stresses and deformations of structures and machines at working loads at ordinary temperatures are essentially elastic. The permissible working load, as realized now and in the earlier days of engineering, must be chosen as a suitable fraction of the failure load. Therefore, it is the behaviour at failure which governs, not the behaviour at the working load. Excessive elastic deflection may constitute failure in some problems of design, but, in the design for strength or load carrying capacity, failure is defined as either excessive deformation in the inelastic range, or fracture. Fracture in metallic structures most often is preceded by large plastic deformation and almost always involves appreciable local plastic flow, even when the appearance of the fracture is brittle. The analysis of the response of a body to load or imposed deformation is extremely simple in principle. All equations or equilibrium or motion must be satisfied at all times. Familiar examples are the force summation equations at joints of a truss, the relation between moment and shear or moment and transverse loading in a beam, or the more elaborate forms for plates, shells, or three-dimensional continua. All conditions of geometric constraint and compatibility also must be met. Included here are the relation between the change in length

of a member of a truss and the end (panel point) displacement, the expression for curvature of a beam im terms of its lateral deflection, the relation between circumferential and radial strain in a thick-walled sphere or cylinder under interior pressure, and the general equations of compatibility in two or three dimensions. Neither Newton's Law nor geometry depend upon the material of the body. Therefore, these sets of equations hold for all bodies of all materials.

It is the stress-strain relation, or more generally the constitutive relation, which distinguishes the theory of plasticity from the theory of elasticity and from the many other specialized or idealized representations of the real world. Real materials are enormously complex in their response to stress even under isothermal conditions. No real structural metal is exactly linear elastic over any stream range and no metal is entirely free of some time dependence at ordinary rates of loading and at ordinary temperatures.

The real behaviour of actual metals appears to be infinitely complex. For this reason, models are therefore constructed which simplify or idealize the behaviour of particular materials a little or a lot. The model may be assumed to work harder, as real metals do, or to be perfectly plastic and deform indefinitely at constant stress. Work hardening may be of the isotropic stress-hardening type with a yield criterion of the Mises form, or may be more complex with a Bauschinger effect. A work-hardening assumption is much more realistic, but this realism is gained at the expense of excessive effort in the solution of problems in more than one dimension. Perfect plasticity leads to much simpler results

and to more powerful general theorems. Much of the realism which is lost by ignoring the work-hardening can be regained by selecting the level of the flow stress in accord with the level of strain to be expected. Often it is not necessary to determine this level in advance, the solution can be obtained in general form and then can be used to guide the choice of the flow stress.

Certainly, no material is perfectly plastic, but the idealization does retain the essential characteristics of plastic behaviour, time independence, a very low plastic modulus by comparison with the elastic, and relatively little if any plastic deformation upon unloading the perfect plasticity region constitutes a mode of classifying which is still quite broad. One criterion of yield may be the simple maximum shear stress criterion of Tresca, the octahedral shear stress of Maxwell, Huber, Mises and Nadai or their extensions to anisotropic material. It may, on the other hand, be a criterion as elaborate as that employed by Chen for concrete, which combines a Coulomb-Mohr hypothesis with a non-zero tension cut-off. Once again, the simplest of all idealizations should be used in order to keep the essence of the physical behaviour for the problem under control.

The limit theorems of Drucker et al.[32] hold for all consistent perfectly plastic idealizations from the simplest to the most complex. When load carrying capacity is therefore sought, it is not necessary to over-simplify the material to obtain an answer. The theorems state:

Theorem I (lower bound). If any equilibrium distribution of stress can be found which is in balance with the applied load and is everywhere below yield, the body, structure, or microstructure will not undergo large plastic deformation on a gross scale. (Collapse).

Theorem II (upper bound). The body, structure, or microstructure will collapse if there is any compatible pattern of plastic deformation for which the rate at which the external forces do work equals or exceeds the rate of internal dissipation.

The lower bound theorum T states that the body will adjust itself to carry the imposed load, if there is any way in which it may. This desirable attribute is characteristic of both a ductile structure on the macroscale and a ductile metal alloy on the microscale. Slip occurs on the microscale long before the working stress of the metal is reached, just as plastic deformation occurs in local regions of a structure far below the working load. However, until the limit (collapse) load is reached, the plastic deformation is contained, and all strains are of the order of gross elastic strains multiplied by elastic stress or strain concentration factors.

When the limit load is reached, gross plastic deformation occurs, and local strains are no longer limited by the small gross elastic strain levels and so can become extremely large. Nevertheless, the resulting displacements are not always as obvious to an observer as they are in the bending of a beam or portal frame of structural steel or even in a

simple tension specimen at yield. Sometimes the deformation is localized to the vicinity of a single cross section, as in a deeply notched circular bar under tension, a special brittle fracture specimen, or to a sharply curved knuckle region of a thin-walled pressure vessel. Under these circumstances, fracture often does occur in a real metal when the limit load is exceeded. The fracture of a metal like steel is likely to appear brittle, despite the reaching of fully plastic conditions (limit load) and the consequence reduction in stress concentration from the high elastic values associated with sharp discontinuities of shape or material.

The upper and lower bound theorems of limit analysis also provide the basis for most of the studies of extrusion and other processes of metal deformation. At first this seems rather surprising, because metals are far from time-independent at the temperatures of hot deformation processes. Their flow stresses at near zone rates of strain are extremely small when compared with the appreciable stress levels reached in commercial processes with their attendant very high strain rates.

2.7.2 Plastic Zone, Formation and size

All structural materials contain stress concentrations of some types (e.g. fillets and sharp dimensional changes). Generally these have little effect on the load at which elastic and plastic failure of the entire member takes place, although they can induce premature fracture in brittle material. It is well defined that the

maximum stress concentration factor (K_{max}) = 3 for the hole in a thin wide plate, where local yielding can occur in its vicinity of a load $P_y/3$ where P_y is the yield load for a plate having the same gross cross section but with hole absent. $P_y/3$ is called the elastic limit load and it is that load which causes initial plastic deformation of the most highly stressed volume element in the plate. When the load is increased to $P_1 > P_y/3$ the plastic zone spreads further from the hole, but the maximum tensile stress that exists in the plate is still σ, since the material is non-strain hardening and plane-stress conditions exist. A further increase in load from, say, P_1 to P_{GY} where P_{GY} is the general yield load causes the plastic zones to spread completely across the plate, which then becomes completely plastic. This is why P_{GY} is sometimes called a fully plastic load. Low values of yield stresses relative to E/10 (E = elastic modulus) imply: (1) relatively large plastic zones near the crack tip, (2) relatively large values of plastic $\gamma_p = 10^3\gamma_s$ where γ_s is the surface energy and (3) relatively large plastic strains in regions adjacent to the crack tip. In fact, it is these localized plastic strains which cause the crack to grow. Consequently, fracture is plastically induced. All types of crack propagation, with the exception of continuous cleavages, fall into this category. Normal rupture and shear rupture which occur by void formation (at small particles) and void coalescence require plastic deformation to cause the void to join together.

Localized plastic deformation occurs when the appropriate yield criterion is satisfied in the vicinity of the crack and a plastic zone is created near the crack tip. In non-strain hardening materials the

shear stresses inside the plastic zone are equal to k, the yield stress in pure shear, but outside the plastic zone the shear stresses are less than k. The size and shape of the plastic zone depend on the node of deformation that acts on the crack and on the criterion for yielding (Tresca or Von Mises) that is applicable. The simplest method of determining the plastic zone size is to treat the problem as one of plane stress and to assume that yielding occurs in those regions where the stresses at the crack tip are greater than the tensile yield stress. The material is assumed to be non-strain-hardening unless otherwise stated.

More than one model has been constructed to measure the plastic zone size; firstly, the Dugdale model, secondly the linear elastic fracture mechanics approach, and thirdly Smith's model.

The Dugdale Model

This model has a wedge shaped plastic zone ahead of the crack tip as shown in figure 5.

The plastic zone may be replaced by an internal stress distribution acting on the boundary of the plastic zone and this model is based on the following assumptions.

1. The material in the plastic zone is under a uniform stress which is equal to the yield stress of the material.

2. The material outside the extended crack 2C is elastic.

3. The plastic zone size S is such that no stress singularity appears at the end of the extended crack.

From these assumptions, Dugdale obtained the following solution for the plastic zone size:

$$s = a(\text{Sec}\ \frac{\pi\sigma}{2\sigma y} - 1) \tag{30}$$

It may be of interest to note that a mathematical method developed by Muskhelishvili was used by Goodier and Field[55] to solve the crack boundary displacements for the Dugdale model. The displacement at the tip of the actual crack (x = a) in the model is

$$v_a = \frac{4\sigma y a}{\pi E}\ \ell n\ \text{Sec}\ \frac{\pi\sigma}{2\sigma y} \tag{31}$$

In cracked plate tests on steels Dugdale[35], Rosenfield, Dai and Hahn[130] and Forman[46] have observed a zone of plastically deformed material consistant in shape and magnitude with the wedge shaped zone assumed in the Dugdale model. On the other hand, Aulf and Soretnak[4] with sharp notches in molybdenum, and Gerberich[60] with cracks in several aluminium alloys have observed a plastic zone which differs considerably from the wedge-shaped zone. However, the simplicity of the Dugdale model allows a mathematical treatment of plastic yielding at the crack tip. One of the assumptions of the Dugdale model is that the internal stress distribution in the plastic zone is constant. In actuality, this stress distribution is not constant and varies with the material properties.

Linear Fracture Mechanics Model

Analysis from the point of view of fracture mechanics centres attention upon the leading edge of a real crack. Figure 6 shows, schematically a cross-section of such a region. The leading edge extends

indefinitely to the plane of the figure and is regarded as a line disturbance zone. Striking similarities exist between fracture mechanics and crystalline dislocation mechanics which also deals with line disturbance zones.

In both cases the strains close to the disturbance line are too large to correspond to linear stress-strain behaviour and, in both cases, the concept of a force driving the process is obtained from a linear analysis in which the local non-linear strains are neglected.

From previous literature it will be recalled that crystalline dislocations were first introduced as a 'device' for explaining a mystery. Straightforward estimates of the force necessary to slip one layer of atoms rigidly across an adjacent layer suggested the yield strength should be about E/10, where E is Young's modulus, and this was too high by several orders of magnitude. In the 1930's Orowan, Taylor and Burgess[121] showed how this mystery could be explained, if we imagined that crystalline imperfection lines (termed dislocations) already existed on the slip planes. Then the large strains locked in at the dislocations locally provided the equivalent of the E/10 stress level, and easy glide of dislocations in sufficient numbers could produce macroscopic plastic yielding at low stress levels. The resulting estimates of theoretical strength then went from too high to too low. It was, in fact, necessary to introduce realistic interferences to easy glide, such as grain boundaries and interstitial atoms, before the explanation was satisfying relative to the behaviour of structural metals.

In the case of fracture, the mystery to be explained was brittle fracture failures well below the limit load for failures by yielding. Clearly, if every region of the section to be fractured is brought simultaneously to a tensile strain large enough for fracture, then that section must support an average tensile load high enough for general plastic yielding, and a below-yield separation is impossible. However, if one could imagine a prior crack is present, then a relatively small tensile load may produce strain large enough for fracture adjacent to the leading edge of the crack and progressive forward motion of such a crack can completely sever the structural component. However, if one regards the resistance of crack motion as provided by energy dissipation from yielding within the crack border zone of plastic strains, then the idea of explaining low stress fractures in terms of progressive crack extension fits the experimental facts quite well[85, 88]. The stress analysis then says there is an inverse square root dependence of stress which therefore goes to infinity at the leading edge of the crack model, and close to the crack borders, the stress terms possessing this singularity dominate. The figure shows, for example, the dominant term for the stress σ_y on the plane of expected crack extension where θ and r are zero.

The same stress intensity parameter K appears in the expression for σ_x and σ_{xy} and also in the equation for the parabolic shape of the elastic crack opening displacements. All of the effects of loads, crack size, and specimen shape are contained in the K value[89].

Since the only energy reservoir of this model is the elastic stress field, the rules of theoretical mechanics say that the 'force' conjugate to a forward speed of the crack is the same stress field energy loss rate which was employed in the Griffiths'[63] crack theory. This quantity, represented in fracture mechanics by the symbol G is the basic force concept. Because both stresses and opening displacements are proportional to K one might expect to find G is proportional to K^2, the actual relationships are shown in figure 6 for plane-stress and plane-strain. These are for the opening or tensile mode in which the crack surfaces are pulled directly apart.

There are two principal two-dimensional models for the leading edge of the crack. In one of these, the leading edge disturbance is considered small relative to length of the zone perpendicular to the figure. The disturbance zone is then held in a plane-strain elastic stress field in which there would be a stress σ_z equal to Poisson's ratio ν times the sum, $(\sigma_x + \sigma_y)$. For a plate containing a long through crack the appropriate two dimensional analysis model is the one corresponding to generalized plane-stress. In this model the stress σ_z is assumed to be zero and, since only averages through the plate thickness are significant, the leading edge of the model crack then has no significant Z direction dimension. The behaviour of material in which the plastic zone is relatively small and surrounding stress field is primarily one of the plane-strain is corresponded to brittle fracture conditions. The K values for onset and arrest of rapid fracturing would be termed K_{IC}. The Roman numeral subscript designates the first or opening mode.

In general, the tensile crack toughness depends upon the amount of elastic constraint around the elastic zone and thus upon the plate thickness. In early studies of critical values termed G_c (or K_c) for onset of rapid fracture in high strength aluminium alloys, a trend for these was found to decrease with increase of plate thickness. This was expected as an influence of elastic constraint. However, it was also found that a tendancy for the G_c values to increase when the crack and plate size were increased. Most of this was due to improper positioning of the leading edge of the analysis-model crack and the dependency upon lateral dimensions was nearly eliminated when the plasticity correction was added to the crack size. The amount added at each crack end was[90].

$$r_y = \frac{1}{2\pi} \left(\frac{K}{\sigma_y}\right)^2 \qquad (32)$$

where for plane stress σ_y was taken to be the 0.2 per cent offset tensile yield strength, σ_{ys}. This crack size adjustment can be derived from the stress equation

$$\sigma_y = \frac{K}{\sqrt{2\pi r}}$$

Simply be defining r_y as the r value where $\sigma_y = \sigma_Y$. In other words if the plastic zone is thought of as circular with the leading edge of the model crack at its centre, then $2r_y$ represents a guess at the diameter of this circle. Studies of elastic-plastic models of cracks show that the plastic zone of the crack is rarely circular and that it changes shape with materials dimensions. Nevertheless, the procedure appears to position the leading edge of the model crack about at the centre of

the area of plastic yielding and seems satisfactory for its purpose. Other than the crack size, the plastic zone size was the first new length factor introduced by fracture mechanics. Equation 3 could be simplified by substituting for the value of K which $K = \sigma\sqrt{\alpha\pi C}$ and α is a parameter depending on specimen and crack geometry the following equation results:

$$2r_y = \alpha\pi C\left(\frac{\sigma}{\sigma_y}\right)^2 \qquad (34)$$

Smith's Model

In this model Smith refers to the recent years great advances which have been made towards obtaining a clear understanding of the brittle fracture characteristics of large engineering structures. This subject was the topic for discussion at a recent Royal Society Discussion Meeting[36]. Particular attention is now being given to the determination of the safe operating stress level of a large structure when it contains known defects which may arise as a consequence of welding procedures or fracture of design. Alternatively, given the operating stresses, it is required to know the maximum defect size that can be tolerated, this critical then being related to appropriate inspection procedures. In order that these procedures can be made sufficiently accurate, and the behaviour of laboratory size test specimens related to that of large structures. It is of paramount importance to understand the manner in which plasticity spreads from a defect and how fracture propagates from such a size. From the theoretical viewpoint it has been possible to make appreciable progress by assuming that plastic deformation is confined to infinitesimally thin regions[35]. Smith originally adopted this approach for the case of an isolated defect in an infinite body.

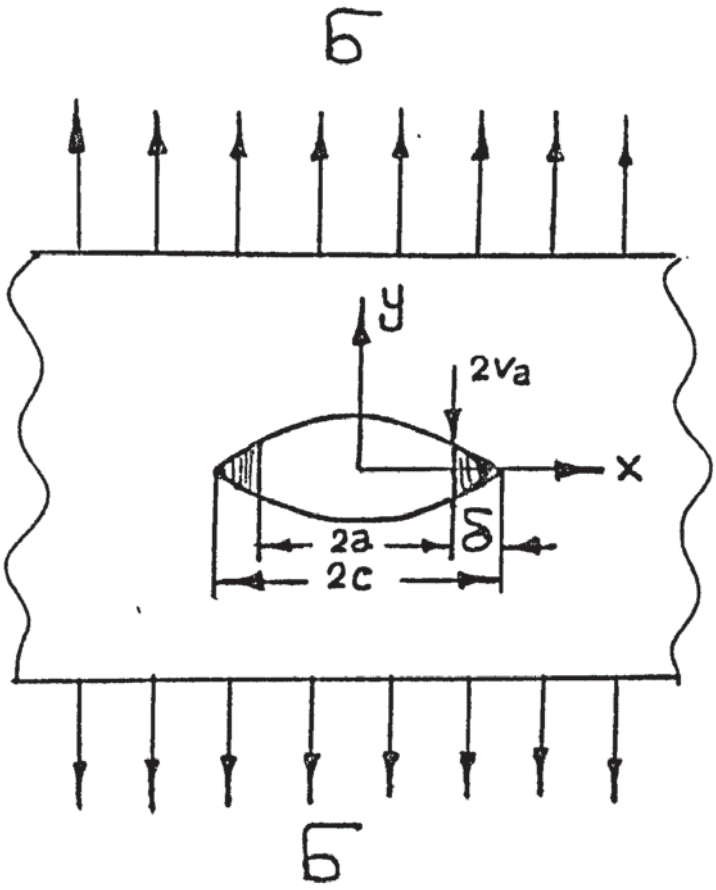

Figure 5

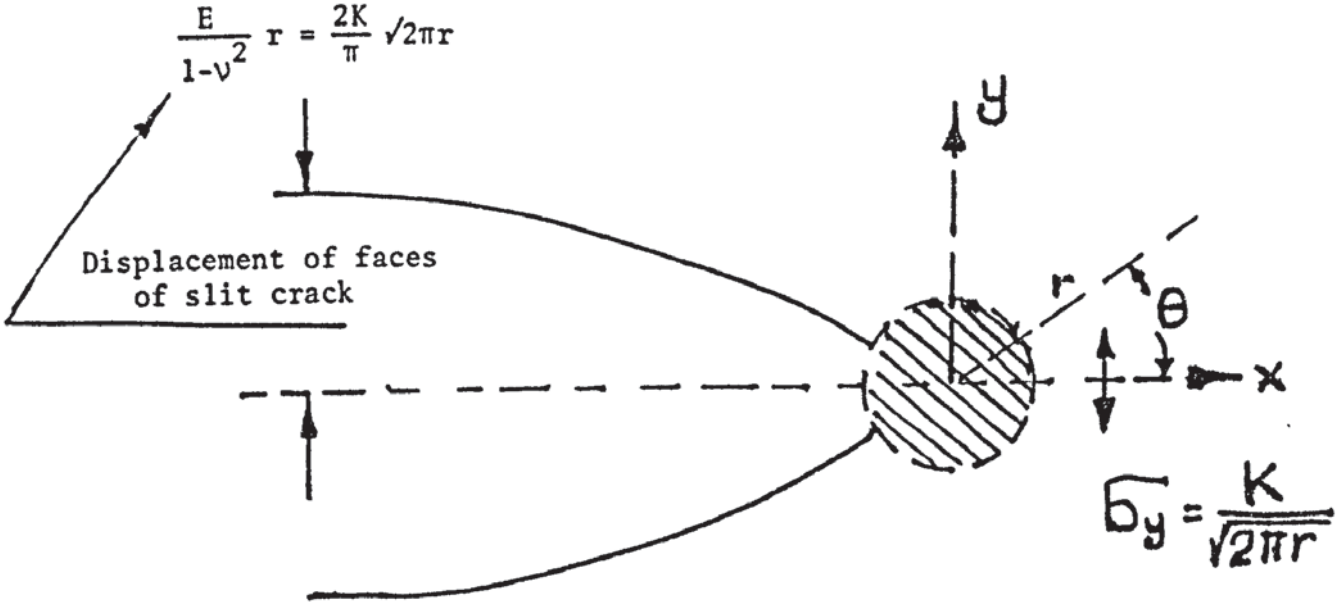

X,Y = Coordinates
σ_y - stress normal to crack plane as Y = 0
ν - Poissons Ratio

Figure 6

$G = (\frac{1}{E})K^2$ plane stress $\qquad$ $G = (\frac{1-\nu^2}{E})K^2$ plane strain

but since an anti-plane strain model of deformation was assumed here this model was used to represent the behaviour of a semi-infinite body containing a surface defect. Subsequent work[12,13] has considered the behaviour of defects in bodies of limited size and the effects of various distributions of defects in an infinite body, interaction effects between defects and free surfaces being taken into account.

One of the basic assumptions in the preceding theories is that the defects are infinitely sharp, enabling plastic deformation to proceed at infinitesimally low applied stresses. Thus anomalies clearly arise when the sharp crack theories are applied to notches where, of course, there are no plastic deformation until the locsl stress at the notch root exceeds the yield stress of the material[146]. Proceeding further and assuming that the criterion for fracture initiation is the achievement of a critical displacement at a defect tip, the predictions of the sharp crack theories applied to notches can give fracture stresses lower than that at which even local yield occurs. To remove these incompatibilities, Smith[146] considered the spread of plasticity and the initiation of fracture at an elliptical notch in the surface of a semi-infinite body deforming under anti-plane strain conditions. Smith produced the following model for anti-plane strain but one can assume that it is approximately correct for plane strain. It is worth mentioning that Smith's theory predicts that there is no yielding ahead of a blunt notch of root radius R until the stress is greater than

$$\sigma = \sigma_y \frac{(R/C)^{\frac{1}{2}}}{[1+(R/C)^{\frac{1}{2}}]} \qquad (34a)$$

for stresses greater than this the plastic zone size (S) is given as

$$\frac{\sigma}{\sigma_y} = \frac{(R/C)^{\frac{1}{2}}}{[1+(R/C)^{\frac{1}{2}}]} + \frac{2.0}{\pi[1+(R/C)^{\frac{1}{2}}]} \cos^{-1}\left\{\frac{1-(R/C)}{1+\frac{S}{C}-(\frac{R}{C})^{\frac{1}{2}}[(1+\frac{S}{C})^2-(1-\frac{R}{C})]^{\frac{1}{2}}}\right\} \quad (35)$$

where: σ applied stress, σ_y = yield stress, C = crack length

For large stresses the plastic zone sizes given in equation (35) approach those given by equation (1) discussed earlier.

The latest development of plastic zone size influenced by the stress state by Aurich[5].

$$r_y = \frac{1}{2} \frac{K_I^2}{(\sigma_y + \sigma_{zz})^2} \quad (36)$$

where σ_y is the yield point and σ_{zz} is the principal stress.

Vitek Model

This model was to study the situation of plane strain yielding from an embedded crack with finite root-radius loaded in uniform tension. Also the study of the anti-plane strain situation was carried out and the application of these results to the study of crack initiation from a blunt notch.

The Vitek model was based on the theory established earlier by Dugdale (1960) and Bilby, Cottrell and Swinden (1963) which was concerned with the spread of plastic deformation from sharp cracks. This represented the yielded region ahead of the crack by coplanar array of dislocations and their solution is valid for both the situations and anti-plane strain and of plane strain, i.e. cracks loaded in pure shear and in uniform tension respectively. In his work (Vitek), he studied

yielding from a crack of elliptical cross-section embedded in an infinite isotropic body loaded in uniform tension. He represented the plastic zone as in the model of Bilby et al. by a coplanar array of edge dislocation with the Burgess vectors parallel to the tension axis. Beside the equilibrium condition Vitek was talking about in his paper, (the condition determining the dislocation in the plastic zone at every point of the plastic zone) he made a comparison for the situation of anti-plane strain when $\rho/a = 0.5$ (derived by Smith (1967) is shown as the dotted curve. Vitek results are shown plotted in figure 6a and 6b. He showed that for a blunt crack of root radius ρ and length a, a stress $\sigma > \sigma_1(\rho/a)^{\frac{1}{2}}/[2 + (\rho/a)^{\frac{1}{2}}]$ is needed to initiate plastic deformation. Hence for small stresses, both ρ and ϕ have values smaller than those for a sharp crack. For higher stresses, the same is true for ϕ, which for a given applied stress is always the smaller, the larger is ρ (figure 6b). However the size of the plastic zone may be larger for a blunt crack than for a sharp one if a high enough stress is applied (figure 6a).

This also reflected the fact that for the situation of plane strain the stresses at a distance comparable with the crack length are higher in the case of a blunt crack than in that of a sharp one (Vitek 1975). This circumstance does not occur for the situation of anti-plane strain and consequently the size of the plastic zone is always the largest for the sharp crack. Figure 6a and 6b show a good comparison of the situations of plane strain and anti-plane strain where the plastic zone for a given applied stress is always smaller for the latter.

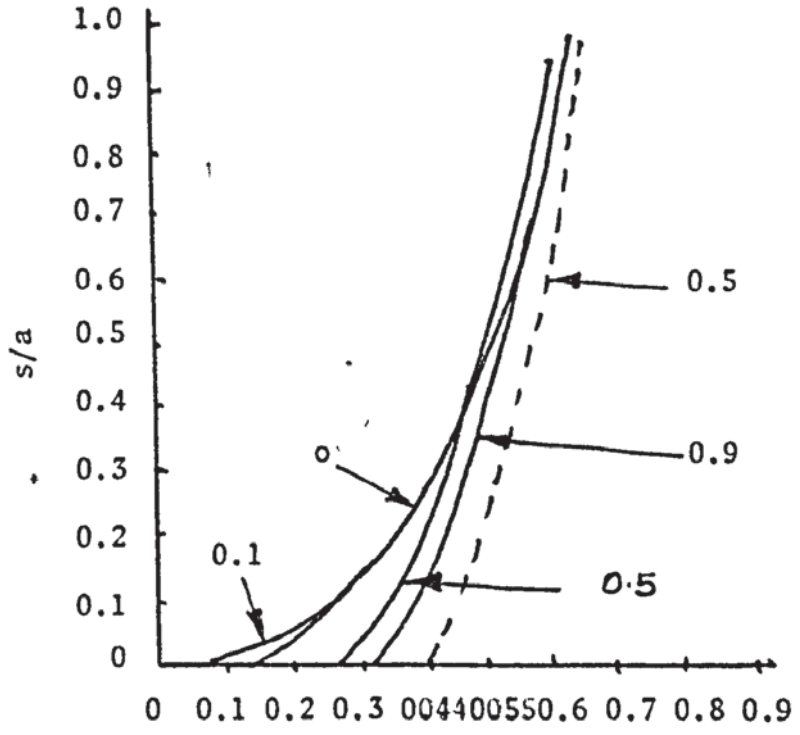

Figure 6a - (Vitek) curves show the dependence of S/a and σ/σ_1 for ρ/a = 0, 0.1, 0.5 and 0.9

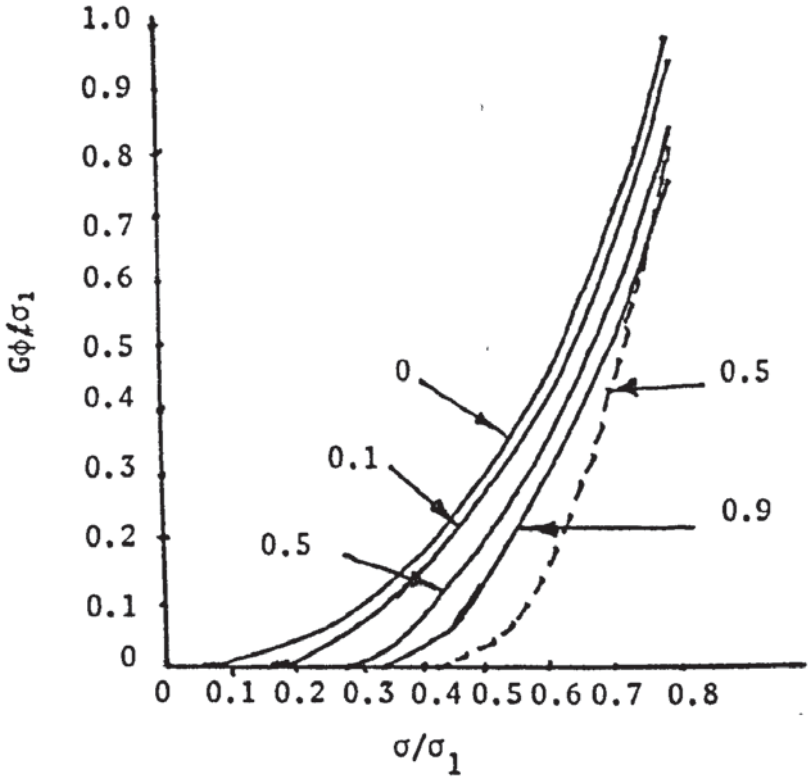

Figure 6b - (Vitek) shows the dependence of $G\phi/\sigma_1$ for the same ρ/a values.

2.8 Micro- and Macro-scopic aspects of Fatigue Crack Nucleation and Growth

2.8.1 Microscopic Aspects

Nucleation

Fatigue cracks can be initiated in a number of ways, but the important fact is that they are usually nucleated at free surfaces. Exceptions exist, as in rolling contact fatigue, in which shear stresses are greatest beneath the surface[112] but even so cracks are probably nucleated at an interface between a particle and the matrix[161]. The surface condition in fatigue is vitally important to increase fatigue life[118]. In this example a high strength structural steel alloy in the polished condition tested in pulsating tension has a fatigue strength at high cyclic life twice that of the as-received material. The stronger the material the greater the influence of surface condition, because the sensitivity to surface flaws and notches generally increase with tensile strength. The low fatigue strength of the as-received alloy is due to the presence of mill-scale which is easily cracked, thereby creating stress concentrations. Decarburisation, especially of forgings is another common cause of the reduction in fatigue strength. Although some of this loss can be avoided by machining off, the decarburised layer, even the method of machining is an important factor. Recarburising, surface rolling, and shot peening can also improve fatigue resistance, and it is significant that the benefits developed in the shot peening of notched specimens are greater than in un-notched specimens.

In addition to cracks initiated at stress-raisers in millscale coatings, cracks can appear at a variety of sites, at particles, either surface or subsurface. In some other cases a soft zone existing along a grain boundary can lead to crack initiation at a triple point. There were other cases which are fundamentally more interesting, for they represent examples of crack initiation at slip bands created during cyclic loading. Each effect can lead to the localisation of plastic strain by the creation of discontinuities on a previously featureless surface. It has been observed that regions beneath these fatigue slip bands are softer than the adjacent matrix[17]. It appears that this recovery facilitates further dislocation motion within the regions. Recent studies of the subsurface dislocation arrays have indicated a correlation with the surface disturbance[114]. The soft zones have been found to penetrate some distance beneath the surface in axially loaded copper single crystals. Substructures have been observed within such persistant slip bands, but their dimensions are an order of magnitude larger than those observed in the H region. The presence of the substructure suggests that cross slip and climb are involved in the recovery process[74].

In materials whose slip systems are such that cross slip dose not occur easily, these surface defects are not developed. Ionic crystals (e.g. LiF) which do not contain two glide planes with a common slip direction, are of this type[113]. Another example is zinc tested at low temperatures wherein slip occurs primarily on the basal plane. The resistance to cyclic stressing of materials that cannot form surface stress raisers is quite high, and in general, fatigue resistance increases with decreasing stacking fault energy.

The geometry developed if screw dislocations cross slip to cause non-recurring plastic deformation, based on Mott[117] mechanism, as indicated in his simplified model.

Growth of a crack

Stage I growth. Once a crack is initiated at a surface slip band in a single crystal it will continue to advance into the material along the primary slip planes involved in the creation of the slip band before veering onto a plane macroscopically at right angles to the principle tensile stress. Crack growth before the transition is referred to as Stage I growth, that after the transition as Stage II growth[53]. The transition is governed by the magnitude of the tensile stress, and the lower the magnitude of this stress, the larger the extent of the first stage of growth. For this reason Stage I growth is favoured in torsion testing, for the tensile component at right angles to the Stage I crack is low. If the tensile stresses are high enough, Stage I may not be observed at all, as in sharply notched specimens, and growth occurs entirely in the second mode.

In polycrystalline metals Stage I growth usually terminates when the slip band crack encounters a grain boundary. In polycrystalline brass, for example, if the stress amplitude is high enough to nucleate a Stage I crack in a large-grained specimen, that stress would also be sufficient to cause the crack to propagate through the adjacent grains. On the other hand, in fine-grained specimens cracks may be initiated at a stress that is insufficient for propagation into the adjacent gains.

In one case the event resulting in final failure is nucleation of a crack, whereas in the other propagation is the important factor [49].

Relatively little is known about the mechanism of Stage I growth largely because of the fine scale of the processes involved. It has been proposed that inclusion, a type of reverse extrusion, may develop and facilitate this mode of growth. If so, there would be no clear-cut distinction between initiation and propagation[113]. It has also been proposed that a component of tensile stress may assist in the growth of Stage I cracks, in which case the mechanism would be similar to that of Stage II growth to be discussed.

Stage III growth can be investigated under conditions of high strain amplitude. As a consequence, the plastic deformation taking place at the tip of a crack can be directly observed, a circumstance that contributes greatly to the understanding of the process. One of the most important characteristics is that the crack advances a finite increment in each loading cycle[54]. Another is that a mark, referred to as a striation, is created on the fracture surface in each load cycle and provides a record of the passage of the fatigue crack front. These two aspects are not unrelated as shown in the schematic diagram of the growth process in figure 8[100]. At the start of a loading cycle the crack tip is sharp, but during extension, as the crack advances, it simultaneously becomes much blunter, and the plastic zones at the tip expand. Both effects are involved in establishing a balance between the applied stress and the amount of plastic deformation at the crack

tip. It is during the loading stage that a new fracture surface is created by this plastic shearing process. During the unloading portion of the cycle as the sharp tip of the crack is re-established the extended material at the tip is heavily compressed and exerts a back stress which causes the deformation marking or striation on the fracture surface as the crack closes. There appears to be no correlation between the sub-surface dislocation arrangements and these striations. The resharpened crack is then ready to advance and blunted in the next cycle. The repetition of this blunting and resharpening process is the basic aspect of Stage II growth. The mechanism can be modified but not altered in principal if the crack advance along only one of the two shear zones at the crack tip, as it sometimes observed, at the surface.

Stage II growth continues until the crack becomes long enough to trigger off final instability. In brittle materials the instability criterion is simply that a critical displacement be achieved at the crack tip, at which point the crack runs unstably. This implies that the crack length reaches a critical value $2C_F$, for nominal stresses in the elastic range. In ductile materials Stage II continues until the remaining cross-sectional area can no longer support the applied load. Fracture usually occurs by shear rupture, on shear planes inclined at 45° to the tensile axis. Thus, the extent of Stage II growth is also governed by the materials toughness G_C, for this determines the critical sized crack that can exist before causing final instability at a given peak stress.

2.8.2 Macroscopic aspects

Net section stresses in the elastic range

Two factors that are important in determining the rate of crack growth are the applied stress or strain amplitude and the length of the crack itself, for they determine the stress intensity factor K. To measure the rate of growth as a function of these parameters, one can measure the spacing of adjacent striations on the fracture surface and obtain directly the rate of growth per cycle[75]. Another method is to test sheet specimens and observe the length of the crack as a function of the number of cycles applied and then determine the rate of growth by graphical analysis of a plot of crack length as a function of the number of load cycles applied. These two techniques are equivalent, but it is usually simpler to use the second. In this method cracks are started at a stress raiser in the central portion of the sheet specimen, and their growth along the surface under pulsating loading is followed with a low power microscope. Usually, the crack front beneath the surface is in advance of that at the surface, but the difference in actual length is small in sheet specimens. In notched sheet specimens crack growth occurs initially in the Stage II mode, but after some distance a gradual shift occurs to a plane containing the width direction but inclined 45° to the sheet thickness. This transition region occurs when the radius of the plastic zone at the tip of the crack equals one-half of the sheet thickness.

A large number of tests with sheet specimens indicate that the results can be correlated by means of the parameter $\sigma\sqrt{C}$, where σ is the peak gross stress and C is one-half of the tip to tip length of a crack

started at a stress raiser in the centre of the sheet. The parameter $\sigma\sqrt{C}$ is related to K, the stress intensity factor $\frac{K}{\sqrt{\pi}} = \sigma\sqrt{C}$ for a small crack in a wide sheet. With experimental scatter the rol@ of crack growth is a single values function of this parameter for net section stresses in the elastic range. The trend of fatigue crack propagation rates obtained for an aluminium alloy as a function of the parameter $\sigma\sqrt{C}$ is shown in page 300 [159]. For rates in excess of 10^{-5} - 10^{-4} in/cycle the plane stress mode of propagation is dominant in sheet specimens. For this alloy the rate of crack growth under fully reversed loading does not differ greatly compared with just pulsating tensile loading, indicating that compression stresses do little to advance the crack to an alloy of low strain hardening capability.

There is no simple relationship between the rate of crack growth and the stress intensity factor that holds precisely over the entire range, but a straight line approximation can be made. The slope of this line is such that the rate of propagation is proportional to $\sigma\sqrt{C}$ raised to the fourth power[75]. At low values of $\sigma\sqrt{C}$ the rate is much less than given by this relationship and in fact at very low stresses crack growth may not be detected over a period of observation of more than 10^8 cycles. At high values of the net section stress, approaching or exceeding the yield strength, crack growth occurs at a higher rate than predicted by the fourth power approximation. This approximation holds for other alloys as well as aluminium[112] but there is a wide variation in the resistance to fatigue crack growth from alloy to alloy. It is interesting to consider the factors that are responsible for this difference.

In contrast to the fatigue strength at 10^7 cycles for a material such as copper (which is related simply to the yield strength), crack propagation, involving as it does large strains at the crack tip in each cycle, depends more on the total plastic response of the material. The result of an analysis [165] of crack growth in an elastic plastic solid based on the continuum dislocation model of plastic yielding at a notch is useful in determining the relative importance of the parameters affecting resistance to crack propagation. The rate of growth given by this analysis [165] is

$$\frac{dc}{dN} \alpha \frac{(\sigma\sqrt{C})^4}{\gamma G \sigma_y^2} \tag{37}$$

where γ is a surface mark term, G is the shear modulus and σ_y is the yield stress. Relation [37] has been empirically modified [112] to incorporate the effects of strain-hardening by replacing γ with the area under the stress-strain curve up to the point of necking instability. This area is given approximately by $(\sigma_y + \sigma_u)/2\varepsilon_u$ where ε_u is the strain at necking. Young's modulus is used in place of G, and σ_u^2 is used instead of σ_y^2 to include more strongly the effects of strain hardening. The result is

$$\frac{dc}{dN} \alpha \frac{(\sigma\sqrt{C})^4}{[(\sigma_y + \sigma_u)/2]E\sigma_u^2\varepsilon_u} \tag{38}$$

It seems that except for the aluminium alloy 7075-T6, which may be metallurgically unstable under the test conditions, the results fall in a fairly narrow band. From [38] it appears that significant improvements in resistance to crack growth by alternation of mechanical properties are not likely.

For cracks initiated at sharp notches Stage II growth occupies most of the fatigue lifetime. Certain predictions about the dependence of the lifetime can therefore be made in terms of the fourth power relationship. For example, if

$$\frac{da}{dN} \alpha \sigma^4 C^2 \tag{39}$$

integration between the limits of C_o, the initial crack length, and C_F, the critical crack length, leads to

$$N_F \alpha \frac{1}{\sigma^4} \left(\frac{1}{C_o} - \frac{1}{C_F} \right) \tag{40}$$

If C_F is always much larger than C_o, the slope of a log σ - log N curve should be equal to 1 - ¼ in the range in which the fourth power approximation is applicable.

Net section stresses in the plastic range

In the low cycle range it has been shown that fatigue crack propagation in the Stage II mode occupies most of the lifetime[99]. The fatigue lifetime of a large number of un-notched ductile metals and alloys is remarkably similar when tested under fully reversed strain range ε_r. This correlation serves to emphasize the importance of plastic strain in the fatigue process, for its stresses rather than strains had been used this correlation would be lacking. In addition to the similarity in lifetime, it is noted that the slope is such that the following relationship due to Mansion[103] and Coffin[75] holds:

$$N^n \varepsilon_r = C \tag{41}$$

when n often has a value of ½.

It is thought that the similarity in lifetime of materials of such dissimilar mechanical properties results from the similarity in the deformation processes at the tip of the growing crack. By counting the striations on the fracture surface it is possible to account for at least 75% of the lifetime in this range. In addition, by measurement of the spacing of the striations it is possible to determine the rate of advance of the crack. This would be better seen if such results were plotted in terms of a strain intensity factor, $\varepsilon_r\sqrt{C}$ where ε_r is the total strain range. This factor is similar in concept to the $\sigma\sqrt{C}$ (stress intensity factor) parameter described earlier. The rate of crack growth can be expressed empirically as

$$\frac{dc}{dN} \alpha (\varepsilon_r\sqrt{C})^2 = \varepsilon_r{}^2 C \qquad (42)$$

Assuming that Stage II growth starts when the strain intensity factor $\varepsilon_r\sqrt{C}$ at the base of a slip-created notch reaches a critical value $(\varepsilon_r\sqrt{C})_1$ and final fracture occurs when a second critical value $(\varepsilon_r\sqrt{C})_2$ is reached, one can find the total number of cycles spent in Stage II by integrating[86] between appropriate values of ' for a constant value of ε_r.

$$\varepsilon^2 N_{11} = K \ln \frac{C_2}{C_1} = C^1 \qquad (43)$$

where N_{11} denotes the number of cycles spent in Stage II growth and K and C^1 are (approximately) constants. It is known from experimental determinations that for lines less than 10^3 cycles almost the entire lifetime N is spent in Stage II growth; therefore N can be substituted for N_{11} to obtain the result that:

$$N^{\frac{1}{2}}\varepsilon_r = C \qquad (44)$$

which is the expression experimentally found to describe the behaviour of ductile materials in the low cycle range.

At lower strain amplitudes, where the net section stresses remain in the elastic range, the characteristics of the individual materials become more important in crack propagation. As already discussed, crack growth in this range can be given in terms of $(\varepsilon_r\sqrt{C})^4$ or its equivalent $(\sigma\sqrt{C})^4$. If one computes as above the position of total lifetime spent in Stage II growth for an un-notched specimen, one could find that

$$N_{11} \propto \frac{1}{\sigma^2} \text{ or } \frac{1}{\varepsilon_r^2} \qquad (45)$$

This result indicates that the number of cycles spent in Stage II crack propagation in an un-notched specimen depends inversely only on the second process of the stress-strain amplitude. However, the total life may vary by as much as the tenth power on the stress (or strain) level. Hence the life spent in crack growth (Stage II) at low stresses is but a small portion of the total lifetime. Much of the lifetime of un-notched specimens stressed at a level corresponding to a fatigue lifetime of specimens stressed 10^5 cycles or more is spent in slip-band formation and Stage I crack growth[99].

2.9 Fracture Toughness Tests and their Physical Meanings

In Part 8 of this survey the macroscopic aspects of fracture in large structures containing sharp, deep notches as cracks were considered. It was shown that plastically induced fracture begins at the notch root (i.e. crack tip) when a critical plastic strain is produced over a critical distance ahead of the tip. At low nominal stress levels ($\sigma << \sigma_y$) the displacement of the crack faces near the tip Vcc is proportional to the strain in the volume element directly ahead of the tip so that fracture initiates when Vcc reaches a critical value $\overset{*}{V}cc$. The work done in initiating a plane-strain fracture is

$$2Y_p^* = G_{IC} \equiv 2\sigma_y V^*(c) \tag{46}$$

where σ_y is (approximately) the uniaxial tensile yield stress. The nominal fracture stress σ_F is given by the relation

$$\sigma_F = \sqrt{\frac{EG_{IC}}{\pi C(1-\nu^2)}} \quad (\sigma_F << \sigma_y) \tag{47}$$

At higher nominal stress levels ($\sigma_F \to \sigma_y$), $V^*(c)$ may itself be a function of geometry [110] and G_{IC} is no longer a simple function of $\sigma^2 C$ so that the mechanics of the fracture process becomes considerably more complicated.

The macroscopic aspects of fracture are primarily concerned with events in one or two grains of a polycrystal where microcracks or voids are formed by inhomogeneous plastic deformation. Cleavage fracture of an un-notched tensile specimen occurs when the microcracks can spread unstably, at a tensile stress σ_y that is influenced by intrinsic

variables such as microstructures and extrinsic variables such as temperature and strain rate. Tear fracture occurs when the voids coalesce by localised plastic deformation, and this process is also influenced by intrinsic and extrinsic variables. The choice between these two modes of fracture depends on many factors and is very involved.

2.10 The Mechanics of Fracture

Fracture is a non-homogeneous process of deformation that causes regions of material to separate and load carrying capacity to decrease to zero. It can be viewed on many levels, depending on the size of the fractured region that is of interest. At the atomistic level fracture occurs over regions whose dimensions are of the order of the atomic spacing (25.4×10^{-8} mm). At the microscopic level fracture occurs over regions whose dimensions are of the order of the frain size (about 12.7×10^{-3} mm); and at the macroscopic level fracture occurs over dimensions that are of the order of the size of flaws or notches. (2.54 mm or greater).

At each level there are one or more criteria that describe the conditions under which fracture occurs. For example, at the atomistic level fracture occurs when bands between atoms are broken across a fracture plane and new crack surface is created. This can occur by breaking bonds perpendicular to the fracture plane (Fig. 7a), a process called cleavage,

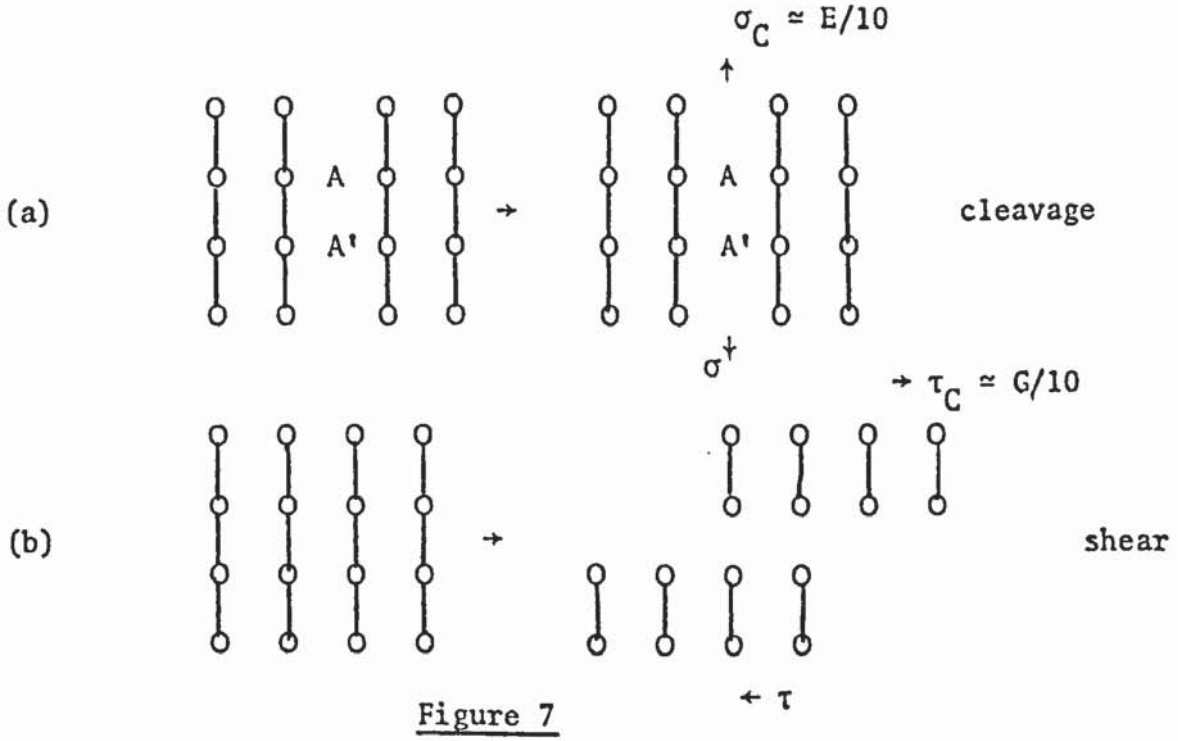

Figure 7

or by shearing bonds across the fracture plane (Fig. 7b), a process called shear. At this level the fracture criteria are simple; fracture occurs when the local stresses build up either to the theoretical cohesion strength $\sigma_C \simeq E/10$ or to the theoretical shear strength $\tau_C \simeq G/10$ where E and G are the respective elastic and shear modulii.

The high stresses required to break atomic bonds are concentrated at the edges of inhomogeneities that are called microcracks(cracks which are one or two grain diameters in length) or macrocracks (flaws, notches, cracks). At the microscopic and macroscopic levels fracture results from the passage of a crack through a region of material. The type of fracture that occurs is characterized by the type of crack responsible for the fracture. Early work[159] showed that fracture occurs when the product of the applied (nominal stress) and stress concentration factor of a flaw reaches the cohesive stress, σ_C.

Few structural materials are completely elastic; localized plastic strain usually precedes fracture, even when the gross fracture strength is less than the gross yield strength. From the principles of fracture mechanics it is possible to determine macroscopic fracture criteria in terms of the nominal fracture strength, the flaw length, and the critical amount of plastic work required to initiate unstable fracture (the fracture toughness).

Since the role of dislocation in slip and yielding is partially understood, it has been suggested by various authors that specific combinations of dislocations may initiate cracking on the atomic scale,

which, in turn, may propagate throughout a specimen. Alternative mechanisms for the initiation of cracking invoke grain boundary sliding, twin-twin interactions and twin-grain boundary interactions. From the theory by Griffith[62], the condition for crack propagation in very brittle material, such as glass, was given by:

$$\sigma > [8\gamma G/\pi(1-\nu)C]^{\frac{1}{2}} \qquad (48)$$

where G is the shear modulus, ν Poisson's ratio, γ the surface energy per unit area, C is the crack length, and σ the stress normal to the crack. Orowan [122] suggested that some plastic flow took place prior to fracture in even the most brittle metals, and, therefore, an extra term representing the energy associated with plastic flow around the crack should be introduced. The Griffith energy criterion then became

$$\sigma > [8(\gamma+P)G/\pi(1-\nu)C]^{\frac{1}{2}} \qquad (49)$$

where P is the work per unit area required for plastic deformation. In fact, $(\gamma + P)$ may be regarded as an effective surface energy in metals and is rather difficult to evaluate.

Experimental evidence of plastic flow prior to fracture below the ductile brittle transition temperature has appeared in the literature[153]. This flow, however, may be due to dislocations which can themselves co-operatively cause cracking in a number of ways. Several theories involving dislocation pile-ups have been suggested to provide an understanding of how cracks large enough to satisfy the Griffith criterion can be formed. Zener [178] suggested that edge dislocations forces together would form an incipient crack. Stroh [154] considered ways

in which dislocations piled up on a slip plane could cause cracking at a grain boundary or some obstacle to slip. Cottrell[27] discussed methods by which <111> dislocations on intersecting {110} slip planes could cause {100} cracks in the BCC lattices. The experimental evidence for all these mechanisms is somewhat scant, and an alternative but much less sophisticated explanation may evoke simply cracking around impurity inclusions in the metal matrix. From this point of view, it is noteworthy that the very pure BCC metals usually fail by ductile fracture at all temperatures.

Twins are very often observed around fracture surfaces both above and below the ductile brittle transition temperature, and, therefore it has been suggested that intersecting twins can cause cracks[84, 81]. Absolute proof that failure in tension began at the site of intersecting twins was not established and the suggestion was backed only by strong, circumstantial evidence. It is quite possible that apparently intersecting twins may be produced by shock waves around a rapidly moving crack. Reid et al.[136] investigated brittle fracture in molybdenum and found that twins were not connected with the initiation of fracture, but were present elsewhere on the fracture surface. In compression, on the other hand, cracks are so commonly observed at twin-grain boundary and twin-twin intersections that is is almost certain that accommodation stresses around the twins are responsible for them.

2.10.1 Fracture at Low-temperature (Atomistic Consideration)

Slip plane

It has been generally accepted that the principal slip

direction in BCC metals is <111> , but there is no general agreement concerning the slip plane. Various authors[102] have concluded that slip does not occur on a specific crystallographic plane in iron. Others have observed straight slip lines and a definite preference for {110}, {112}, and {123}. All investigators have found a definite tendency toward {110} slip at lower temperatures. Probably, {123} slip is a consequence of slip on {110} and {112} planes.

It has been suggested that screw dislocations are not limited to slip in specific crystallographic planes, since, theoretically, dislocations do not dissociate in BCC metals, and, hence, steps on the surface of a crystal, due to their motion, will tend to be non-crystallographic and will appear to follow the trace of the maximum shear stress planes. Edge dislocating on the other hand, cannot move out of the slip planes except by climb, and hence, these planes can be deduced, provided their motion may be observed.

The mode of slip is determined largely by the crystal structure and anisotropy of the elastic constants. Recently, it has been found that slip can take place in the <100> direction, in special circumstances. Reid et al.[137] have found that crystals of Nb tested in tension at 77°K ≃ - 200°C underwent catastrophic plastic flow; the shear plane being close to {110} and the shear direction <110> . They also concluded that the slip on the {112} planes occurs at a lower stress in the direction appropriate for twin formation than in the opposite sense. Their results can be understood in terms of dislocation theory which

takes the crystal anisotropy into account. From the work of Reid[137], it is suggested that the {110} <100> dislocation may be mobile in Nb, Cr, Mo and V. However, the phenomenon has not yet been observed in the latter three metals.

Twinning Modes

Early work in iron by Paxton[128] established that Neumann lamellae or twins in α iron have a {112} twinning plane in a <111> shearing direction. Since then, the twinning modes in all the BCC transition metals and several BCC alloys have been established. All the unalloyed and most of the alloyed transition metals have been observed to have the {112} composition plane, and so it is generally accepted that they have the same twinning elements as iron. These elements were predicted by Jaswan and Dove[94] on the principle that they should involve the smallest possible homogeneous shear capable of twinning the lattice.

In addition to the above form of twinning, others have found alternative systems in the BCC alloy Fe-5Be with {013} habit planes and also with {0, 4, 5} and {2, 3, 10} planes.

2.10.2 Fracture at low-temperature (Macroscopic viewpoint)

In this section, the influence of major macroscopic parameters such as test procedures (strain, rate and stress system), microstructure, (grain size and prior cold work), and chemistry (alloy additions and impurities) on fracture in the low temperature region will be discussed. The relative differences or similarities between these metals will be dealt with. This section will be concerned

primarily with the influence of these parameters on the ductile-to-brittle transition temperature and the stress at which fracture occurs below the transition range. Several authors have completed a comprehensive review of the influence of structural and mechanical variables on the ductile-to-brittle transition of particular alloys[155].

Characterization of a Material

Although there have been many studies of the ductile-to-brittle transition, for example, in the refractory metals, there are few, if any, well-documented studies characterizing the mechanical behaviour of a material in the transition region. Most researchers have been content merely to show the change in some ductility parameters with temperature, composition or test conditions. The results of one attempt to characterize the mechanical behaviour of molybdenum have been shown[102, p.377]. In that sample, the resistance to plastic deformation increases below 100°C. Below about -75°C, brittle fracture occurs without prior macroscopic plastic deformation, and the stress at fracture is independent of temperature. (Microscopic yield always precedes fracture and occurs at much lower stress than the macroscopic yielding.) The manner in which ductility increases through the transition region, and thus the width of the transition temperature zone, is determined by the relative rates at which the resistance to slip, and the resistance to fracture, change with strain. In the experience of one of the authors, the latter is by far the most important fracture parameter albeit the least studied in practice.

It was shown experimentally that the resistance to brittle fracture increases rapidly with strain. These results were plotted and indicated by the "isostrain fracture" curves[102]. These curves were determined by prestraining specimens in the transition range and testing in the brittle range. Since the stress for brittle fracture increases more sharply with strain than the flow stress, ductility increases rapidly with temperature and the transition zone is narrow.

Unlike strain hardening, fracture resistance does not always increase with strain. It can, in fact, decrease, in which case the ductility will increase slowly with increased temperature and the transition zone will be broadened. Not only will the transition zone be broad and brittle fracture persist to higher temperatures, but the influence of variables such as strain rate, notches and pre-existing cracks will be much greater in material whose fracture resistance decreases rather than increases with strain. At some temperatures, the fracture mode changes from bright brittle intergranular or cleavage fracture to a dull fibrous rupture.

It would be satisfying to discuss fracture as a function of composition, microstructure and test method and derive information about (a) the temperature dependence of yielding, (b) the stress at which fracture occurs without macroscopic yielding[103], (c) the change in flow stress with strain, and the change in fracture resistance with strain. Unfortunately, this is impossible, as the data does not exist.

Test Parameters (Stress System and Strain Rate)

By stress system is meant that the manner in which the specimen or part is loaded, i.e. Compression, Tortion, Uniaxial tension, Biaxial strain, etc. Brittle fracture occurs only in the presence of tensile stresses, and it will not occur under hydrostatic compression in isotropic or polycrystalline metals. It does not occur under uniaxial compression until barrelling of the specimen or other non-uniformatives result in local tensile stresses; thus, a compression specimen of, for example, a refractory metal will be ductile at a much lower temperature than a tensile specimen. Beckfold et al.[9] did some work comparing the properties of a sample of molybdenum tested in tension and uniaxial compression. Above -100°C the yield strength was about the same in tension and compression. Below -100°C, the tensile specimens fractured at very low strains and at a stress essentially independent of temperature. The compression specimen exhibited macroscopic ductility to as low as was studied and the stress at yield continued to increase on a smooth extrapolation of data from higher temperatures as long as the strain rates were slow enough to ensure isothermal conditions.

The transition temperature determined from torsion tests is below that determined from tensile tests. This is because the ratio of tensile to shear stress is 1:1 rather than the 2:1 in the tensile tests. Weinstein[168] reported that a sample of molybdenum which, in the tensile test, showed zero ductility at 25°C, still exhibited some ductility at 100°C when tested in torsion.

Weinstein (1961) stated that the most studied, least understood, and most important mechanical variables are biaxial and triaxial stresses due to notches and crack-like defects. A special area of mechanical properties behaviour, usually identified as fracture mechanics, has been developed in recent years to treat this problem in steels. Fracture mechanics approaches have not progressed far enough in all different materials. It was also shown that ductile to brittle transition temperature in molybdenum increases as the test severity increases from a single tensile to an un-notched impact, and notched impact, specimen.

The properties of notched tensile specimens of molybdenum are found to be a function of temperature, reduction in area and true stresses increase as temperature increases. The stress at which macroscopic yielding is observed is not greatly different from that of an un-notched specimen if the pulling rate is adjusted so that the strain rate at the root of the notch is the same as in the un-notched specimen. Well below the transition range, the fracture stress is much reduced - approximately by the elastic stress concentration factor. However, just below the transition range, this is not true and the temperature of zero ductility is not greatly different for notched and un-notched specimens. The ductility in the transition zone increases more slowly with increased temperature with notched specimens, and the transition zone is wider. This is due to a higher ratio of normal to shear stress due to the plastic constraint of the notch. Because of the plastic constraint at the root of the notch once yielding occurs, the ratio of normal to shear stress is greater than the 2:1 in the un-notched test, and the specimen acts essentially as if it work-hardened more rapidly than an un-notched specimen. This spreads out the transition zone.

The yield and flow strength in the transition region behaves as if governed by an activation energy. Thus, these properties are functions of time or strain rate, as well as temperature. Fracture therefore depends on strain rate and because of the dependence of yielding entering the strain rate. An increase in strain rate raises the transition temperature because of its influence on the yield and flow properties. The three decadesin change in strain rate, which, in most more common metals, would not cause a change in strength much greater than that due to normal scatter, triples the yield strength and changes the fracture from a ductile shear with 50% reduction in area to a brittle cleavage without macroscopic elongation. This is equivalent to a 100°C change in the test temperatures.

Electrical Potential Techniques

The basic idea of this technique is directly related to Ohm's law when the resistance of the tested specimen is dependent completely on the cross sectional area through which the chosen current is passing. On this basis, if a constant current is passed through a specimen containing an increasing crack in length, an increase in resistance will be expected as a result of decreasing cross sectional area, this will lead to an increase in the potential difference across the crack faces. Supplying the constant current, which certainly will generate heat in the specimen, this technique is continuous, cheap, reliable and claimed to have no disadvantage (Cooke & Robinson 1971 and Holder 1976). Although many workers (Sidey 1973, Smith R.A. 1974, Beevers & Halliday 1975) did not agree with this method, they pointed out that to get accurate and reproducible results great care must be taken to obtain voltage-crack length calibration curves and carefully designed equipment is most important. Work in this department showed that calibration curves may be obtained by various experimental techniques or by theoretical treatment.

Although several theoretical treatments were performed (Holder 1976) the more rigorous one was performed by Gilby and Pearson (1966) which was based on both centre cracked and edge cracked panels. This consists of centrally notched sheet symmetrical about the cracking plane X-Y with a crack of a certain length in this plane, the potential distribution in the specimen depends on the current application mode.

The equi potential lines will be parallel to the cracking plane in the uncracked specimen if the current is introduced at a large distance

from that cracking plane. If the current is introduced close to the cracking plane, it will give a non-uniform current distribution and equi potential lines may not be parallel to that plane in the uncracked specimen. The solution for Gilbey and Pearson model is given by (Cooke and Robinson 1971):

$$V = \text{Imaginary part of} \quad K \cos^{-1} \frac{\text{Cos}(\pi t/2W)}{\text{Cos}(\pi a/2W)}$$

where V is the potential between the potential probe and cracking plane.

t is x + i(y)

W is the specimen width.

a is the crack length.

K is proportionally constant, the magnitude of which depends on the material, specimen geometry and electrical condition. Other attempts to obtain a calibration curve were made by Smith (1974) and Clark & Knott who used a resistive paper electrical analogue and conformal mapping techniques respectively. All these techniques were different in detail only from a simple analysis of the voltage change across a conductor of steadily decreasing cross sectional area. Using the electrical potential method the following changes could result changes in potential across a crack:

a) Crack growth reducing the cross sectional area of the specimen.

b) Increase in the resistivity of the material due to cold work or plastic zone formation.

c) An apparent increase in the separation of the potential probes due to specimen bending.

The sensitivity of this technique will depend on the material, specimen geometry, the position of the potential probes, the potential measurement equipment and the electrical current magnitude and mode of application. All these factors are well described by Holder (1976) in his thesis. To use this technique one should obtain an accurate experimental calibration before attempting any study of crack growth or initiation.

2.12 The J-Integral Technique

Recently the J-Integral has been adopted as a failure criterion (Rice et al. 1968) and analytical estimation procedures have been developed for its use. It was shown that the J-Integral can be evaluated from a single load-displacement record (Broberg 1971) and (Bucci 1972).

In review, with the framework of a total strain formulation of elastic-plastic deformation, a path independent integral was defined for two dimensional problems:

$$J = \int_r (Wdy - T. \frac{\partial u}{\partial x} ds)$$

where: K & Y are rectangular co-ordinates normal to the work point, Y being perpendicular to the work surface.

ds is an increment of arc length along any contour, r, beginning along the bottom surface of the crack and ending along the top surface.

T is the stress vector entered on the material within the contour.

U is the displacement

W is the integral of stress working density (or strain energy density)

Other alternate and equivalent of J was also given by

$$J = \int_0^{\delta} (-\frac{\partial p}{\partial a})_{\delta} d\delta, \text{ or } J = \int_0^{P} (\frac{\partial \delta}{\partial a})_p dp$$

these relate J to the rate of change with respect to crack size, a, of the area under the load versus load-point-displacement, p versus δ, curves. Here p is the force per unit length of crack front and the curves are considered to be generated for different crack sizes, a, in virgin specimens subject to monotonic loading. It is interesting also to note that for bodies loaded in the linear-elastic range

$$J_{elastic} \equiv G \equiv \frac{K^2}{E}$$

where $J_{elastic}$ is the well known Griffith energy release rate, but only for this special case.

Rice considered the case where:

$$\delta_{Total} = \delta_{no\ crack} + \delta_{crack}$$

or alternatively as the elastic displacement, $\delta_{elastic}$, plus the displacement due to plasticity, $\delta_{plastic}$. Estimates of J from single points on load displacement records were made (Bucci & Pavis 1972) and in order to discuss elastic displacement they had to use the method developed by Paris 1957 relating energy principles to usual methods of linear-elastic fracture mechanics analysis.

Start by considering the strain-energy, U, of a cracked configuration as that with no crack present, $U_{no\text{-}crack}$, plus that due to introducing the crack, U_{crack}, then:

$$U_{total} = U_{no\text{-}crack} + U_{crack}$$

without going through the complete derivation the final equation used by

Rice 1968 and Barnby & Al Daimalaini 1976 could be written as:

$$J = \frac{2}{B(W-a)} \int_{o}^{\delta_{crack}} p \, d \, (\delta_{crack})$$

where δ_{crack} is the load-point-displacement arising from the presence of the crack. B is the specimen thickness, W is the specimen width and, a is the crack length.

The critical plane strain stress intensity factor could be concluded then using the following equation:

$$K_{IC} = \sqrt{\frac{J_{IC} E}{(1-\nu^2)}}$$

where E - elastic modulus

and ν - Poisson's ratio.

CHAPTER 3

THE EXPERIMENTAL PROCEDURE

3.1 The Materials

The experimental programme was designed to provide design information which led to the requirement that the number of specimens tested should be at least two for each condition. The two Cast Steel materials to be compared were produced to the specifications listed in Table 4.

Detailed chemical composition in weight percentage and mechanical properties are listed in Tables 5 and 6. Heat treatment listed in Table 7 produced the mechanical properties listed in Table 6. Several pieces 0.25 inches thick each were cut from various parts of each material. A repeated polish and etch technique was used prior to final etching in 2% nital. The structure of both materials was found to be pearlitic as shown in Figure 8.

Material 'A' was received in the form of blocks with dimensions 153 mm x 178 mm x 305 mm. These blocks were flame cut from an anchor and given the heat treatment shown in Table 7. Material B was casted in smaller size blocks at Steel Castings Research and Trade Association (SCRATA), and received as cast without any heat treatment. It was initially thought that material B was heat treated and based on that

assumption fatigue test was carried out on material B at three different temperatures namely, room temperature, +50°C and +100°C. During the polishing, technique processes material A was found to be a cleaner steel than B. Material A was produced using an arc-furnace, while Material B was produced using an induction furnace. The mechanical properties of both materials examined are shown in Table 6. The uniaxial tensile properties were obtained using No.11 Hounsfield tensile test pieces tested in Hounsfield tensile test machine.

Steel Code	General specification	
A	B.S. 1458A	1.4% - Ni - Cr - Mo
B	B.S. 1456A	0.1% Cr - 1.6% Mn - 0.09%Ni-0.07% Mo

TABLE 4 - Materials General Specification

Material	C	Si	S	Mn	P	Ni	Cr	Mo	V	Cu
A	0.24	0.41	0.023	1.4	0.035	0.11	0.1	0.28	0.01	0.12
B	0.25	0.37	0.029	1.6	0.022	0.09	0.1	0.07	0.00	0.13

TABLE 5 - Materials Chemical Composition

* Average hardness(10.0 kilos)

Material	Ultimate tensile strength (MNm^{-2})	Yield stress 0.2% proof stress (MNm^{-2})	VPN*	% Elongation	Reduction of area %
A	680	545.0	208		40.0
B	641	425.0	198		50.0

TABLE 6 - Materials Mechanical properties

Material	Heat treatment		
A	3 hours	935°C	Furnace Cool
	3 hours	900+C	Air Cool
B	2 hours	885°C	Air Cool
	2 hours	650°C	Water Quinch

TABLE 7 - Materials heat-treatment

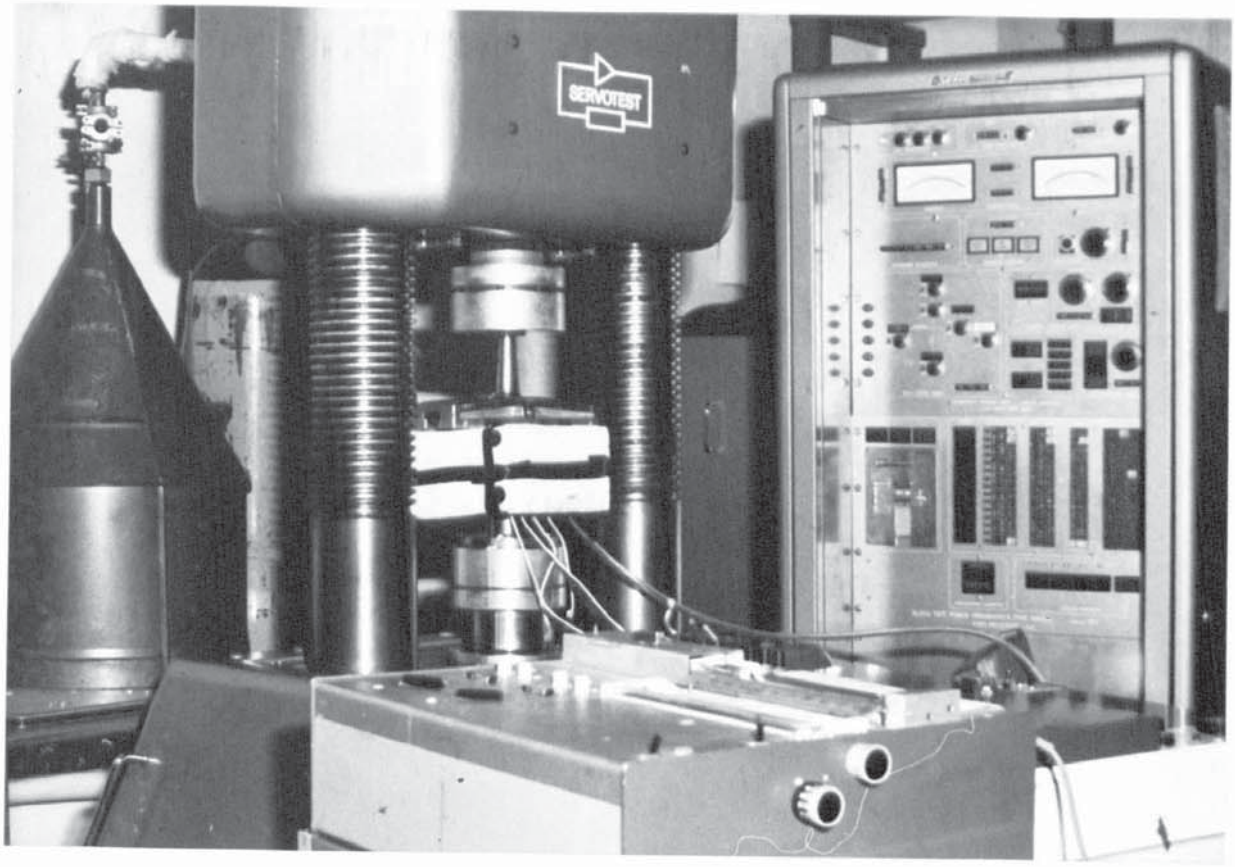

(a) Specimen mounted in the machine before the sub-zero tests provided

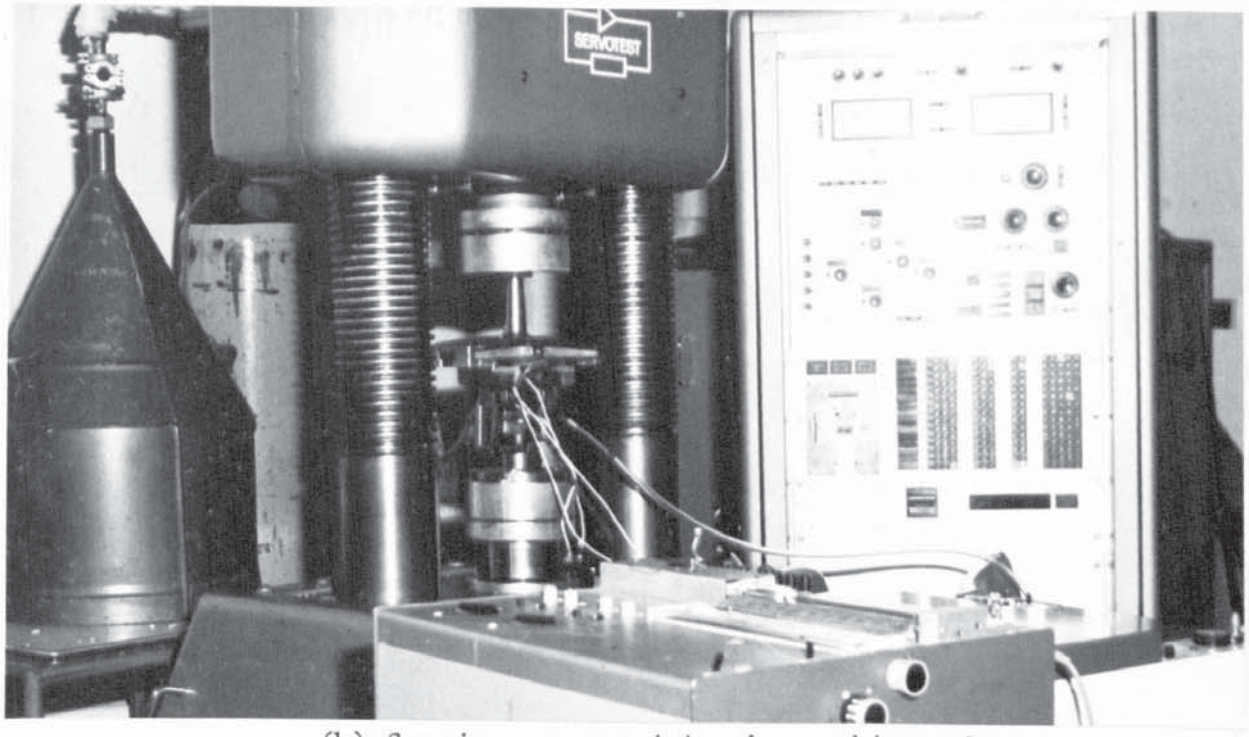

(b) Specimen mounted in the machine after the sub-zero tests provided

Figure 7S

$d = 38.67 \times 10^{-2}$ mm

Material B as cast x 75

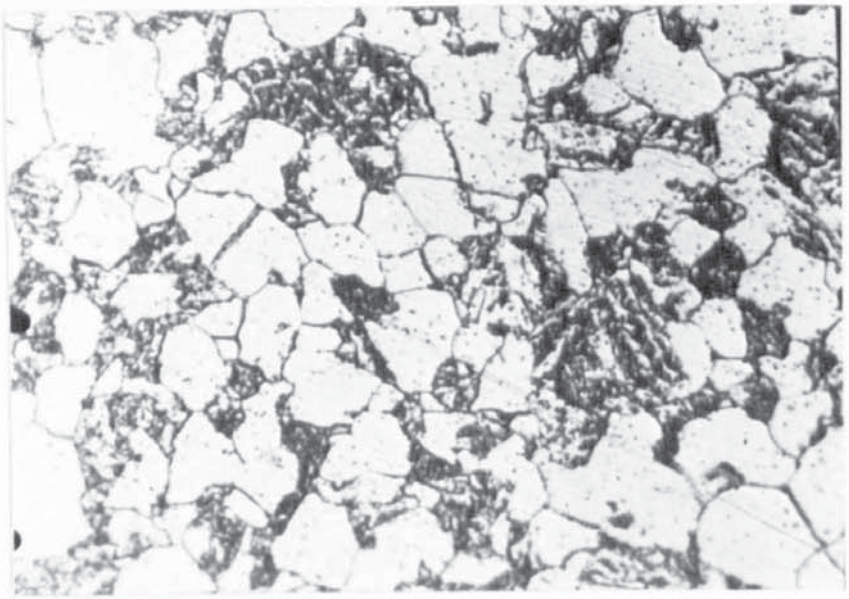

Material A x 600

$d = 1.368 \times 10^{-2}$ mm

Figure 8.

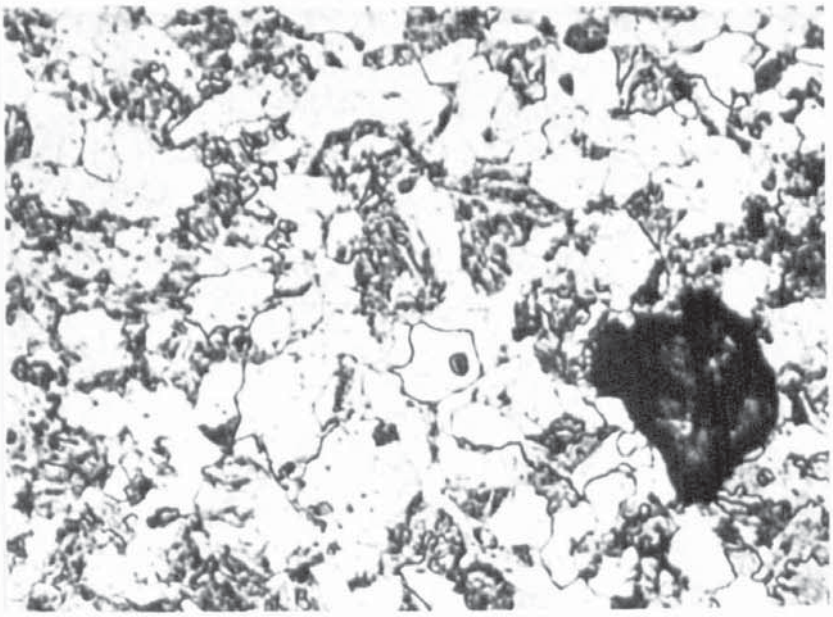

Material A x 300

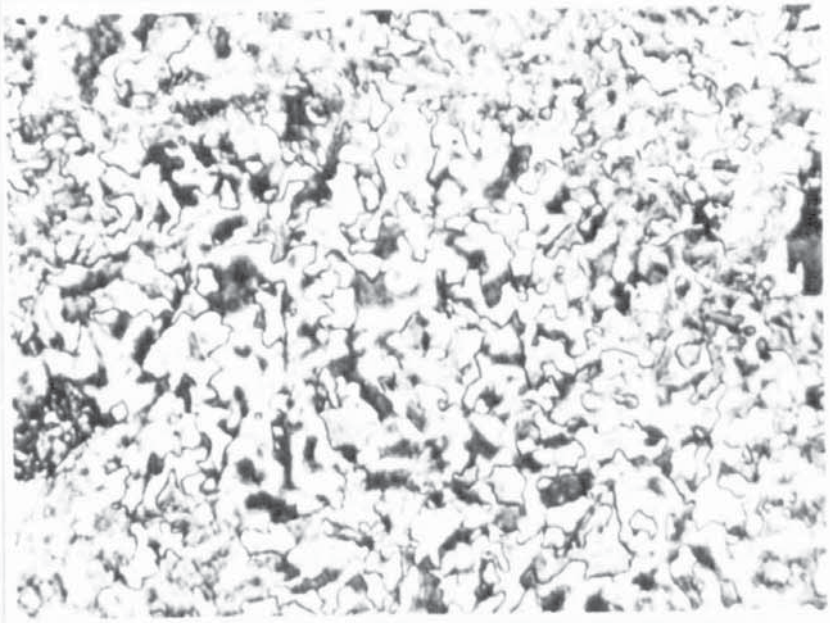

Material B x 300

as after heat treatment provided

Figure 8 cont.

3.2 Specimens preparation

Specimens of both materials were of single edge-notched type for use in three point bending and were machined to the design shown in Figure 9 with the following dimensions:

A = 5.0 mm B = 20.0 mm W = 25.0 mm L > 120 mm

and b - depends on the notch root radius.

From material A blocksnumber 1, 2, 5 and 6 were cut, which can be seen in Appendix 1 (directions and positions were shown with respect to the original casting) to small and large specimens, roughly finished as can be seen in detail in Appendix 1. The location of any specimen in the original cast block can be identified through the diagrams and code number of Table 1 Appendix 1, fatigue test specimens designed to the dimensions and specification mentioned to satisfy two criteria. Firstly, the specimen should be tested under plain strain conditions. This sets a lower limit on the specimen thickness such that the plastic zone size at the crack tip should be less than 1% of the thickness. The plastic zone size (which will be discussed later) in fatigue is approximately on sixth of the monotomic plastic zone size and for most of the materials the plastic zone size calculated from the equation

$$r_p = \frac{1}{2\pi} \left(\frac{K}{\sigma_y}\right)^2$$

produced a minimum thickness of 10 mm.

The second criteria was that to avoid the possibility of single crystal tests, the specimen thickness should be no less than six times the cast grain size of the material.

The minimum thickness for all specimens tested was therefore 20.0 mm. The specimen overhang requirements suggested in ASTME-79 for three point bend specimens dictated that the maximum specimen span should be 100 mm.

The K-calibration curves available (Walker & May) are calculated for a span/width ratio of 4 or 2. The former value gives a width of 25.0 mm and was selected for all test spieces except the large fracture toughness test piece.

The final dimensions were attained by wet grinding and were within a tolerance of ± 0.01 mm. All the faces except the ends were parallel and perpendicular to within 0.02 mm per 10 mm. The side faces were ground in the length direction to facilitate the observation of growing fatigue cracks.

Few specimens were stress relieved at 400°C for eight hours before being prepared to establish the effects of the residual stresses. All notches of all specimens were highly polished with silicon carbide paper down to grade finish. The small amount of 'flash' was also removed. The machined notches with 0.127 mm root radius were then scribed with three lines on opposing sides of the notch. The positions of these lines is shown in figure 9. The first of these was positioned at the specimen mid-point and was used to accurately position the specimen on the loading points of the fatigue machine, the other two were used for the accurate location of the electrical potential probes. The

first was 1 mm from the notch edge, and the other was 1 mm above the notch root. An automatic centre punch fitted with a fine tip was positioned at the intersection of these lines and a "dimple" produced in the metal surface. For specimens with 12.7 mm and 25.4 mm notch root radii the location lines for the electrical potential probes were, however, positioned 1 mm above the notch root and 1 mm from the notch surface.

The potential probes shaped from 0.15 mm michrome wire were spot welded into the dimples immediately before testing. The welding was carried out using a converted battery charger.

3.3 Planning the work

3.3.1 The Equipment

A ±50KN capacity electro-hydraulic test machine (Servotest 177-F8) was used to carry out all fatigue tests in three point bending. A sinusoidal wave form at a frequency of 20 Hz was used. All thermal and electrical stabilization was expected to be taken place, since the machine was switched on at least forty minutes before the start of any experimental work.

To follow the initiation and growth of fatigue cracks the potential drop method was used. The constant source (Farnell F2111M 7/50 ST) was the only current supply for this technique. A woven heavy current cable was used to introduce the current through to the specimen. This type of input lead was flexible and had sufficient cross-sectional area to reduce resistive heating to a negligible degree. These loads were connected to the power supply output of the power supply from one, end and the other end grilled with a 6 mm hole to fit the input clamps. The clamps were toolmakers clamps with strips of electrical purity copper braced to the surfaces which are in direct contact with the specimen side. The clamps were positioned at either end of the specimen and the adjusting screws tightened. The current supply was then switched on and the output adjusted to twenty amperes. The voltage between the potential probes was then measured using a D.C. chart recorder (Tekman TE 200). The voltage across the sharp notch was about 0.085 mv and about 0.15 mv across the blunt notch. This large potential was opposed by a variable millivolt source (Time Electronics Type 2003 0.006%) enabling a 50 μv full scale deflection to be used on the chart recorder.

3.3.2 Fatigue tests at five different temperatures

Five different temperatures were chosen to carry out fatigue tests at a frequency of 20 Hz for each material. A three point bending was used on an electro-hydraulic machine. Test variables were five temperatures, three different load amplitudes in fatigue, and three different notch root radii. Each test was duplicated and further tests were devised for each condition if the first two tests revealed significant scatter of material properties. The minimum number of specimens required for these tests was 180 pieces from both materials, that is each batch of 60 specimens contained a notch root radii of 0.127 mm, 12.70 mm and 25.4 mm respectively.

Temperatures selected were (-100°C), (-50°C), room temperature, (+50°C) and (+100°C). The three values of the load amplitude assumed were as follows for each notch root radius.

Notch root radius (mm)	$\Delta K/\rho^{\frac{1}{2}}$ (MNm^{-2}) Range		
	minimum	average	max.
0.127 (0.005")	1000	1800	3000
12.70 (0.500")	300	470	550
20.40 (1.000")	130	300	400

Some of the fatigue tested specimens were planned to proceed up to fracture, which gives the opportunity to cut a thin piece off the fractured surface and using the scanning electron microscope to study these surfaces. The fatigue crack, initiation propagation and direction was detected by the electrical potential method. Part of this programme on fatigue crack initiation was planned to carry on using the acoustic emission techniques as well as the potential drop technique which is discussed in the next section

3.3.3 Fatigue tests using acoustic emission application

Steel 'B used in the form of blanks 20 mm x 25 mm x 140 mm for a fatigue test purpose. Total number of specimens used was 27, these specimens were heat treated (Table 7). For a fatigue test purpose three shapes of notches were used all 8.0 mm deep from the surface of a three point bend bar these notches are:

a) Zero flank angle 1.5 mm wide ending in nominal 60° included angle with a 0.127 mm root radius.

b) Circular profile with a 12.70 mm root radius.

c) Circular profile with a 25.40 mm root radius.

A fatigue test was planned to be provided in each case at a fixed range of stress intensity factor. During fatigue tests two transducers were coupled to the specimen with a thin layer (film) of high-vacuum grease and held in place with the help of an insulated tape. One transducer was enabling to record the summed number of acoustic emission counts, the other was to sample the form of signals by taking spot to second recordings with a high speed tape recorder. These played back on to an oscilloscope and the form of the acoustic emission was seen at various stages of test.

In fatigue testing the summed number of acoustic counts was measured against the number of fatigue cycles, N as well as against time. The acoustic count rate was determined and a plot of count rate (counts/minute) against time (minutes) was concluded. The total number of cycles to fatigue crack initiation Ni was identified by the potential

drop technique. The potential drop trace and fatiguing was continued until the fatigue crack is no less than 2.0 mm long. This would allow recording of the summed emission counts during fatigue crack propagation as well as initiation. A constant current of 20.0 amperes through the specimen was used providing the specimen electrically insulated from the rig. Figure 10 indicates how the equipment was connected during fatigue testing of specimen. All experimental fatigue results were carefully collected, cross referenced and catalogued with specimen reference number. All tests carried out at room temperature, frequency used was 20 Hz and the $\Delta K/\rho^{\frac{1}{2}}$ levels were based on established values of the report written to SCRATA by Professor J.T.Barnby and R.Holder, these values are identical to the values given in the previous section.

The circuits used for detecting the emission is shown in figure (10), the amplifier gain was 1000 and the frequency band was between 150-250 k Hz. The tape-recorder speed was 60 inches/sec. Each transducer was coupled to the width face of the specimen placed about one inch from the edge. The play back speed of the tape recorder was slowed down to 1⅞ inches/second a frequency reduction of 32 could be obtained. Due to a spurious low frequency signal superimposed on the output signals from a fault in the tape recorder the output signals had to be filtered from the tape recorder. The filtering was done between 4500 and 7800 Hz which is a reduction by a factor of 32 of the input filtering frequency. Table 4 shows the details of specimens tested as well as the type of test provided.

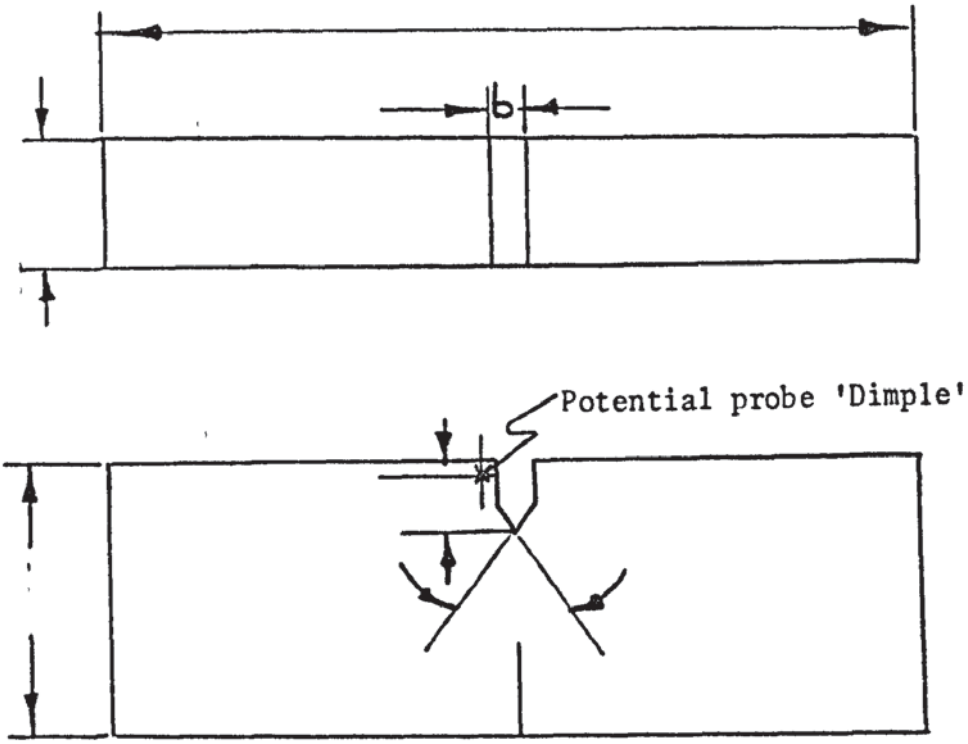

Figure 9.

Notched 3-point bend specimen specification and potential probe position

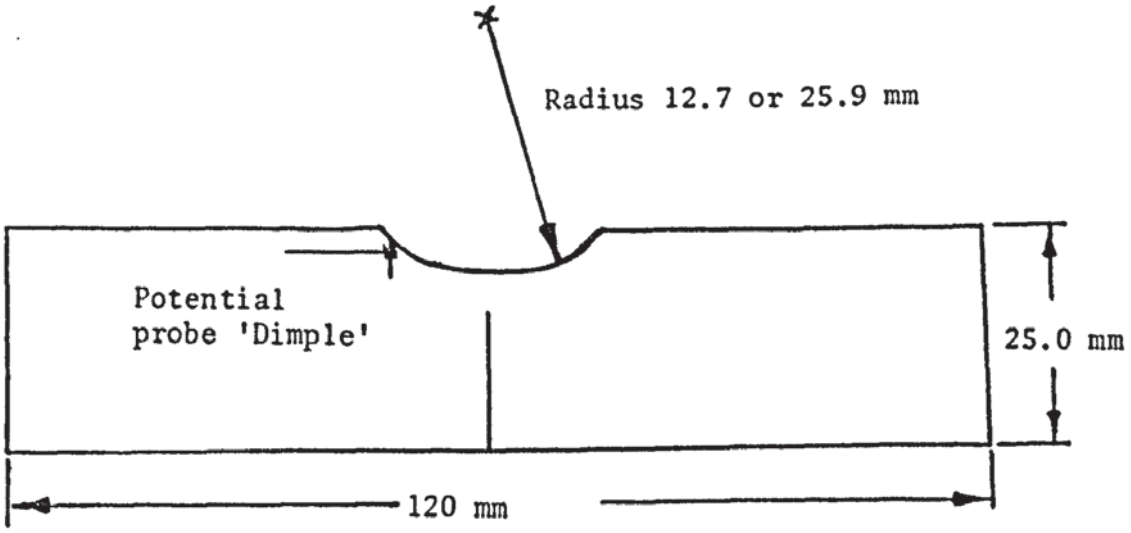

20 mm thick

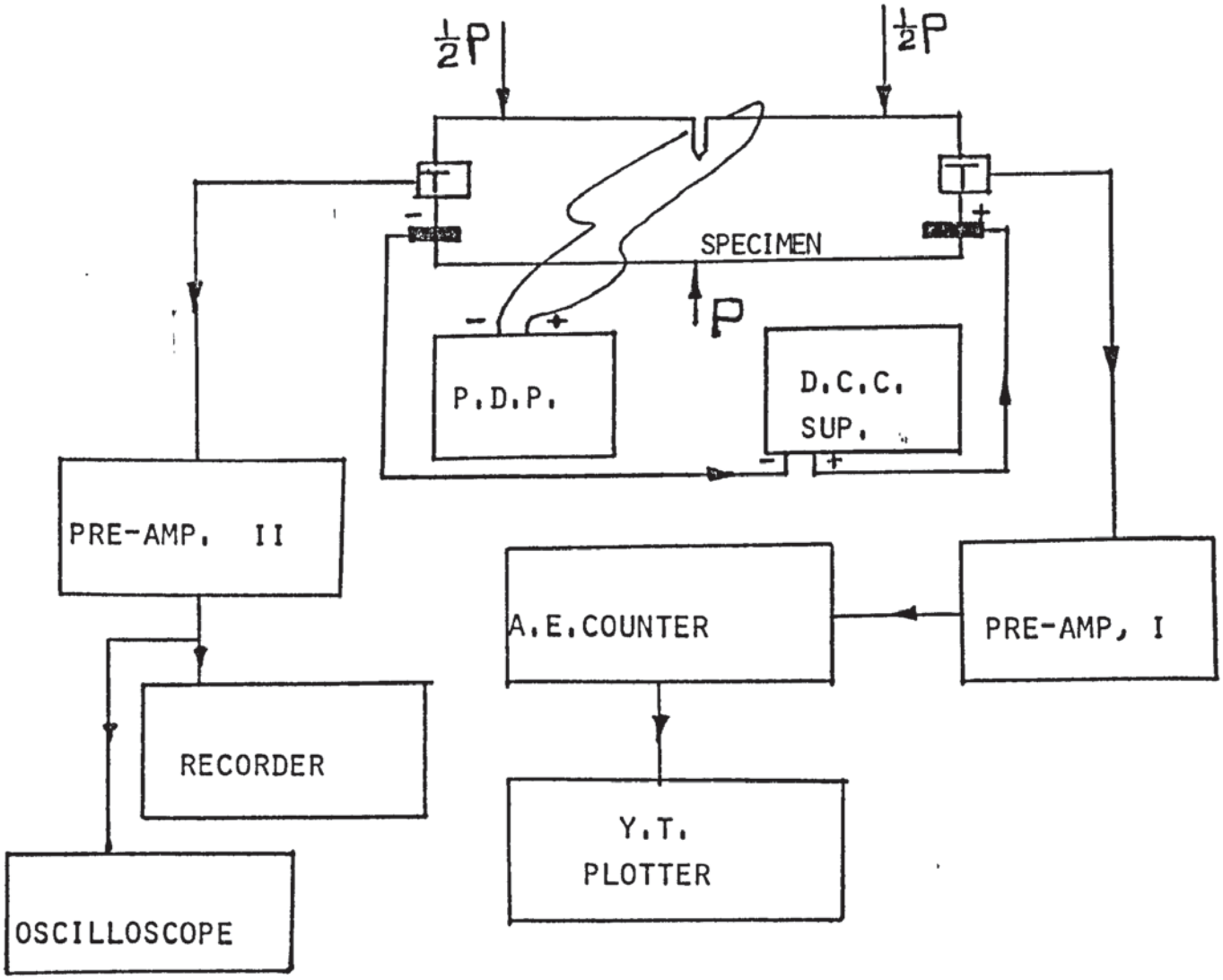

1. Pre-amplifier (pre-amp.)
2. Direct Current Supply (D.C. Sup.)
3. Potential Drop Plotter (P.O.P.)
4. Transducer (T.)

Figure 10

In all fatigue crack initiation tests provided the initiation criterion selected for all these tests was defined as the first deviation from the study value of the potential across the notch. The initiation criterion for all specimens tested using the acoustic emission application was carefully defined as acoustic emission first starts to deviate from the steady state recording and as the count rate (counts/total time) starts to decrease in value.

3.3.4 Microstructure and mechanical properties

The microstructure, yield strength (0.2% proof stress), ultimate tensile strength, hardness and the chemical composition of each cast was checked to make sure of the values given in the sheet received from SCRATA. For material B, part of which tested at sub-zero temperature in both fatigue and fracture toughness test, the same procedure was followed to detect any changes in microstructure and mechanical properties. In both cases the results produced as shown in Tables 5 and 6 as well as figure 8. The test showed that residual stresses after machining have no significant effect on fatigue and fracture toughness properties. Before going into details of how the load was approximated the author would like to explain how the fracture toughness test was provided through the next section.

Types of test	Total number of specimens used	Frequency	Specimen size(BxW) mm x mm	Material	Remarks
Fatigue test at five different temperatures.	90	20 Hz	20 x 25	A	Three different notch root radii with a notch depth of 5.0 mm
	90	20 Hz	20 x 25	B	
Fatigue test with acoustic emission at room temperature only.	27	20 Hz	20 x 25	B	- ditto -
Fatigue test at room temperature	3	20 Hz	20 x 25	B	Done after heat treating material B. Two spark cut the others are not.
	4	20 Hz	20 x 90	A	
Fatigue testing a specimen mechanically polished	1		20 x 25	B	Replicas were taken at fourteen different stages.
K-calibration tested specimens	30		20 x 25	A	10 at -50°C and 10 at room temperature, last 10 test provided at R.T.
				B	
Fracture toughness test at five different temperatures	15		20 x 25	A	Crack prefatigued before the test.
	15		20 x 25	B	
	15		40 x 50	A	
	15		40 x 50	B	
Fracture toughness tests at room temperature using the acoustic emission	8		20 x 25	B	Prefatigued no stress coat without prefatiguing but stress coated
	8		20 x 25	B	
Three point bend compression loading of electrically polished specimens of five different temperatures.	5		20 x 25	A	Notch root radius for all was 0.127 mm

341 Total Specimens used in this programme

Table 8

3.3.5 Fracture toughness tests at five different temperatures

a) Room Temperature Tests

Thirty specimens were required for the fracture toughness testing of each material A and B. Half of the thirty specimens were the same size as the fatigue test specimens. Material A was received, heat treated while material B received as cast. Even though the information at early stages was not clear about material B (Heat treatment information), fracture toughness test was not provided specially for material B until heat treatment was provided by the author. Each batch of 30 specimens was divided into five groups, each group containing three large specimens with a notch root radii of [0.127 mm (0.005"), 12.70 mm (0.500"), and 25.40 mm (1.00")], plus three small size specimens with identical root radii as in the large size specimens. Specimens quantity, size and condition of the test could be seen in Table 8. For all these 60 specimens of both materials a crack was prefatigued at certain loads to about half the width of each specimen. The load then dropped to propagate the crack for the last 1.25 mm to half the width. During monotonic loading the onset of cracking was independently detected using the potential pick-up across the notch passing a constant current of 20.0 amperes through the small size specimens and 40.0 amperes through the large size ones. A transducer was used to get a permanent record of the load/load point deflection traces on the X-Y plotter, load/crack opening displacement trace was also recorded using a clip gauge. Together with a load/load point deflection characteristic curve for single unnotched specimen the later information provided toughness estimates so long as the fracture initiation point is clearly identified.

Figure 11

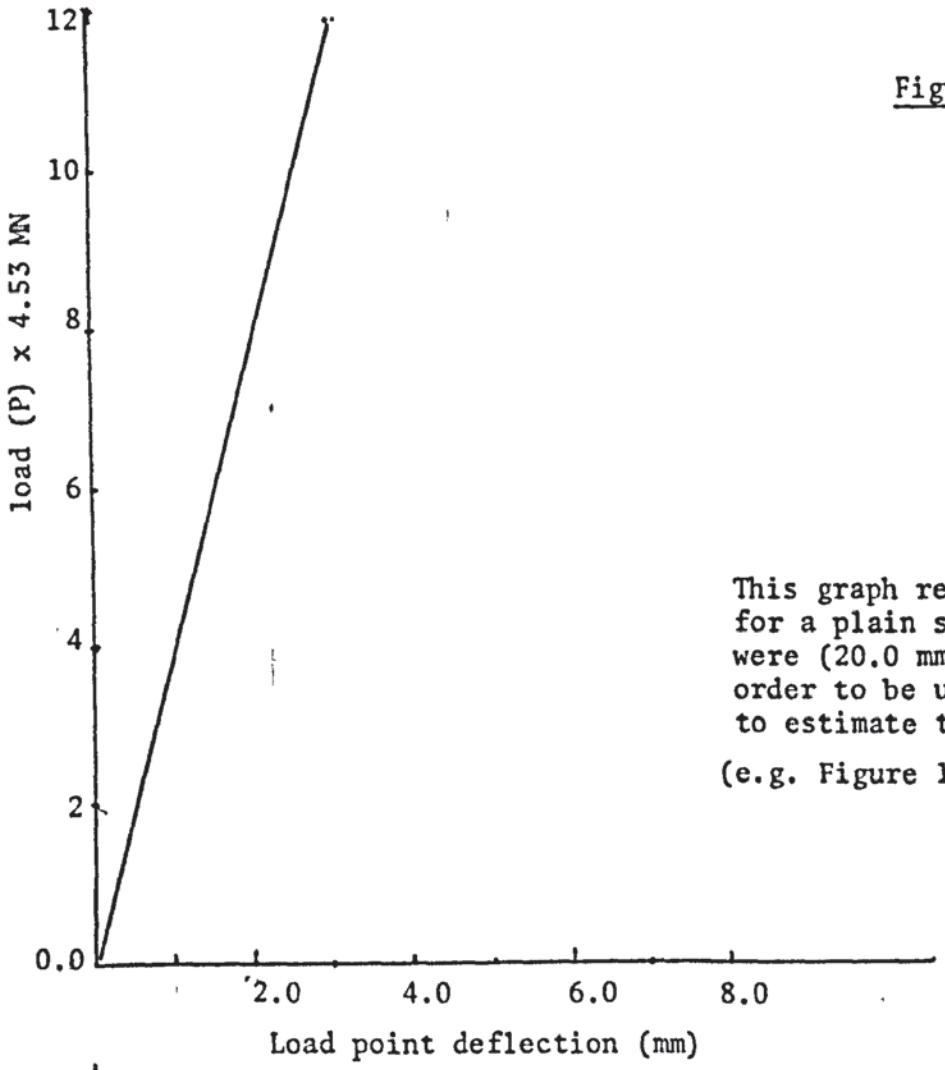

This graph represents a monitoring test for a plain specimen dimensions of which were (20.0 mm x 25.0 mm x 120 mm) in order to be used in the J-integral method to estimate the area

(e.g. Figure 11a below)

Figure 11a

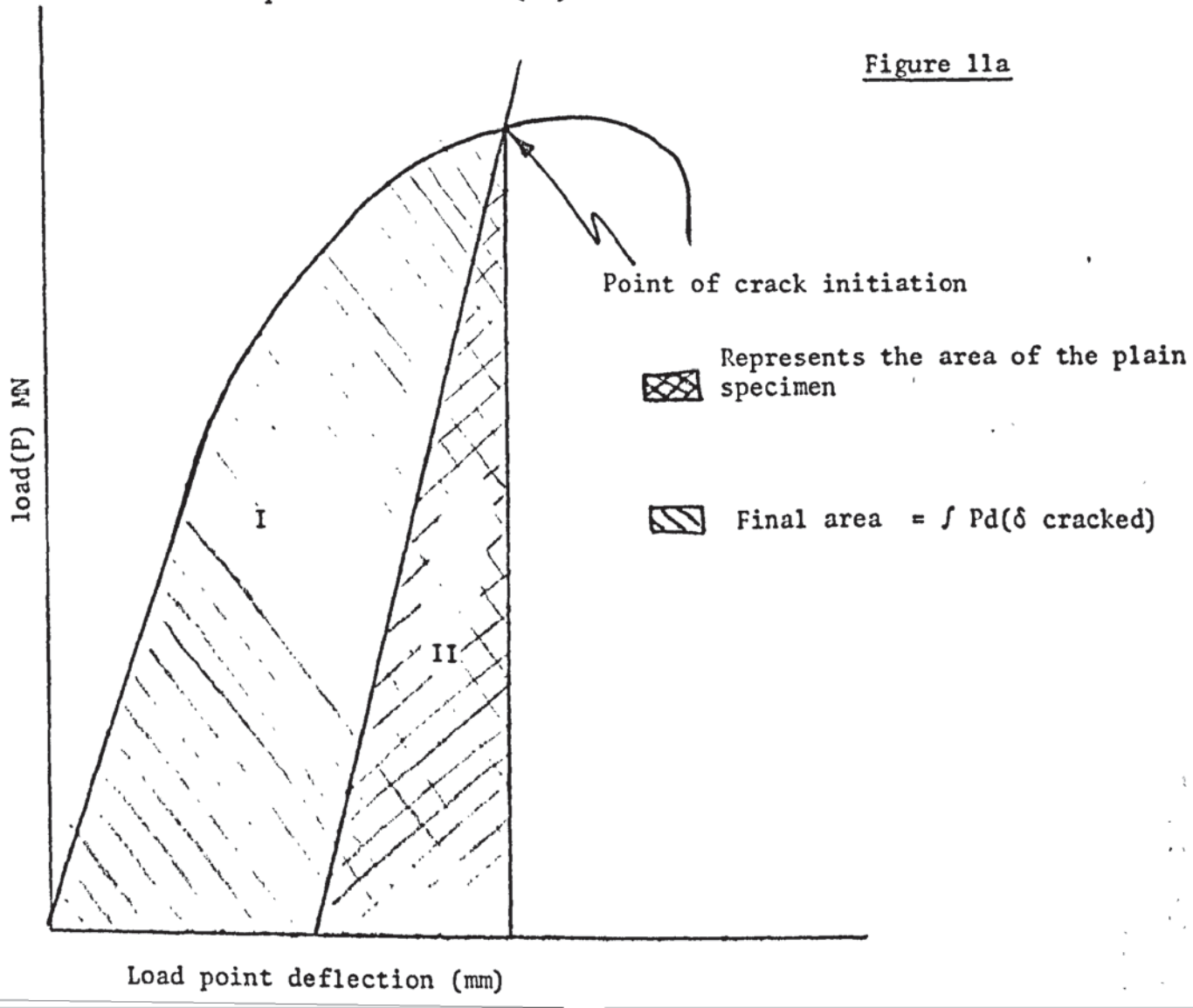

Using the J-integral method [138] to calculate K_C from the load/load point deflection the total area under the curve (I & II) figure 11a, taking from that area under the elastic straight line (II) using the triangle method. To obtain the right temperature for a sub-zero and above-zero temperature the following techniques were used.

b) +50°C and +100°C

An electrothermal heating tape (H.T.) type (HT 95506) which was one inch wide and about seventy-two inches long was coiled to the specimen to heat it up to the required temperature. A thermocouple was spot welded to the specimen in order to get the reading from a millivoltmeter which coincides with the required temperature. The British Standard Tables were the reference to this check. The tape was also connected to a temperature controller to ensure the tape from getting burned, the maximum temperature the tape could reach was 450°C. Figure 12 shows the connection in a diagram form.

c) -100°C and -50°C

The diagram in figure 13 shows how each specimen was coiled with a plastic hose taped to the specimen and the vapour of the liquid nitrogen was passed through it. The pressure build-up within the liquid nitrogen container was due to the nitrogen gas passing from another container through a rubber pipe. The millivolt reading from the recorder was cross checked with the B.S. 1827:1952 tables for this purpose. The millivoltage reading was recorded through a thermocouple spot welded to the face of the specimen. The thermocouple was well insulated up

to the welded point. When the temperature reached the desired value the nitrogen gas container valves closed tight. It is worth mentioning here that in both cases (higher and lower than zero temperature) the thermocouple was calibrated using ice and boiled water and the room temperature reading was determined to be equal to 1.06 mv which corresponds to ≃ 23°C.

3.3.6 Fracture toughness tests with acoustic emission applications

A monotonically increasing load test at room temperature was carried out to general yield and fracture, two batches of specimens were used. Each batch contained eight specimens dimensions of each was 20 mm x 25.0 mm x .20 mm. Batch 1 specimens were all prefatigued and a crack length to width ratios (a/w) were: 0.2, 0.34, 0.5 and 0.6 and a notch root radii were 0.127 mm, 12.70 mm, 25.4 mm and 0.127 mm respectively. Alteration of such a ratio produced intentionally to compare the total acoustic count for specimens of differently prefatigued in depth. The difference in root radii was not expected to affect the total acoustic counts produced. Since all specimens were prefatigued and the crack tips are all sharp. The second batch of 0.127 mm, 0.250 mm, 0.5 mm and 1.5 mm notch root radii in pairs. The depth of the notch in all eight specimens was 12.5 mm (that is $\frac{a}{W} = 0.5$). Also these specimens monotonically loaded to failure in experiments as described earlier (Section 2.3.4a), the recommendation of BSI draft for development (DD3) was followed with the J-integral method. The block diagram in figure 14 shows the equipment connected and used during

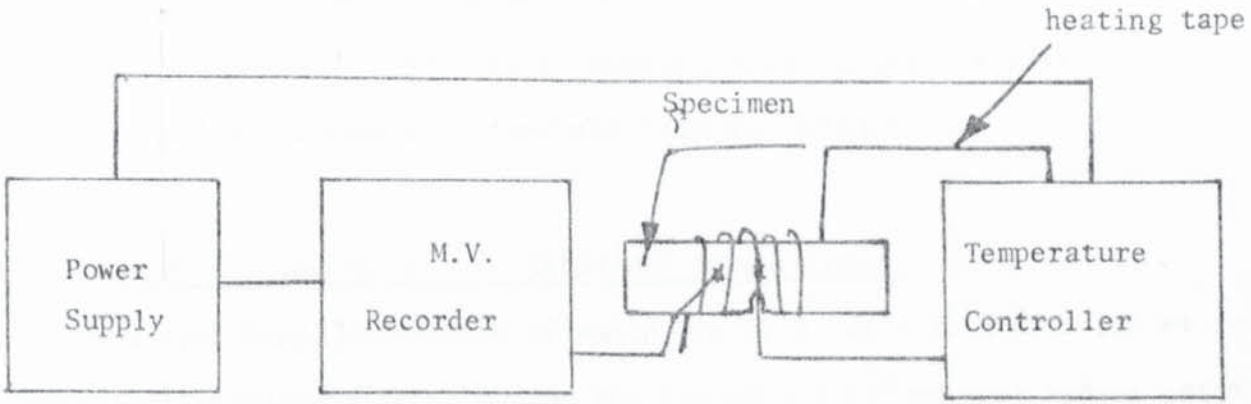

Figure 12 - Diagram of heating the specimen

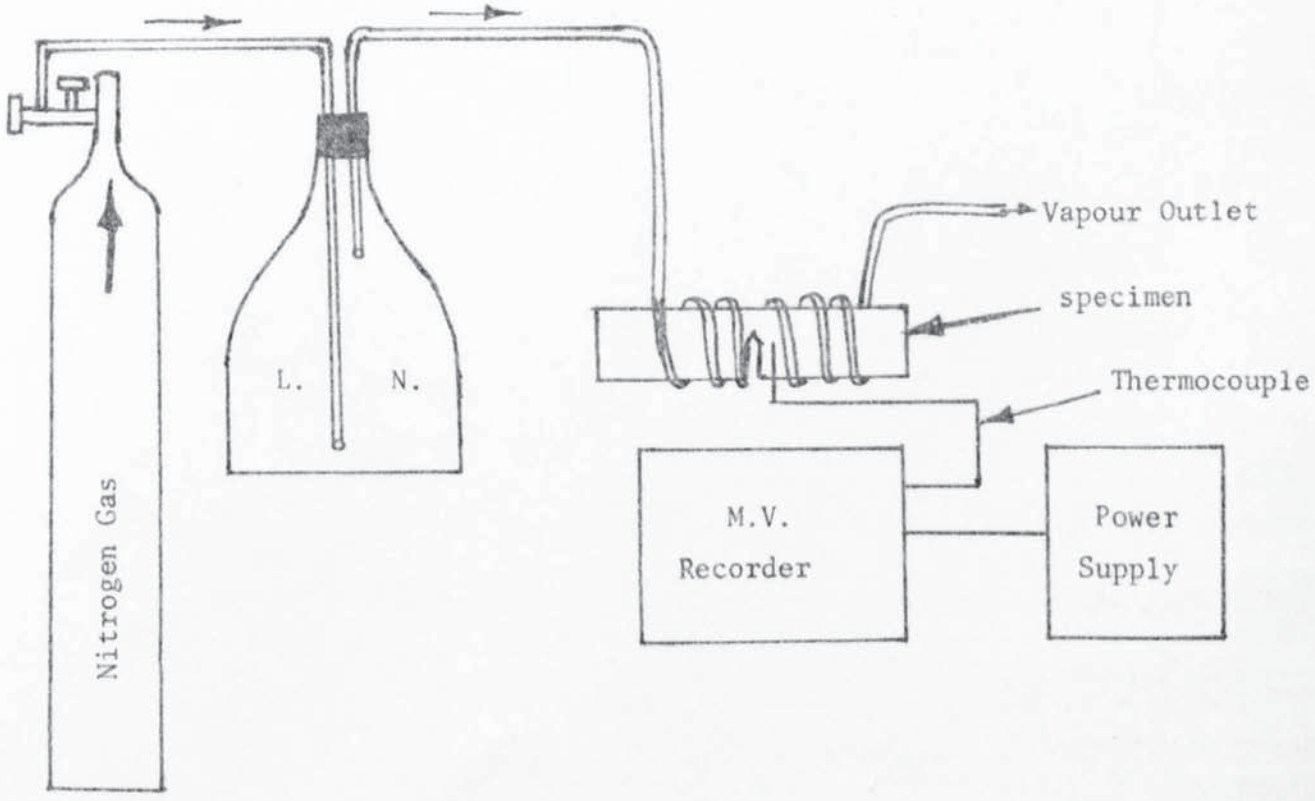

Figure 13 - Cooling technique in a diagram form

that test using a 50 tonne Instron machine available in the department. A more magnified diagram in figure 15 shows how the specimen with the clip gauge one placed in the machine. One side of several specimens were stress-coated. This was to enable photographing the plastic enclave before, during and after the fracture point.

a) Monotonic loading at five different temperatures

Five specimens, dimensions of which are 20.0 mm x 25.0 mm x 120 mm were electrically polished around the tip of a 0.127 mm root radius notch. They were monotonically loaded to approximately half the K_C value of material A at temperatures (room temperature, +50°C, +100°C, -50°C and -100°C) to enable photographing of the slip lines shape and orientation. Unfortunately, the results of this test were not encouraging ones.

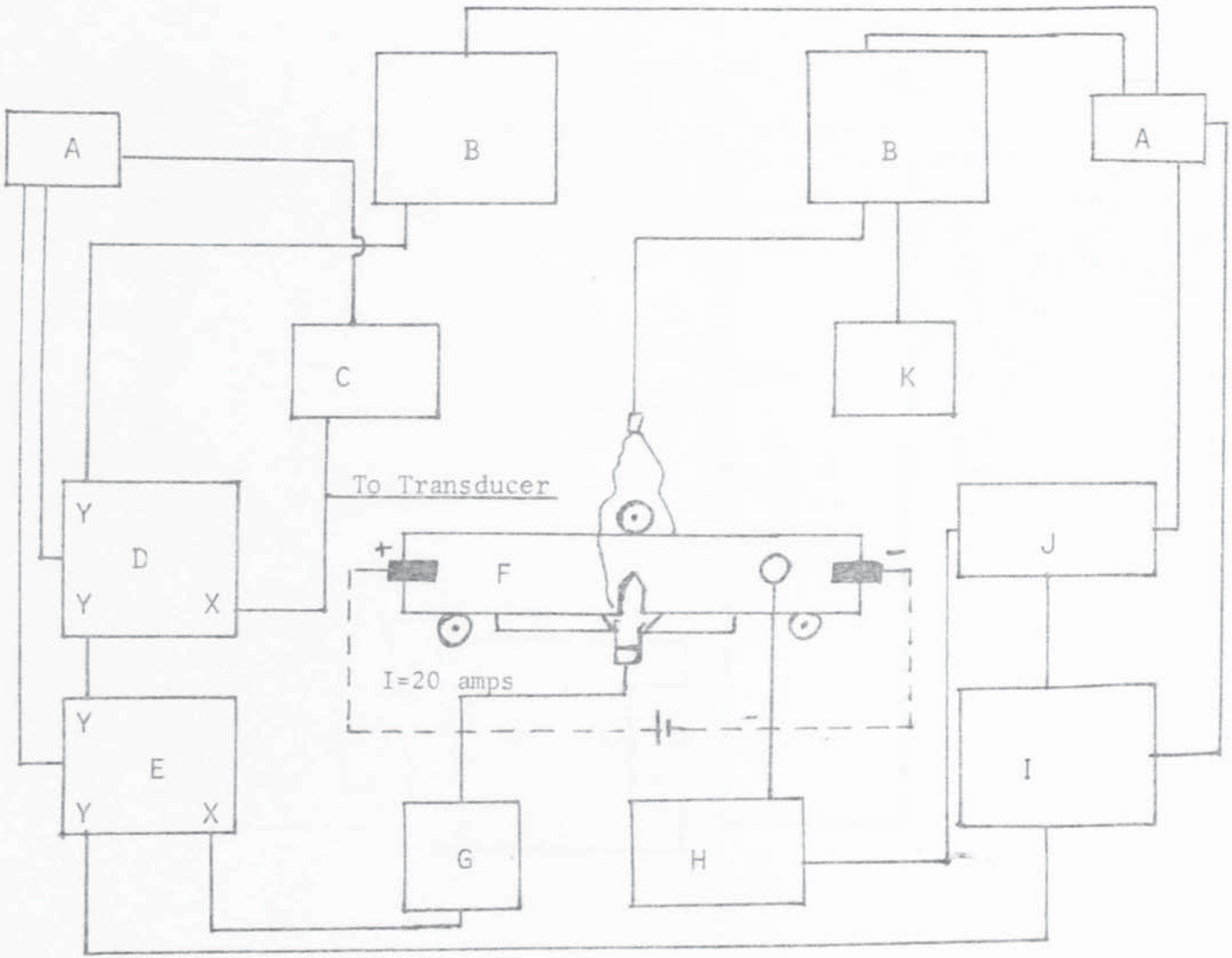

A - Power source 240 v

B - Potential drop Recorder produce Time v.s. Voltage Permanent chart

B - Potential drop Recorder procedure Load v.s. Time records.

C - Power Supply

D - Brayns X-Y recorder

E - Electronics X-> recorder

F - Specimen

G - Amplifier

H - Pre-Amplifier with a gain of 60

I - Twin-pen recorder

J - Acoustic Emission counter

K - D.C.millivoltmeter

Figure 14

Block diagram for a fracture toughness test using acoustic emission equipment.

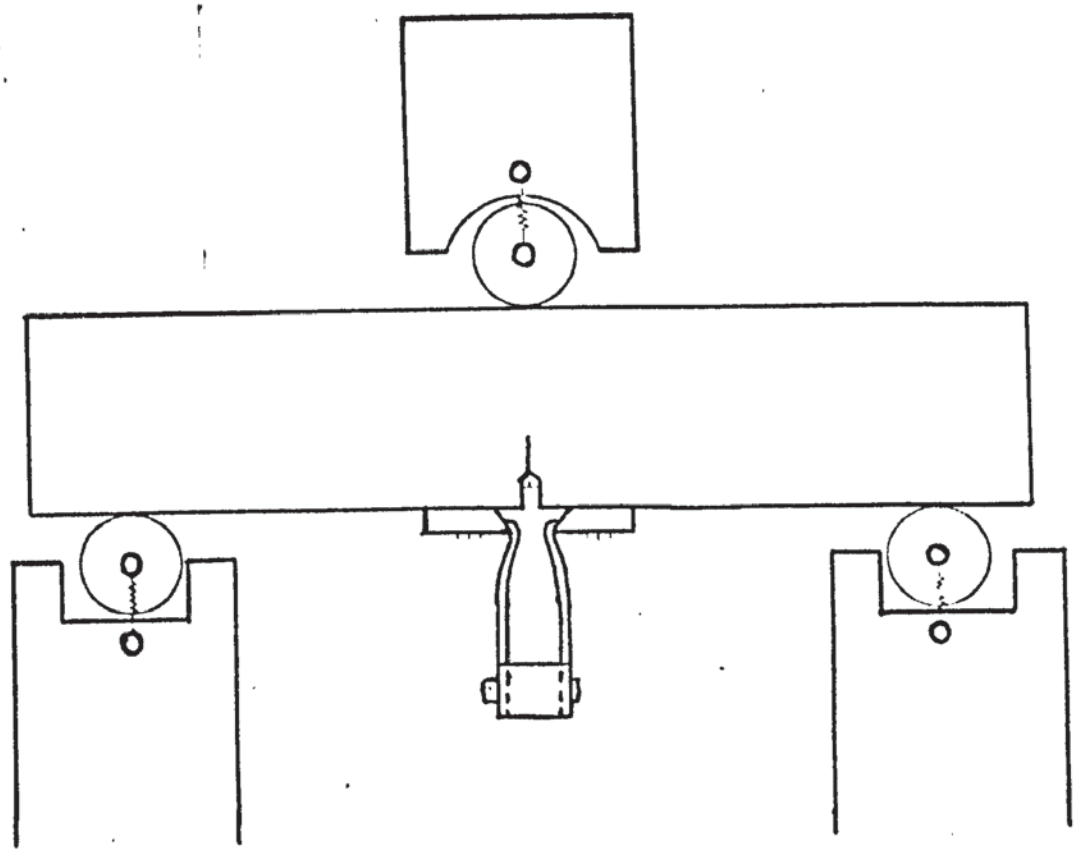

Figure 15 - Bend Test Fixture Design

3.4 Approximating the load range

All fatigue test specimens (for both materials) were arranged in five groups, and each group was tested at one of the following temperatures (room temperature, +50°C, +100°C, -50°C and -100°C).

Each of these five groups contained three sub-groups. Every sub-group contained six specimens with the same notch root radii. This was done in order to establish the effect of stress intensity, notch configuration and temperature (for both materials) on the number of cycles necessary to initiate a fatigue crack at the tip of the notch. It was therefore decided to test at three different load amplitudes for each of the different notch root radii. For ρ = 0.127 mm specimens the following load amplitude ($\Delta K/\rho^{\frac{1}{2}}$) were used (1000 MNm^{-2}, 1500 MNm^{-2} and 2500 MNm^{-2}). For specimens with a notch root radii equal 12.70 mm, the load amplitudes were 350 MNm^{-2}, 450 MNm^{-2} and 550 MNm^{-2}. Finally, for specimens of a notch root radii equal to 25.4 mm the load amplitudes were 200 MNm^{-2}, 250 MNm^{-2}, 250 MNm^{-2} and 350 MNm^{-2}. The alteration of load amplitudes was made on account of the stress concentration variation at the bottom of each notch. The sharper the notch the higher the nominal stress concentration at the bottom of the notch and vice-versa.

The load was calculated by writing the moment expression for the three point bending case.

$$\frac{\sigma}{Y} = \frac{M}{I} \tag{50}$$

where:

σ - is the stress applied ($\frac{P}{area}$)

M - is the moment $\frac{PL}{2} = PW$, $(2L = 4W)$

I - is the second moment of area

Y - is half a distance $\frac{Bh^3}{12}$ from the centre of beam rotation

from the specimen design it is also clear that:

W - is the specimen width

B - is the specimen thickness

a - is the crack length (notch depth)

P - is the applied load

2L equals 4W, that is 4:1 span ratio

Substituting these values in the expression for Y_o value taken from BISRA technical report, where Y_o is a unitless polynomial function of a/W which could be written as:

$$Y_o = A\left(\frac{a}{W}\right)^{\frac{1}{2}} - B\left(\frac{a}{W}\right)^{3/2} + C\left(\frac{a}{W}\right)^{5/2} - D\left(\frac{a}{W}\right)^{7/2} + E\left(\frac{a}{W}\right)^{9/2} = \frac{K_1 BW^{3/2}}{6M}$$

where A, B, C, D and E are constants

K_1 is the stress intensity factor (material properties).

$$Y_o = \frac{K_1 BW^{3/2}}{6PW} \qquad \text{let } Y = \frac{K_1 BW^{\frac{1}{2}}}{P}$$

Hence $K_1 = \frac{YP}{BW^{\frac{1}{2}}}$ or $P = K_1 \frac{BW^{\frac{1}{2}}}{Y}$ (51)

The last expression is applied for the single edge notch bend specimen loaded in three-point bending, and all span to specimen width ratio = 4:1. During load calculation the Y values were taken from BISRA Tables related to the a/W values of specimens.

Test results from fatigue test specimens will provide design data and will also be used to study the mechanism of fatigue crack initiation and propagation from notches in relation to microstructural fractures of the alloys.

The depth of each notch for the fatigue specimens of dimensions 20 mm x 25 mm x 120 mm was 5.0 mm. The fatigue testing frequency was 20 Hz, although in testing very few specimens at lower load amplitude the frequency was 80Hz.

The D.C. electric current passing through the specimen during each test was 20.0 amperes. Photomicrographs of fracture surfaces of fatigue tested specimens were taken to study the mechanism of the fatigue crack during initiation and propagation.

To carry out high temperature fatigue tests an electrothermal heating tape was secured to heat up the specimen to the required temperature. The tape was wrapped around the central section of the specimen in two places. This tape which could be seen in figure 12 is one inch wide and seventy-two inches long. To maintain a constant temperature the specimen was surrounded by two half tube mild steel pieces and

covered with insulating material. A calibration test provided to indicate the tapes temperature which could produce a constant testing temperature measured from the specimens surface via the spot welded thermo-couple. This calibration indicated that

a) To obtain a +50°C the tapes temperature should be held at 99°C for at least one hour before the test can be started.

b) To obtain a +100°C the tapes temperature should be held at 175°C for at least one and a half hours before the test can be started.

The sub-zero fatigue tests required a double-walled stainless steel box insulated between the walls to give better control over the specimen and to provide a stable temperature. The box was also wrapped all round with a plasticising material to cut down the vibration as well as to prevent any resonance from taking place which could break the box during a fatigue test. The box was set flat on the cycling point of the servo-test machine. The two point jig was fixed to the non-moveable crosshead. The above box was provided with a fixed third point inside it made especially for this purpose from a tool steel. The -50°C temperature was obtained using a mixture of dry ice (Solid CO_2) and acetone. This mixture was sufficient to keep the temperature at the above mentioned value.

To obtain a -100°C new techniques have to be used, since several different chemical mixtures did not give the temperature needed. The new method of obtaining a -100°C was to pass the liquid nitrogen vapour through a plastic hose coiled around the specimen covering the

area in both sides of the notch Figure 13. The liquid nitrogen container was connected to a nitrogen gas bottle from one side and to the specimen from the other. When the nitrogen gas bottle was turned on it built up pressure inside the liquid nitrogen container which resulted at passing the liquid nitrogen vapour through the hose. A thermo-couple was spot welded to the specimen to record the millivolts reading for the required testing temperature. All attachments to the specimen as well as the specimen itself were insulated from the atmosphere by means of plastic material to obtain a constant temperature figure (A). The potential drop was also used here to detect the initiation of a fatigue crack. It required up to 45 minutes to cool the specimen to -100°C as well as for the potential drop to be settled down. Several other tests were experimentally provided for checking some aspects. Results of these tests will be shown in the next chapter but the technical experimental work done should be shown here in this section.

a) Three specimens of material B were chosen after heat treatment was provided. The dimensions of each specimen were: 20.0 mm x 25.0 mm x 120.0 mm. The notch was 5.0 mm deep and contained root radius of 0.127 mm. The same fatigue test condition at room temperature was applied to these specimens. The test was aimed to these with identical condition of material A.

b) Four specimens of material A with the same dimensions as in (a). Two were containing a spark cut along the thickness B using a knife of 0.127 mm thick and the cut was about 0.025 mm deep. The other two specimens were tested as machined without a spark cut. All notch root

radii were 12.70 mm and 5.0 mm deep. This experiment was to define the fatigue life difference between spark cut and just machined and notched specimens only.

c) An experimental test was provided on 1 specimen of material B to show the plastic damage which is believed to take place before a fatigue crack initiates. This plastic damage could be slip lines, slip planes or a mixture of both. A specimen of 20.0 mm x 25.0 mm x 120.0 mm was chosen for this purpose. A sharp (namely 0.127 mm) notch root radius was machined in it. The specimen was mechanically polished using different grades of sand paper as well as a six and one micron diamond wheels. A servo- test machine was used for this test. The total span was 100.0 mm (2L = 4W). A direct current of a value of 20.0 amperes was passed through the specimens to enable measuring the voltage across the specimen using the potential drop techniques. The frequency used was 20.0 Hz. A plastic replica was taken before the test started and at six different stages of a fatigue test from both sides of the specimens by stopping the test. These plastic replicas then enriched with carbon in a vacuum chamber and they were examined and the results are shown in the next chapter.

In all fatigue and fracture toughness tests the initiation criterion selected for all these tests was defined as the first deviation from the steady value of the potential across the notch.

3.5 Fatigue crack propagation

Fatigue crack propagation date for both materials are to be obtained because they are to be useful for the characterisation of the fatigue properties. This data should be obtained over a wide range of ΔK. The value of the parameter ΔK was calculated from the published K-calibration curves (Walker & May) assuming the notch to be a sharp crack, thus:

$$\Delta K = \frac{Y\Delta P}{BW^{\frac{1}{2}}}$$

the crack propagation rates were determined using Holder R. techniques[74].

3.6 Fracture surface examination

A random selection of the fractured specimens at up to failure tests were used for this purpose, this selection covered all five testing temperatures. A slice of 10 mm x 10 mm and 3.0 mm thick was cut from, in a parallel direction of the crack movement. These samples were then connected to an SEM specimen stub ready for an examination. These samples were then studied and photographed throughout both initiation and propagation areas at several different magnifications.

CHAPTER 4

RESULTS

4.1 Fatigue Test Results

Tables (9 - 13) show all the results of the fatigue crack initiation tests for each specimen of both materials namely A and B. These results were arranged in such a way that in each table one can compare these two materials tested at the same conditions. Different load amplitudes applied for different notch configuration specimens as well as different test temperatures. The number of cycles to initiate a fatigue crack was detected. The results from these tables plotted in figures 16 - 20 on a 4 x 4 scale log-log papers which represents the number of cycles required to initiate a fatigue crack against the load amplitude value ($\Delta K/\rho^{\frac{1}{2}}$ MN m^{-2}). All five figures (16 - 20) were plotted for five different temperatures (room temperature, +50°C, +100°C, -50°C and -100°C) respectively. The material constant (M,B) are also represented in Tables (9 - 13). Statistics of the log Ni (number of fatigue cycles to initiate a fatigue crack) versus $\Delta K/\rho^{\frac{1}{2}}$ produced the following values.

Material	m	B_o	Test temperatures
A	-4.84	$10^{6.941}$	Room temperature
B	-4.81	$10^{6.638}$	" "
A	-5.79	$10^{4.25}$	+50°C
B	-5.80	$10^{6.991}$	+50°C
A	-5.43	$10^{5.974}$	+100°C
B	-5.40	$10^{6.57}$	+100°C
A	-5.0	$10^{4.40}$	-50°C
B	-4.8	$10^{5.27}$	-50°C
A	-3.98	$10^{4.5}$	-100°C
B	-3.67	$10^{5.25}$	-100°C

Anyone looking through these statistical results should always remember that Tables 9, 10 and 11 contain specimens of material B which were not heat-treated, but machined as cast. In the same tables material A was given the heat-treatment shown in Table 7. The last two Tables 12 and 13 both materials were given the heat-treatment shown in Table 7, with one exception and that is Material A heat-treated in big blocks as shown in Appendix 1, while material B was given the heat-treatment in smaller size specimens (22 mm x 22 mm x 120 mm) and 45 mm x 55 mm x 250 mm.

Fatigue crack initiation results for both materials tested at room temperature

Material A Heat-treated

Specimen Code	$\Delta K/\rho^{\frac{1}{2}}$ MN m^{-2}	ΔK(MN $m^{-3/2}$	Ni (cycles)	ρ mm
AZ1	10000	11.27	3.5×10^6	0.127
AZ36	1000	11.27	3.1×10^6	
AZ2	1500	16.91	1.16×10^5	
AZ37	1500	16.91	1.2124×10^5	
AZ3	2500	28.18	4800	
AZ38	2500	28.18	6600	
AZ26	300	33.81	1.233×10^5	12.70
AZ39	300	33.81	1.1×10^5	
AZ6	470	52.97	2400	
AZ40	400	45.08	2.4×10^4	
AZ23	550	62.00	1200	
AZ41	500	56.35	10180	
AZ22	130	20.72	2.832×10^6	25,40
BZ26	200	31.88	1.1816×10^6	
AZ24	200	31.88	1.06325×10^5	
AZ42	250	39.85	1.6925×10^5	
AZ25	300	47.82	10500	
AZ43	300	47.82	7.5×10^4	

$m = -4.84$, $B = 10^{6.92}$

Frequency = 20 Hz Room temperature test

Table 9

Material B (no heat-treatment provided)

Specimen Code	$\Delta K/\rho^{\frac{1}{2}}$ (MNm^{-2}	ΔK(MNm$^{-3/2}$)	Ni (cycles)	ρ mm
6	1100	12.40	4.44×10^5	0.127
3	1200	13.52	1.052×10^5	
58	1500	16.91	3.81×10^4	
25	1800	20.286	1.334×10^4	
37	2500	28.18	3380	
17	2800	31.56	1900	
60	300	33.81	2.926×10^5	12.70
27	300	33.81	2.931×10^5	
24	400	45.08	20640	
40	400	45.08	32060	
23	500	56.35	4300	
21	500	56.35	6980	
10	200	31.88	1.6445×10^5	25.40
64	200	31.88	5.0×10^5	
11	250	39.85	38950	
67	250	39.85	50590	
42	350	55.79	1020	
41	350	55.79	3300	

$m = -4.8$ $B = 10^{6.64}$

Fatigue crack initiation results for both materials tested at +50°C

Material A Heat-treated

Specimen Code	$\Delta K/\rho^{\frac{1}{2}}$ MN m^{-2}	ΔK(MN $m^{-3/2}$	Ni (cycles)	ρ mm
AZ4	1000	11.27	9.8625×10^5	0.127
AZ44	1200	13.52	7.495×10^5	
AZ5	1500	16.91	3.513×10^5	
AZ45	1800	20.29	3.85×10^5	
AZ46	2500	28.18	18000	
AZ7	2800	31.56	8900	
AZ29	350	39.45	2.31×10^5	12.70
AZ50	300	33.81	1.054×10^5	
AZ35	450	50.72	3.87×10^4	
AZ51	400	45.08	2.174×10^4	
BZ1	500	56.35	1800	
AZ52	500	56.35	4210	
AZ27	200	31.88	1.15×10^6	25,40
AZ56	200	31.88	3.18×10^5	
AZ28	250	39.85	2.252×10^5	
AZ57	300	47.82	0.7475×10^5	
BZ11	300	47.82	1.033×10^5	
AZ58	400	63.76	5000	

Table 10

+50°C Freq. = 20 Hz

Material B (no heat-treatment provided)

Specimen Code	$\Delta K/\rho^{\frac{1}{2}}$ (MNm^{-2}	ΔK(MNm$^{-3/2}$)	Ni (cycles)	ρ mm
13	1100	12.40	1.2×10^6	0.127
02	1200	13.52	0.25×10^6	
20	1400	15.78	6.6×10^4	
44	1800	20.29	1.50×10^4	
29	2500	28.18	6200	
01	2800	31.56	1040	
15	350	39.45	3.0×10^4	12.70
46	300	33.81	21.58×10^4	
32	450	50.72	5.356×10^4	
31	400	45.08	1.44×10^4	
38	550	62.00	3150	
47	500	56.35	7370	
22	200	31.88	1.72×10^6	25.40
09	200	31.88	0.6×10^6	
16	300	47.82	8.88×10^4	
75	300	47.82	2.2×10^4	
30	400	63.76	2450	
81	400	63.76	3070	

Fatigue crack initiation results for both materials tested at +100°C

Material A Heat-treated

Specimen Code	$\Delta K/\rho^{\frac{1}{2}}$ MN m^{-2}	ΔK(MN $m^{-3/2}$	Ni (cycles)	ρ mm
AZ8	1000	11.27	3.1965×10^6	0.127
AZ47	1200	13.56	3.0×10^6	
AZ9	1500	16.91	0.622×10^5	
AZ48	1800	20.29	0.6369×10^5	
AZ10	2500	28.18	0.6290×10^4	
AZ49	2800	31.56	0.575×10^4	
BZ2	300	33.81	90.31×10^4	12.70
AZ53	300	33.81	87.4×10^4	
BZ3	400	45.08	40.15×10^3	
AZ54	400	45.08	109.8×10^3	
BZ4	500	56.35	23.95×10^3	
AZ55	500	56.35	14.210×10^3	
BZ12	200	31.88	2.277×10^5	25.40
AZ59	200	31.88	2.103×10^5	
BZ13	250	39.85	3.0×10^4	
AZ60	250	39.85	16.254×10^9	
BZ14	350	55.79	19.450×10^3	
AZ61	350	55.79	75.59×10^3	

m = -5.43 B = $10^{5.974}$

Material B (no heat-treatment provided)

Specimen Code	$\Delta K/\rho^{\frac{1}{2}}$ (MNm^{-2}	ΔK(MNm$^{-3/2}$)	Ni (cycles)	ρ mm
14	1200	13.56	2.8744×10^5	0.127
39	1200	13.56	2.658×10^5	
18	1800	20.29	2.06×10^4	
55	1800	20.29	1.9×10^4	
19	2800	31.56	1.43×10^3	
65	2800	31.56	1.25×10^3	
41	300	33.81	5.178×10^5	12.70
54	300	33.81	1.392×10^5	
45	400	45.08	1.137×10^4	
59	400	45.08	1.405×10^4	
51	500	56.35	6.74×10^3	
88	500	56.35	9.0×10^3	
33	200	31.88	1.245×10^5	25.40
92	200	31.88	0.85×10^5	
72	250	39.85	10.4×10^4	
93	250	39.85	6.4×10^4	
73	300	47.82	18.15×10^3	
94	300	47.82	8.3×10^3	

m = -5.4 B = $10^{6.6}$

+ 100°C

Table 11

Fatigue crack initiation results for both materials tested at -50°C

Material A Heat-treated

Specimen Code	$\Delta K/\rho^{\frac{1}{2}}$ MN m^{-2}	ΔK(MN $m^{-3/2}$	Ni (cycles)	ρ mm
AZ11	1200	13.52	0.6×10^5	0.127
A47	1200	13.52	0.65×10^5	
AZ12	1500	16.91	5.0×10^4	
A48	1800	20.29	2.7×10^4	
AZ16	2500	28.18	4.3×10^3	
A49	2800	31.56	3.2×10^3	
BZ6	400	45.08	5.5×10^4	12.70
A53	400	45.08	4.413×10^4	
BZ5	450	50.72	2.72×10^4	
A54	450	50.72	2.4×10^4	
BZ7	500	56.35	16.18×10^3	
A55	500	56.35	12.0×10^3	
BZ15	250	39.85	1.44×10^4	25.40
A59	250	39.85	2.36×10^4	
BZ16	300	47.82	8.4×10^3	
A60	300	47.82	8.1×10^3	
BZ17	350	55.79	9.9×10^3	
A61	350	55.79	6.4×10^3	

m = -5.0 B = $10^{4.4}$

-50°C

Material B (heat-treatment provided)

Specimen Code	$\Delta K/\rho^{\frac{1}{2}}$ (MNm^{-2}	ΔK(MN$m^{-3/2}$)	Ni (cycles)	ρ mm
63	1200	13.52	0.294×10^5	0.127
FEG	1200	13.52	0.357×10^5	
85	1800	20.29	1.5×10^4	
FZH	1800	20.29	1.48×10^4	
84	2800	31.56	5.45×10^3	
FZI	3000	33.81	4.35×10^3	
57	400	45.08	2.44×10^4	12.70
FZD	400	45.08	2.871×10^4	
62	450	50.72	1.4×10^4	
FZE	450	50.72	1.51×10^4	
F4	500	56.35	4.92×10^3	
FZF	500	56.35	4.01×10^3	
95	250	39.85	8.38×10^4	25.40
FZA	250	39.85	6.73×10^4	
96	300	47.82	16.6×10^3	
FZB	300	47.82	9×10^3	
97	350	55.79	6.4×10^3	
FZC	350	55.79	7.04×10^3	

m = -4.8 B = $10^{5.3}$

Table 12

Fatigue crack initiation results for both materials tested at -100°C

Material A Heat-treated

Specimen Code	$\Delta K/\rho^{\frac{1}{2}}$ MN m^{-2}	ΔK(MN $m^{-3/2}$	Ni (cycles)	ρ mm
AZ17	1200	13.52	2.2×10^5	0.127
A66	1200	13.52	2.8×10^5	
AZ18	1800	20.29	1.03×10^5	
A76	1800	20.29	0.85×10^5	
AZ19	3000	33.81	9200	
A77	3000	33.81	9160	
BZ8	400	45.08	5.127×10^4	12.70
A8	400	45.08	4.87×10^4	
BZ9	450	50.72	1.32×10^4	
A68	450	50.72	1.15×10^4	
BZ10	500	56.35	1110	
A82	500	56.35	2800	
BZ18	250	39.85	5.785×10^4	25.40
A98	250	39.85	10.7×10^4	
BZ19	300	47.82	7.4×10^4	
A99	300	47.82	6.5×10^4	
BZ25	350	55.79	2.32×10^4	
A100	350	55.79	2.8×10^4	

m = 4.0 B = $10^{4.5}$

-100°C Freq. = 20 Hz

Table 13

Material B (heat-treatment provided)

Specimen Code	$\Delta K/\rho^{\frac{1}{2}}$ (MNm^{-2}	ΔK(MNm$^{-3/2}$)	Ni (cycles)	ρ mm
HT1	1200	13.52	1.5×10^5	0.127
HT4	1200	13.52	1.38×10^5	
HT3	1800	20.29	0.38×10^5	
HT5	1800	20.29	0.45×10^5	
HT2	3000	33.81	9000	
HT6	3000	33.81	15000	
HT7	400	45.05	10.46×10^4	12.70
HT10	400	45.05	9.58×10^4	
HT8	450	50.72	3.4×10^4	
HT11	450	50.72	3.57×10^4	
HT9	500	56.35	11770	
HT12	500	56.35	10200	
HT13	250	39.85	1.086×10^5	25.40
HT16	250	39.85	1.106×10^5	
HT14	300	47.82	4.86×10^4	
HT17	300	47.82	4.52×10^4	
HT15	350	55.79	1.23×10^4	
HT18	350	55.79	1.08×10^4	

m = -3.67 B = $10^{5.25}$

Code	notch root radii mm
X	0.127
O	12.70
Δ	25.40

Fatigue crack initiation results.
(Test provided at room temperature)

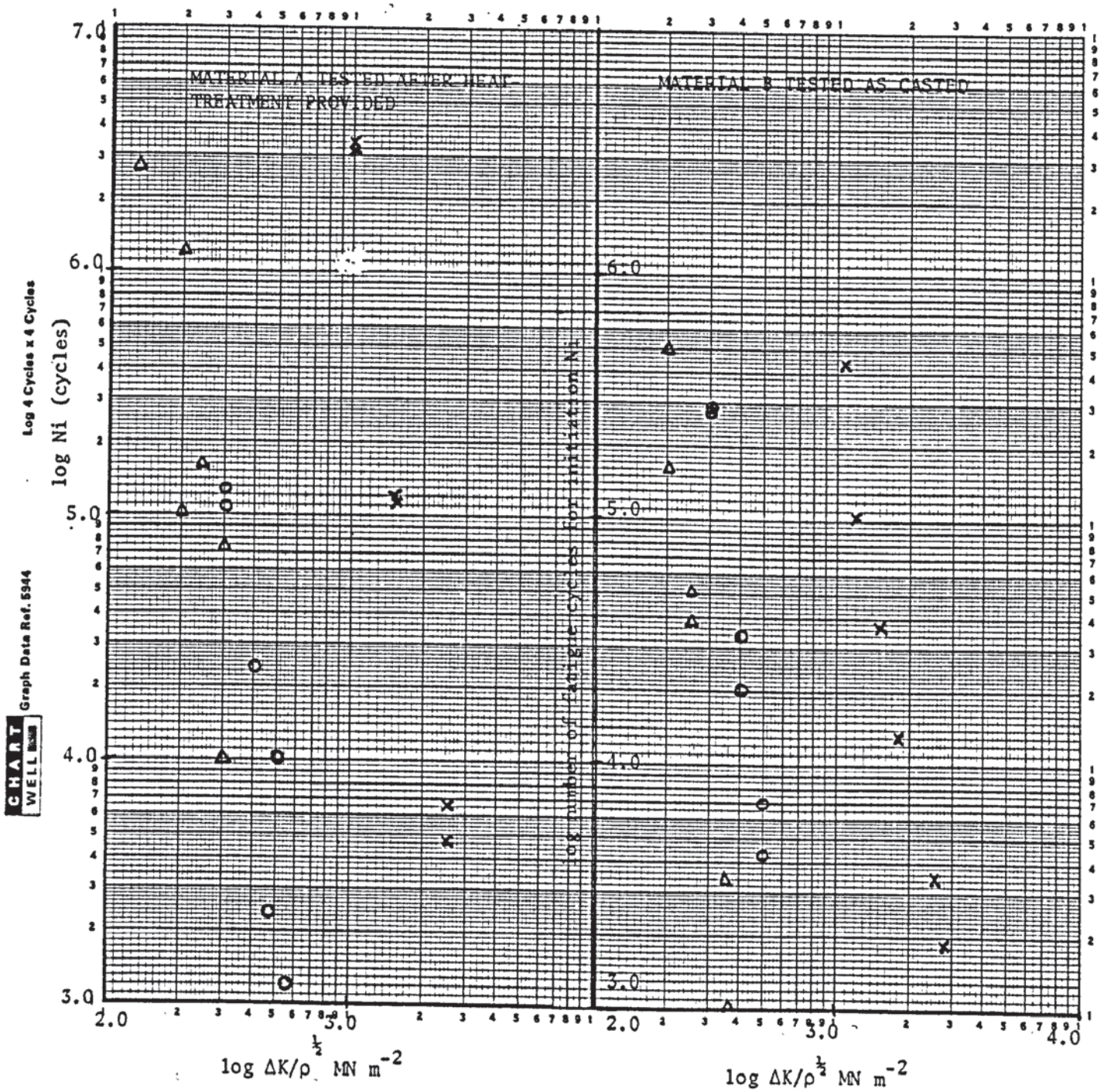

Figure 16.

Fatigue crack initiation results of specimens

Tested at +50°C

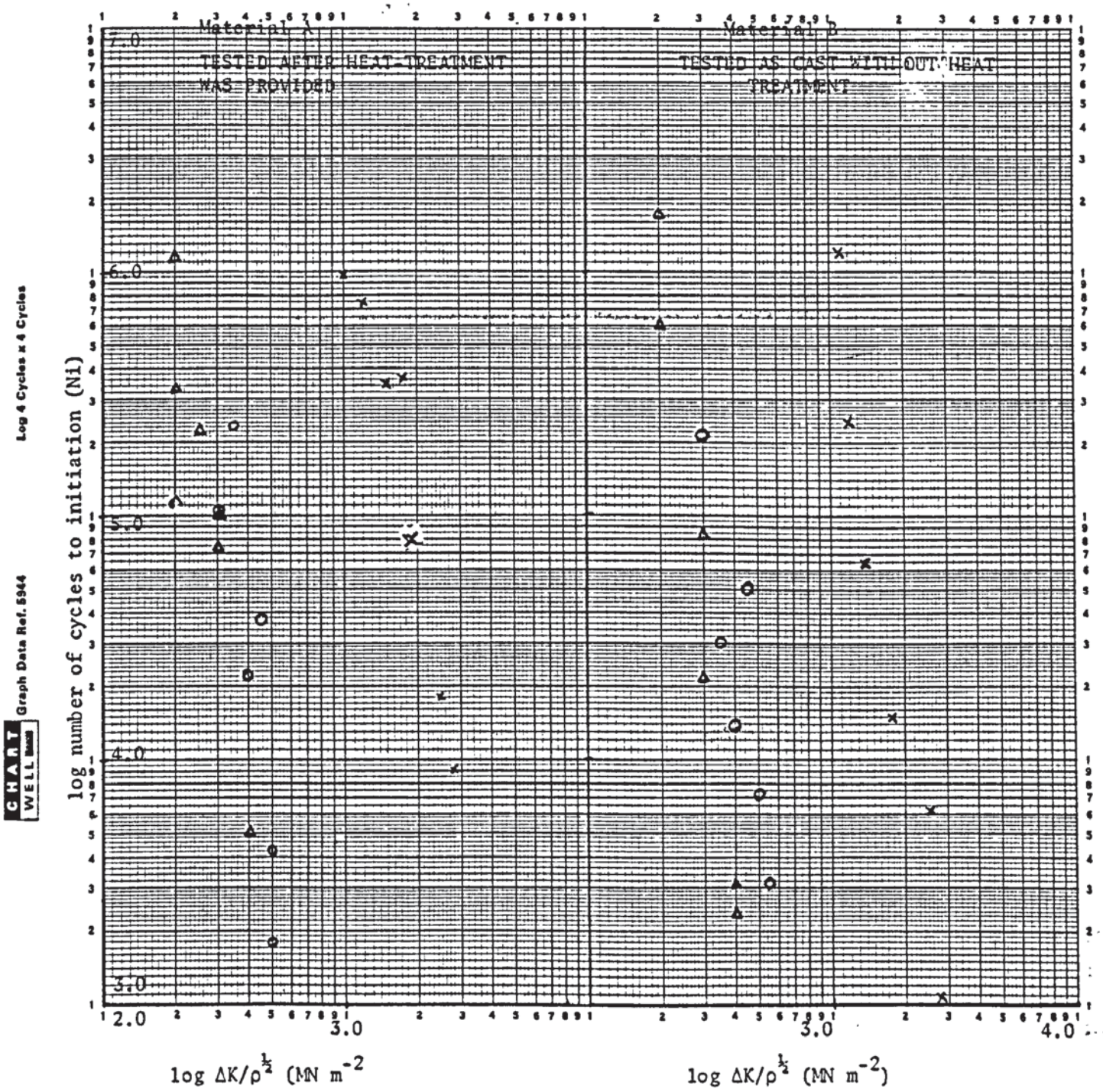

Figure 17

Fatigue Crack Initiation Results

(Test provided at +100°C)

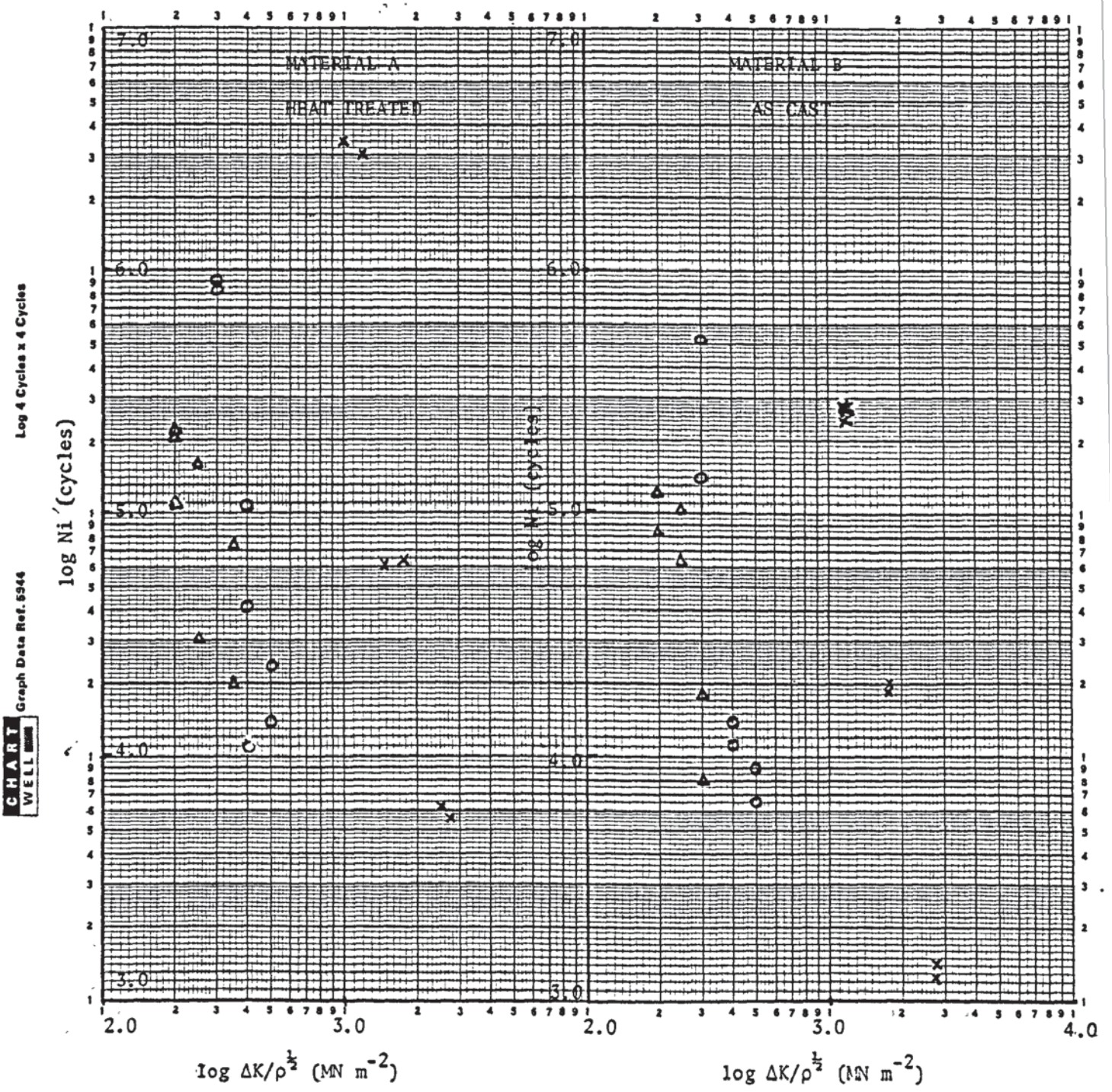

Figure 18

Fatigue crack initiation results

1. Test provided at (-50°C)
2) Both materials were heat treated.

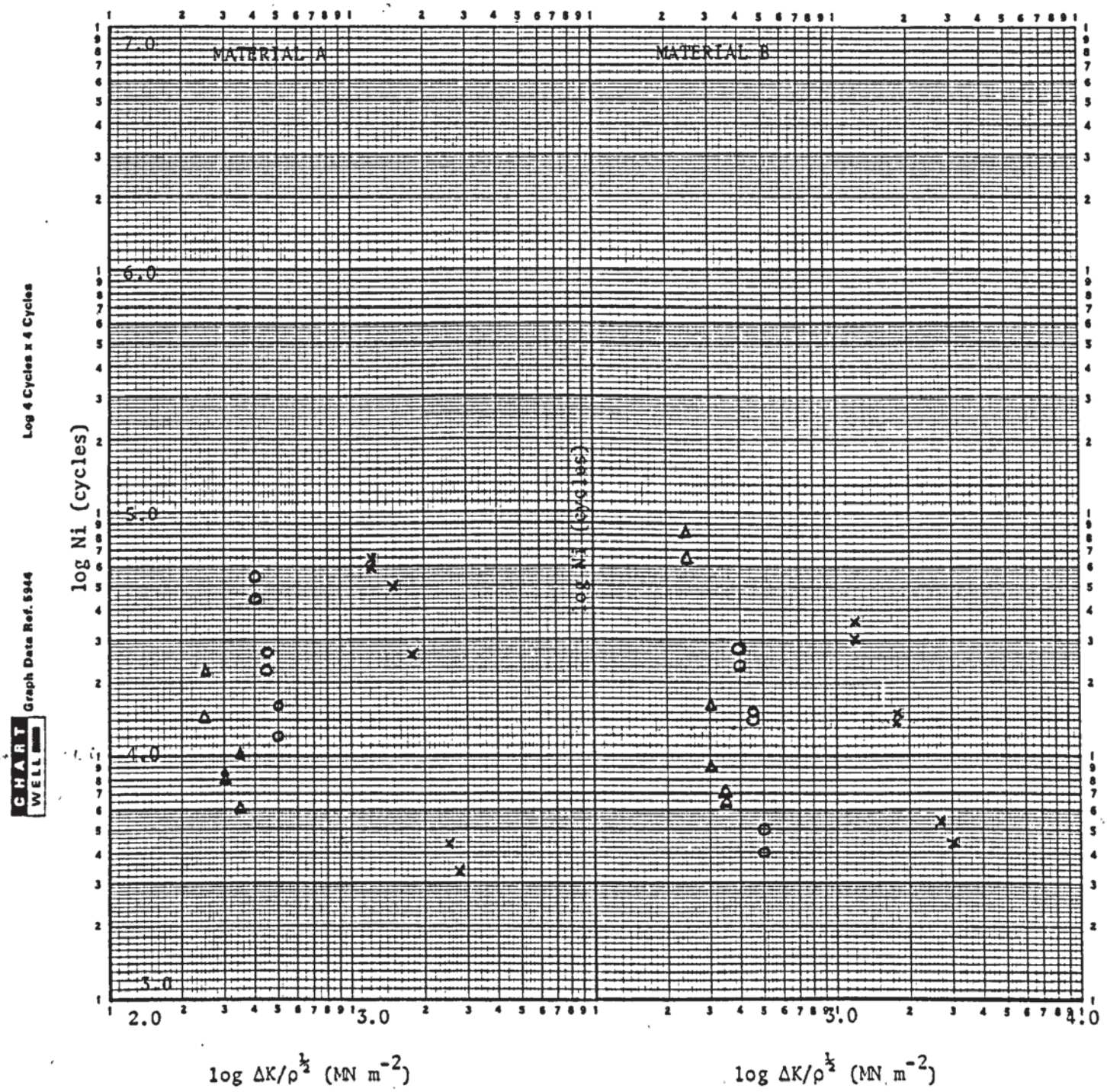

Figure 19

Fatigue crack initiation results

1. Test provided at (-100°C)
2. Both materials were heat-treated

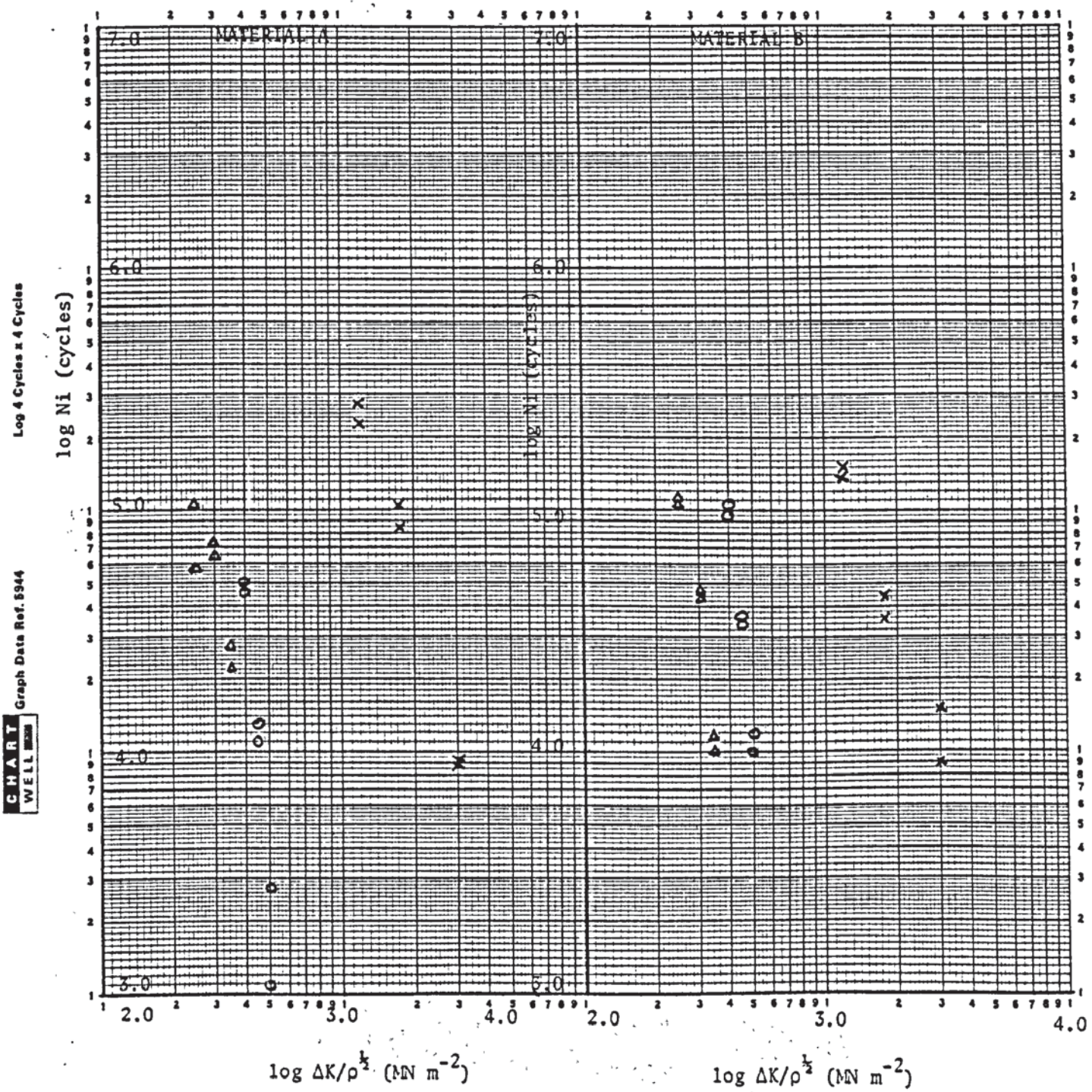

Figure 20

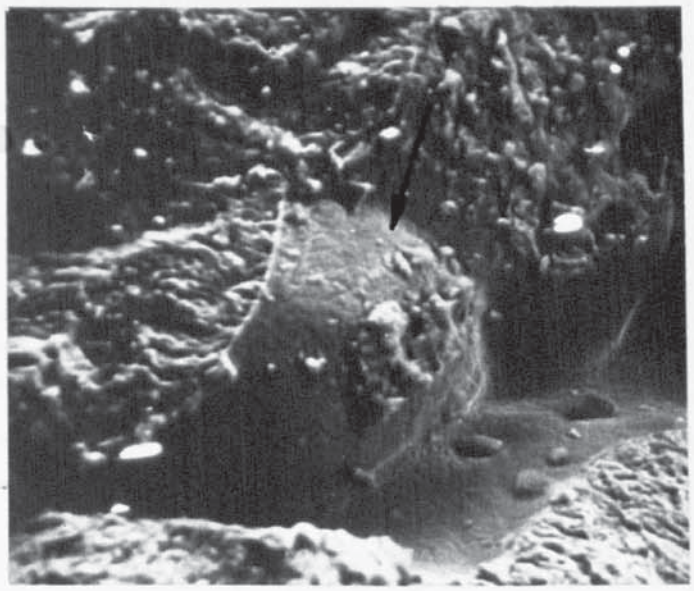

Specimen AZ38 X 500
Figure 20a Initiation Fractography Of

Material A Tested at room temperature

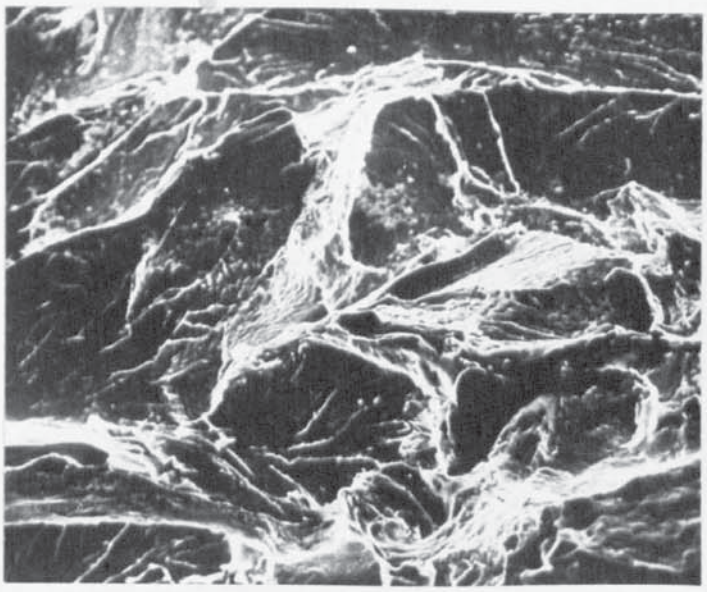

Specimen 6 X500

Figure 20b Initiation Fractography of
Material B tested at room temperature

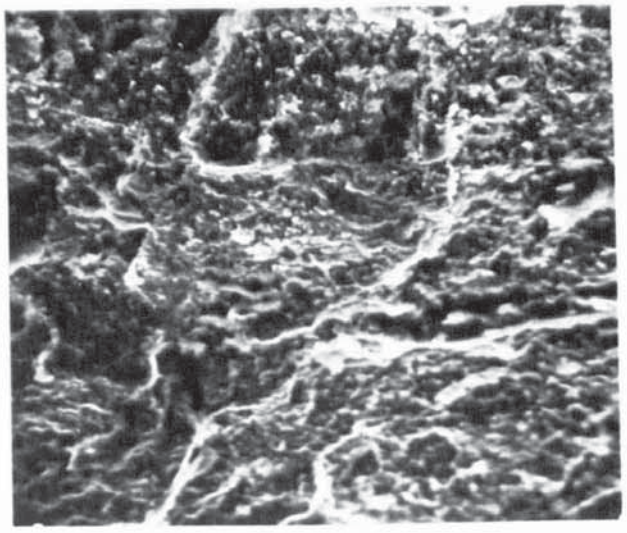

Specimen AZ27 X 1100

Figure 20c Initiation Fractography of Material A tested at + 50C

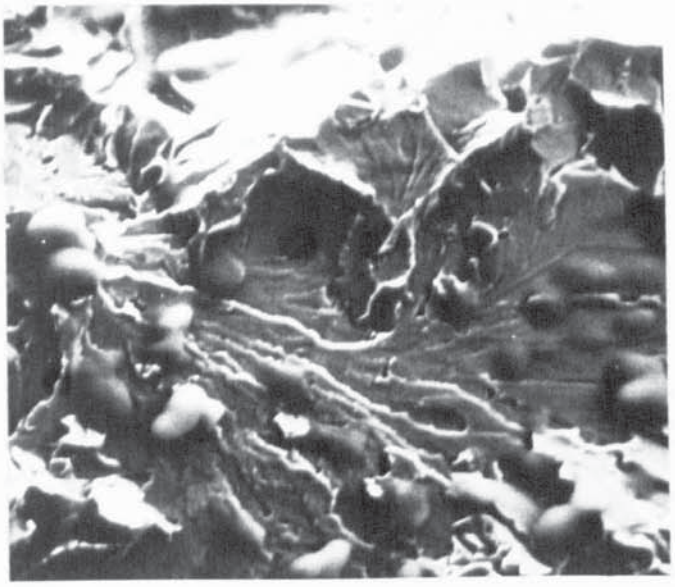

Specimen 15 X 500

Figure 20d Initiation Fractography of Material B tested at + 50C

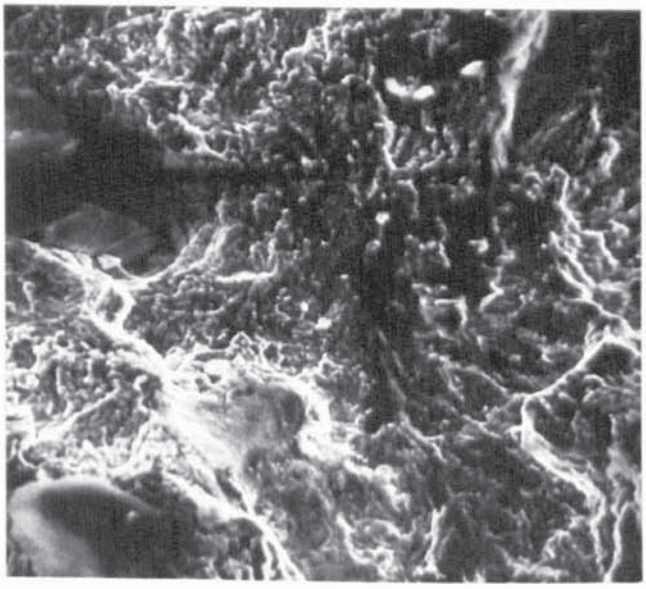

Specimen AZ10 X1000

Figure 20e Initiation Fractograp hy of Material A tested at + 100°C

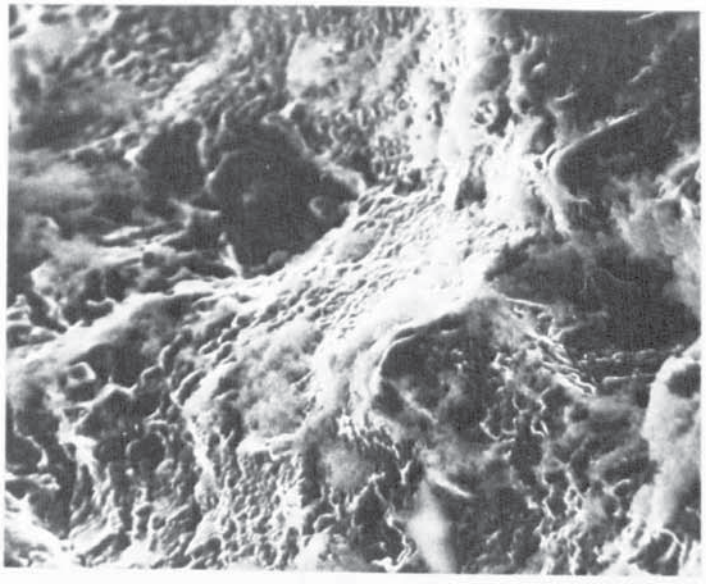

Specimen 45 X500

Figure 20f Initiation Fractography of Material B tested at + 100°C

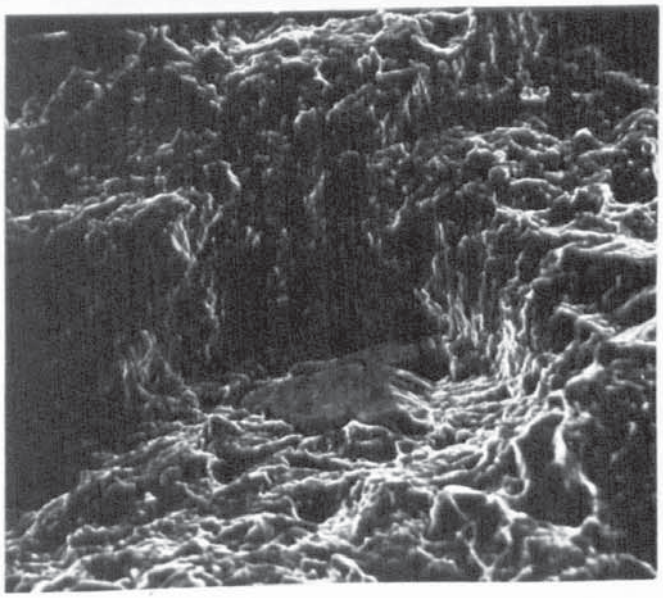

Specimen B29 X1050

Figure 20g Initiation Fractography of Material A tested at - 100°C

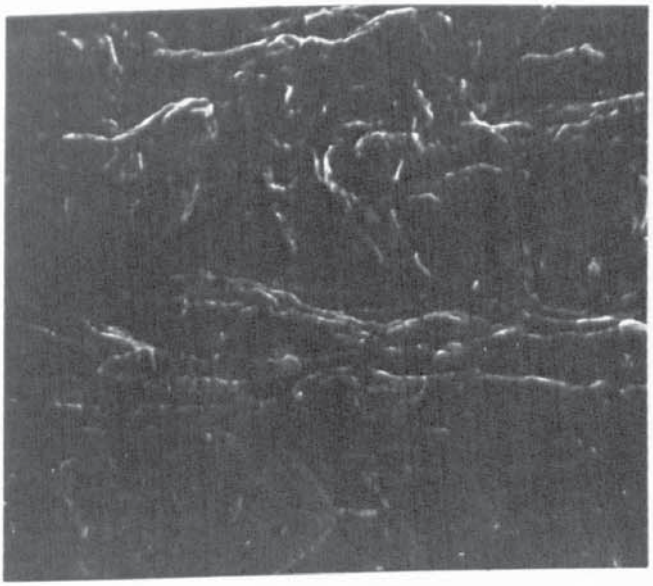

Specimen MT9 X1100

Figure 20h Initiation Fractography of Material B tested at - 100°C

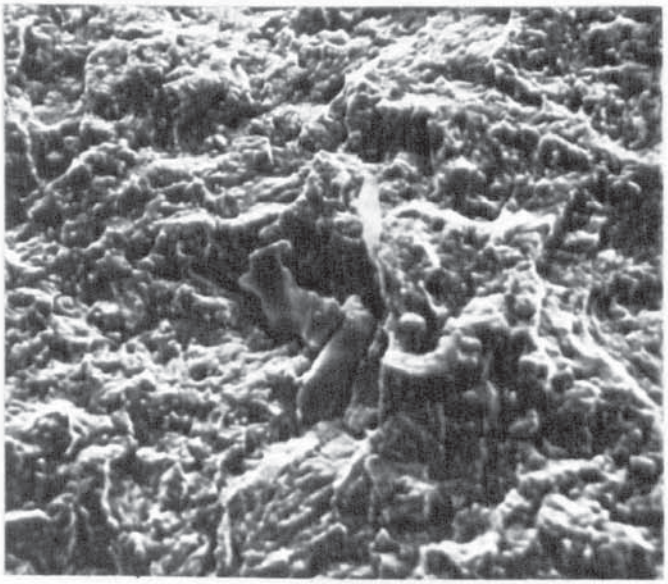

Specimen AZ2 X1100

Figure 20i Propagation Fractography of Material A tested at Room Temperature

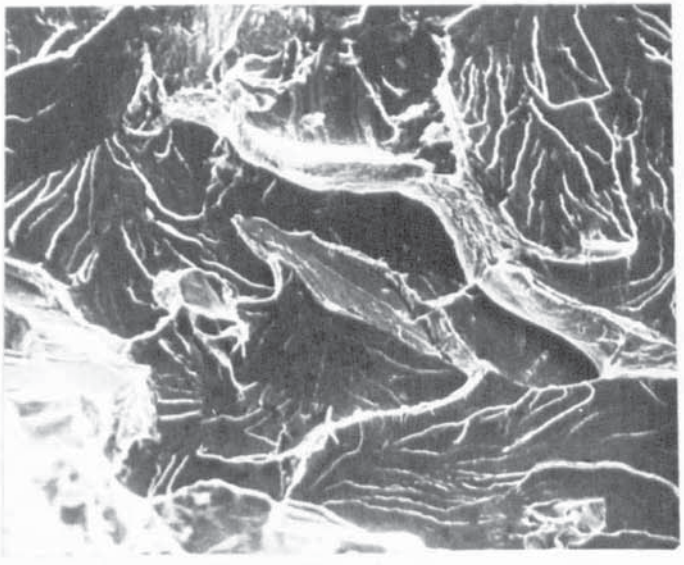

Specimen 6 X500

Figure 20j Propagation Fractography of Material B tested at Room Temperature

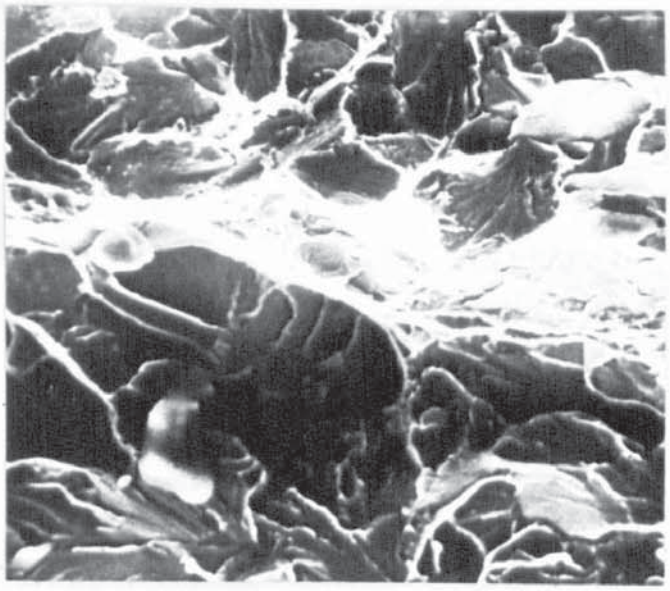

AZ Specimen AZ7 X1200

Figure 20k Propagation Fractography of Material A tested at + 50°C

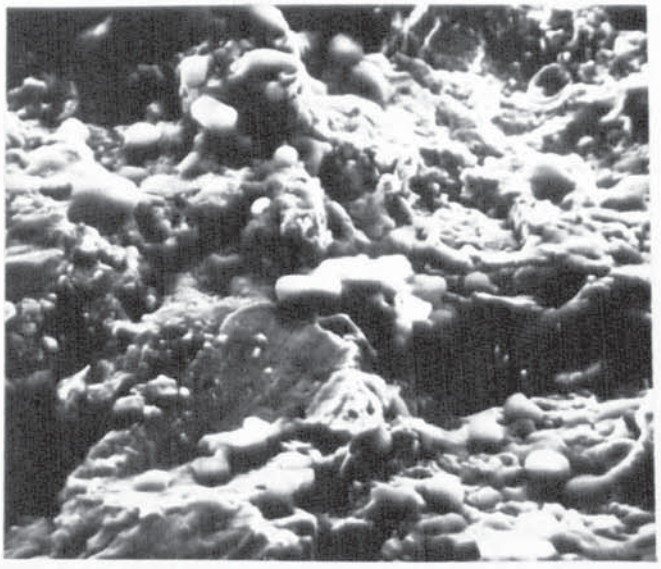

Specimen 2 X1200

Figure 20l Propagation Fractography of Material B tested at + 50°C

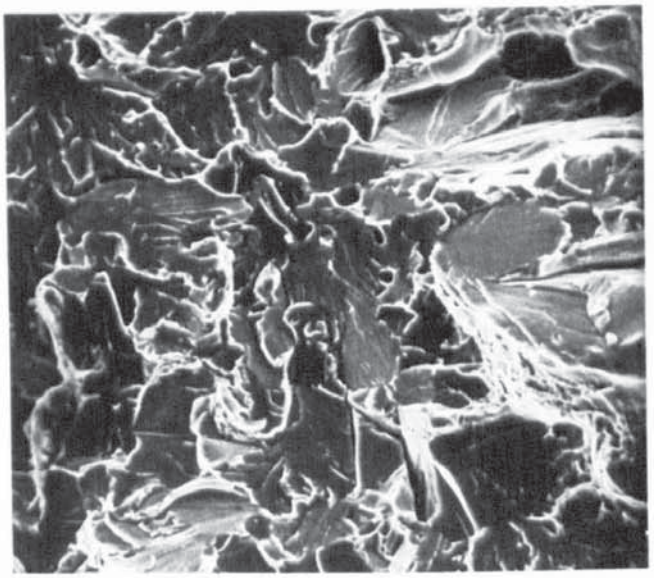

Specimen AZ47 X1100

Figure 20m Propagation Fractography of Material A tested at + 100°C

Specimen 45 X1100

Figure 20n Propagation Fractigraphy of Material B tested at + 100°C

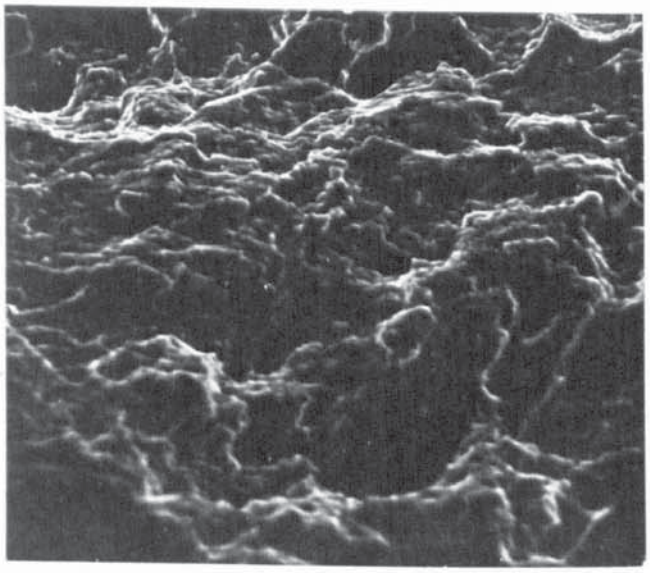

Specimen BZ9 X600

Figure 20p Propagation Fractography of Material A tested at - 100°C

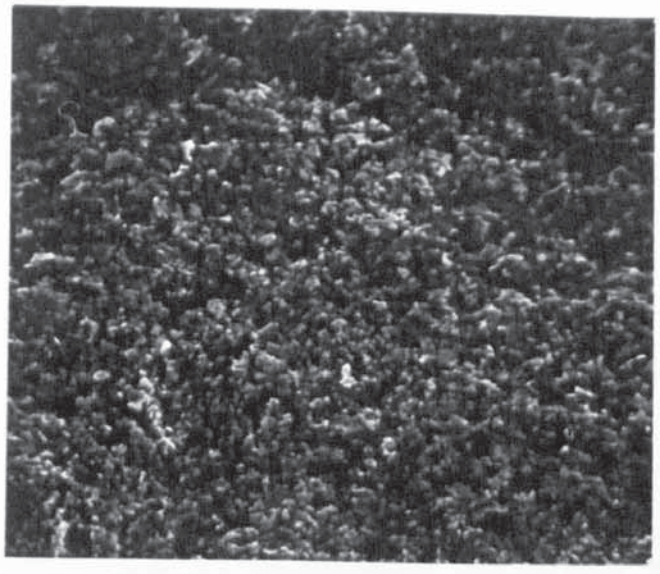

Specimen HT9 X1200

Figure 20r Propagation Fractography of Material B tested at - 100°C

A fatigue test at room temperature was provided to predict the plastic damage, which is believed to take place before a fatigue crack initiates. A specimen of 20.0 mm x 25 mm x 120 mm was chosen for this purpose. A sharp (namely 0.127 mm) notch root radius was machined in it, so that the uncracked ligament cross section was 20 mm x 20 mm. The specimen was mechanically polished using different grades of grinding paper as well as six and one microns diamond wheels. A servo-test machine used as well as a potential drop equipment to detect the crack. All conditions were the same as during fatigue tests at room temperature. Photographs of the surface in several stages of the tests will be shown in the next Chapter. Figure 22 shows the type of specimen used for this investigation. Figures 21, 23 and 24 show how the plastic zone formed as a result of slip lines at low magnification in figure 23 right and in detail in figure 23 left and 24. This replica was one out of fourteen replicas which were taken at such an investigation.

The tests mentioned in Chapter 2 Section 4 concerning the effect of a spark cut on a fatigue crack initiation showed that a fatigue crack always initiated earlier in a spark cut material to that without a cut. In this particular test the number of cycles required to initiate a fatigue crack, using identical conditions, was about 20% higher for those specimens not containing a spark cut than those with a spark cut.

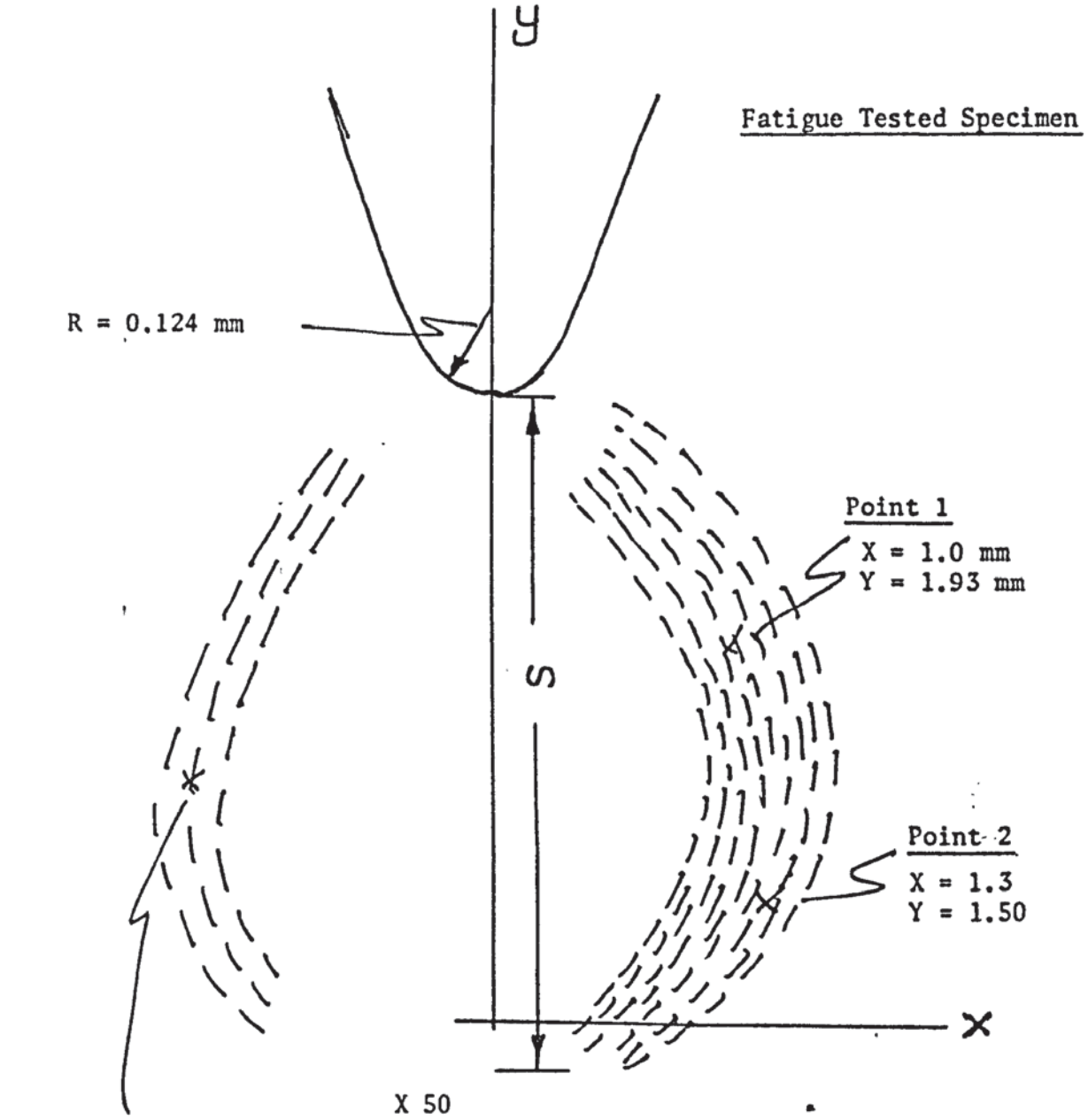

Figure 21

Represents a sketch of the top of the notch and slip lines formed due to the plastically deformed surface.

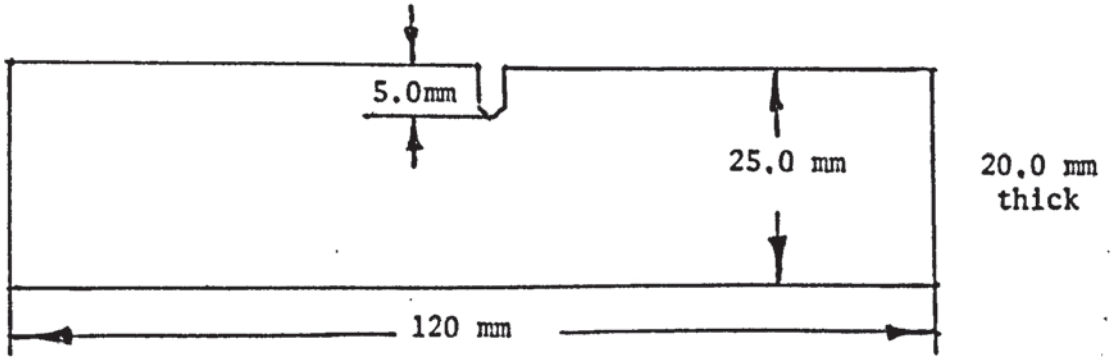

Figure 22

Dimensions of specimen used in this test.

No.	Condition of Test	$\Delta K/\rho^{\frac{1}{2}}$ (MN m^{-2})	mm.	Ni(cycles)
1	with spark cut	450	12.70	143,700
2	" " "	"		145,170
3	without spark cut	"	12.70	173,170
4	" " "	450	"	170,230

The last fatigue test was provided to material B after heat-treatment was carried out using specimens FT1, FT2 and FT3. These results showed that the number of cycles to initiate a fatigue crack was about the same found out for material A under the same conditions. These three specimens were tested at room temperature and produced the following results: (a = 5.0 mm. B = 20.0 mm, W = 25.0 mm and ρ = 0.127 mm)

Specimen code	$\Delta K/\rho^{\frac{1}{2}}$ MN m^{-2}	ΔK-3/2 MN m	Ni
FT1	1200	13.52	161400
FT2	1750	19.72	52000
FT3	2500	28.17	6900

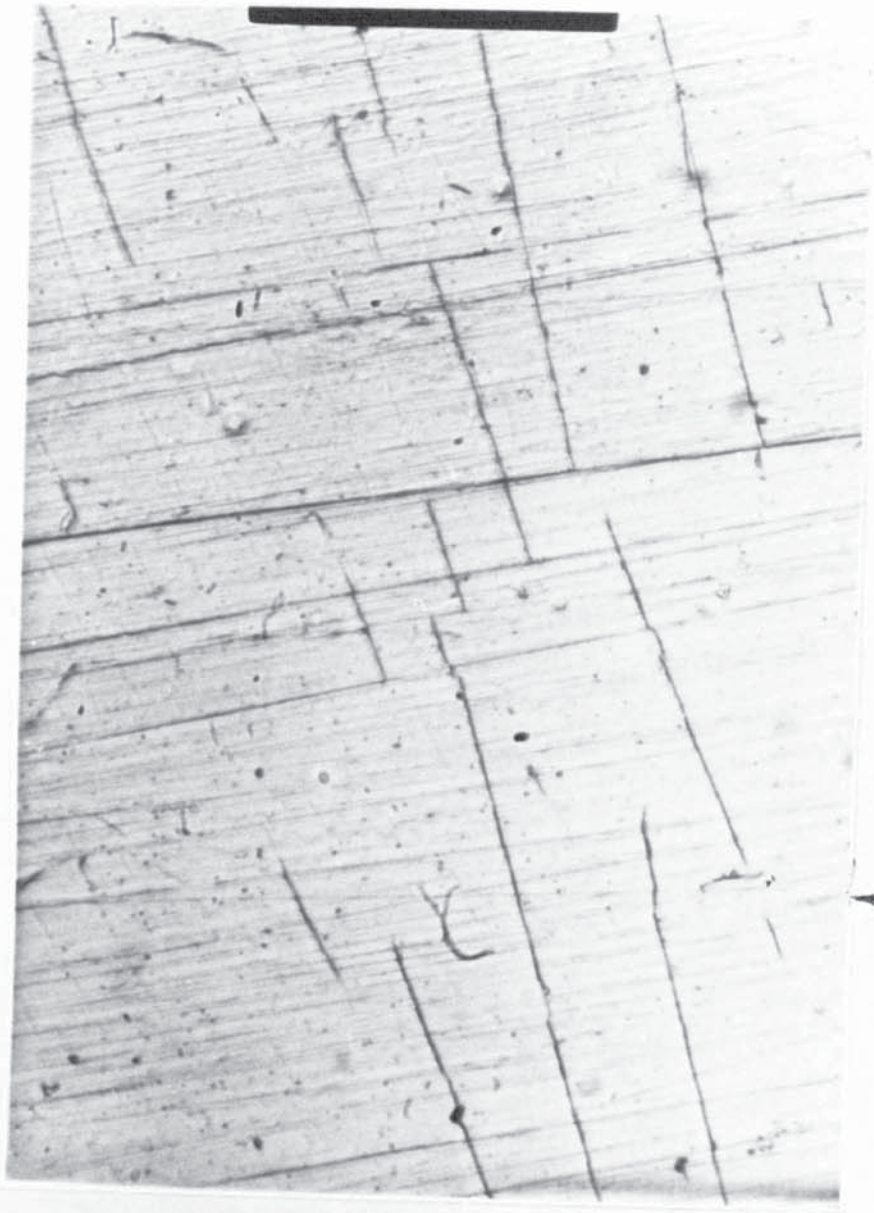

X400
Point 3

X50

Figure 23

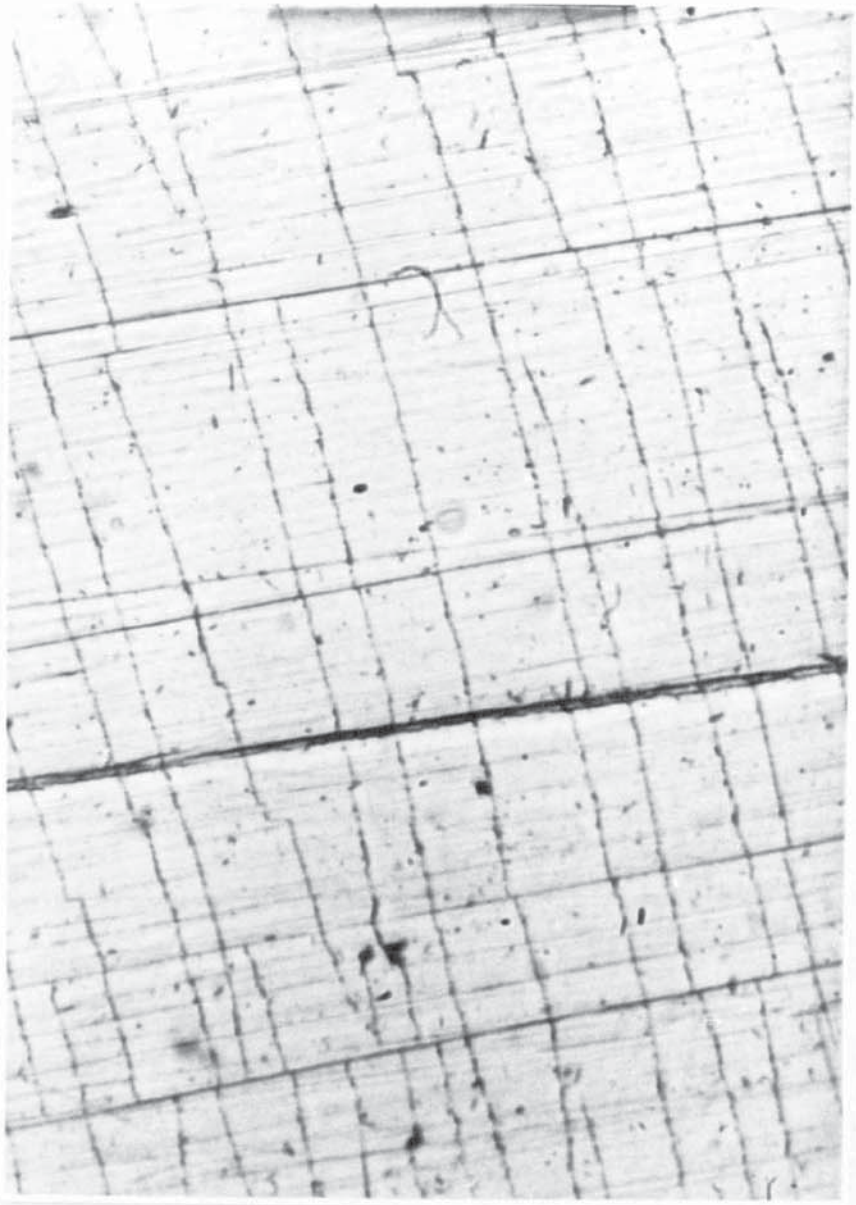

X400

Point 1 of figure 23

Figure 24

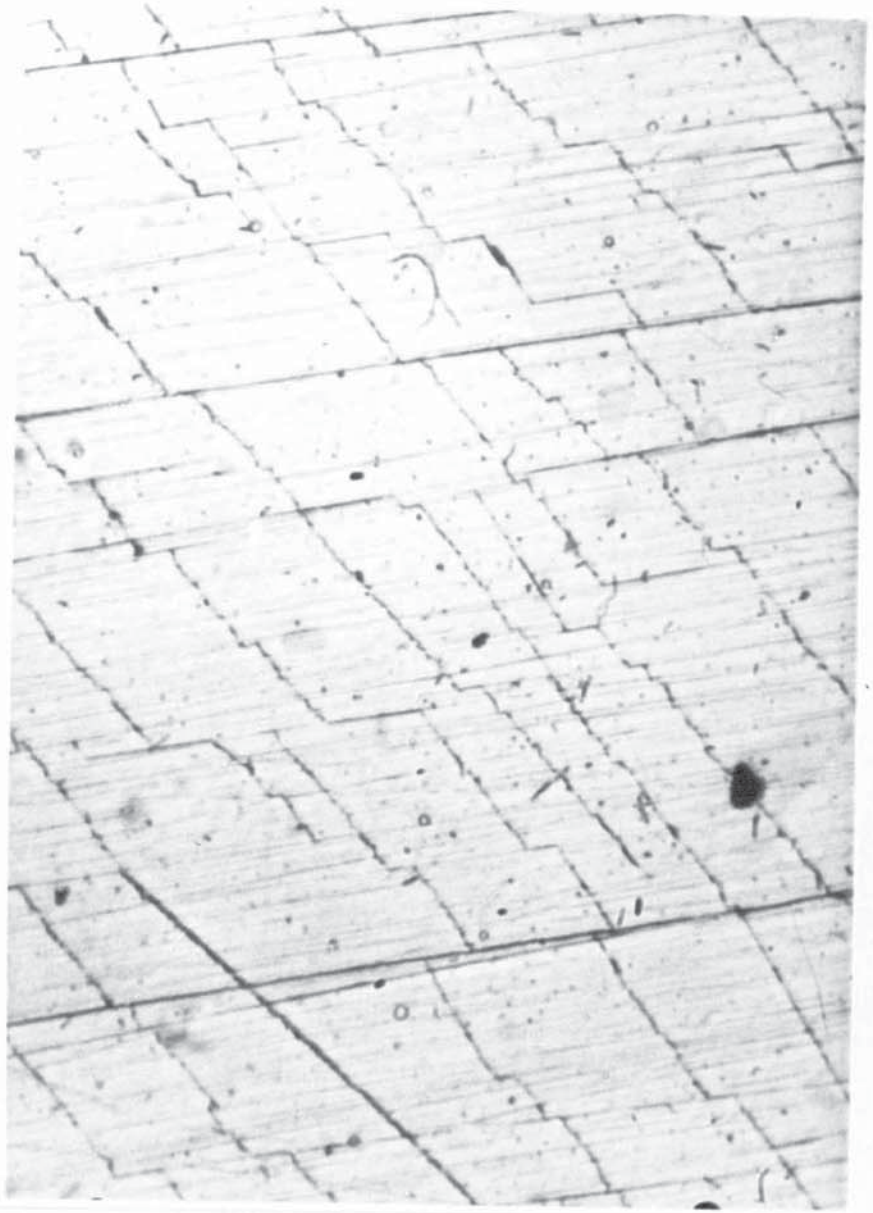

X400

Point 2 of figure 23

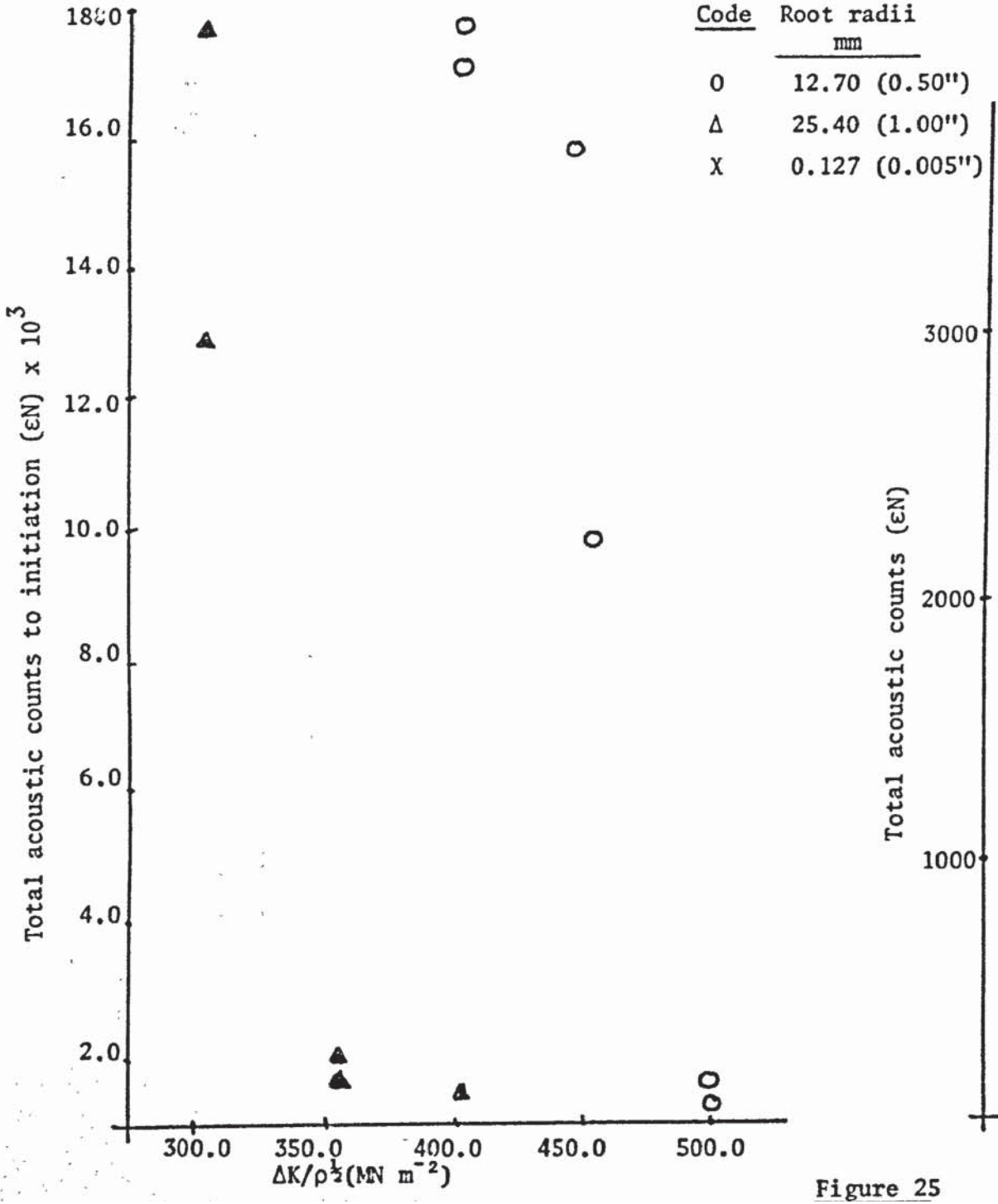

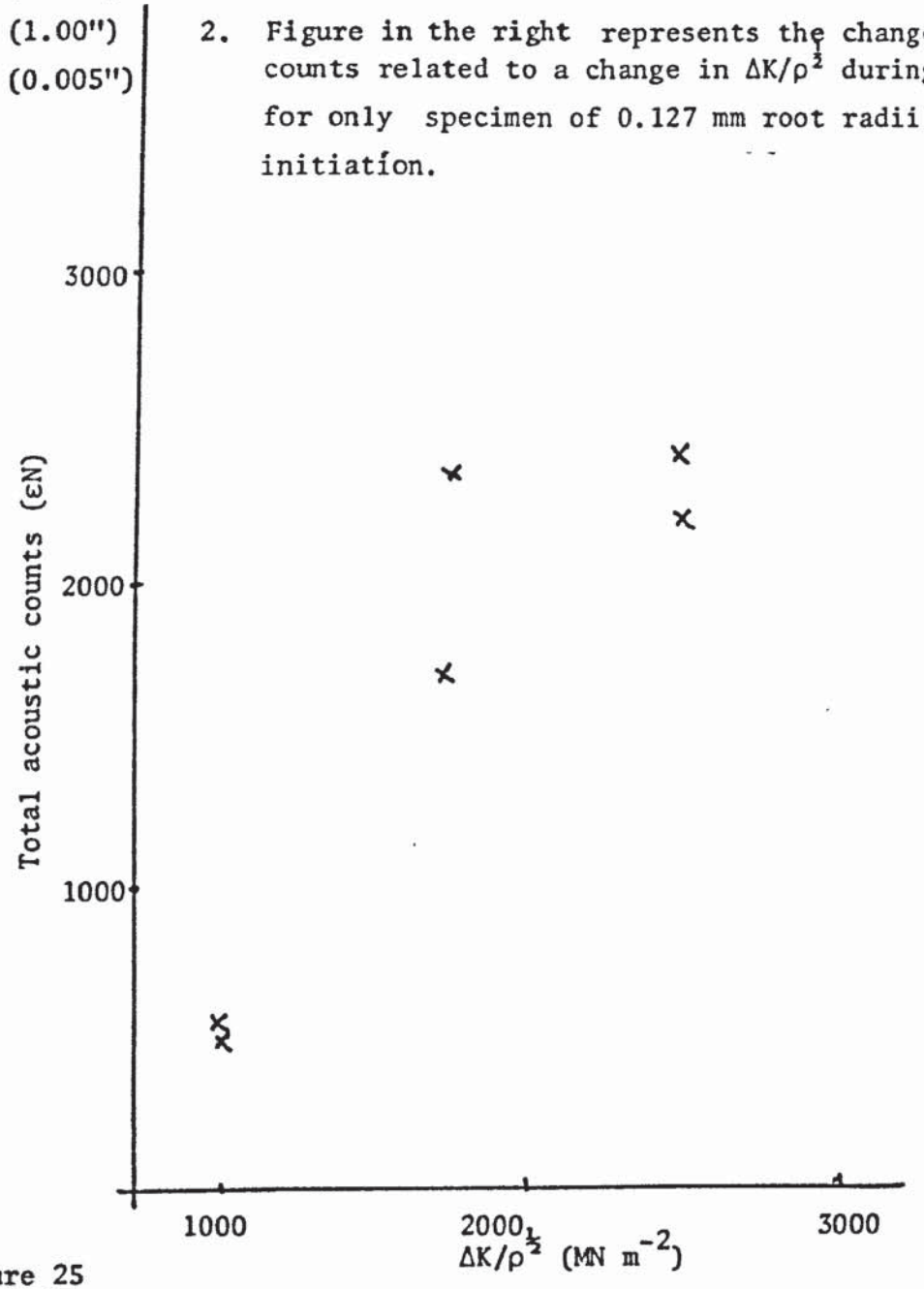

1. Figure left represents the change in total counts related to a change in $\Delta K/\rho^{\frac{1}{2}}$ during fatigue for 12 specimens with 1270 mm and 25.40 mm root radii only.
2. Figure in the right represents the change in total counts related to a change in $\Delta K/\rho^{\frac{1}{2}}$ during fatigue for only specimen of 0.127 mm root radii up to initiation.

Figure 25

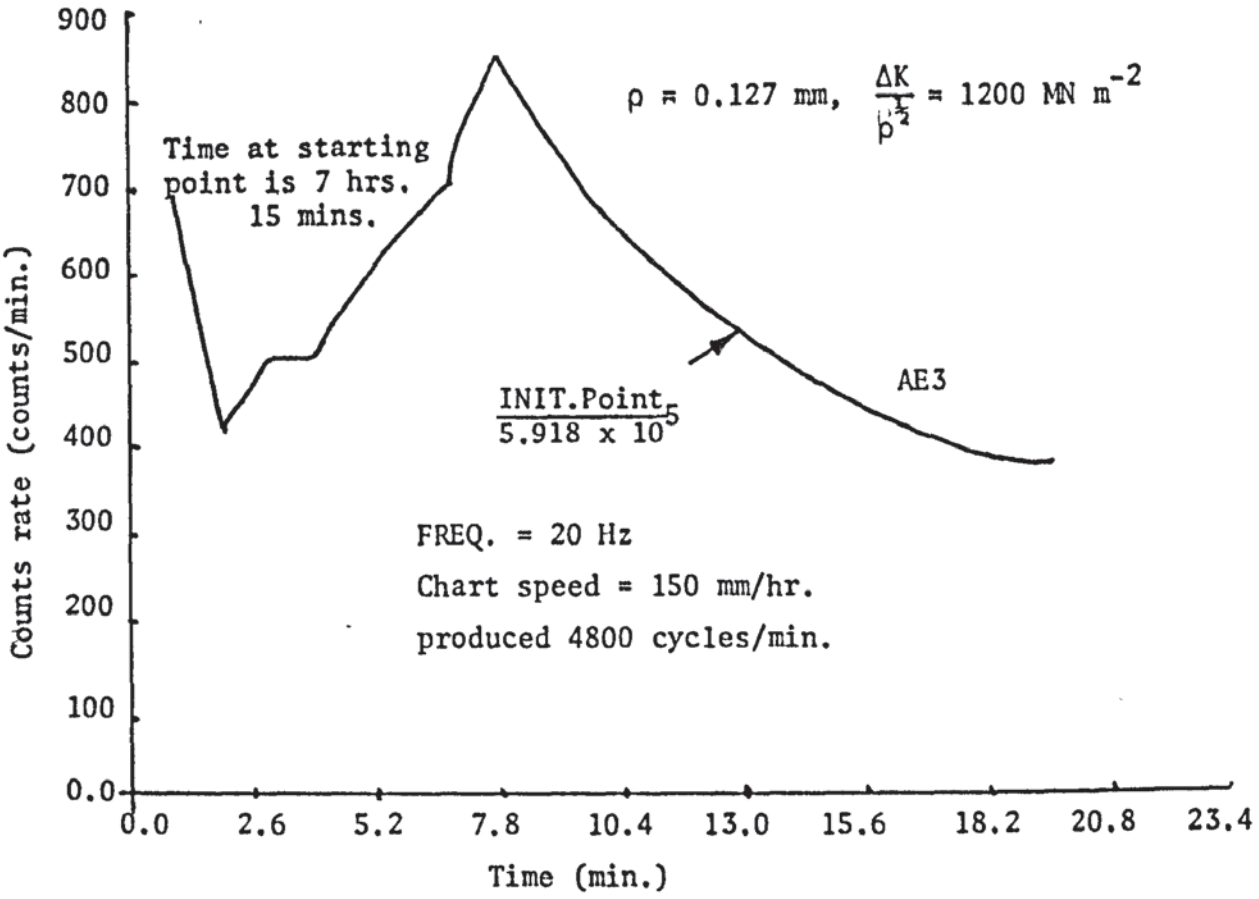

Figure 26

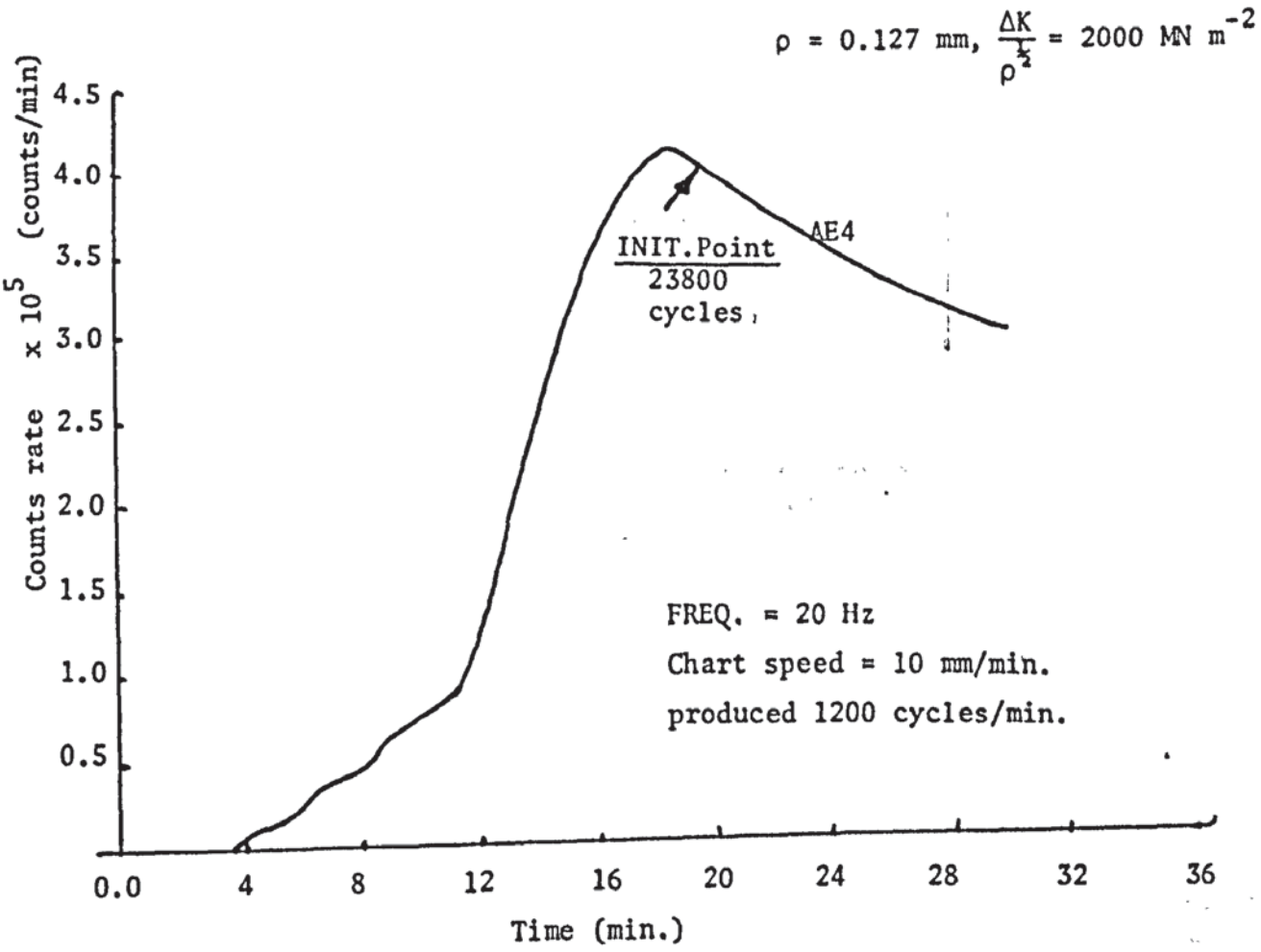

Figure 27

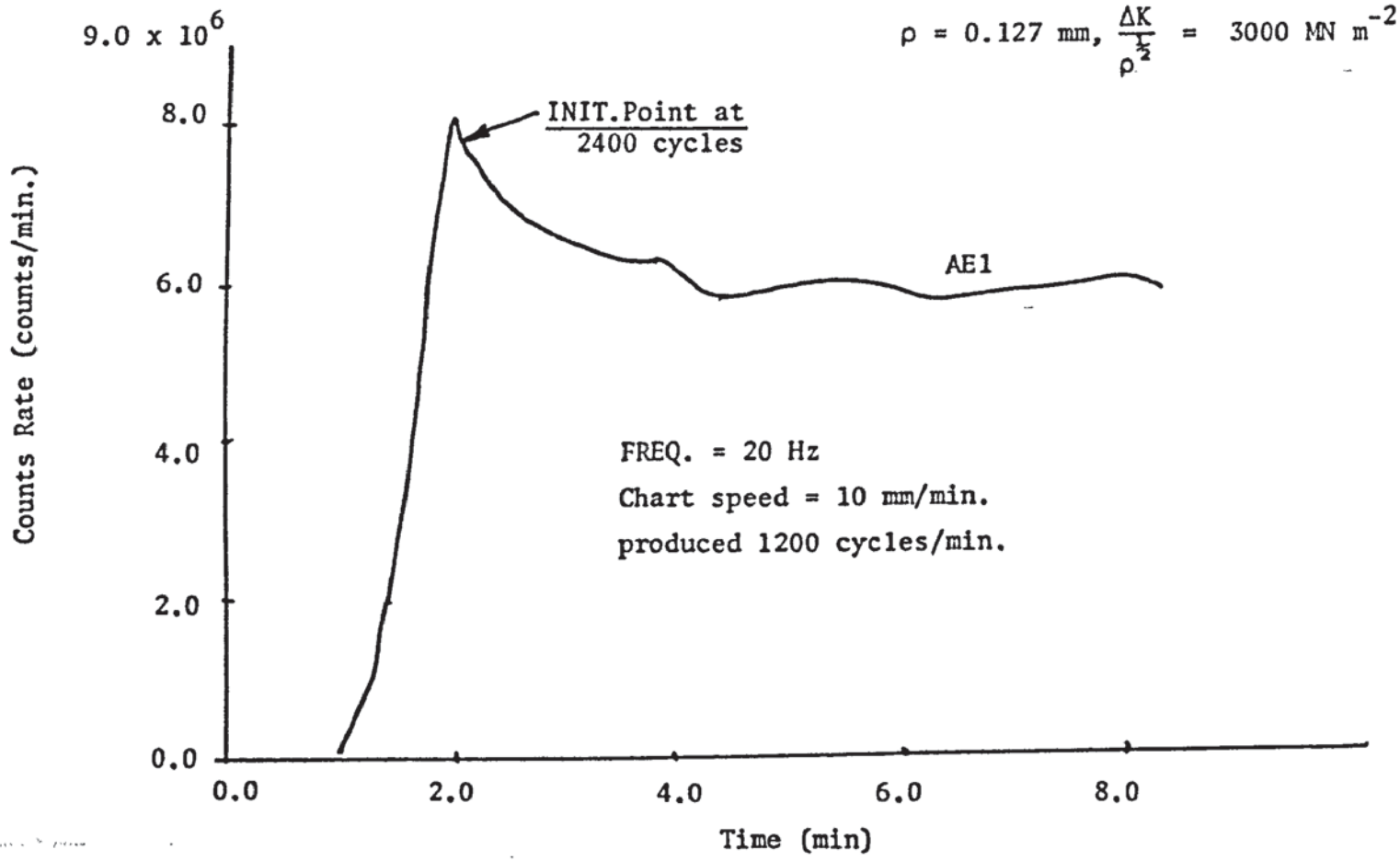
9.0 x 10^6
8.0
6.0
4.0
2.0
0.0
Counts Rate (counts/min.)
ρ = 0.127 mm, ΔK/ρ^½ = 3000 MN m^-2
INIT.Point at
2400 cycles
AE1
FREQ. = 20 Hz
Chart speed = 10 mm/min.
produced 1200 cycles/min.
0.0
2.0
4.0
6.0
8.0
Time (min)

Figure 28

ρ = 12.70 mm $\frac{\Delta K}{\rho^{\frac{1}{2}}}$ = 400 MN m^{-2}

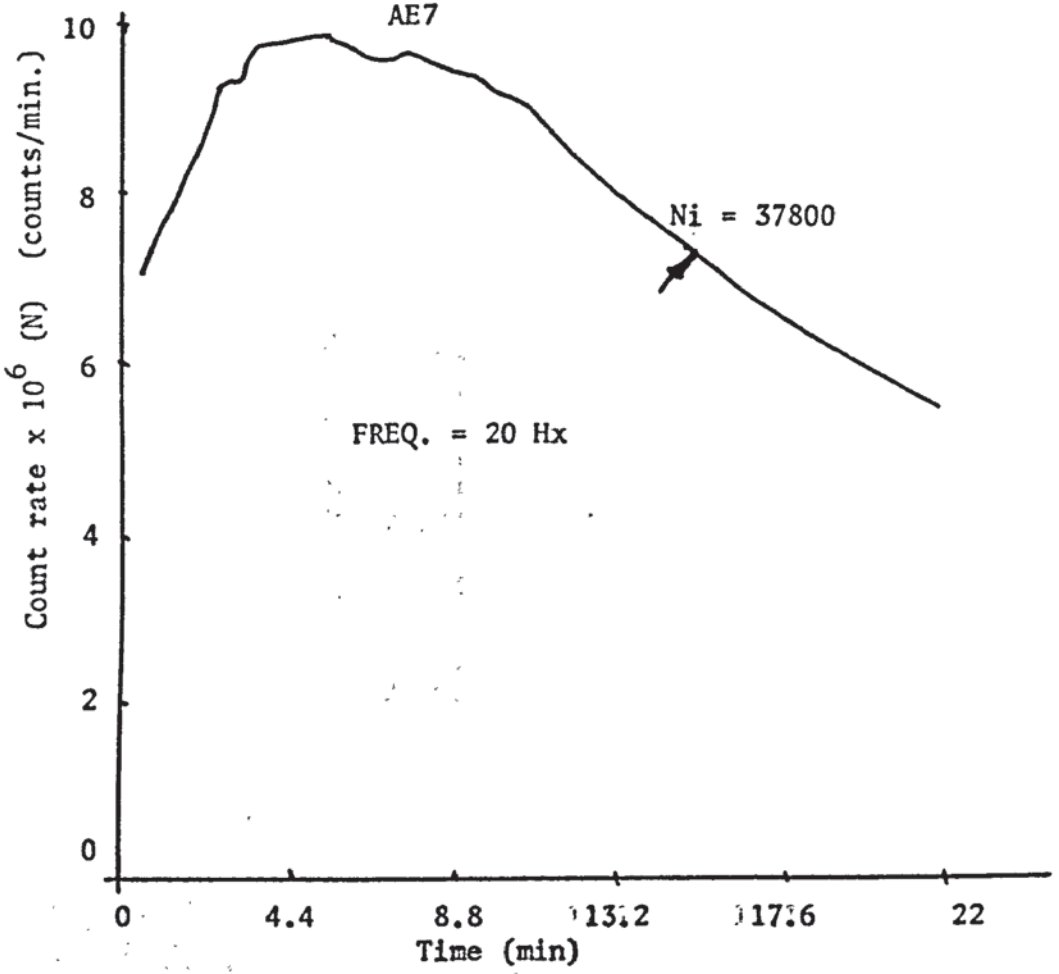

ρ = 12.70 mm, $\frac{\Delta K}{\rho^{\frac{1}{2}}}$ = 450 MN m^{-2}

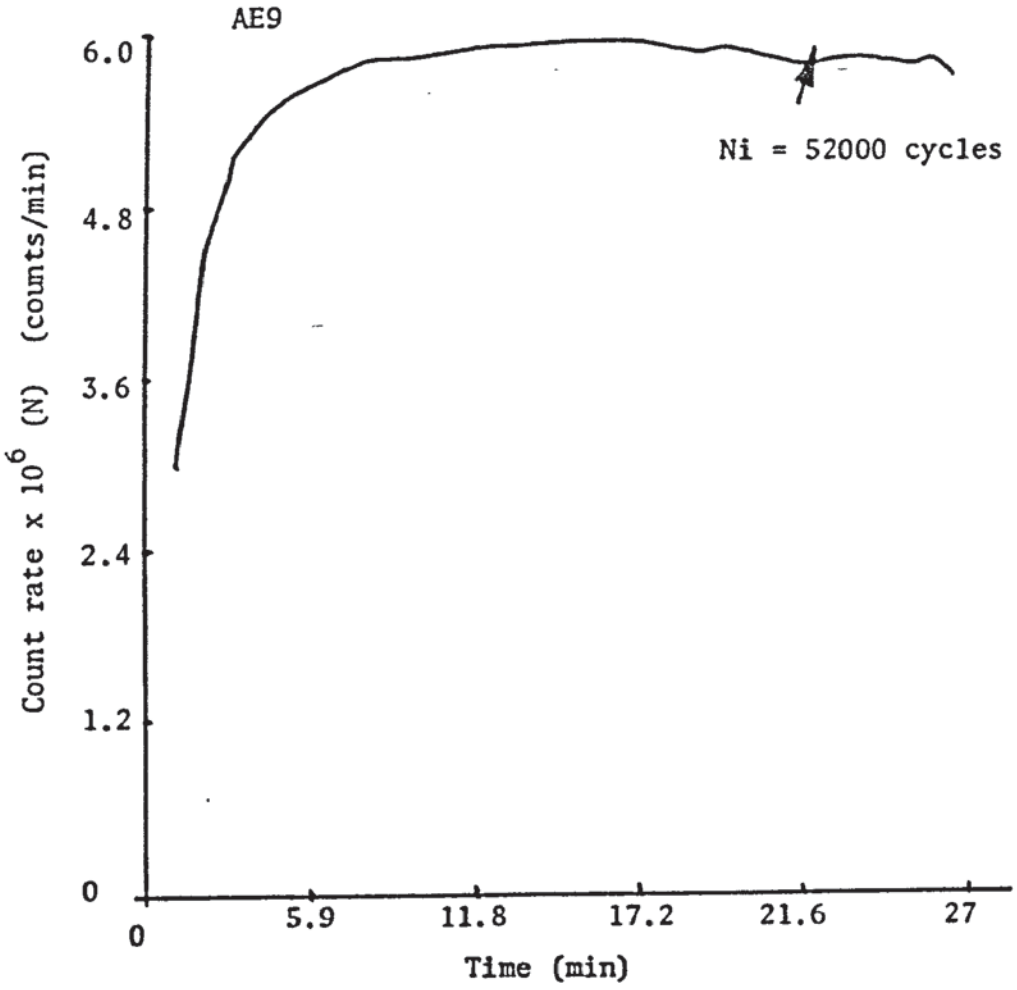

Figure 29

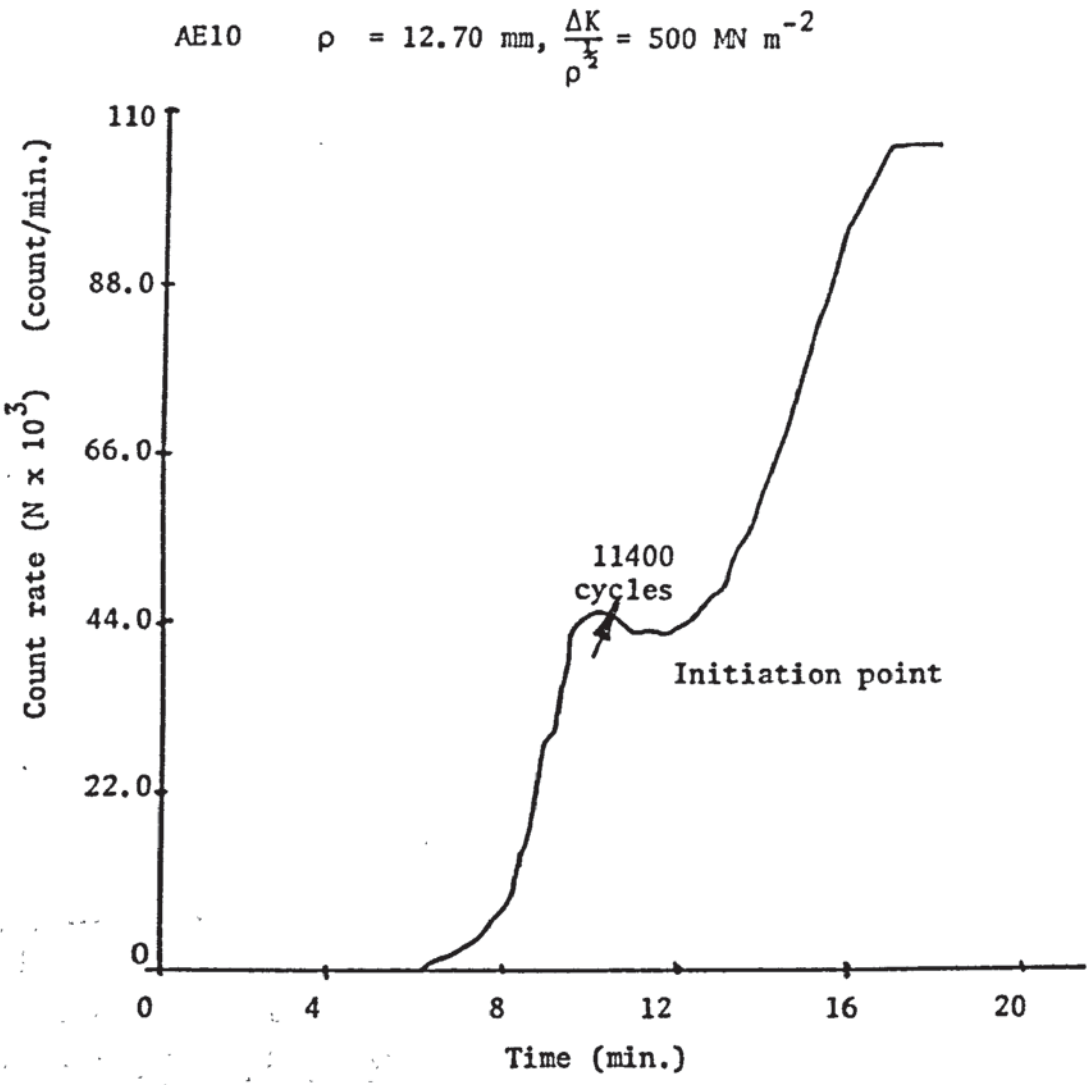
AE10 ρ = 12.70 mm, $\frac{\Delta K}{\rho^{\frac{1}{2}}}$ = 500 MN m^{-2}
Count rate (N x 10^3) (count/min.)
110
88.0
66.0
44.0
22.0
0
11400 cycles
Initiation point
0
4
8
12
16
20
Time (min.)

Figure 30

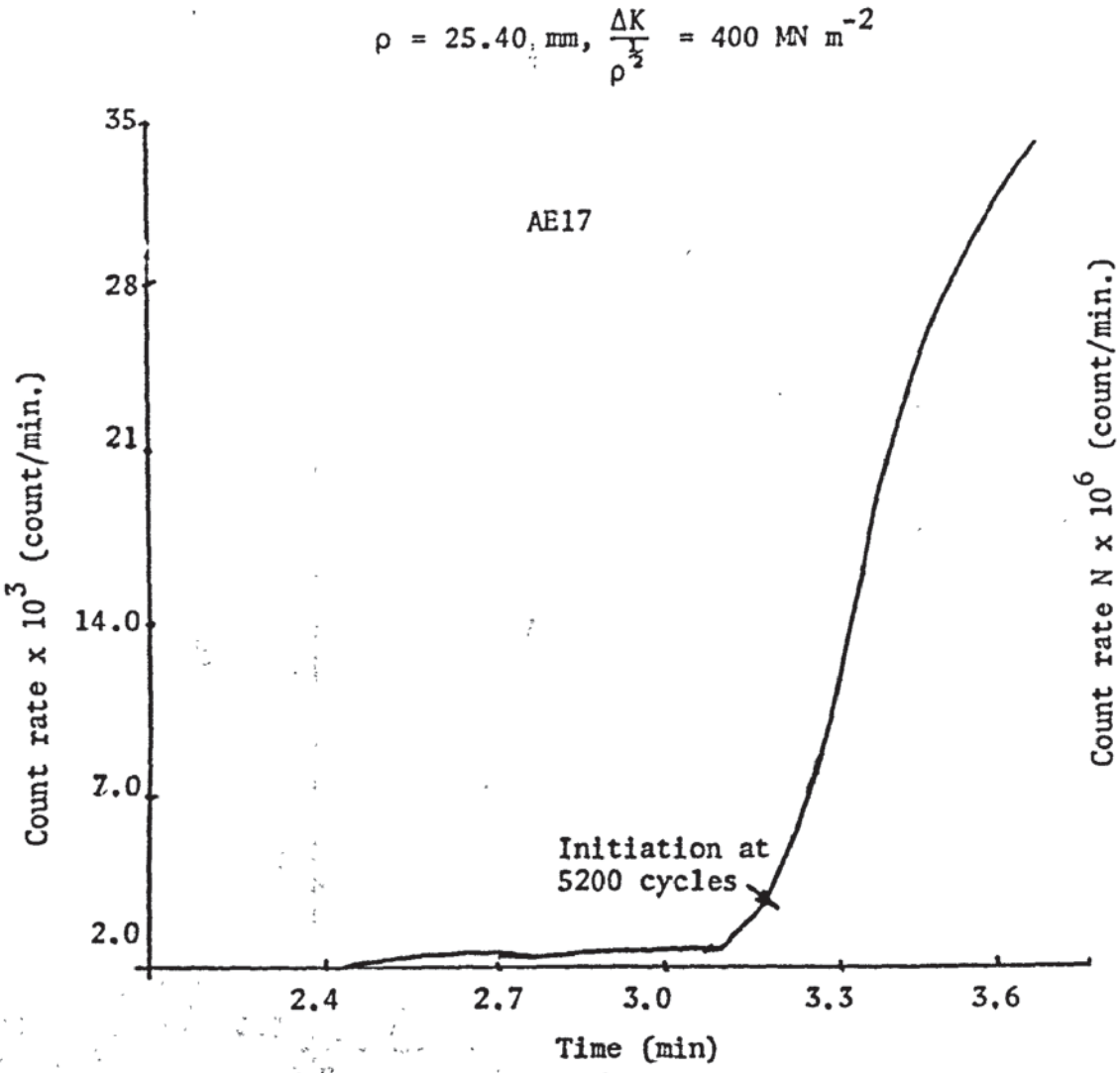

Figure 31

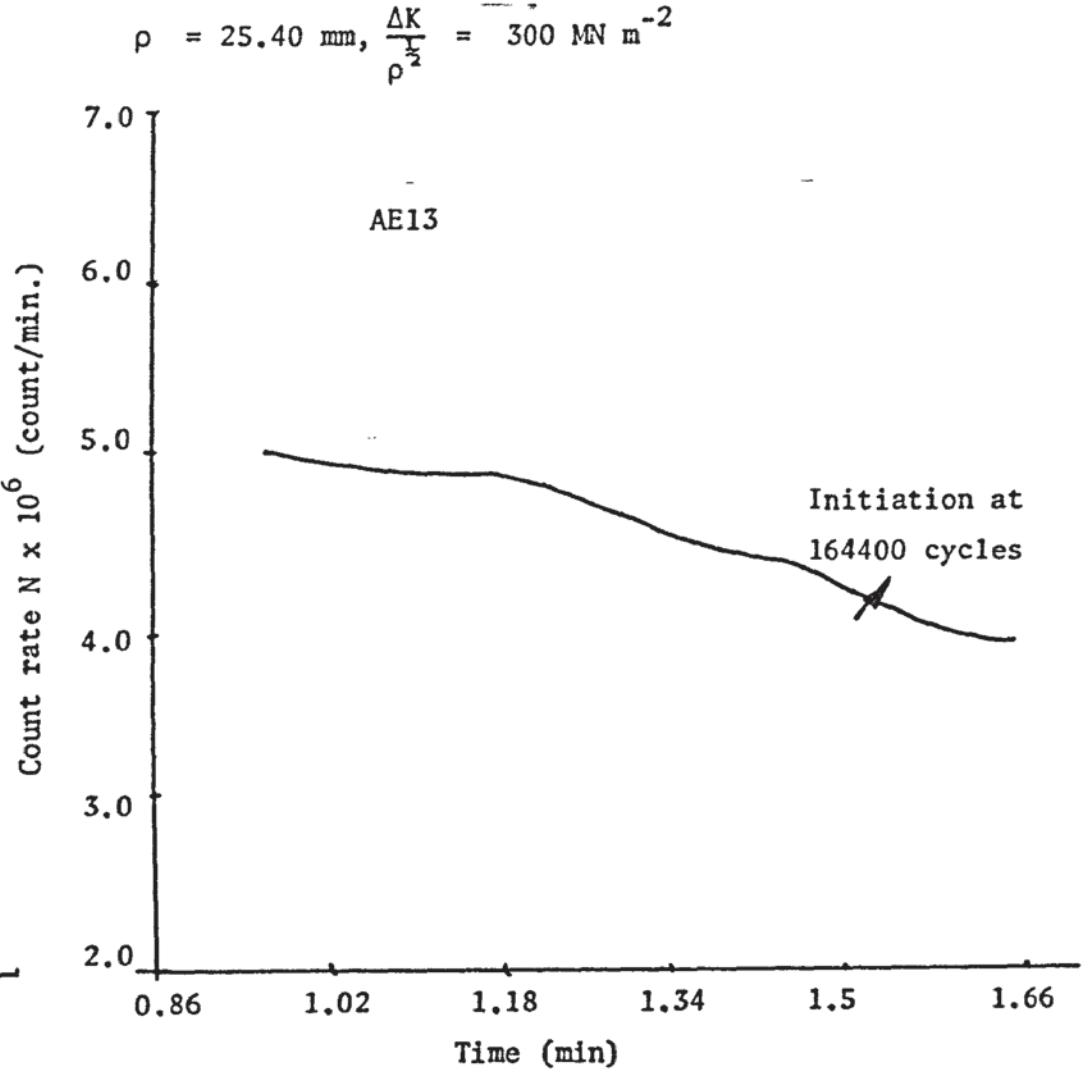

Figure 32

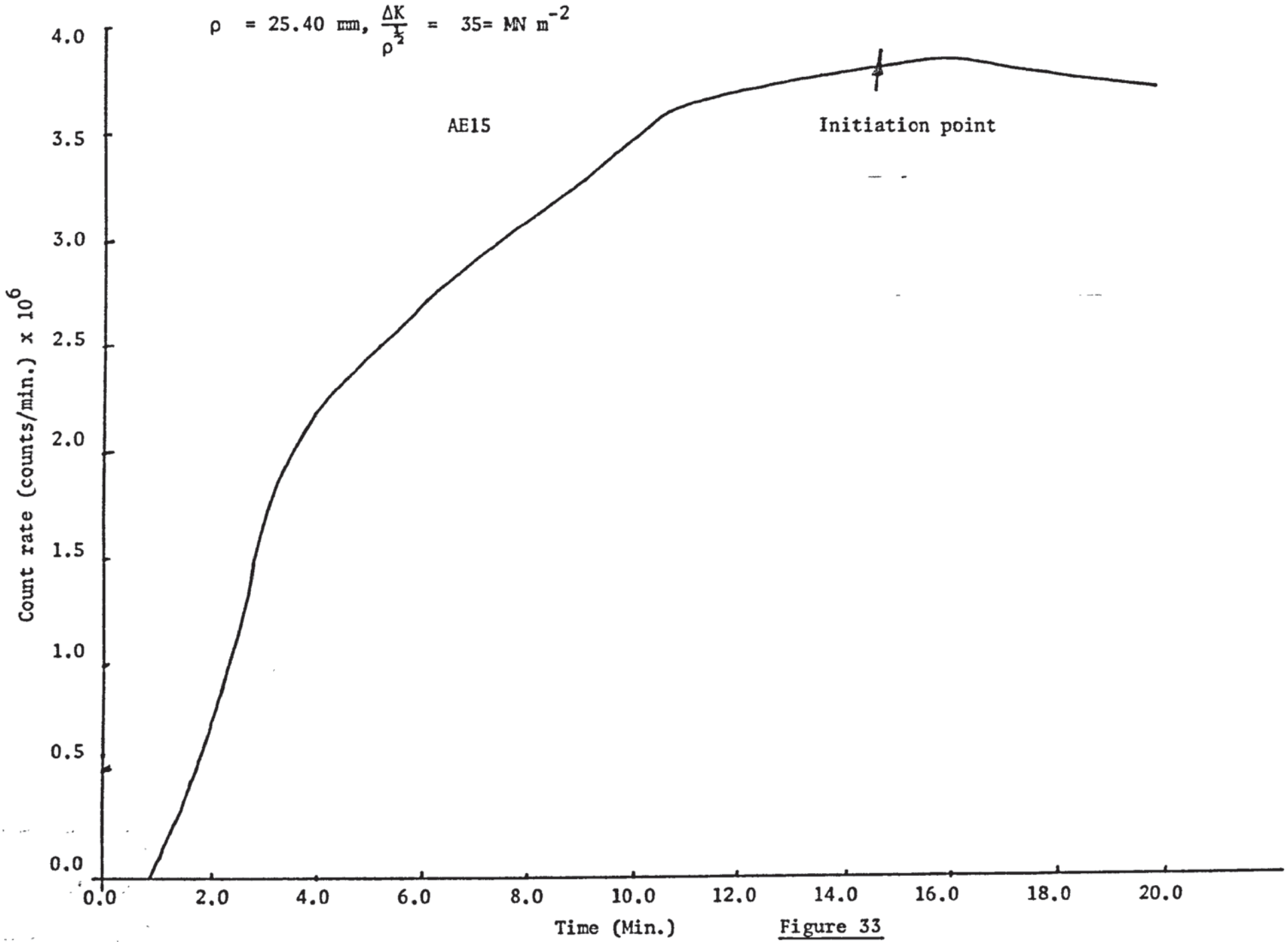
ρ = 25.40 mm, $\frac{\Delta K}{\rho^{\frac{1}{2}}}$ = 35= MN m^{-2}
AE15
Initiation point
Count rate (counts/min.) x 10^6
4.0
3.5
3.0
2.5
2.0
1.5
1.0
0.5
0.0
0.0
2.0
4.0
6.0
8.0
10.0
12.0
14.0
16.0
18.0
20.0
Time (Min.)

Figure 33

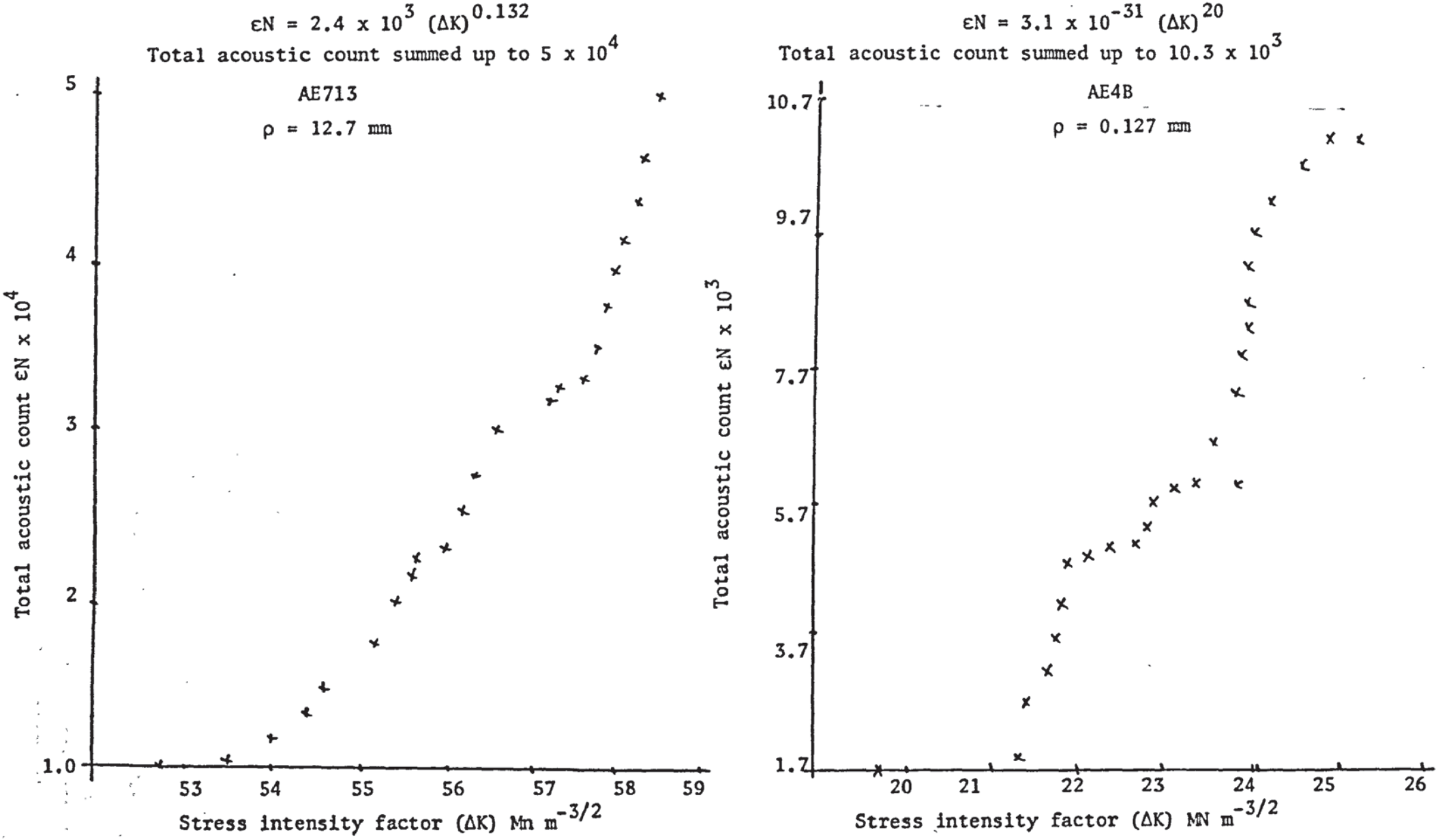
εN = 2.4 x 10^3 (ΔK)^0.132
Total acoustic count summed up to 5 x 10^4
AE713
ρ = 12.7 mm
Total acoustic count εN x 10^4
5
4
3
2
1.0
53
54
55
56
57
58
59
Stress intensity factor (ΔK) Mn m^-3/2
εN = 3.1 x 10^-31 (ΔK)^20
Total acoustic count summed up to 10.3 x 10^3
AE4B
ρ = 0.127 mm
Total acoustic count εN x 10^3
10.7
9.7
7.7
5.7
3.7
1.7
20
21
22
23
24
25
26
Stress intensity factor (ΔK) MN m^-3/2

Figure 34

Number	Specimen code	Notch root radius mm	$\Delta K/\rho^{\frac{1}{2}}$ MN m^{-2}	Total fatigue cycles to initiation Ni	Total acoustic counts at initiation	dB
1	AE1B	0.127	1000	1.35×10^6	500	62.4
2	AE2B	0.127	1000	1.90×10^6	570	62.4
3	AE3B	0.127	1750	6.3×10^4	2380	62.4
4	AE4B	0.127	1750	5.0×10^4	1700	62.4
5	AE5B	0.127	2500	2.8×10^3	2460	62.4
6	AE6B	0.127	2500	3.2×10^3	2200	62.4
7	AE11B	12.70	400	4.11×10^4	17200	62.4
8	AE12B	12.70	400	4.9×10^4	17800	62.4
9	AE7B	12.70	450	2.33×10^4	10000	63.0
10	AE8B	12.70	450	2.64×10^4	16200	62.4
11	AE9B	12.70	500	1.5×10^3	1700	62.4
12	AE10B	12.70	500	3.2×10^3	500	62.4
13	AE15B	25.40	300	5.76×10^4	13000	62.4
14	AE16B	25.40	300	8.32×10^4	18000	62.4
15	AE13B	25.40	350	11.64×10^3	2020	64.0
16	AE14B	25.40	350	14.15×10^3	1650	63.6
17	AE17B	25.40	400	3.72×10^3	1020	64.0
18	AE18B	25.40	400	1.8×10^3	420	64.0
19	AE3	0.127	1200	5.918×10^5	* 550	62.4
20	AE4	0.127	2000	2.38×10^4	$*4.1 \times 10^5$	62.4
21	AE1	0.127	3000	2.4×10^3	$*7.8 \times 10^6$	62.4
22	AE7	12.70	400	1.63×10^5	$*7.2 \times 10^6$	62.4
23	AE9	12.70	450	0.52×10^5	$*5.85 \times 10^6$	62.4
24	AE10	12.70	500	1.14×10^4	$*0.44 \times 10^6$	62.4
25	AE13	25.40	300	17.6×10^6	$*4.2 \times 10^6$	62.4
26	AE15	25.40	350	34.32×10^3	$*3.8 \times 10^6$	62.4
27	AE17	25.40	400	4.7×10^3	* 3200	62.4

Table 14 - Test results of a fatigue crack initiation with acoustic emission application.

* These values represent the count rate (counts/min).

4.2 Fatigue Test Results using Acoustic Emission Application

Table 14 contains the fatigue test results of 27 specimens. This table shows how the total acoustic emission count varies with load variation as well as for different values of notch root radii. The last nine specimens of this table show how the count rate at initiation changes by changing the value of the stress intensity factor as well as the notch root radii. For the first eighteen specimens in Table 14 the gain range from the amplifier was between 62.4 dB to 64.0 dB, while for the last nine specimens the gain was 75 dB. Table 14 was used to produce figures 25 - 33 which give the value of the total counts to the count or the count rate required for each specimen at certain loads to initiate a fatigue crack for sharp and blunt notch root radii. Figure 34 represents the relation of the acoustic emission counts to the stress intensity ofactor (ΔK) right from the initiation point of a fatigue crack for sharp and blunt notched specimens. This figure gives also the total counts for different values of (ΔK) where the total fatigue cycles are known.

Statistics were run for these specimens to calculate the material constants of the fatigue crack initiation law

$$Ni = B(\Delta K/\rho^{\frac{1}{2}})^{m}$$

and came out to be as follows:

Notch root radii (mm)	B	m
0.127	10^4	-4.80
12.70	$10^{2.9}$	-4.76
26.40	$10^{2.87}$	-4.82

On the other hand these constants came out to be for all specimens, regardless of the notch size $B = 10^{2.898}$, $m = 14.80$

The initiation point was carefully detected using the potential drop technique which was coincided (the initiation point) with the acoustic emission tracing. The voltage gain used through the acoustic emission system was within the range of (62.4 - 64.0)dB. This means

$$20 \log (\text{voltage gain}) = 62.4$$

$$\text{Voltage gain } \left(\frac{\text{output voltage}}{\text{input voltage}}\right) = \text{Anti log } \left(\frac{62.4}{20.0}\right)$$

therefore: Voltage gain = 1318.3

Although the potential drop and the acoustic emission techniques were detected the same point of a fatigue crack initiation, it was useful to provide the system with another element to check that. The recorded sound waves picked up by the recorder were analysed before, during and after the initiation took place. Permanent traces were provided and samples of these are shown in figure 35. Figure 35 indicates that there was no sign of acoustic emission pulses with a steady count rate before the fatigue crack has initiated, some pulses

were detected just before initiation and continued as the crack proceeded to grow. It was not possible to decide on a unique fixed count rate since the gain was varying from one specimen to another.

Going back to figure 34 which is again representative of the total acoustic emission count variation against the stress intensity factor in fatigue right after the initiation and through propagation for both sharp and blunt notches. The best fit to these two figures as an equation which was supposed to represent the crack propagation law statistically was found to be as:

1. $N_2 = 3.1 \times 10^{-31} (\Delta K)^{2.0}$ sharp notch
2. $N_2 = 2.4 \times 10^{3} (\Delta K)^{0.132}$ blunt notch.

Results plotted in figure 25 show how the total number of acoustic counts varies with $(\Delta K/\rho^{\frac{1}{2}})$. So far the results are still not complete in fatigue. Figures 36, 37 and 38 represent three specimens with a notch root radii of 0.127 mm, 12.7 mm and 25.4 mm respectively. In all these figures and before any plastic damage could take place the acoustic emission recorder was plotting an equally spaced lines which represents a full scale deflection reading in each case. These figures indicate that the spread becomes wider after a period of time (during plastic deformation). This indicates that as plastic damage takes place it suddenly effects the elastic wave of the acoustic emission. The results of these three tests produced the following results in total counts.

Specimen code	Notch Root Radii (mm)	Total acoustic counts the onset* of plastic deformation	Total of counts at initiation	Figure corresponding.
AE4	0.127	2.34×10^6	2.811×10^6	36
AE7	12.70	96.0×10^6	109.82×10^6	37
AE13	25.40	105.0×10^6	175.65×10^6	38

* The onset of plastic deformation was taken to be indicated by the reduction in rate of acoustic emission counts as indicated by wider spacings of the lines, for example, in figures 36, 37 and 38.

4.3 Fracture Toughness Tests Results at five different temperatures

It was shown earlier in Section 2.3.4 that two types of specimens were treated for the fracture toughness tests namely 20 mm x 25 mm x 120 mm and 40 mm x 50 mm x 240 mm. Tables 15 and 16 contain the results produced from this work. The first seven columns of each figure show the details of material A beginning from the number of specimens and ending with the notch root radii. The other right hand side of these tables shows the results of material B produced from the test. The average K_C(MN $m^{-3/2}$) value of each condition of each material at different temperatures could be estimated from these tables. Although the K_C value of each material was not the same at all temperatures, but the average value could be written as follows:

Average K_C values derived from J-Integral technique

Material \ Temp.	Room temperature	+50°C	+100°C	-50°C	-100°C
A	147.17 MN $m^{-3/2}$	174.3	150.00	48.14	25.42
B	139.00	159.04	154.66	47.58	24.35

Valid K_{IC} was as follows at room temperature:

Material A 165.2 MN $m^{-3/2}$

Material B 154.0 MN $m^{3/2}$

Figures 39 and 40 represent the ductile and cleavage fractures of both materials taken after the fracture toughness tests were provided.

Material A σ_y = 525 MN m^{-2}							Material B σ_y = 425 MN m^{-2}						
Number	Specimen Code	B x W mm x mm	Testing temperature °C	P_Q KN	K_C Using the J-integral MN $m^{-3/2}$	Notch Root radius mm	Number	Specimen code	B x W mm x mm	Testing temperature	P_Q KN	K_C using the J-integral MN $m^{-3/2}$	Notch Root radius mm
1	FAZ15	20 x 25	25	18.0	146.16	o.127	1	FBZ1	20 x 25	+25	18.2	146.7	0.127
2	FAZ30	"	25	12.0	99,38	12.70	2	FBZ2	"	+25	14.0	105.0	12.70
3	FAZ13	"	25	15.0	128.44	25.40	3	FBZ3	"	+25	15.6	130.00	25.46
4	FBZ21	"	+50	16.9	133.58	0.127	4	FBZ4	"	+50	16.0	131.0	6.127
5	FAZ31	"	+50	7.5	66.85	12.70	5	FBZ5	"	+50	12.0	99.38	12.70
6	FAZ14	"	+50	16.44	155.33	25.40	6	FBZ6	"	+50	15.0	128.44	25.40
7	FBZ22	"	+100	13.95	111.0	0.127	7	FBZ7	"	+100	14.00	111.50	0.127
8	FAZ32	"	+100	16.94	126.42	12.70	8	FBZ8	"	+100	16.40	155.0	12.70
9	FAZ20	"	+100	13.95	122.30	25.40	9	FBZ9	"	+100	15.0	128.44	25.40
10	FBZ23	"	-50	8.00	67.0	0.127	10	FBZ10	"	-50	7.5	66.90	0.127
11	FAZ33	"	-50	6.70	47.63	12.70	11	FBZ11	"	-50	6.5	47.00	12.70
12	FAZ21	"	-50	4.00	30.36	25.40	12	FBZ12	"	-50	3.8	29.40	25.40
13	FBZ20	"	-100	3.99	28.41	25.40	13	FBZ13	"	-100	2.5	22.30	0.127
14	FBZ24	"	-100	4.0	25.00	0.127	14	FBZ14	"	-100	3.5	25.00	12.70
15	FAZ34	"	-100	2.80	22.00	12.70	15	FBZ15	"	-100	2.8	23.60	25.40

Table 15 - Fracture toughness tests results of both materials at five different temperatures
All specimens are prefatigued ($\frac{a}{W}$ = 0.5)

	Speci-men Code	B x W mm x mm	Testing temper-ature °C	P_Q KN	K_C using the J-integral MN $m^{-3/2}$	Notch Root radius mm		Speci-men Code	B x W mm x mm	Testing temper-ature °C	P_Q KN	K_C using the J-integral MN $m^{-3/2}$	Notch Root radius mm
1	FZ1	40 x 50	+25	67.8	227.86	0.127	1	FB1	40 x 50	+25	35.00	160.0	0.127
2	FZ6	"	+25	50.0	152.88	12.70	2	FB2	"	+25	52.00	154.0	12.70
3	FZ14	"	+25	34.0	128.31	25.40	3	FB3	"	+25	40.00	137.5	25.40
4	FZ2	"	+50	69.75	216.83	0.127	4	FB4	"	+50	62.00	180.0	0.127
5	FZ7	"	+50	56.0	182.75	12.70	5	FB5	"	+50	56.00	180.78	12.70
6	FZ11	"	+50	65.76	183.36	25.40	6	FB6	"	+50	60.00	175.00	25.40
7	FZ3	"	+100	64.80	188.10	0.127	7	FB7	"	+100	62.00	180.00	0.127
8	FZ8	"	+100	63.80	169.80	12.70	8	FB8	"	+100	61.80	177.00	12.70
9	FZ12	"	+100	63.31	182.64	25.40	9	FB9	"	+100	60.50	176.00	25.40
10	FZ4	"	-50	15.94	50.0	0.127	10	FB10	"	-50	15.50	49.00	0.127
11	FZ10	"	-50	15.05	47.33	12.70	11	FB11	"	-50	14.50	45.00	12.70
12	FZ13	"	-50	18.00	46.51	25.40	12	FB12	"	-50	17.00	47.00	25.40
13	FZ5	"	-100	10.90	28.30	0.127	13	FB13	"	-100	11.53	30.05	0.127
14	FZ9	"	-100	10.00	25.80	12.70	14	FB14	"	-100	9.72	24.00	12.70
15	FZ15	"	-100	9.6	23.0	25.40	15	FB16	"	-100	8.5	21.15	25.40

Table 16. Fracture toughness tests results of both materials at five different temperatures..
All specimens are prefatigued ($\frac{a}{W} = 0.5$)

4.4 Results of fracture toughness tests using the acoustic emission application tests enabled to obtain the following traces:

1. Load v.s. load point deflection.
2. Load v.s. crack opening displacement.
3. Load v.s. time.
4. Load v.s. voltage.
5. Time v.s. total acoustic counts.

To relate these to Table 17 one should keep in mind that the first eight specimens in the left hand side of this table contain three different notch root radii namely 0.127 mm, 12.70 mm and 25.40 mm. Although these specimens contained both sharp and blunt notches, they were still considered as sharply notched, because a crack was prefatigued in each one to the required depths shown in Table 17 (a/W).

Figures 41, 42 and 43 show how load varies with load point deflection and indicates the values of the acoustic counts at any load for all three notch root radii. Figure 44 represents the shape of the plastic zone for specimens containing different notch geometry at the fracture point during monotoning loading tests. Figure 45 produced from Table 17 clearly indicates the change in total acoustic counts as the ratio of crack length to width ($\frac{a}{W}$) changes for all specimens concerned, since there is no point in comparing the root radii with the total acoustic counts. The average value of K_C for all these eight specimens tested was found to be equal to 143.4 MN $m^{-3/2}$ using the J-integral method. The (LEFM) method was not reliable without the use of the potential drop to detect the initiation period of fracture.

* L.E.F.M.

Material B Pre-fatigues

Number	Specimen Code	Notch root radius mm.	$\frac{a}{W}$	K_C (J-integral) MN $m^{-3/2}$ *	Total counts at fracture
1	F1	0.127	0.26	158/155	5000
2	F2	0.127	0.26	134.131	4605
3	F3	12.70	0.34	104/100	810
4	F4	12.70	0.34	126/124	1214
5	F5	25.40	0.50	150/147	1200
6	F6	25.40	0.50	221/216	1540
7	F7	0.127	0.60	122/120	2125
8	F8	0.127	0.60	131/128	2400

Material B notches as machined (no pre-fatiguing)

Number	Specimen Code	Notch root radius mm	$\frac{a}{W}$	K_C (J-integral) MN $m^{-3/2}$ *	Acoustic emission count rate (counts/min)	
1	FA1	0.127	0.5	104/103	7.5×10^5	
2	FA2	0.127	0.50	100/98	10.0×10^5	stress coated specimen
3	FA3	0.250	0.50	107/105	1.35×10^5	
4	FA4	0.250	0.50	112/110	0.9×10^5	stress coated specimen
5	FA5	0.500	0.50	114/112	5.7×10^5	
6	FA6	0.500	0.50	117/115	8.0×10^5	stress coated specimen
7	FA7	1.50	0.50	114/112	53×10^5	stress coated specimen
8	FA8	1.50	0.50	121/118	25×10^5	

Table 17. Fracture toughness test results of material B applying to acoustic amission technique.

On Specimens 20 mm x 25.0 mm x 120 mm.

slow propagation pattern

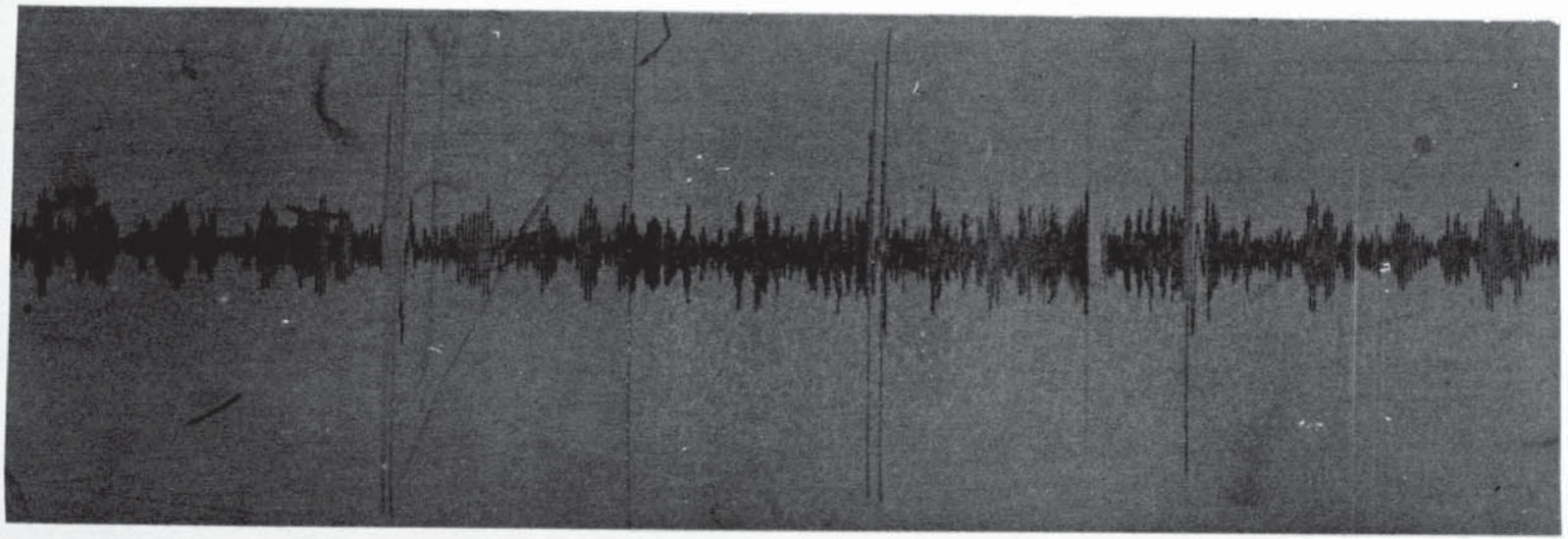

Figure 35.

Fatigue crack before and after initiation

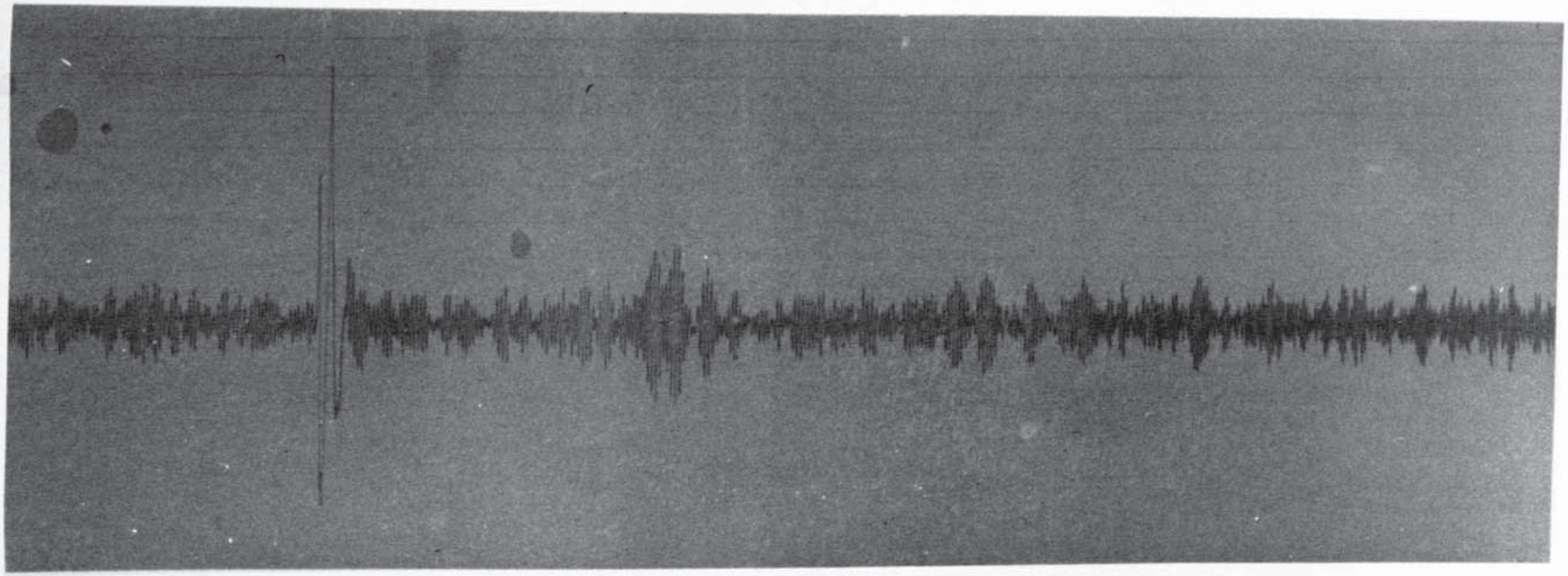

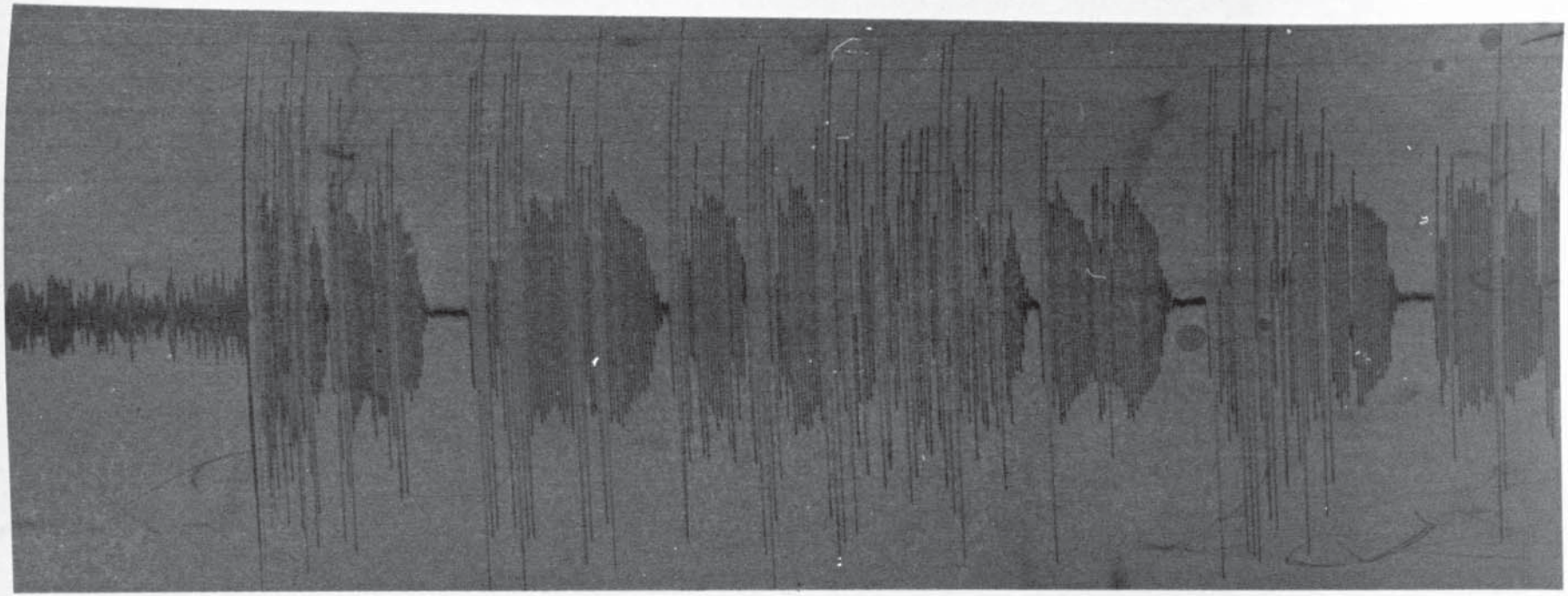

Figure 35 cont'd.,

Fast crack propagation pattern

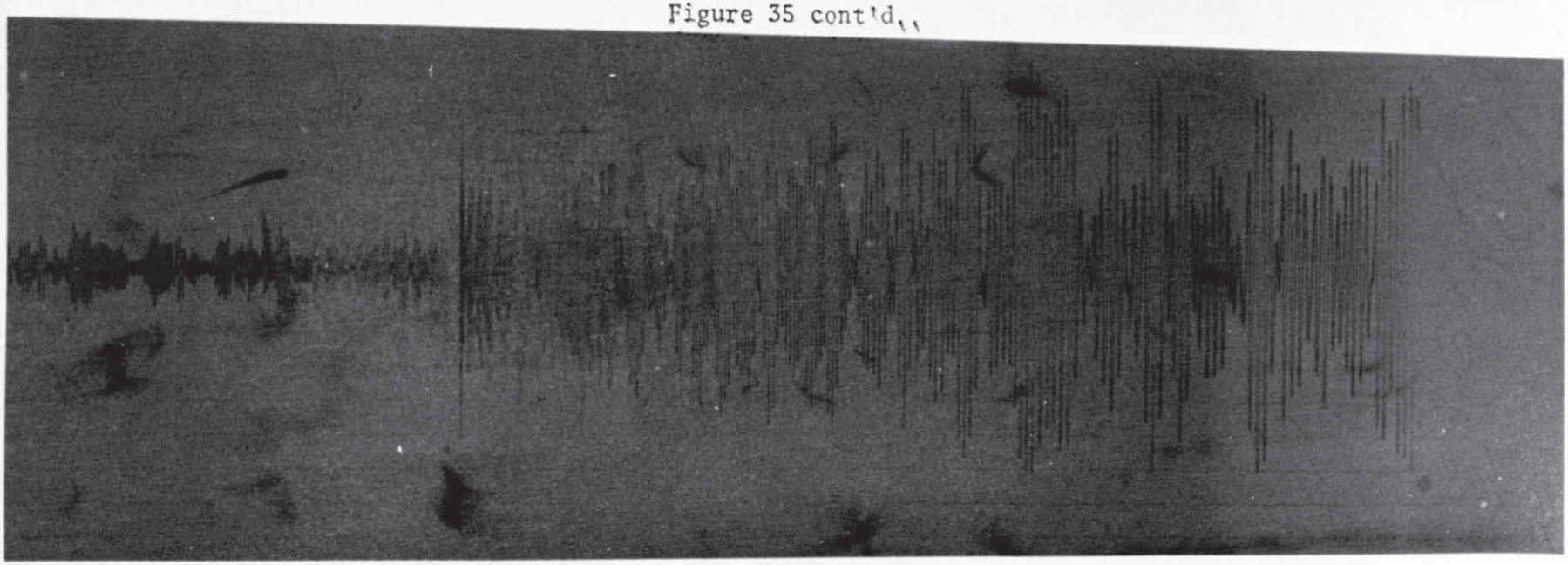

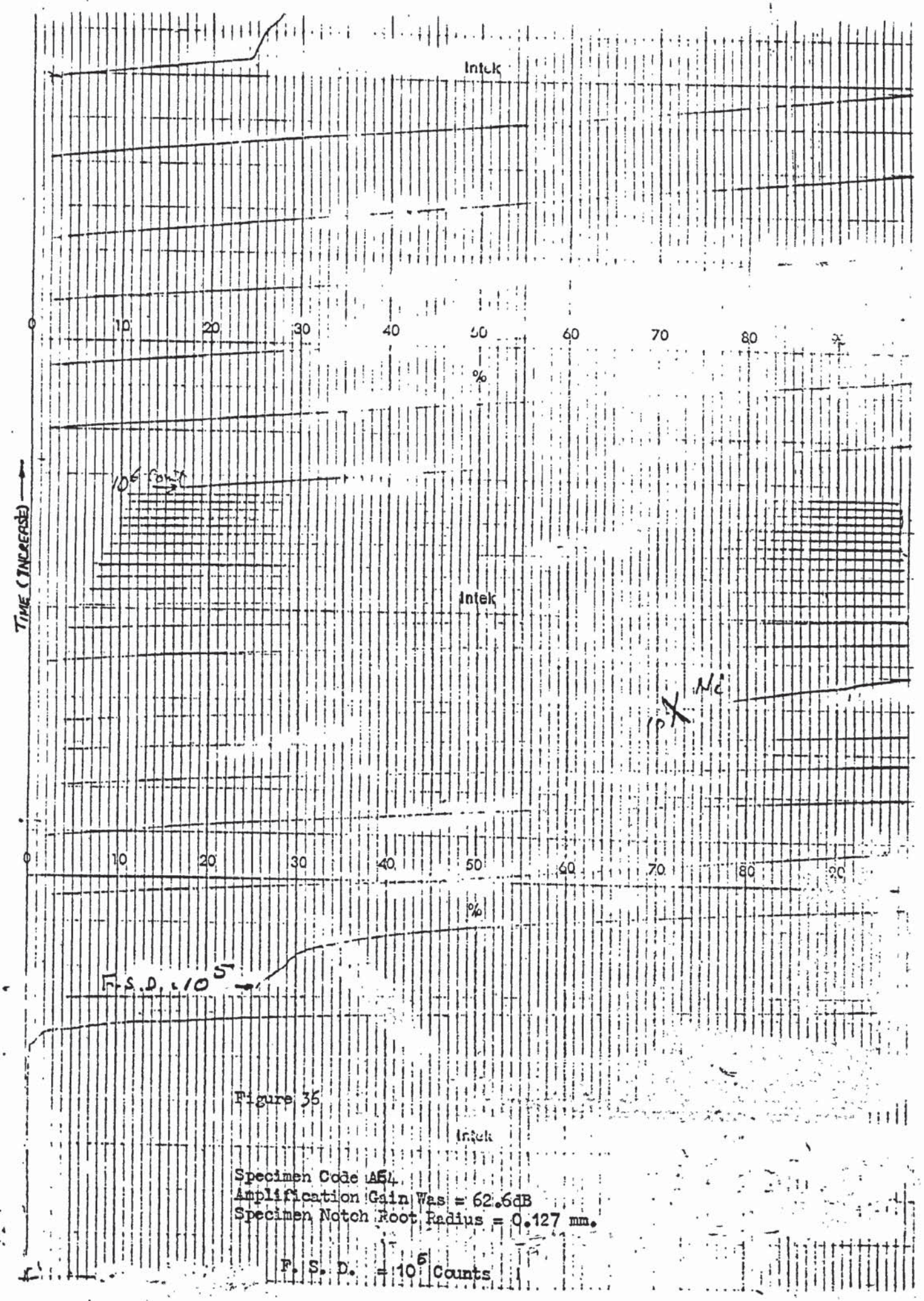

Figure 35

Specimen Code A54
Amplification Gain Was = 62.6dB
Specimen Notch Root Radius = 0.127 mm.

F. S. D. = 10^6 Counts

Figure 37

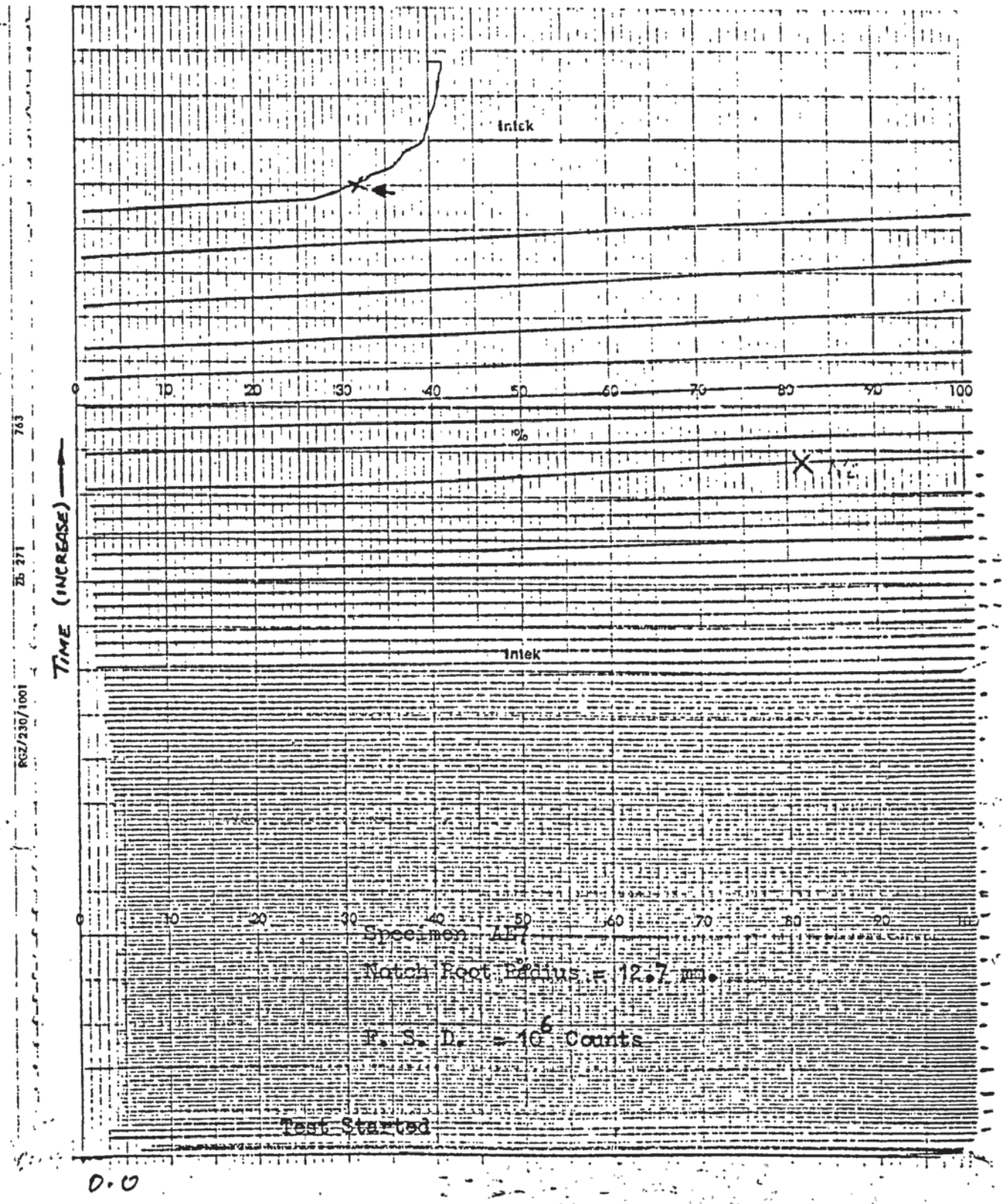
Intek
10
20
30
40
50
60
70
80
90
100
%
TIME (INCREASE)
RGZ/230/1001
25 271
763
Intek
Specimen AE7
Notch Root Radius = 12.7 mm.
F. S. D. = 10^6 Counts
Test Started
0.0

Figure 38

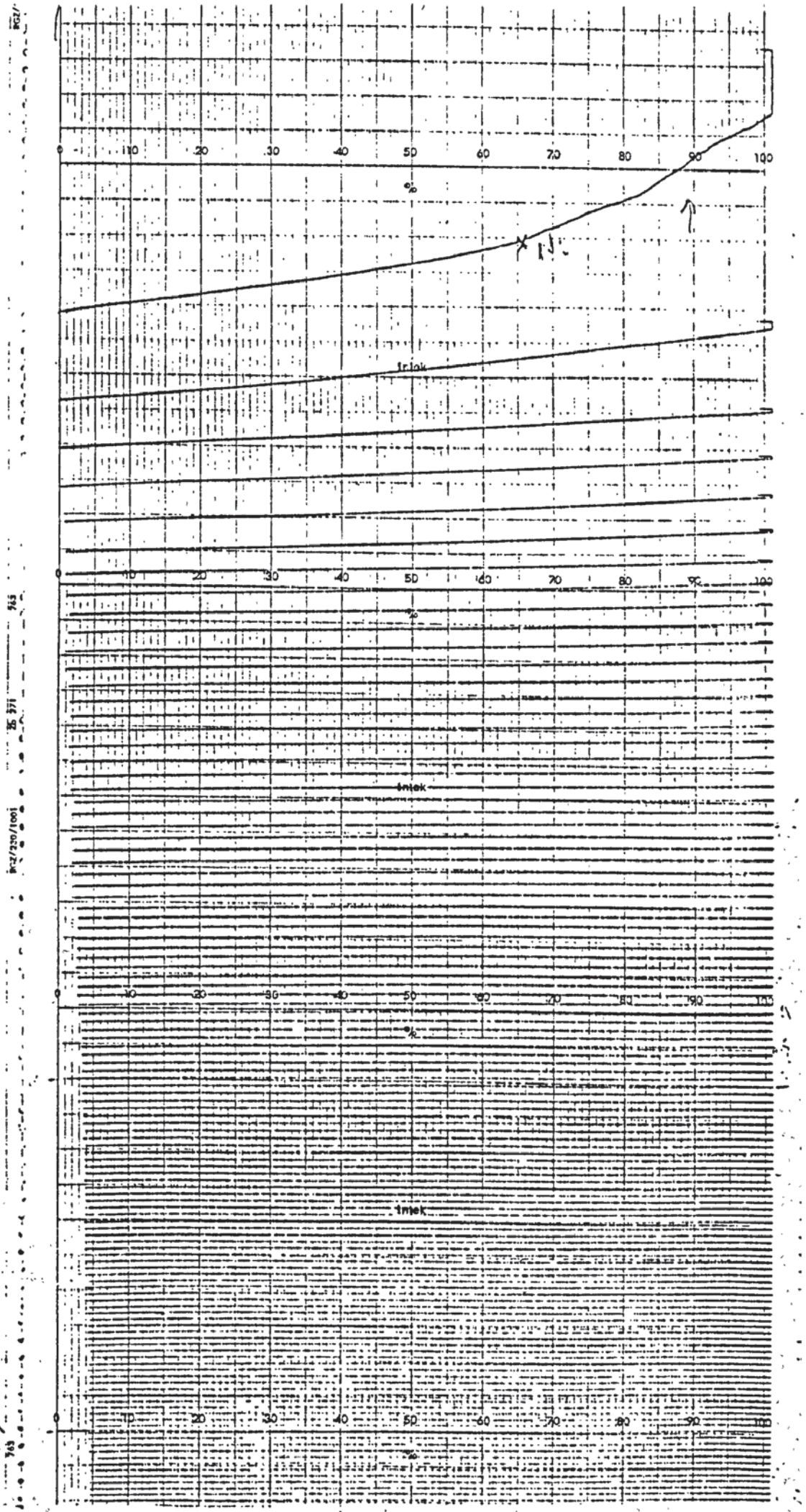

Specimen AE13
R.R. = 25.4mm.
Amplification
Gain = 62.6 dB.
F. S. D. = 10^6 cour

Material A tested at room temperature

Material B tested at room temperature

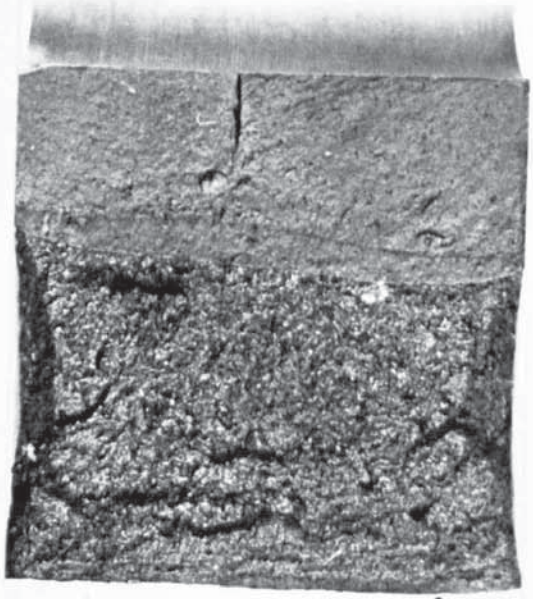

Material A tested at + 50°C

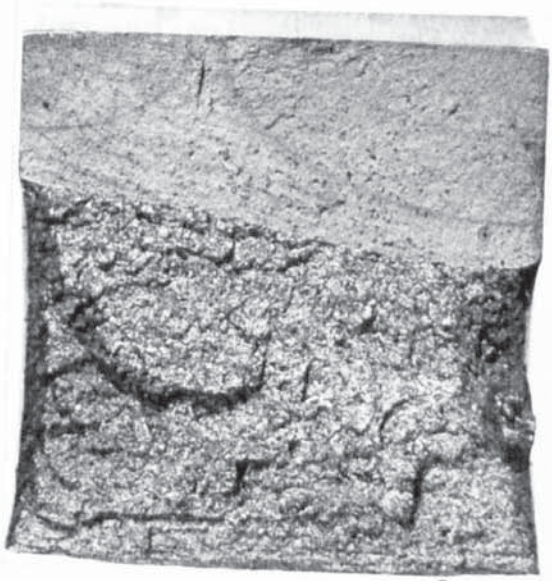

Material A tested at + 100°C

Material B tested at + 100°C

Material B tested at + 50°C

Figure 39 Ductile Fracture of (F.T.T.) results

Material B tasted at - 50°C

Material A tested at - 50°

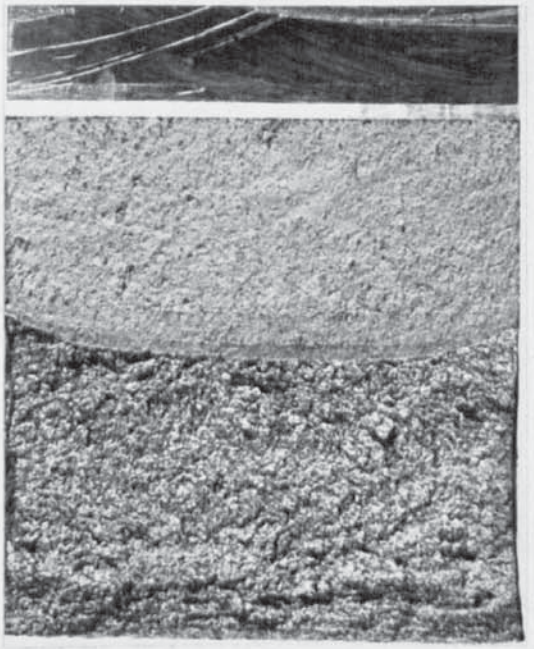

Material B tested at - 100°C

Material A tested at - 100°C

Figure 40 Cleavage Fracture of (F.T.T.) results

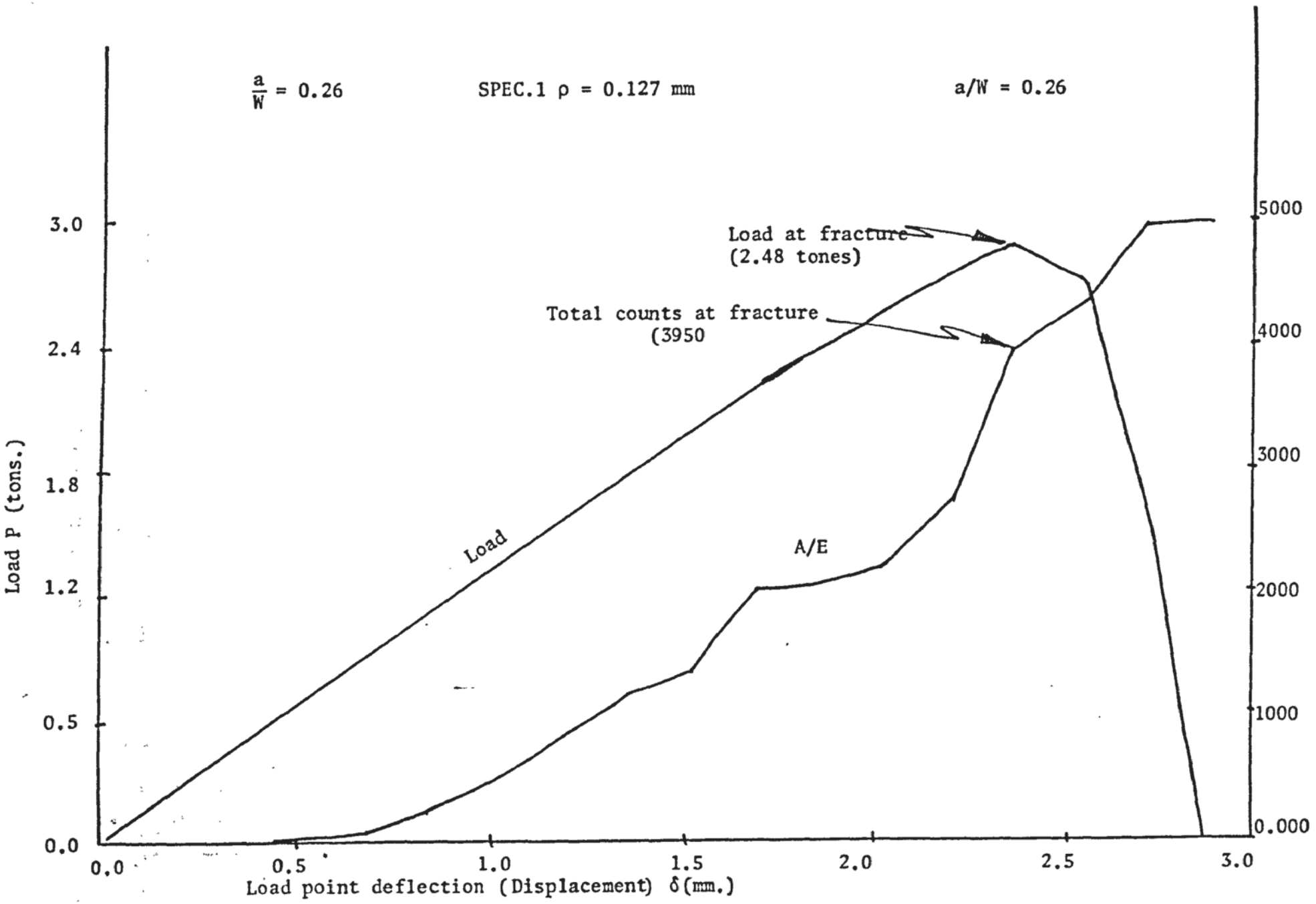
a/W = 0.26
SPEC.1 ρ = 0.127 mm
a/W = 0.26
Load at fracture
(2.48 tones)
Total counts at fracture
(3950
Load
A/E
Load P (tons.)
3.0
2.4
1.8
1.2
0.5
0.0
5000
4000
3000
2000
1000
0.000
0.0
0.5
1.0
1.5
2.0
2.5
3.0
Load point deflection (Displacement) δ(mm.)

Figure 41

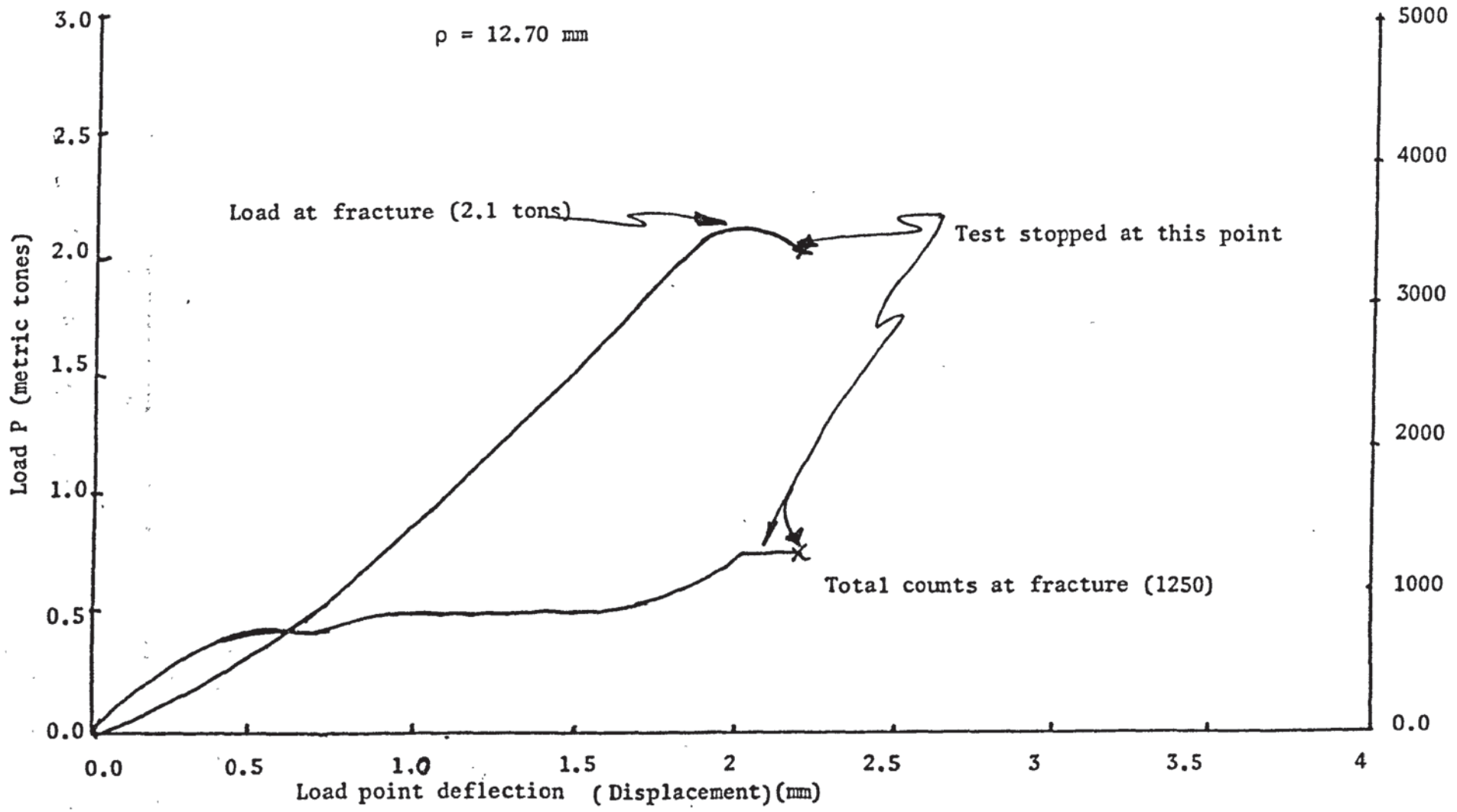
SPECIMEN (AE11B)
ρ = 12.70 mm
Load at fracture (2.1 tons)
Test stopped at this point
Total counts at fracture (1250)
Load P (metric tones)
Load point deflection (Displacement) (mm)
3.0
2.5
2.0
1.5
1.0
0.5
0.0
5000
4000
3000
2000
1000
0.0
0.0
0.5
1.0
1.5
2
2.5
3
3.5
4

Figure 42

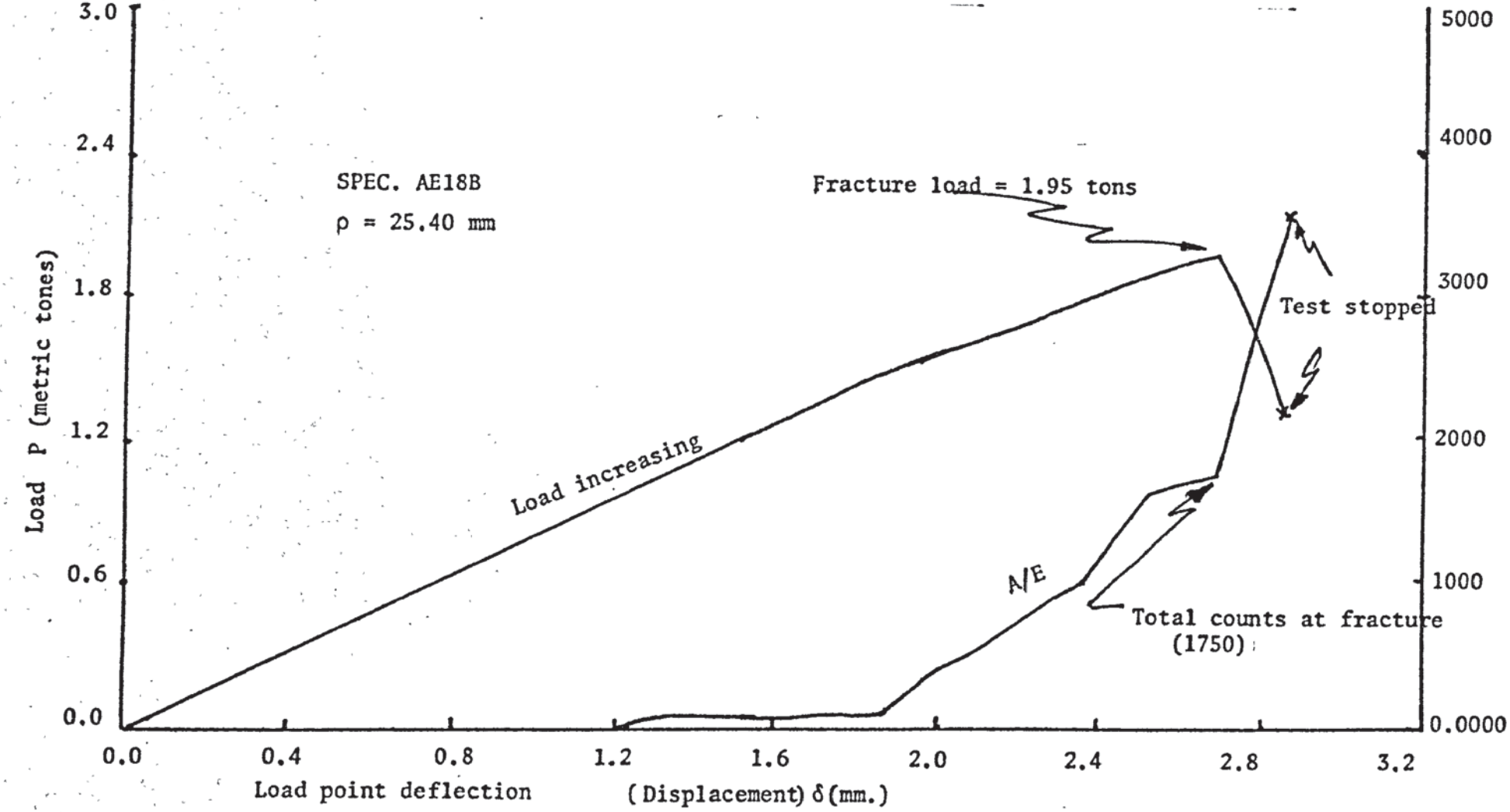
SPEC. AE18B
ρ = 25.40 mm
Fracture load = 1.95 tons
Test stopped
Load increasing
A/E
Total counts at fracture
(1750)
Load P (metric tones)
3.0
2.4
1.8
1.2
0.6
0.0
5000
4000
3000
2000
1000
0.0000
0.0
0.4
0.8
1.2
1.6
2.0
2.4
2.8
3.2
Load point deflection
(Displacement) δ (mm.)

Figure 43

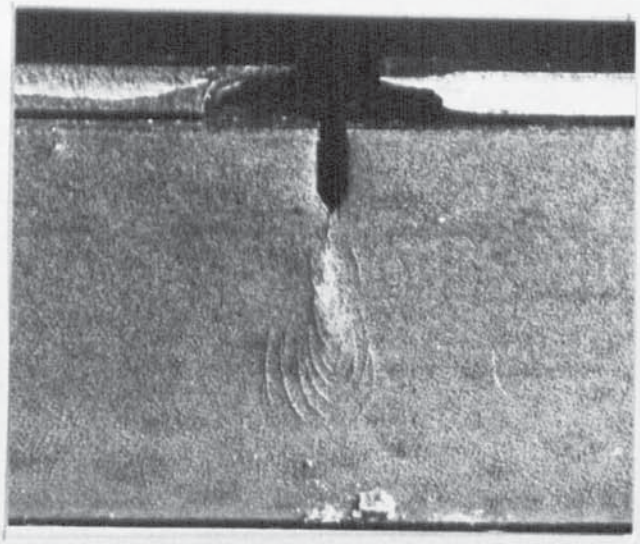

Specimen F1 X2.0 ρ = 0.127 mm

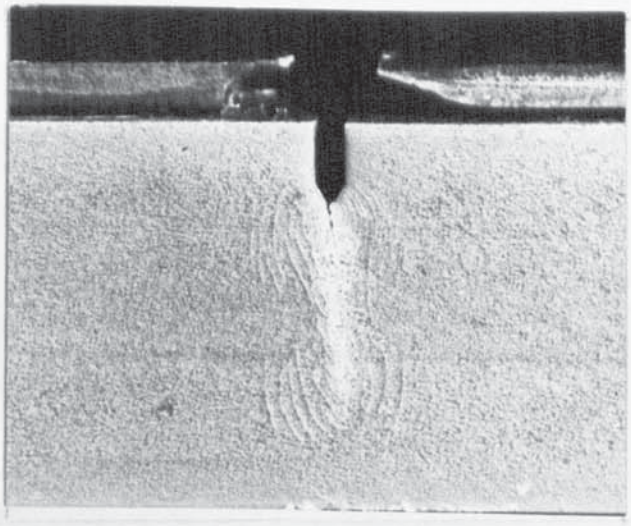

Specimen AE4B X2.0 ρ = 0.127 mm

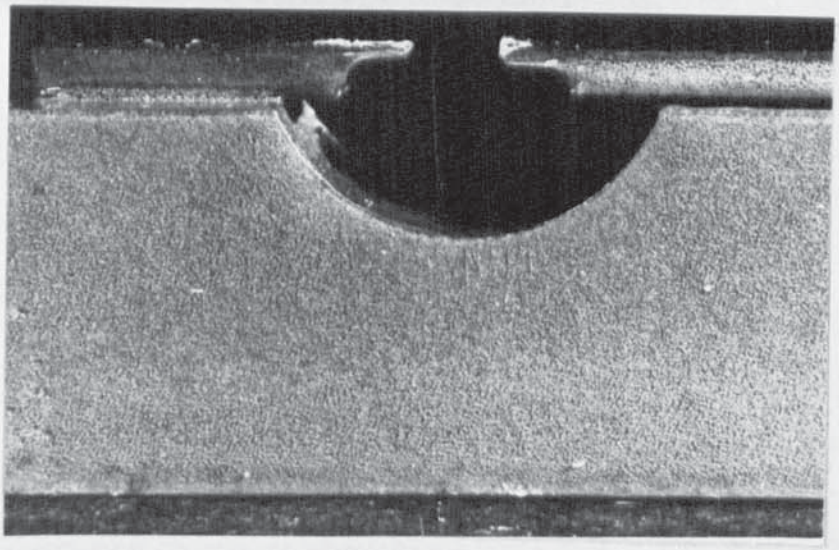

Specimen F6 X2.0 ρ = 25.4 mm

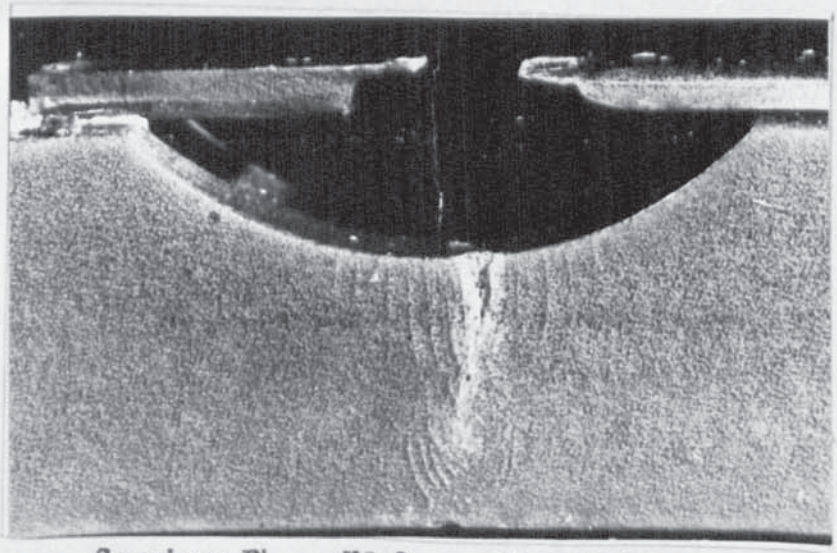

Specimen F4 X2.0 ρ = 12.7 mm

Figure 44 Plastic Zone shape at fracture point during the monotoning loading.

Pre-Fatigued Specimens

From Table 2.

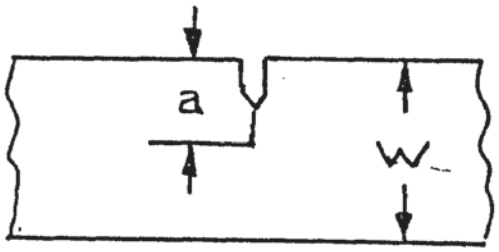

Fracture toughness test piece where total acoustic counts varies as a/W changes.

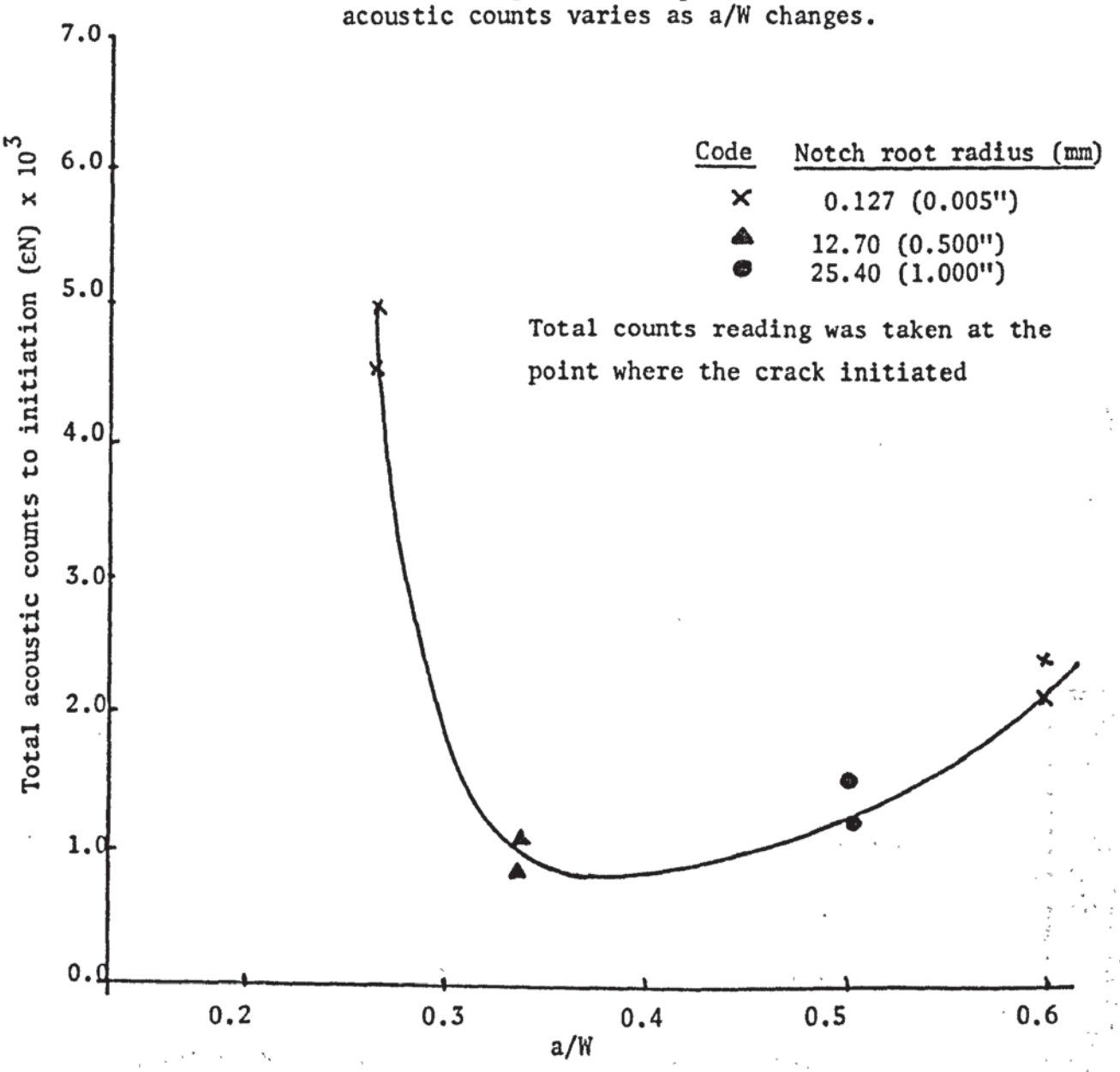

Figure 45

This represents the change in total counts due to the change in the machined root radius of a specimen

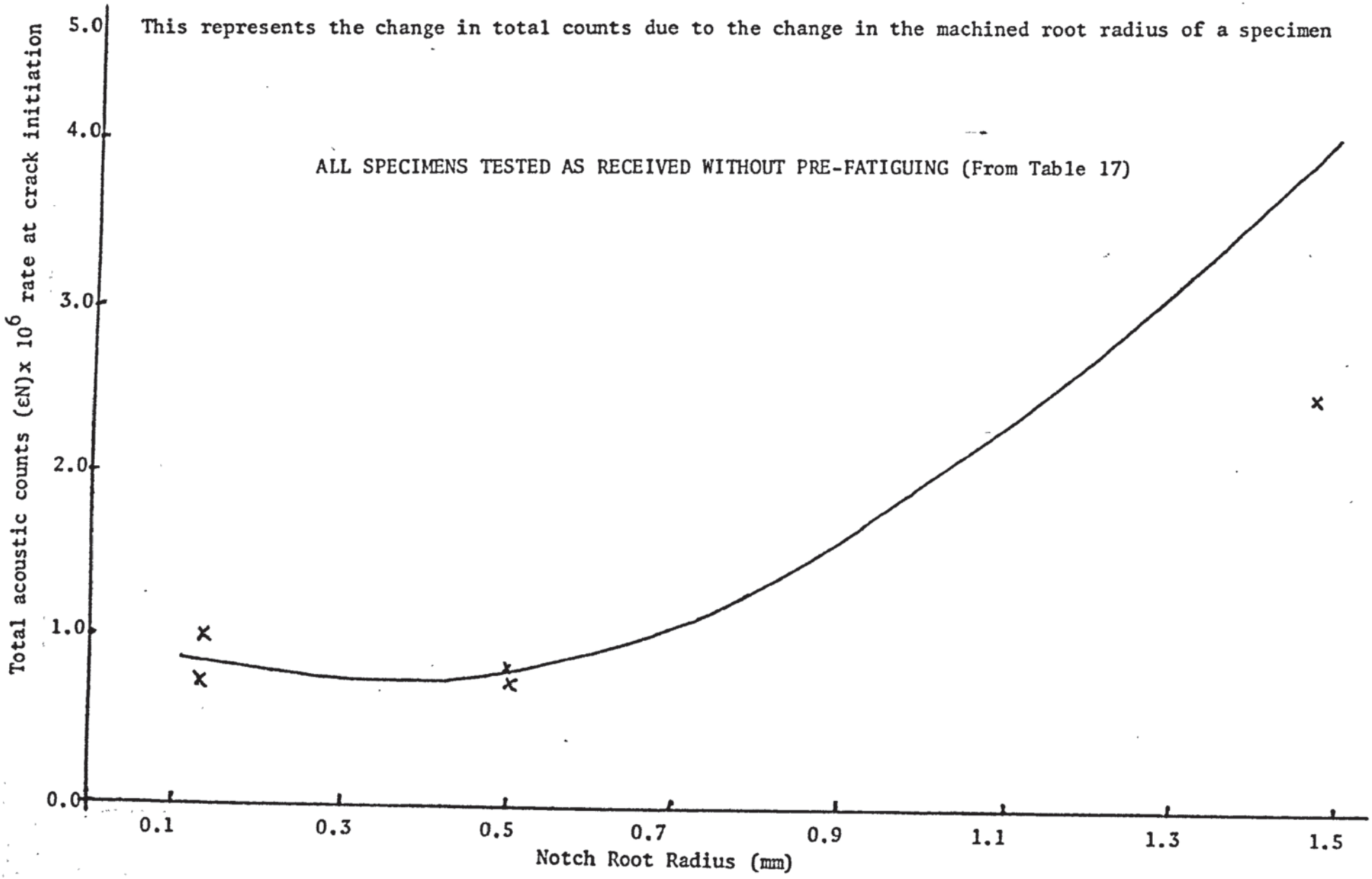

Figure 46

Effective K_C sharp and blunt notched specimen from Table 17. Both the J-Integral and theLEFM techniques were used to calculate K_C. All specimens tested as notched without prefatiguing.

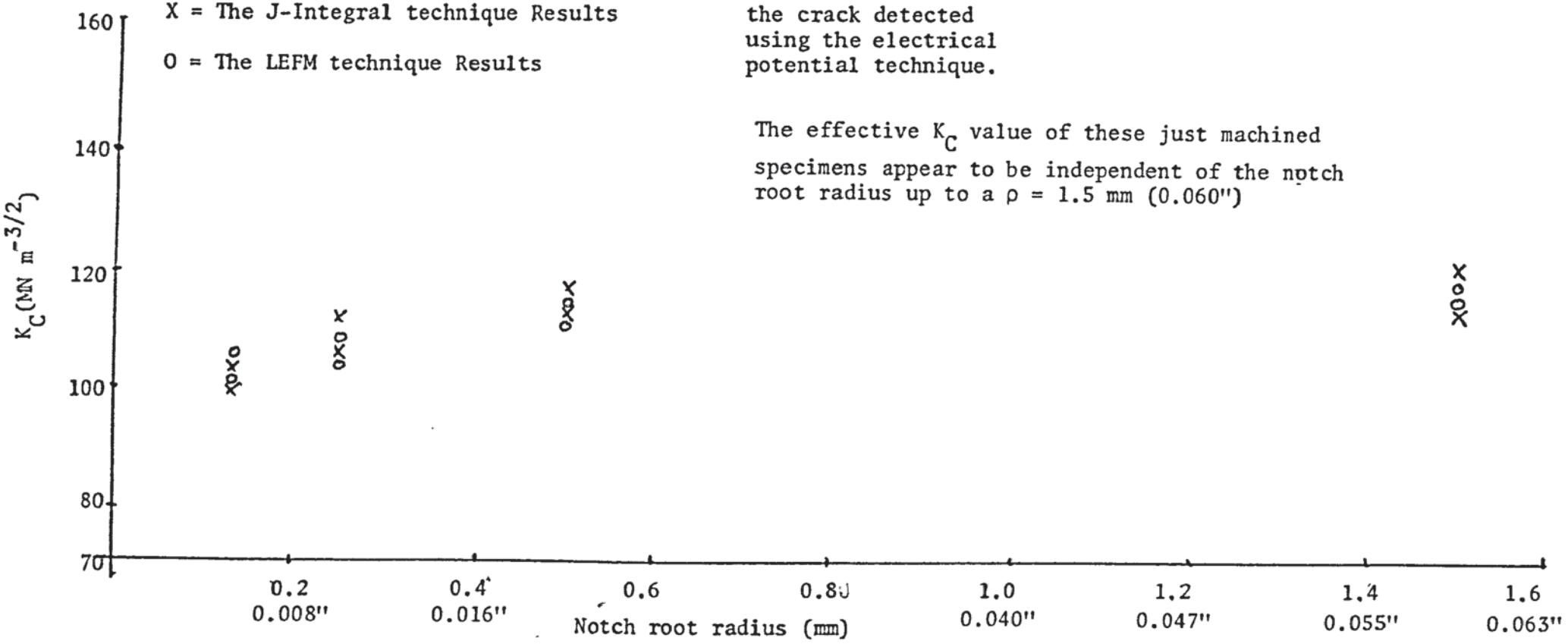

Figure 47. The effective value of K_C v.s. the notch root radius changes for Steel B

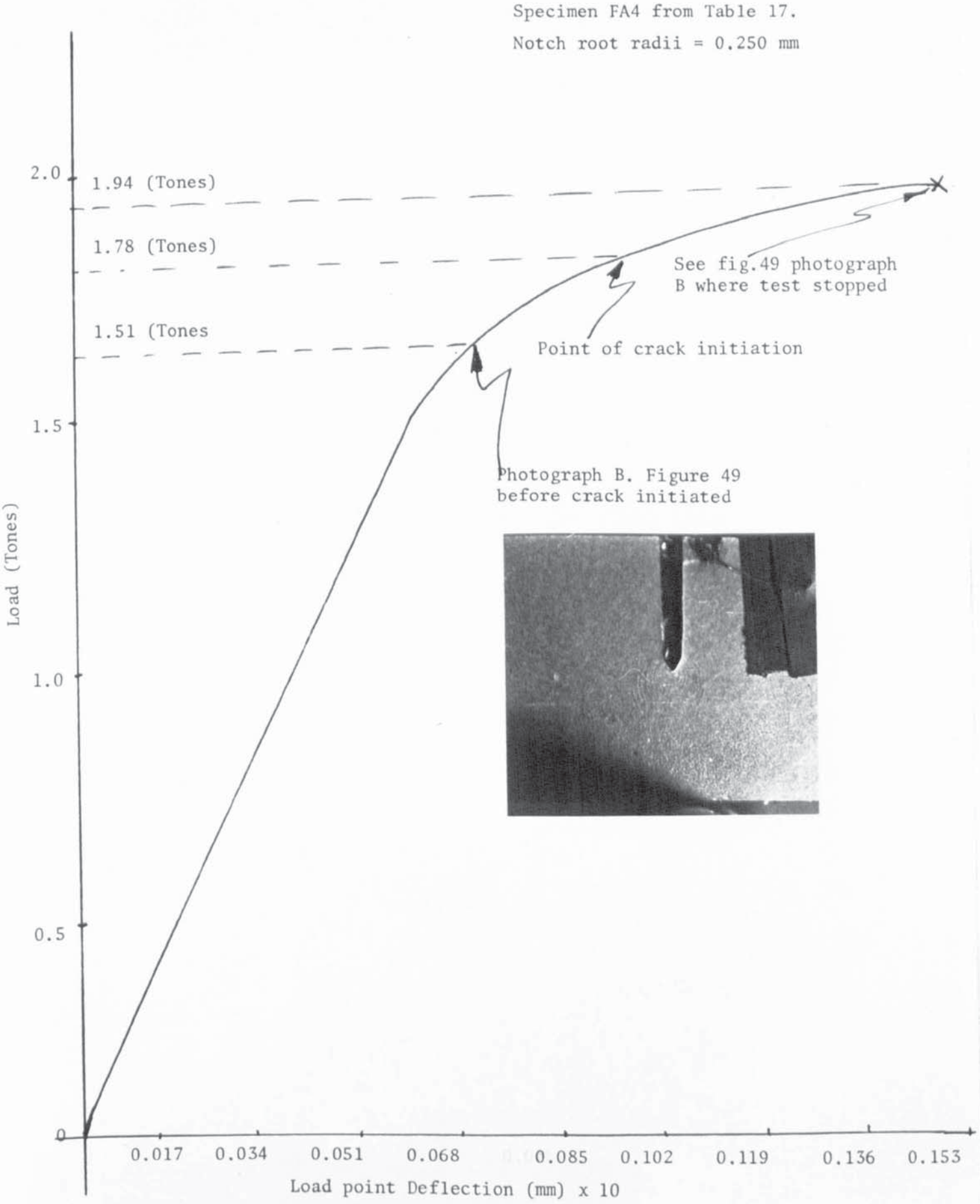
Specimen FA4 from Table 17.
Notch root radii = 0.250 mm
2.0
1.94 (Tones)
1.78 (Tones)
1.51 (Tones
1.5
1.0
0.5
0
Load (Tones)
See fig.49 photograph B where test stopped
Point of crack initiation
Photograph B. Figure 49 before crack initiated
0.017
0.034
0.051
0.068
0.085
0.102
0.119
0.136
0.153
Load point Deflection (mm) x 10

Figure 48

Using the (LEFM) method and taking 5% secant produced an average value of K_C for these specimens about 2% less than that found by the J-Integral.

The J-Integral Equation used (F):

$$J = \frac{2}{B(W-a)} \int_0^{\delta_{crack}} Pd\ (\delta_{crack})$$

The other eight specimens in the right hand side of Table 17 produced figures 46 and 47. These specimens were not prefatigued and all notches were 12.5 mm deep (a/W = 0.5). Four of these were stress-coated to enable photographing the area at the tip of the notch before crack initiates. Figure 48 represents specimen FA4 from Table 17 where the plastic deformation lines show clearly before the monotonic loading crack initiated. Figure 49 shows the shape of the plastic enclave when test stopped for coated specimens of four different notch root radii.

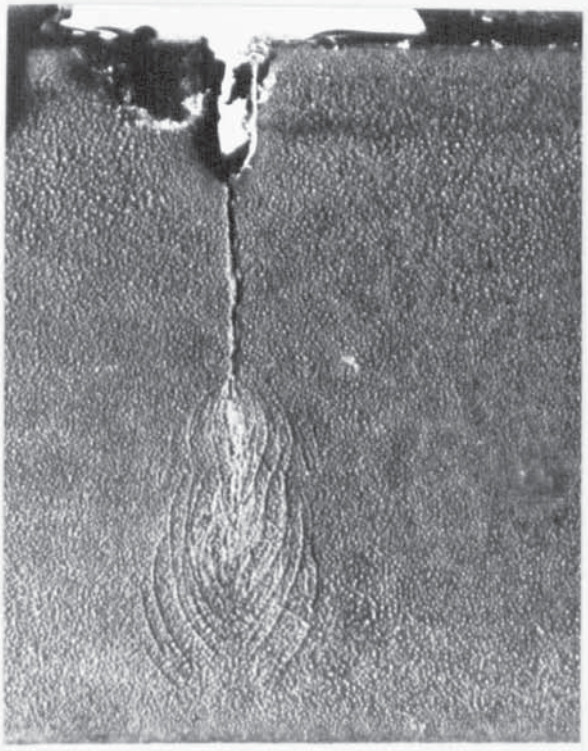

A X3.6 ρ = 0.127 mm.
Specimen NO. 11
Photo taken when test stopped
at P = 1.22 tones.

Deformation Area = 648 mm.^{2}

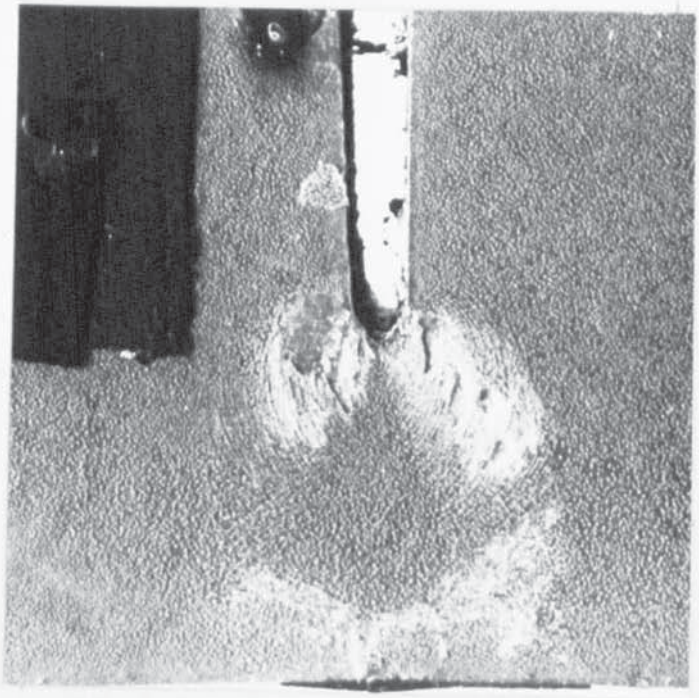

B X3.6 ρ = 0.25 mm.
Specimen NO. 13
Photo taken when test stopped
at P =1.88 tons

Deformation Area =831.0 mm.^{2}

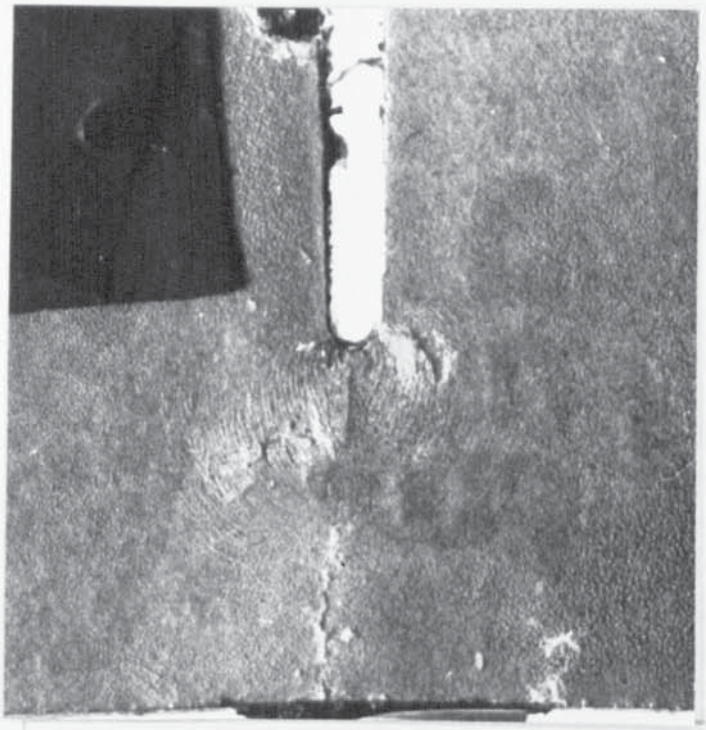

C X 3.6 ρ = 0.50 mm.
Specimen NO. 15
Photo taken when test stopped
at P =2.22 tones.
Deformation area = 494.0 mm.^{2}

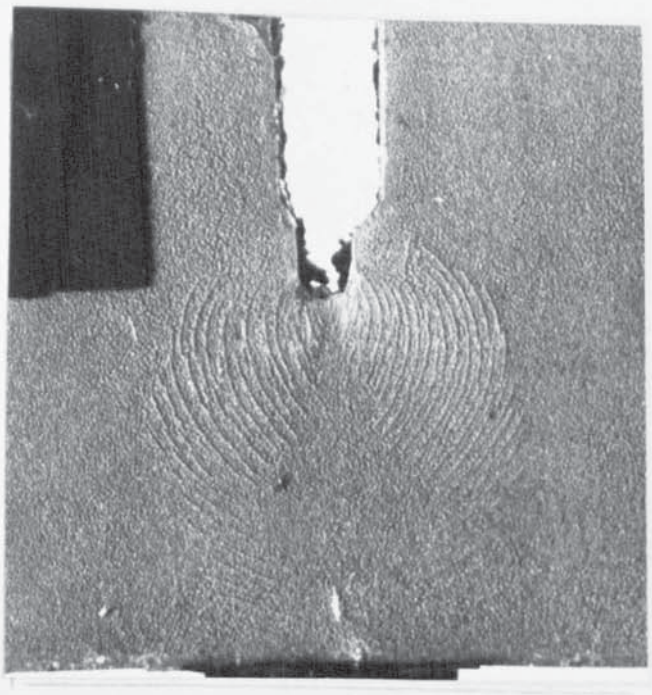

D X 3.6 ρ = 1.5 mm.
Specimen NO. 16
Photo taken when test stopped
at P = 2.24 tones.
Deformation area = 1376 mm.^{2}

Figure 49

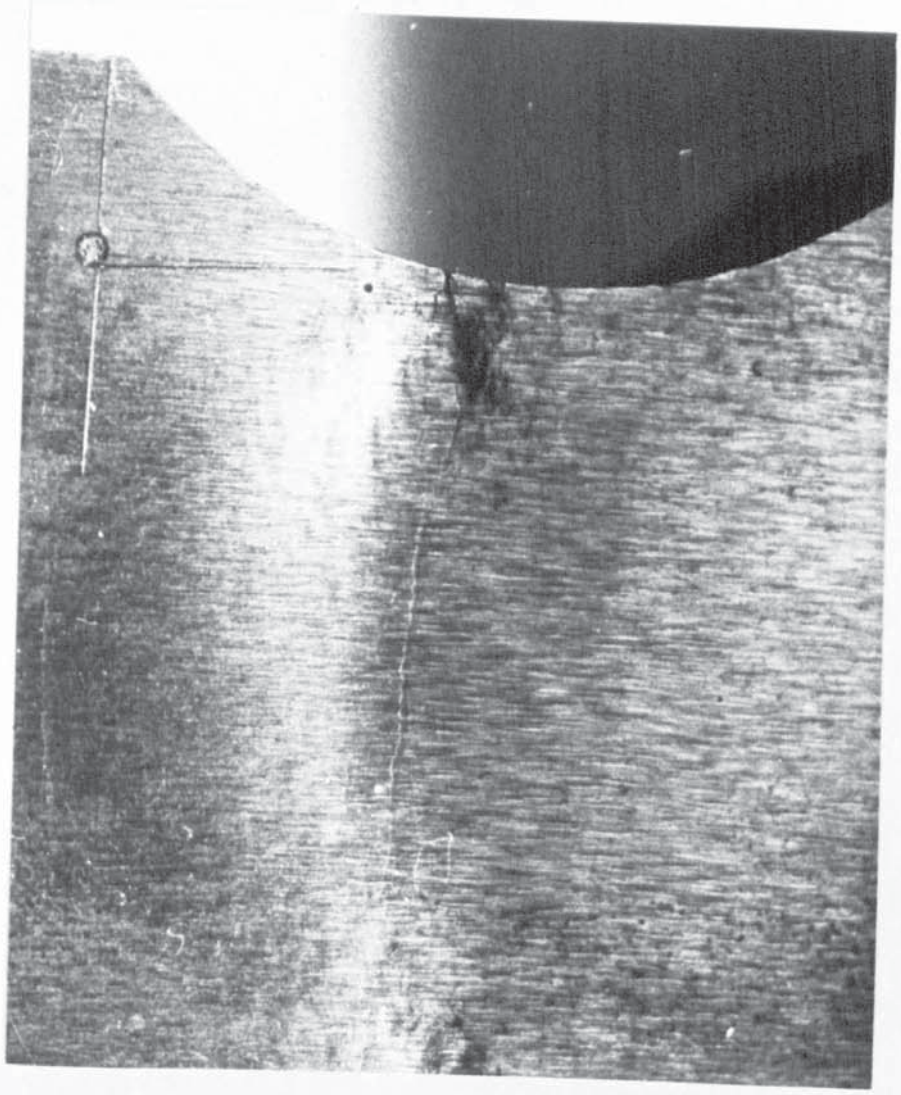

X5.0

Blunt notch ϱ = 12.7 mm

Figure 50 Represents one sided crack propagation

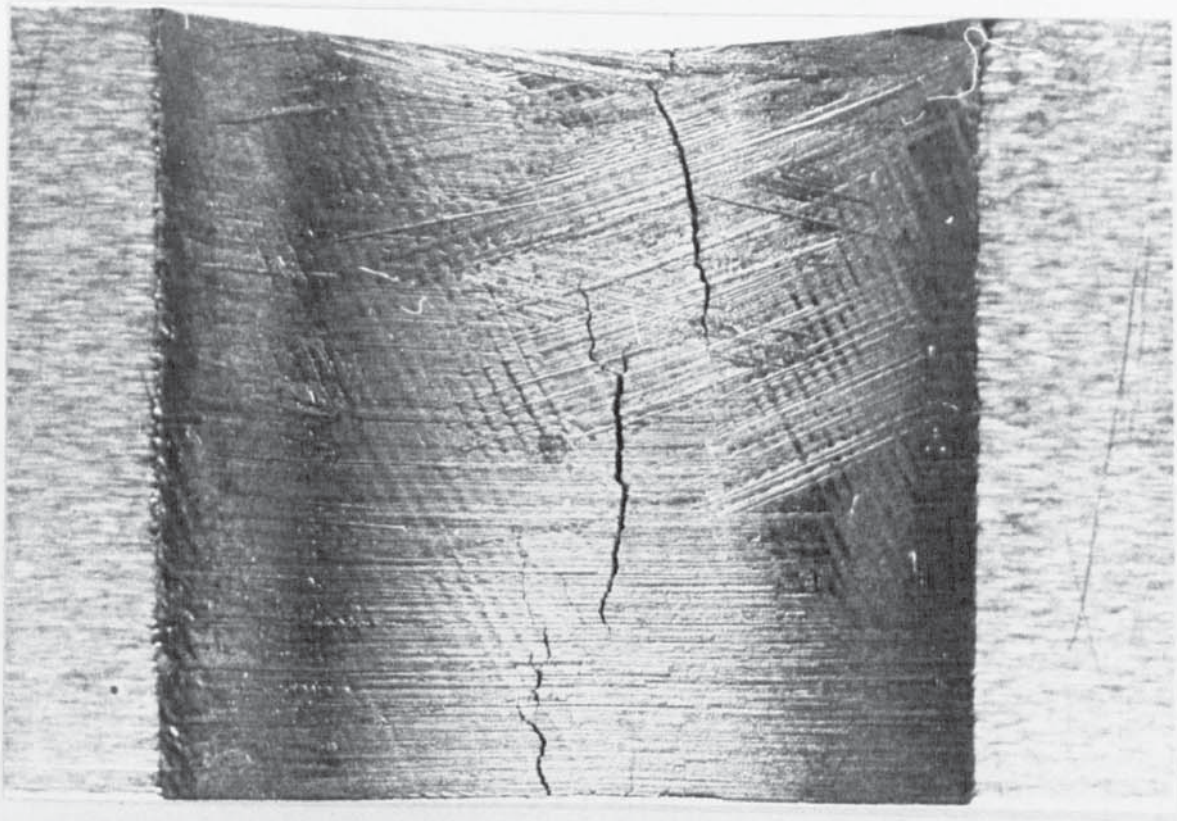

X5.0

Figure 51 Several macro-cracks for a 12.7 mm notch root radius specimen

X5.0

Figure 51a Several macro-Cracks for a 25.4 mm notch root radius Specimen

CHAPTER 5

FATIGUE CRACK INITIATION AT FIVE DIFFERENT TEMPERATURES

5.1 At Room Temperature (≃ 25°C)

If one considers the fracture mechanics approach which was the basic assumption of this work one should keep in mind that this approach requires the discontinuity, which is a through thickness crack, growing in an elastic continuum. Paris suggested earlier that this approach is applicable to blunt cracks providing that one takes an account of the stress concentration factor at the tip of the crack. If that was taken care of then the stress intensity factor, calculated from a sharp crack K-calibration curve, was modified by the square root of the notch root radius ($\rho^{\frac{1}{2}}$). This work confirms the results of R.Holder and Jack with a clear relationship between Ni (number of cycles to initiate a detectable fatigue crack) and the parameter $\Delta K/\rho^{\frac{1}{2}}$.

This approach appears to be valid for both orders of magnitude of sharp flow and blunt flow, (0.125 mm, 12.5 mm and 25.40 mm). The restriction of this theory still stands which states that if the plastic zone size is less than 1% of any specimen dimension then the plasticity effect at the notch root radius can be ignored.

Although material B had a larger grain size than material A in the as cast and machined condition, the definition of N_i shows a good dependence on the factor $\Delta K/\rho^{\frac{1}{2}}$ with exponent of 4.8 - 5.8, these exponents are slightly different to those obtained in Holder's experiments. The growth rate in the initiation region is proportional to (-m) which can be represented by this equation

$$\frac{da}{dN} = C \quad (\Delta K)^m$$

where m = -4.8 to -5.8.

The fatigue crack initiation is an important factor of fatigue life particularly in a design situation, not only initiation, but also propagation must be taken into account. If one assumes N_c to represent the number of fatigue cycles to accumulate sufficient fatigue damage to initiate a fatigue crack, and N_a as the number of fatigue cycles to grow the crack to a certain length, a, then the fatigue nuclear could be written as

$$N_i = N_a + N_c$$

this approach has been successfully used by Bluhm [14] and Holder[80] and Pearson[129].

Although the range of the notches is very wide but results show that they are capable of application to a wide range of practical situations where the machined notch is in the form of a screw thread or fillet.

For both materials A and B at room temperature the results of plotting N_i versus $\Delta K/\rho^{\frac{1}{2}}$ generally indicate that the initiation lives for sharply

notched specimens are higher than the lives for blunt notched specimens tested, applying the same value of $\Delta K/\rho^{\frac{1}{2}}$. It has been known earlier that to achieve the same level of local stress the blunt notch specimen will have to have a higher applied stress than that with a sharp notch radius during fatigue tests.

Plots of Chapter 4 (figure 16) which represent N_i versus $\Delta K/\rho^{\frac{1}{2}}$ in a log-log scale of this work suggest that for identical values of $\Delta K/\rho^{\frac{1}{2}}$ comparing the two materials generally the number of cycles required to initiate the detectable fatigue crack was always higher for material A by a factor ranging from 3 - 9. This factor is not significant in fatigue size since it is less than ten, which suggests that both materials have the same fatigue properties providing they were given the same heat treatment. It also appeared from tests that, although a fatigue crack initiates at both surfaces, it penetrates through the thickness of the specimen, and propagates with almost the same speed of both sides of the specimen. This does not seem to be the case with blunt notched specimens of both materials. Tests showed that the crack could grow as long as 16.0 mm in on one side and was optical undetectable in the other side (Figure 50). The fatigue damage right after the process of crack initiation indicates that a single macro-crack does exist during the first stages of crack growth for sharp flows which several macrocracks continue to propagate up to fracture after all joints to form the possibility of fracture (Figure 51).

The results of this work at room temperature indicate that these fatigue data of figure 16 is a negative result of what was expected but they are still important from the design point of view.

The initiation results plotted as log Ni versus log $\Delta K/\rho^{\frac{1}{2}}$, figure 16 shows a distinct banding on all levels of notch root radius levets tested. This is the case for both materials A and B. This banding effect may be reduced by annealing the specimens after the machining operation. This was shown by Jack[92] and Price[133] who used mild steel specimens. Although some scatter still exists in these results, comparatively it is a much smaller scatter than those results tested at -100°C,which will be discussed later in this chapter. All notch root radii ρ mentioned here are being the measured root radii for the notches after machining. Material A of these room temperature tests reveals that at stress as low as 1000 MN m^{-2} for sharp flow to detect a fatigue crack at initiation more than 3×10^6 cycles while 2.5×10^5 for material B, which is a factor of more than 12, but this does not seem to be the case for the other values of $\Delta K/\rho^{\frac{1}{2}}$. This exceptional case, as tests show is due to differences in microstructures and grain size, as figure 8 explains.

Frost et al.(1974) predicted that the resistance to fatigue crack initiation increases as testing temperature increases and vice versa. The latest results of this work seem to agree with this theory although the temperature range is not as wide as Frost suggested. Fatigue life of material A showed to be longer by a factor of 5 - 6 than for material B. The reason seems to be due to the grain size difference, since both materials have almost the same chemical compositions. Section 4.1 shows how material B has the same fatigue properties after providing the proper heat-treatment as to material A. This convinced the author that the grain size is the only factor for the fatigue properties not to be identical.

5.2 Tests provided at +50°C and +100°C

The same conclusion could be drawn from the results of tested specimens at both +50°C and +100°C temperatures for both materials as it was found out for room temperature investigation. The only exception is that the value of the exponent was found to be higher compared to room temperature tests. On the other hand to compare the two materials A & B at those temperatures they showed nearly the same fatigue properties. The number of fatigue cycles required to initiate a fatigue crack for both materials was nearly the same. The number of cycles to initiate a fatigue crack is greater by a factor of 2 - 3 for tests provided at +100°C than those provided at +50°C for both materials.

It seemed from the results of Tables 10 and 11, which were plotted in figures 17 and 18, that the higher the temperature the more ductile is the material and the higher would be the yield stress of the material. Results concluded that figures 17 and 18 show a good evidence that the higher the testing temperature the greater the resistance to fatigue which is by a factor of 2 - 3 for sharp notches and nearly the same results for blunt notches. The band of these plotted points seem to be narrower for specimens tested at +50°C than those tested at +100°C. This last result seems to be valid for blunt notches rather than for the sharp ones. There is no evidence throughout this work which might show if there is a change in crack formation (whether it is transgranular or intergranular fracture), since the variation in temperature is not so great. Results of this investigation at these two temperatures would safeguard the designer by using a factor of safety to provide a conservative line, below which he

can be sure no initiation would take place at certain applied loads. Fractured surface examinations showed that both room temperature , +50°C and +100°C tested proved to be ductile surfaces.

5.3 Tests at -50°C and -100°C

Results of specimens tested at -50°C plotted in figure 19 suggests that the number of fatigue cycle required to initiate a fatigue crack was nearly the same for both materials (A & B) in spite of the additional percentage of molybdenum intentionally added to material A. This was found to be also the case for other tests provided at -100°C. The scatter resulted from bluntly notched specimens at -50°C seemed to be greater than at -100°C. For sharply notched specimens the case does not seem to be so where the scatter is nearly identical for both. The exponent (m) which is shown in Section 4.1 lower as for the higher testing temperature. The author would like to mention here again that material B was given the proper heat-treatment for all specimens before the sub-zero test was provided.

5.4 Plastic damage evidence before a fatigue crack initiation

The plastic damage resulted during fatigue testing of the specimen in figure 22 was recorded before the fatigue crack could be detected by the electrical potential technique or optically. Figure 21 is simply an approximate sketch which is represented in figure 23. A mass of slip-lines were formed during the early stages of fatigue. The length of these lines detected were between 0.010 mm and 1.0 mm. To compare this plastic damage in size with that proposed by Smith[147] and the

linear elastic fracture mechanics model Appendix III. The following results could be concluded:

1. Using Smith's proposal the plastic zone size of this should be equal to 11.43 mm.
2. Applying the linear elastic fracture mechanics approach one gets a value of 9.6 mm.
3. Even applying Dugdale's model (Appendix III) concludes a plastic zone size of 10.11 mm.

The resulting plastic zone concluded from this test comes out to be less than half the value they have concluded theoretically, figure 21. The applied stress in this case was 281.5 MN m^{-2}, the yield stress is 425 MN m^{-2} therefore $\frac{\sigma_a}{\sigma_y}$ = 0.662 which implied that the plastic zone size should be equal to the values stated in 1, 2 or 3 above theoretically while practical measurements of these results show that it is equal to 4.0 mm.

5.5 Fatigue with A/E application

The acoustic emission reveals an agreeable approach of detecting a fatigue crack initiated at certain number of fatigue cycles for both sharp and blunt notches, therefore it is a quality control technique rather than an experimental one. The results of this work are applicable for this material since the properties of one material could differ from another due to variation of casting procedure. Size and shape of casting and the resulting cooling rates all these may well influence the fatigue properties of the material. The fatigue test showed that at certain voltage gain (e.g. 62.4 dB), the totalacoustic counts had to reach at

least 500 counts in order for a detectable fatigue crack to be initiated, providing the value of $\Delta K/\rho^{\frac{1}{2}}$ should be 1000 MN m^{-2}. This is only true for specimens containing 0.127 mm notch root radius. The total number of fatigue cycles was greater than 10^6 cycles (Table 14). As $\Delta K/\rho^{\frac{1}{2}}$ values increase by 75% the total counts at the point of initiation increases nearly four times and by a further 75% increase in $\Delta K/\rho^{\frac{1}{2}}$ the total acoustic counts do not increase in the same previous manner.

Tests showed that the blunt notched specimens (e.g. ρ = 12.70 mm) behave somewhat different, that is as $\Delta K/\rho^{\frac{1}{2}}$ increases the total acoustic counts decreases. The case was the same with the 25.4 mm notch root radius except no acoustic counts could be detected at 62.4 dB values, therefore higher voltage gain was used.

The last nine specimens of Table 14 where a gain of 75 dB was used, the acoustic count rate was concluded. These results were plotted as counts rate versus time as shown in figures (26 - 33). These resulting plots suggest that for sharply notched specimens the count rate steadily increases until it gets to the maximum value (peak) then the rate starts to drop. The fatigue crack initiation always took place after the rate had reached its maximum value then the rate started to drop. The fatigue crack initiation always took place after the maximum count rate reached its value then started to decline. For lower load values or at $\Delta K/\rho^{\frac{1}{2}}$ = 1200 MN m^{-2} (using sharply notched specimens) fatigue crack initiation did not take place unless the count rate was about 500 counts/minute. For values of $\Delta K/\rho^{\frac{1}{2}}$ = 2000 MN m^{-2} fatigue crack initiation had not taken

place until the acoustic count rate was about 7.8×10^6 counts/minute. Results of this work also showed that blunt notched specimens namely (AE7 and AE9 of figure 12) showed that a fatigue crack did not initiate approximately ten minutes after the acoustic count rate reached its maximum value and this ten minutes corresponds to (12000) cycles when one can draw from that a conservative line before a detectable crack could initiate. Test number 10, figure 30, is excluded from the above consideration. One inch root radii notched specimens, figures 31, 32 and 33, could not give a clear warning to the operator when the fatigue crack was likely to initiate, while the sharply notched specimens did during tests.

An attempt was made to investigate the direction of the slip lines at either surface of the monotoningly loaded specimens at five different temperatures. All specimens were electro-polished and were tested to about half the value of the load required to fracture the specimen. Results were negative since the sub-zero test both fractured much earlier than they were expected. The attempt was to show if there were any changes in slip line direction from one temperature to another.

5.6 Plastic zone size

Earlier work carried out by Smith[146], Dugdale[35], Vitek[180] and Tetelman & McEvily[159] was concerned with the plastic zone size and the shape of that plastic zone at the tip of the sharp crack during fatigue tests. These results were studied at early stages of this work theoretically, the computer programme written for this comparison is shown in Appendix III. Smith's work suggested that unless the applied stress to the yield stress ratio is greater than a certain value $\frac{(\rho/a)^{\frac{1}{2}}}{2+(\rho/s)^{\frac{1}{2}}}$ where ρ is the measured root radius of the notch, and a is the notch depth, the plastic zone does not exist. Vitek followed this work a stage further and concluded that for the ratios of $\rho/a = 0, 0.1, 0.5, 0.9$, as $\frac{\sigma_a}{\sigma_y}$ (the applied stress to the yield stress ratio) increases the plastic zone increases exponentially, while fitting Smith's curve into Vitek's graph for a ρ/a value of 0.5 it seems that it would follow the same pattern as Vitek suggested than at a certain value of $\frac{\sigma_a}{\sigma_y} = 0.8$ Smith's curve ρ increases sharply and intersects with other ρ/a ratio curves (figure 6a). The plastic zone size seems to be fairly well established either by the linear elastic fracture mechanics approach, the Dugdale proposal, the Smith's results or finally by Vitek, but it is not quite agreeably established for blunt notched specimens. Although Smith's model is for anti-plane strain conditions Palmer[123] has used this model based on the assumption that it is appropriate for tension compression fatigue using a big sheet with a crack in its centre when the sheet is under uniaxial tension. Vitek studied the same situation of plane strain yielding from an embedded crack with finite root radius and loaded in uniform tension

and three point bending as well. To apply Smith's model recent experimental work has shown that it cannot be applied to fatigue while using single edge notched specimens, while the other three models (linear elastic fracture mechanics and Dugdale) suggest that whenever $\frac{\sigma_a}{\sigma_y}$ (σ_a = applied stress and σ_y the yield stress) has a value, a plastic zone does not exist even if it is very small (Appendix III). Smith's, Palmer's and Vitek's models show a cut-off at some values of σ_a/σ_y where the palstic zone size is zero. This work confirms this cut-off for different values of ρ/a but it indicates that the cut-off value (σ_a/σ_y) is smaller than it was suggested earlier. More than a dozen specimens which were tested throughout this work namely (AZ1, 4, 8, 26, 39, 22, 24, 27, BZ12, 15, 18, 26, 16, 19, and 6, 13, 4, 10, 22 and 23) from both materials containing three different notch root radii (Tables 9, 10, 11, 12 and 13) were tested using a stress ratio (σ_a/σ_y) less than that Smith proposed in his theory. In all cases, a fatigue crack initiated at different numbers of cycles with respect to the load used. Results of this work applying $\frac{\sigma_a}{\sigma_y}$ = 0.4, 0.5, 0.6 and 0.8 using three different notch root radii suggests that a plastic zone was existing before Smith's cut-off took place. One of these calculated evidences discussed in Section 5.4 where $\frac{\sigma_a}{\sigma_y}$ used was 0.662 and the plastic zone size was less than half the value predicted from the above models. This last case was detected before the fatigue crack was detectable, but slip lines defined the plastic zone shape and size. The gross stress for this purpose was calculated using the bending equation:

$$\frac{\sigma}{y} = \frac{M}{I}$$

where, σ - is the applied gross stress.

M - Bending moment

I - Second moment of area

Y - $\frac{1}{2}$ (W-a)

W - specimen width, and

a - is the notch depth.

Substituting the values of M, I and Y the following equation can be used to calculate the applied stress of any specimen tested throughout this work. This applied stress is equivalent to Smith's applied stress when using his model for anti-plane strain.

$$\sigma_a = \frac{6pW}{B(W-a)^2}$$

Smith suggested that unless $\frac{\sigma_a}{\sigma_y}$ reaches a specific value, no plastic deformation can take place providing the crack length to width ratio $(\frac{a}{W})$ is equal to 0.20 as shown below:

ρ = 0.127 mm leads to $\frac{\sigma_a}{\sigma_y} \geq$ 0.29 as a condition for a plastic zone to exist.

ρ = 12.70 mm leads to $\frac{\sigma_a}{\sigma_y} \geq$ 0.660 " " " " "

ρ = 25.40 mm leads to $\frac{\sigma_a}{\sigma_y} \geq$ 0.70 " " " " "

For specimens of 12.70 mm notch root radii with a stress ratio $(\frac{\sigma_a}{\sigma_y})$ in the range of 0.208 - 0.222, this work concluded that a fatigue crack initiated. Taking Holder's conclusion as granted (before a crack could be detected a plastic damage has to take place), proves that a plastic zone

existed even before Smith's cut-off. At five different temperatures, the case was the same for specimens of 25.4 mm notch root radii. Figure where the plastic zone size was plotted against the log of $(\frac{1}{\rho})$ (ρ - notch root radius) shows the theoretical and critical root radius is equal to 0.510 mm based on Smith's assumption. This concludes that for a smaller radius the plastic zone size does not change and it is about 12.60 mm. As the radius increases up to one inch (25.4 mm) the plastic zone size decreases and gives a value of S = 6.25 mm (0.25 inches).

5.7 Another evidence of plastic damage before a fatigue crack initiated

This work gave an evidence of a plastic damage before the detectable fatigue crack initiated. This evidence was concluded from the total acoustic counts v.s. time for three different notch root radii. As figure 36 indicates that fatigue testing a specimen with a 0.127 mm notch root radius (the resulting chart with a full scale deflection of 10^6 acoustic counts as an X axis) concluded that before a fatigue crack initiated and even before any plastic damage took place, the acoustic emission recorder was plotting equally spaced lines, which represents a full scale deflection in each line. Once plastic damage initiated these equally spaced lines in figure 36 were spaced wider (count rate decreased). In conjunction with this evidence the recorded replayed elastic wave from the tape recorder shows no pulses exist before any plastic damage took place, figure 35. The theory behind this is because as the elastic acoustic wave travels along the specimen it will reject backwards and forwards. As dislocation starts to move (plastic deformation starts) the recorder begins to pick up disrupted waves and shows some pulses. These pulses will increase respectively as the plastic zone increases and finally the fatigue crack

initiates. The result of this test indicates that the total acoustic emission counts at the point when the fatigue crack initiated was found to be 2.811×10^6 counts. This number of counts is much smaller than it is for a blunt notched specimen tested under the same condition. The last result confirms Palmer's result. Palmer suspected that larger plastic zone should take place for blunt notches than it does for sharp ones. Throughout this work the total counts v.s. times is also recorded for specimens of 12.7 mm and 25.4 mm notch root radii (Figures 36, 37 and 38). The resulting number of total acoustic counts for all these specimens are:

Specimen Code	Notch root radius(mm)	Total acoustic counts where deformation started	Total A/E counts when a crack initiated
AE4	0.127	2.34×10^6	2.81×10^6
AE7	12.70	96.0×10^6	109.82×10^6
AE3	25.40	105.0×10^6	175.7×10^6

These results could give the operator an early warning even before the fatigue crack starts to initiate by carefully watching these equally spaced lines from the recording chart. Once these lines start to get wide apart the plastic damage starts at the tip of the notch. The count rate is a better measure as well as a better warning. The above results in the table give the information to the designer where to be careful once these spacings of figures 36, 37 and 38 begin to be wider apart. The final point from these results is that the total acoustic counts from the start of plastic deformation to a point where the fatigue crack initiated was found to be greater for blunter notched specimens than for the sharper ones. Figures 36, 37 & 38 are an original copy reduced to A4 size. For all these tests the electrical potential technique was used to detect the fatigue crack initiation.

5.8 Fatigue crack propagation

The fatigue crack growth have been plotted in figure (52) for both materials at five different temperatures. All are equally valid in the sense that their originator considered that they accurately represented a set of fatigue crack growth data, although other data can often be found to refute any particular theory. The following results concluded to represent the crack growth equation for both materials. All temperatures are statistically found.

Temperature	Material A	Material B
Room temp.	$\frac{da}{dN} = 10^{-6.82}(\Delta K)^{1.71}$	$\frac{da}{dN} = 10^{6.66}(\Delta K)^{1.7}$
+50°C	$\frac{da}{dN} = 10^{-12.5}(\Delta K)^{3.92}$	$\frac{da}{dN} = 10^{-7.5}(\Delta K)^{2.06}$
+100°C	$\frac{da}{dN} = 10^{-7.28}(\Delta K)^{1.99}$	$\frac{da}{dN} = 10^{-7.35}(\Delta K)^{2.05}$
-50°C	$\frac{da}{dN} = 10^{-7.32}(\Delta K)^{1.95}$	$\frac{da}{dN} = 10^{-7.30}(\Delta K)^{1.91}$
-100°C	$\frac{da}{dN} = 10^{-7.32}(\Delta K)^{1.8}$	$\frac{da}{dN} = 10^{-7.32}(\Delta K)^{1.8}$

These latest results are very close to crack propagation results introduced by Frost and Dixon in their theory of propagation where they found that m = 2.0. Excluding the test of material A at +50°C all the results confirm the above theory and show no significance in this law at various temperatures. All the experimental data in this work pertaining to cracks of overall length of up to 5.0 mm were used in the fracture mechanics analysis. Curves were fitted to the basic crack length versus the number of cycles data for each specimen, and crack growth rates obtained

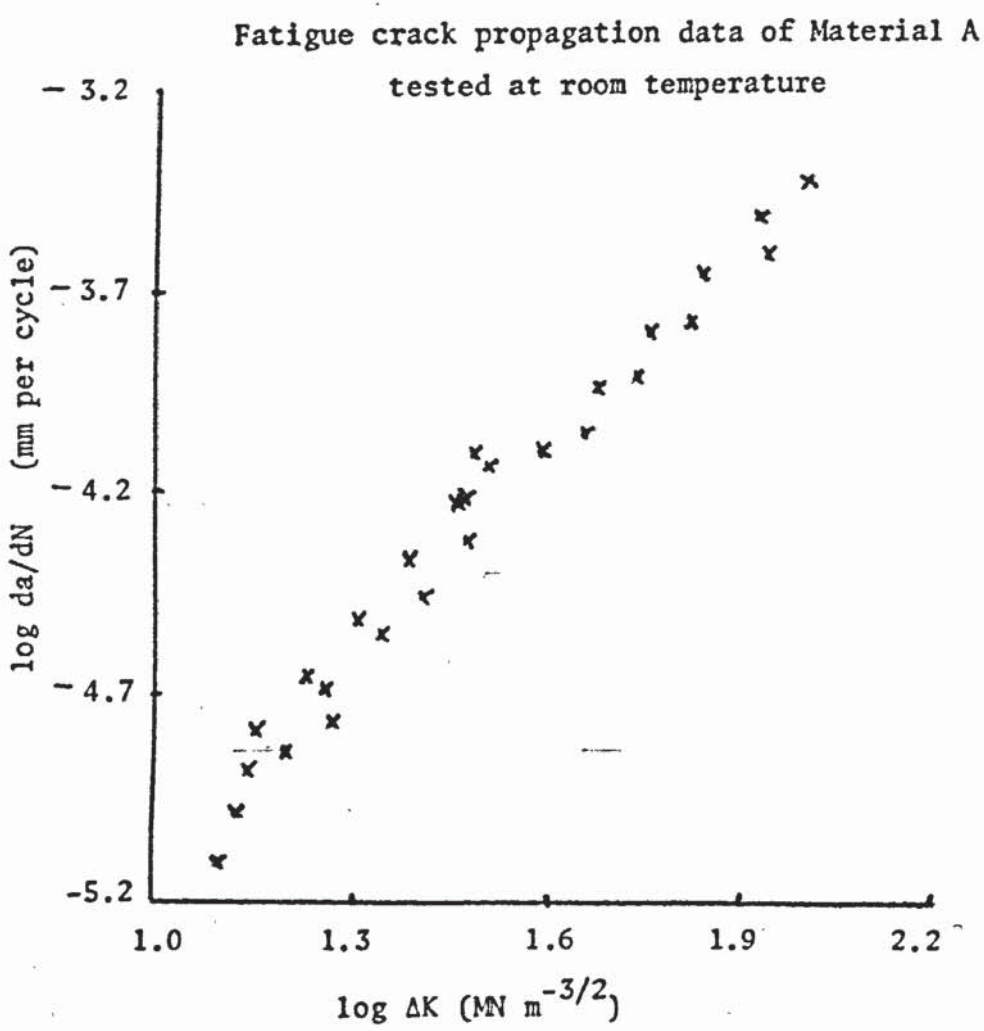
Fatigue crack propagation data of Material A
tested at room temperature
-3.2
-3.7
-4.2
-4.7
-5.2
log da/dN (mm per cycle)
1.0
1.3
1.6
1.9
2.2
log ΔK (MN m$^{-3/2}$)

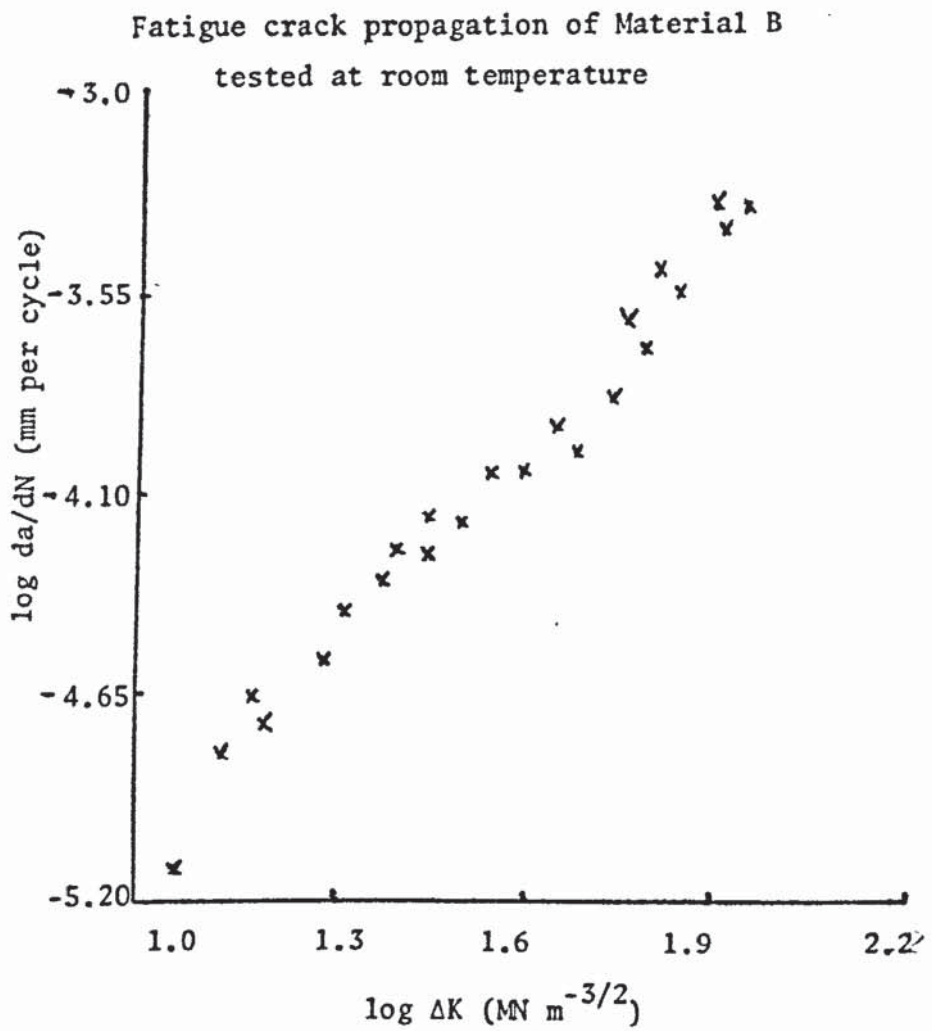
Fatigue crack propagation of Material B
tested at room temperature
-3.0
-3.55
-4.10
-4.65
-5.20
log da/dN (mm per cycle)
1.0
1.3
1.6
1.9
2.2
log ΔK (MN m$^{-3/2}$)

Figure 52

Fatigue crack propagation data of Material A
tested at +50°C

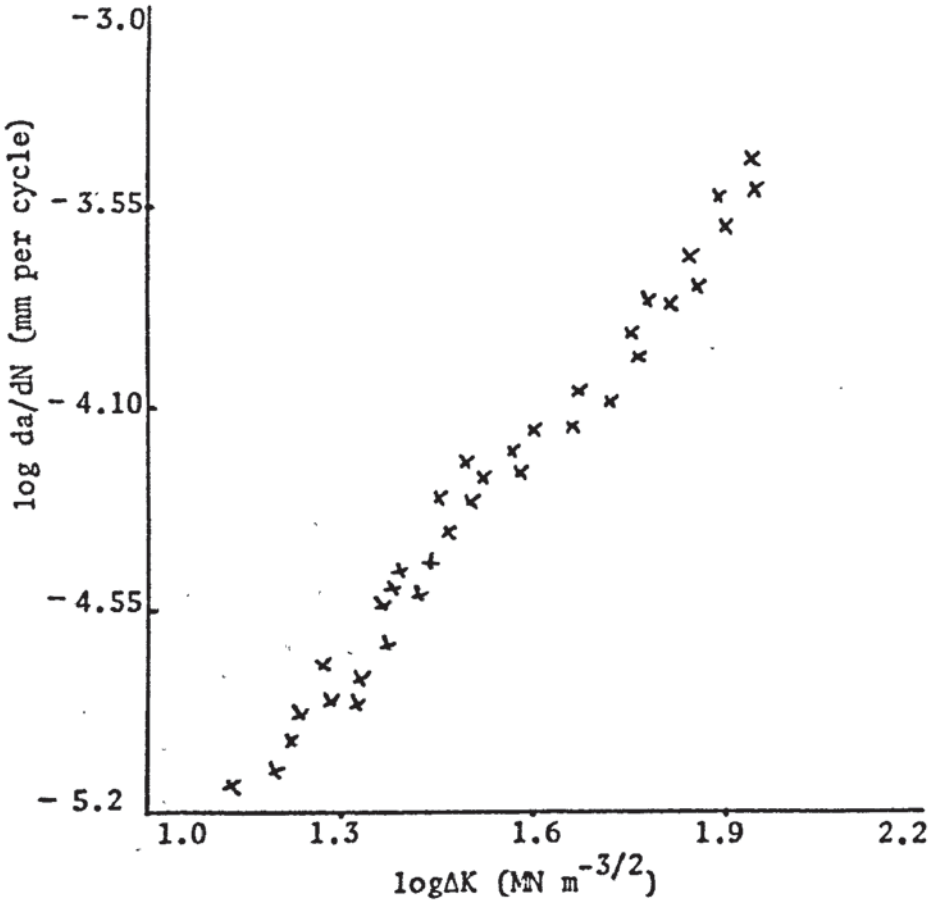

Fatigue crack propagation data of Material B
tested at +50°C

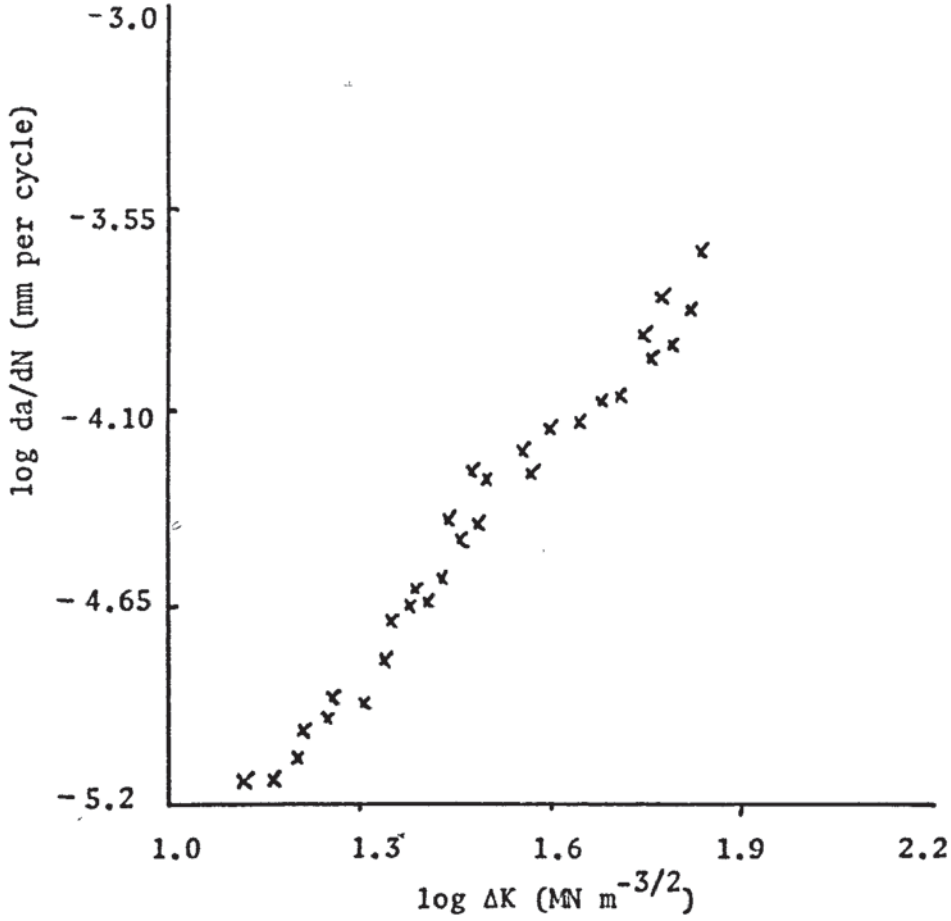

Figure 52 continued..

Fatigue crack propagation data of Material A
tested at +100°C

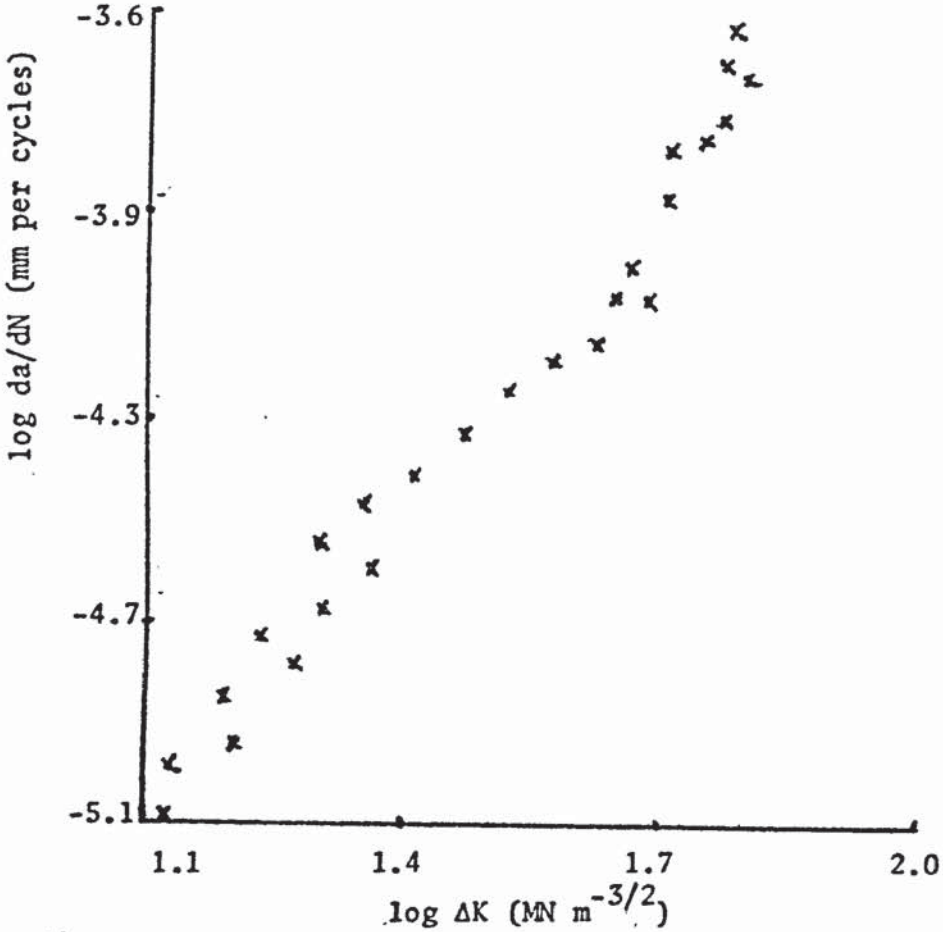

Fatigue crack propagation data of Material B
tested at +100°C

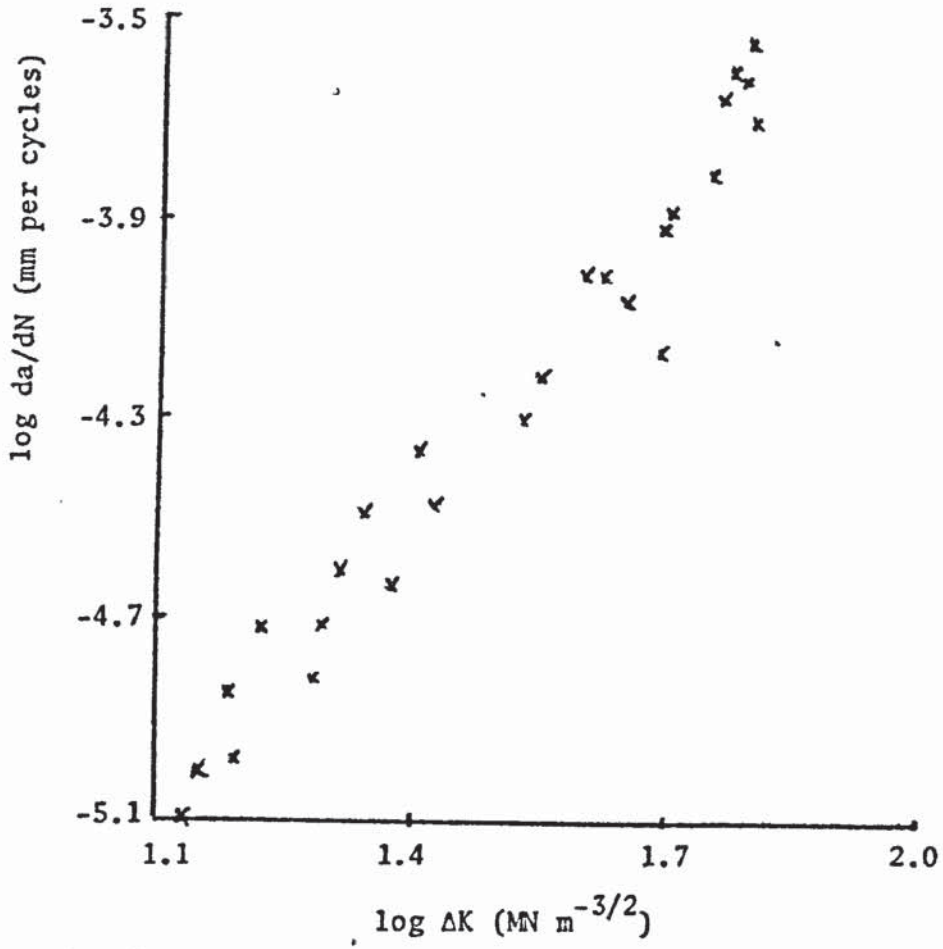

Figure 52 continued..

Fatigue crack propagation data of Material A tested at -50°C

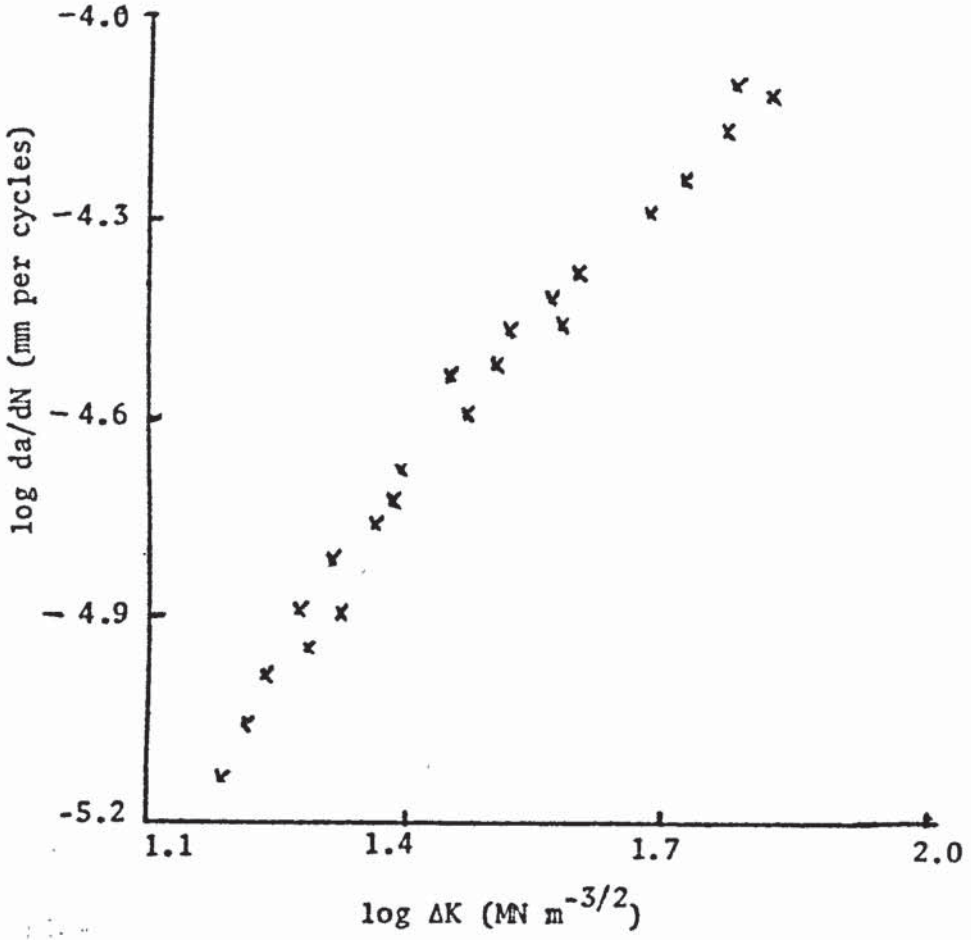

Fatigue crack propagation data of Material B tested at -50°C

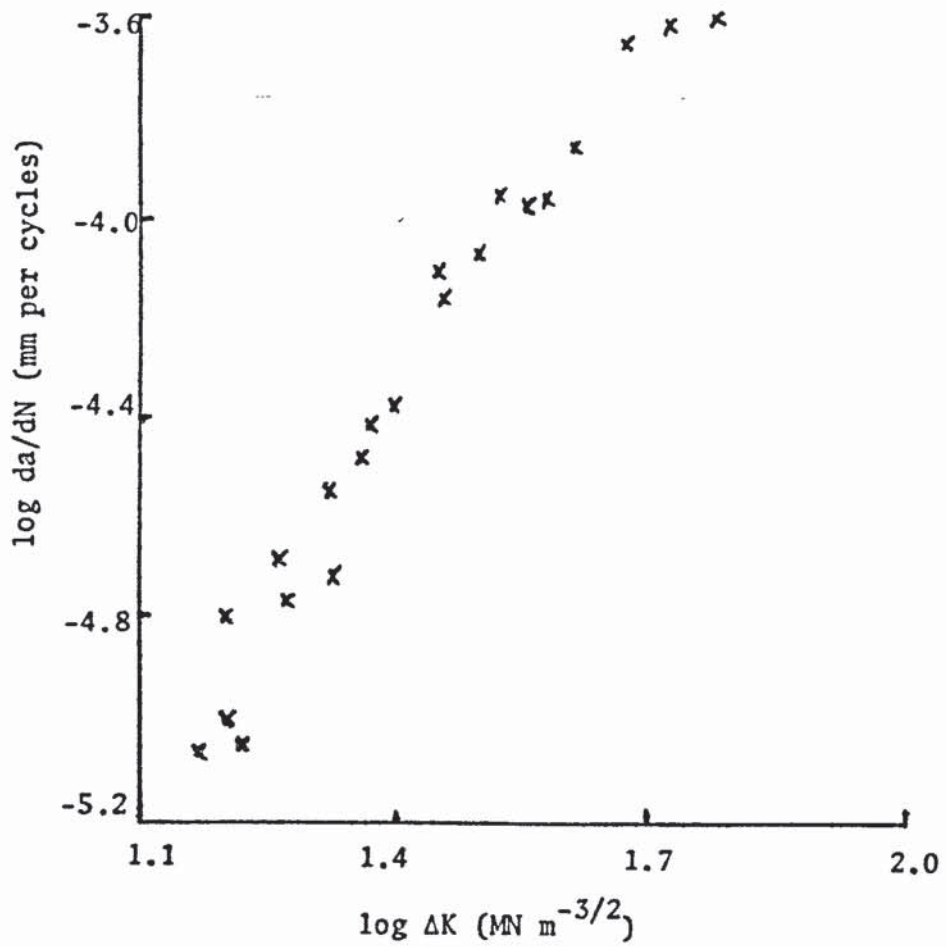

Figure 52 continued...

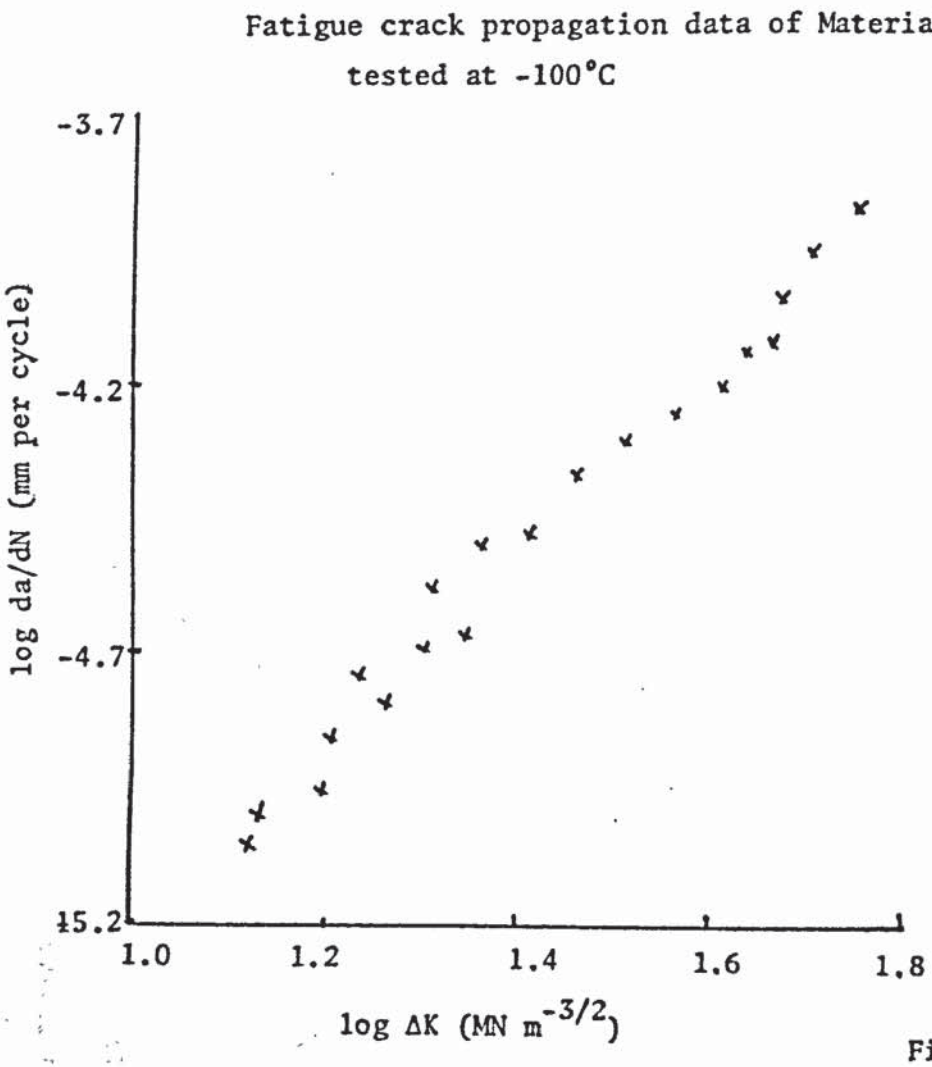

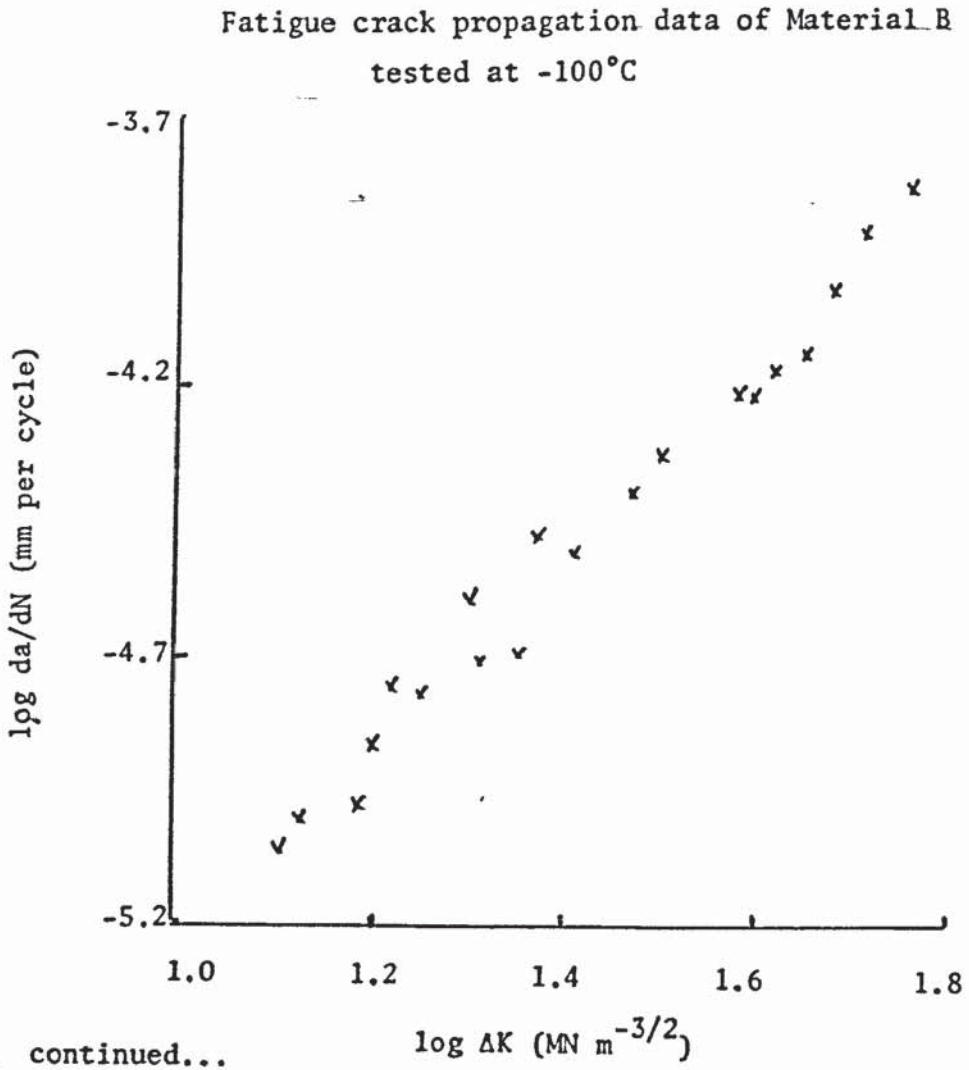

Figure 52 continued...

from the appropriate slopes. As the crack growth does not take place unless a critical value of ΔK, that is, ΔK_c is exceeded by a theoretical minimum crack growth rate can be calculated using the coefficients given in the previous equations by substituting the appropriate value of ΔK_c. The resulting data was plotted in figure 52 where it indicated that at some certain value of ΔK_c (e.g. room temperature $\log \Delta K \approx 1.5 - 1.7$) the crack growth rate is not dependent on ΔK. It seems to be the case for all three first temperatures, which it (the crack growth rate) is always significant of ΔK_c. There is not sufficient evidence throughout this work to determine the element of cracking per cycle in these materials by metallurgical and not even geometric consideration. The element of macro-crack occurring per cycle could be some function of inclusion size, spacing, or mean and alternating stresses. Large inclusions widely dispersed could have the effect of making da/dN highly mean-stress dependent. The difference in over-all growth rates during the first three temperatures was due to the heat treatment difference and grain size difference was resulted. Because fatigue crack growth is a strain in controlled process the behaviour of different steels would be expected to be similar if compared on the basis of strain instead of stress. Unfortunately, there is not sufficient evidence throughout this work to prove this although it was shown by Frost (1974).

These crack propagation data of both steels for five different temperatures plotted in figure 52 represent valuable information for a designer since no information of crack growth rate is available for either steel under such conditions. The expectation of improving the crack growth rate by an addition percentage of molybdenum was negative as a result of this investigation, but still valuable since it indicates how tough these materials are even at sub-zero tests.

5.9 Fracture toughness tests at five different temperatures

For both materials using the linear elastic fracture mechanics approach (LEFM) results showed that they are almost free of defects. For both materials the basic specimen size gave valid assessments of K_{IC}. The K_C values of these materials seem to confirm the general pattern (7) at room temperature. The critical stress intensity factor (K_C) of material A seems to be 6% higher in value than that for material B at room temperature, about 10% higher at +50°C, while 3% lower K_C for material A than it is for material B at +100°C. Results also indicate that K_C values are found to be greater for material A by an average of 11.5% than it is for room temperature. Yielding seemed to take place before the crack initiated, therefore using electrical potential techniques to detect the point of crack initiation was very helpful to calculate K_C for all temperatures. For fracture toughness tests results at sub/zero temperatures namely - -50°C and -100°C the K_C values calculated throughout this survey seemed to be one third of the room temperature tests for material A at -50°C and nearly one sixth of the room temperature value at -100°C. The K_C values of both materials stated in Section 4.3 could be summarized as percentage in relation to room temperature results.

Materials	°50°C	+100°C	-50°C	-100°C
A	118%	102%	32.7%	17.3%
B	114%	111%	34.2%	17.5%

This last conclusion shows that since -50°C and -100°C are far below the transition temperature of both materials it is therefore expected to find the K_C value dropping to about 34% of that value at room temperature

and to about 17% of that value at -100°C. The minimum specimen thickness for a specimen which gave valid critical plane strain intensity (K_{IC}) was found to be 40 mm. The resulting estimates of K_{IC} for material A described here was found to be equal to 135 MN $m^{3/2}$ and 132.5 MN $m^{3/2}$, these seem to be tough materials. The results of surface fractography of random selected areas of these fractured surfaces shows that figures 39 and 40 are ductile and cleavage fracture respectively. At all temperatures the calculated results which depend on the 5% secant of the load C.O.D. curve to correspond to plastic failure and not to crack initiation. This was demonstrated by simultaneous use of the potential technique to detect fracture initiations. Figures 39 and 40 show small shear lips which proves that these fractures are of a plane strain character. To study the toughness of these two materials in more detail several tests were carried out applying not only the L.E.F.M. approach but also the J-integral and the acoustic emission techniques in the next section. All sixty results of the five temperatures are tabulated in Tables 15 and 16 in Section 4.3.

5.10 Fracture toughness test using acoustic emission and J-integral applications

Results of Table 17 show higher values of K_C for specimens half-way prefatigued than those specimens tested as received (just notched). The first part of Table 17 indicates that there is no point in comparing the notch root radius with the total counts produced, since prefatiguing the blunt crack more than 5.0 mm from the crack (notch) tip will produce a sharp crack anyway. The point to state here from these results is that the total acoustic count is lower for a/W value of 0.34. The value of the acoustic emission increased sharply for a/W value of 0.26 which was the maximum number of counts at crack initiation, figure 45. As a/W increased the total acoustic counts increased by about 50% up to a/W = 0.6. Figure 44 the plastic zone shape formed on the surface of the specimen at the times when the crack initiated during monotonic loading. All these specimens were stress cooled to give clear view of the plastic damage. The resulting value of K_C calculated both ways, L.E.F.M. method and the J-integral approach, the two results show a good agreement with about 2% apart. One should always keep in mind that the crack initiation was in both ways,detected using the electrical potential technique. Figure 46 gave a conclusive result, that is, for sharp notches (0.127 mm root radius) the total count at crack initiation was much higher than for ρ = 0.250 mm, nearly the same for ρ = 0.50 mm and it is much lower than for ρ = 1.5 mm. By duplicating the test (one specimen stress was coated, the other was not) Table 17 and figure 46 showed that the stress coating did not effect the number of total counts rate since it was found to be higher and lower for both sharp and blunt specimens. Figure 47 concludes that the effective value of K_C independent of the notch root

radius increases. This was found out by the L.E.F.M. approach as well as the J-integral approach providing the crack detection is by means of electrical potential technique.

The plastic enclave formed before the crack initiated is shown in Figure 48. The plastic zone size and shape before a monotonic loading crack initiated is shown on the surface of the specimen in this figure. The size of this plastic zone, at a load of 1.51 tonnes, was found to be about forty times smaller than it is when the test was stopped at 1.94 tonnes as can be seen from figure 44 for three different notch shapes. Load versus load point deflection (displacement) was represented in figures 41, 42 and 43.

Although figure 48 gives evidence of surface plastic damage, the test was carried out simply by loading the specimens to a point just before the monotonically loaded specimen cracked. The resulting internal examination of this test after sectioning the specimen indicated that no sign of plastic damage could be traced, while the surface damage in the form of slip lines and slip bands was found in the same pattern of figure 48. These latest results suggest that the plastic damage is too small to be detected inside the specimen or no damage could penetrate through the whole thickness.

5.11 Scanning electron microscope fractography

Random samples of scanning electron photographs were selected and displayed for a fatigue crack initiation and propagation. Figures 20a, b,...20h explain the initiation fractography of both materials. Figures 20i,...20r gave details of propagation fractography of both materials. The initial remark could be concluded from these fractographies that material A shows more ductile fracture surface while material B shows brittleness properties (Figures 20a, 20b, 20c, 20d, 20e and 20f) for temperatures namely - room temperature, +50°C and +100°C. Figure 20a shows how the initiation of fatigue crack on the surface contains a carbide inclusion which is about 80 μm in diameter. Separation of inclusion from the matrix was indicated by an arrow. The initiation fracture surfaces indicate that slip bands were present to contain cracks at the end of a test, especially for a specimen which had a long life and the origin of cracking is associated with the free surface (Figures 20a, 20b, 20c, 20d, 20e and 20f). The sub-zero temperature tests did not give evidence to show that extrusion and intrusions could form in slip bands throughout this work, While other workers showed that at even lower testing temperatures the propagation fractography faces produced by a continuously growing fatigue crack have a smooth matt appearance, free from markings visible to the naked eye for all temperatures. Raising the temperature to +50°C and +100°C did not seem to change the mode of cracking from transcrystalline to intercrystalline as previously showed simply because the temperature was not high enough to produce such a change. To change the mode a temperature of 250°C should at least be used. All fractography displayed in Chapter 4 gives a clear picture for both initiation and propagation mechanisms of both materials.

CHAPTER 6

CONCLUSIONS

The following conclusions could be drawn from the results of this investigation.

1. The results of this investigation indicate that the additional percentage of molybdenum did not produce a significant difference in fatigue properties. The grain size difference produced a fatigue property difference which confirms the early theories, which indicate that, the finer the grain size the higher the number of cycles required to initiate a detectable fatigue crack.

2. The use of the acoustic emission technique in conjunction with the electrical potential technique provides a reasonable method to detect the initiation of a fatigue crack providing factors are known (load, the voltage gain (dB) and the specimen notch geometry).

3. Fatigue crack initiation and propagation can be observed by the decreasing value of the count rate or the total accumulated counts during the test. The detection of initiation by acoustic emission was in agreement with the point of initiation indicated by an increase in the voltage across the notch using the potential drop.

4. Average K_C value of both materials at all temperatures produced showed no significant difference. These values are shown in Chapter 5. These values show high toughness at both materials.

5. The J-integral technique for toughness measurement using either the Acoustic emission technique or the Electrical potential technique to detect the point of fracture initiation gave results in agreement with L.E.F.M. methods.

6. The total accumulated number of acoustic emission counts to the initiation of fracture in a J-integral test was found to vary with the a/W ratio. The a/W ratio was itself varied by increasing the length of the fatigue crack at the notch root.

7. Total number of acoustic counts required to give an early warning before fracture was higher for specimens just notched without pre-fatiguing by an average factor of 1.5×10^2 for sharp notches, ($\rho = 0.005"$) and increases to 2×10^3 for blunt notches, ($\rho = 0.50"$ and $\rho = 1.0"$).

CHAPTER 7

RECOMMENDATIONS FOR FURTHER WORK

The author would like to recommend the following proposals for further work:

1. During this investigation the temperature band was between -100°C to +100°C due to the economic situation, therefore expanding the range of temperature say from -400°C ro +400°C would allow us to investigate the extrusion and intrusion formation in more detail. High temperature tests have also been used to investigate the mode change of cracking from transcrystalline to intercrystalline which has been shown for other materials but not for these types of steels.

2. Electro-polished tests are recommended for all temperatures to investigate the plastic damage before a fatigue crack initiates and whether the slip line forms the same pattern and direction or not.

3. More intensive study of the plastic zone size and models is recommended and to be compared with the existing models, e.g. Smith's, Dugdale's, L.E.F.M. and Vitek.

4. It would also be valuable to study the fatigue properties at all temperatures applying lower frequencies (e.g. 1.0 Hz).

5. The acoustic emission technique is a useful one, therefore the author strongly recommends to apply this technique for both fatigue and fracture toughness investigations. In order to define the total counts necessary to initiate a fatigue crack or to initiate a fracture an intensive study should be carried out.

ACKNOWLEDGEMENTS

The author would like to express his indebtedness to Professor J. T. Barnby, for his values advice and encouragement and the criticism of the final draft of this thesis. He also takes the opportunity to thank Professor W.O. Alexander, former Head of this department. Thanks are also due to Professor I.L. Dillamore for providing the necessary equipment to complete this research.

Acknowledgement with gratitude is made to the Ministry of Higher Education and Scientific Research of the Republic of Iraq for providing the financial support for the research programme. The Steel Casting Research and Trade Association (SCRATA) the supplier of testing material for the research programme, their help is gratefully acknowledged.

APPENDIX I

Because both materials A and B were received in the form of large blocks effort was provided to use the Metallurgy Department facilities to cut these blocks to the required size specimens allowing 2.0 to 3.0mm for shaping and grounding.

This Appendix shows how these specimens locate with reference to the original block. The position of the specimen could be affected due to heat treatment and size of the cast.

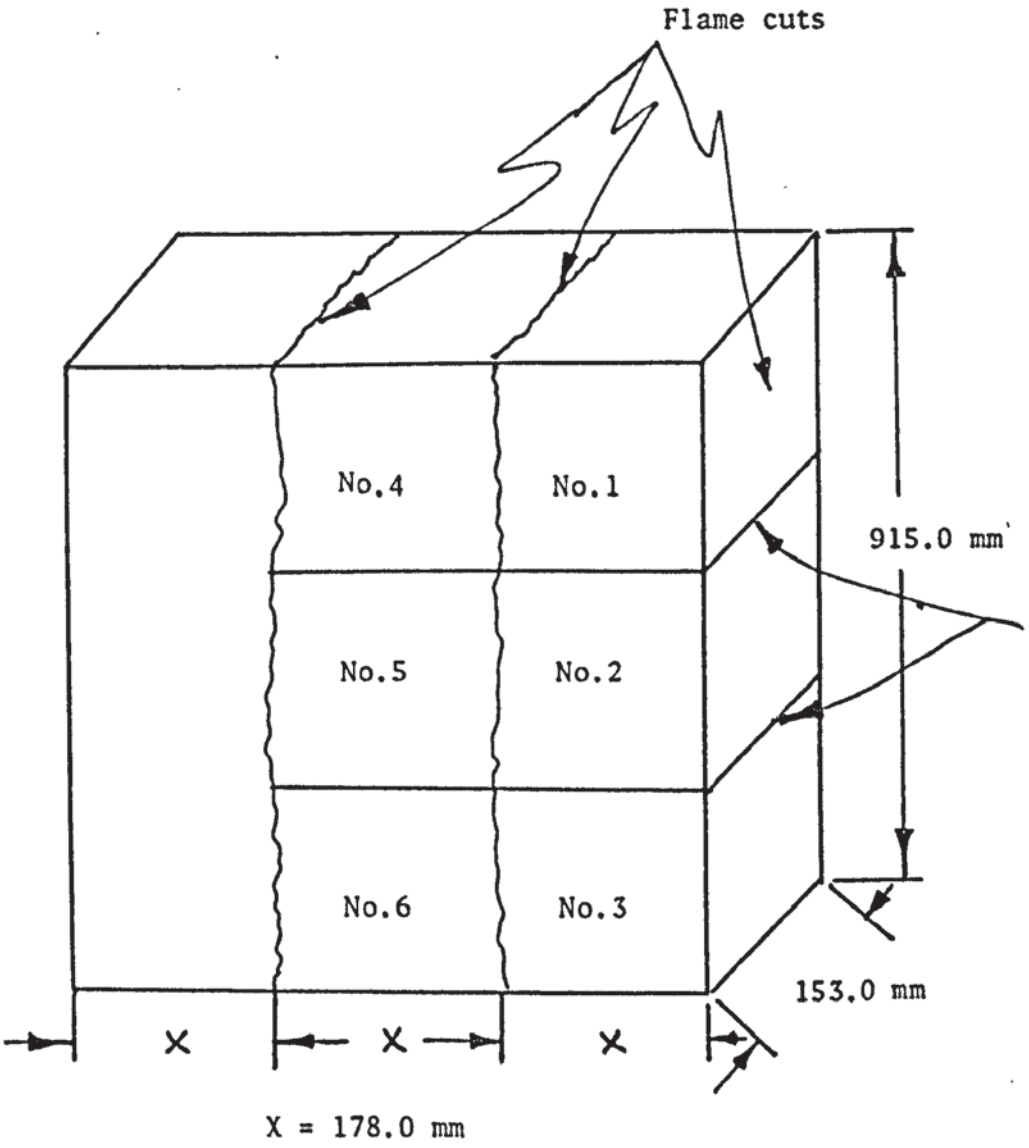

Figure i - Represents the position of the blocks relative to the Anchor piece

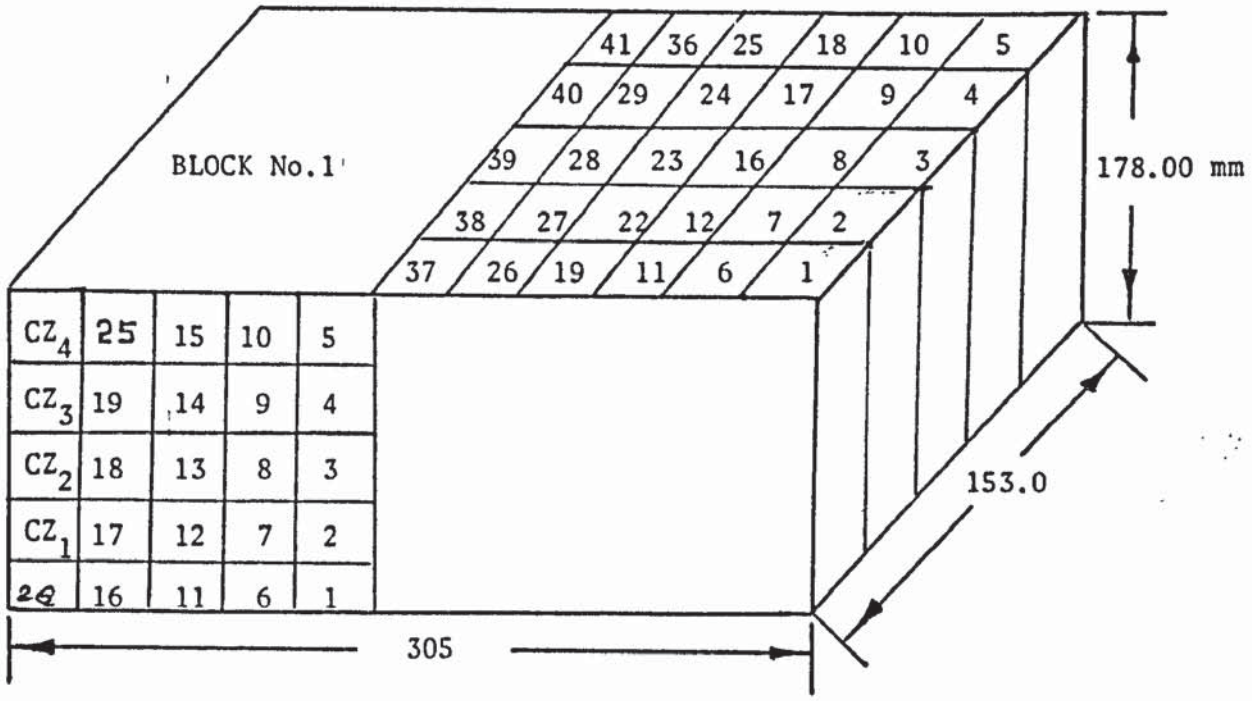

Figure (ii) - 1) Specimens were cut vertically (1-41) are cooled as AZ1, AZ2.....AZ41.

2) while specimens have been cut horizontally (1-26) are cooled as BZ, BZ.....BZ

3) Specimens marked with CZ_1, CZ_2.... are calibration specimens

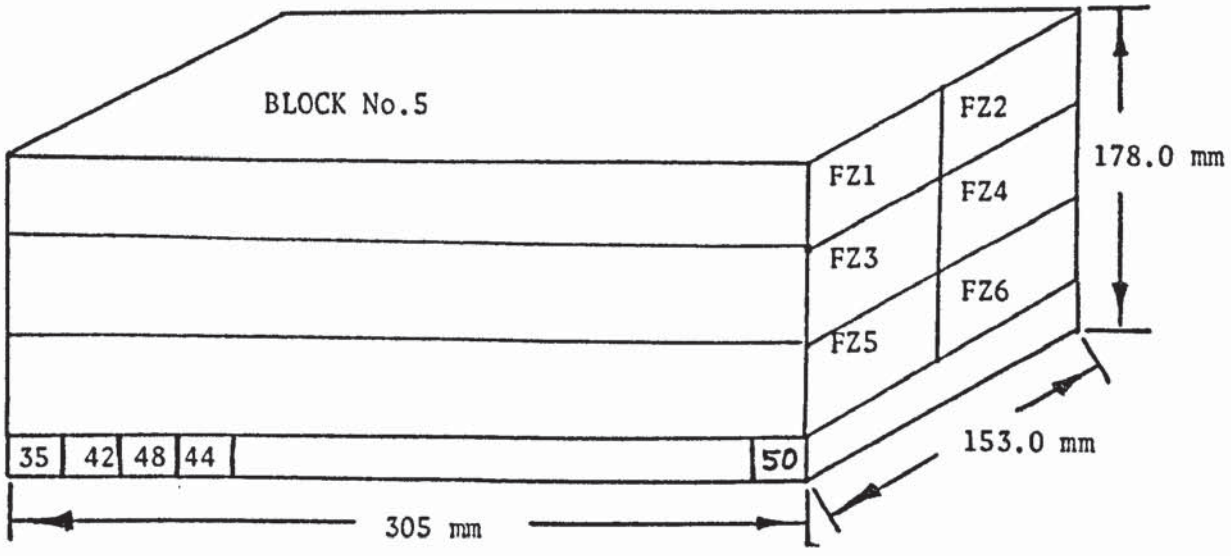

Figure (iii) 1) Specimens numbered 35,42,43...50 are loaded as AZ35, AZ42, AZ43...up to AZ50

2) Other six specimens from this block were large fracture toughness specimens 40 x 50 x 305 mm.

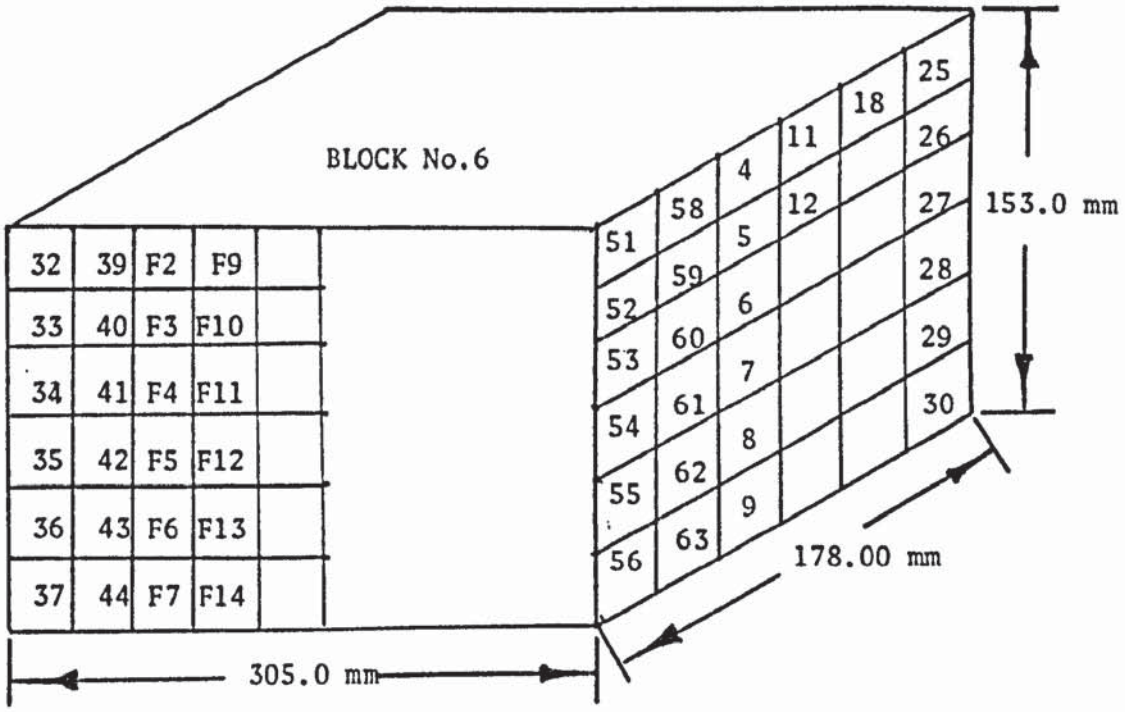

Figure (iv)

1) Specimens numbered 51,52,...61 represented by the following code: AZ51, AZ52,...AZ61 (fatigue test specimens)

2) Specimens numbered 1 to 26 represented by the following code: CZ5, to CZ30 (calibration specimens).

3) Specimens numbered and coded in brackets as shown: 26(A8), 28(A47), 29(A48), 30(A49), 31(A53), 32(A54), 33(A55), 34(A59), 35(A60), 36(A61), 37(A66), 38(A68), 39(A76), 40(A77), 41(A82), 42(A98), 43(A99), and 44(A100), Fatigue Test specimens

4) Specimens numbered F1 to F15 are fracture toughness test specimens Small size (20 mm x 25 mm) coded by FAZ & FBZ in tables.

MATERIAL "B" (BS.1456A)

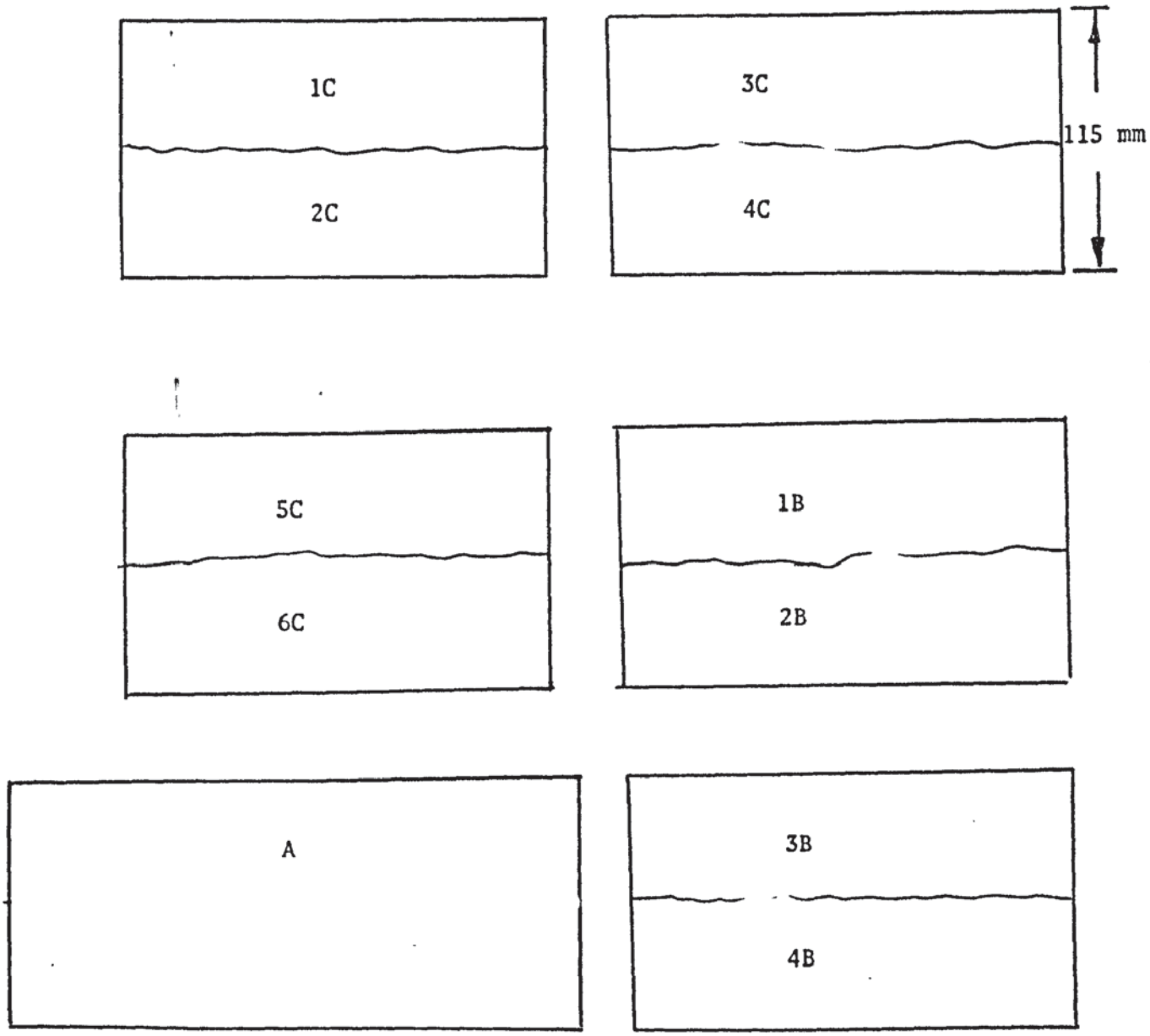

Figure (v) - Blocked received as cast and sawn cut in the middle.

Dimensions: Blocks No.1,2,3,4,5 & 6C were: 30 mm x 115 mm x 300 mm

Blocks No.1,2,3 & 4B were: 65 mm x 132 mm x 250 mm

Block A was 100 mm x 190 mm x 450 mm

Figure (vi)

1	3	9	11	14	16	18	20	22	24
2	6	10	13	15	17	19	21	23	25

1B

27	30	32	37	39	41	44	46	51	55
29	31	33	38	40	42	45	47	54	57

2B

58	60	63	65	71	73	75	84	88	93
59	62	64	67	72	74	81	85	92	94

3B

95	97	HT2	HT4	HT6	HT8	HT10	HT12	HT14	HT16
96	HT1	HT3	HT5	HT7	HT9	HT11	HT13	HT15	HT17

4B

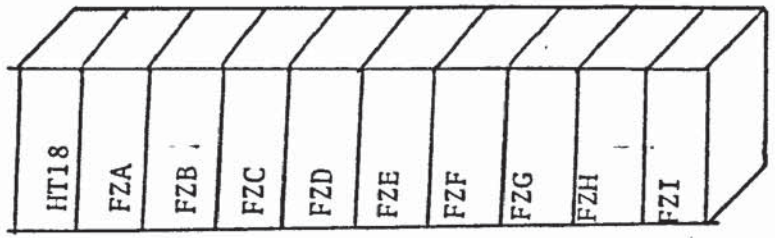

1C

1) 2C was cut to ten specimens 20 mm x 25 mm coded as CB1, CB2,....CB10 as calibration specimens.

2) 3C was cut to ten specimens 20 mm x 25 mm coded as CB11, CB12,...CB15,AE1B,AE2B,AE3B,AE4B & AE5B.

3) 4C & 5C was cut to twenty specimens coded as AE6B, AE7B,....,AE7B.

4) 6C was cut to ten specimens coded as: AE15, AE17, F1,F2,F3,F4,F5,F6,F7,F8

5) Block A was cut to 12 specimens used to fracture toughness test, their size was: 90 mm x 50 mm x 240 mm FB1, FB2,.....FB15 chosen.

6) Broken large fracture toughness specimens were to machine some (four small specimens each) and used as follows:
   a) Eight specimens with blunt notches used for F.T.T. (A.E.), FA1, FA2,...FA8.
   b) Three specimens for a fatigue test to check the heat treatment. FT1, FT2 and FT3.
   c) Fifteen for fracture toughness of 5 temperatures FBZ.

APPENDIX II

Crack length-voltage calibration specimens

Forty-five specimens were necessary for this calibration of both materials, A and B, there were thirty specimens each. Every batch of material 'A' was tested at one of the following temperatures (room temperature and -50°C). The remaining fifteen specimens were of material 'B' which have been tested at room temperature only. All specimens of both materials were the same size as the fatigue test specimens (20 mm x 25.0 mm x 120 mm). Also all specimens contained the same notch root radii (0.127 mm) with a notch depth of 5.0 mm. All specimens were used for the empirical calibration by stopping the fatigue crack growth at various stages, breaking the specimen open and measuring the crack length, corresponding to a given voltage, optically. A constant 20.0 amperes current has been passed through the specimen, a 20.0 Hz frequency was used and the potential drop equipment shown in the figure was used to record the A_a & V_o readings as could be seen in figures (i), (ii) & (iii). Tables 1, 2 and 3 of this Appendix show the results of these calibration tests. These results were plotted in figures (iv), (v) and (vi).

This method was first established by Gilbey and Pearson where the ratio V_a/V_oW determines the effective values of Y. As crack length increases measurement of crack length becomes less sensitive to error in determining the effective value of Y where Y is the material constant, and it is a polonomial function of a/W. As small values of a/W greater

sensitivity to changes in a/W is obtained. The plots of these curves for three different temperatures (figures iv, v, iv) are used to study crack growth rate mechanism for different specimens and two different stress values for all five temperatures to predict the crack propagation law and compare it with other theories discussed through the literature survey in Chapter 2.

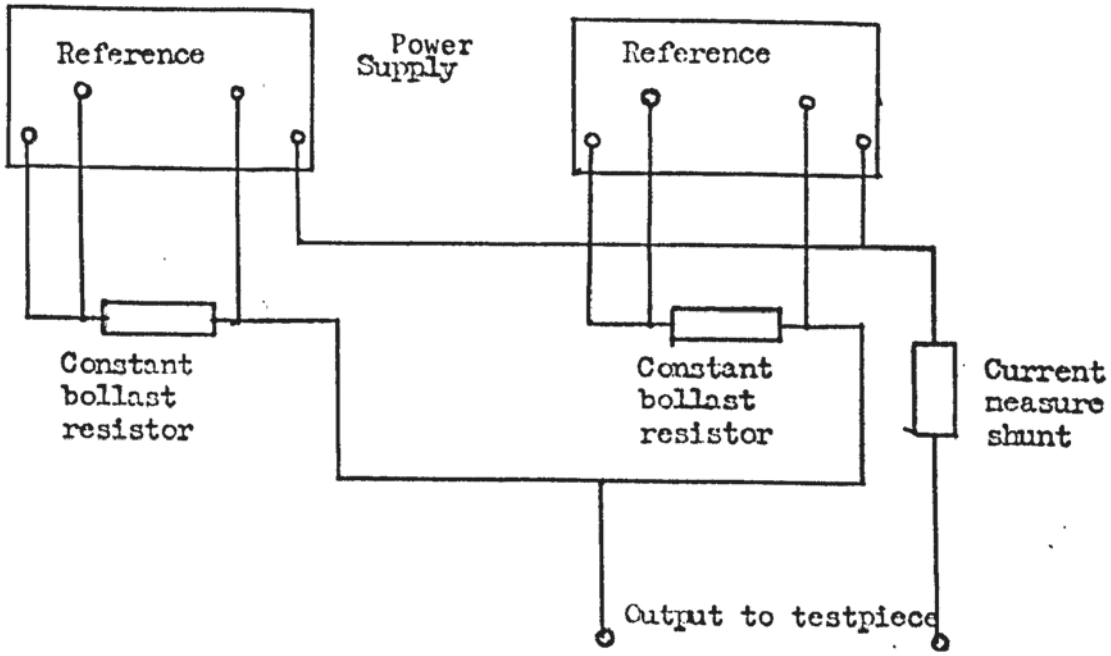

Figure (i) Power circuit

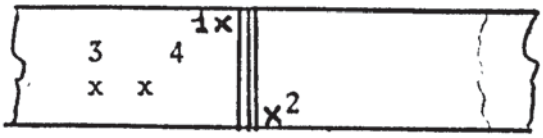

Figure (ii) Position of probes

V_a - potential drop across the crack (1 - 2)

V_o - potential drop across the uncracked material over a unit distance

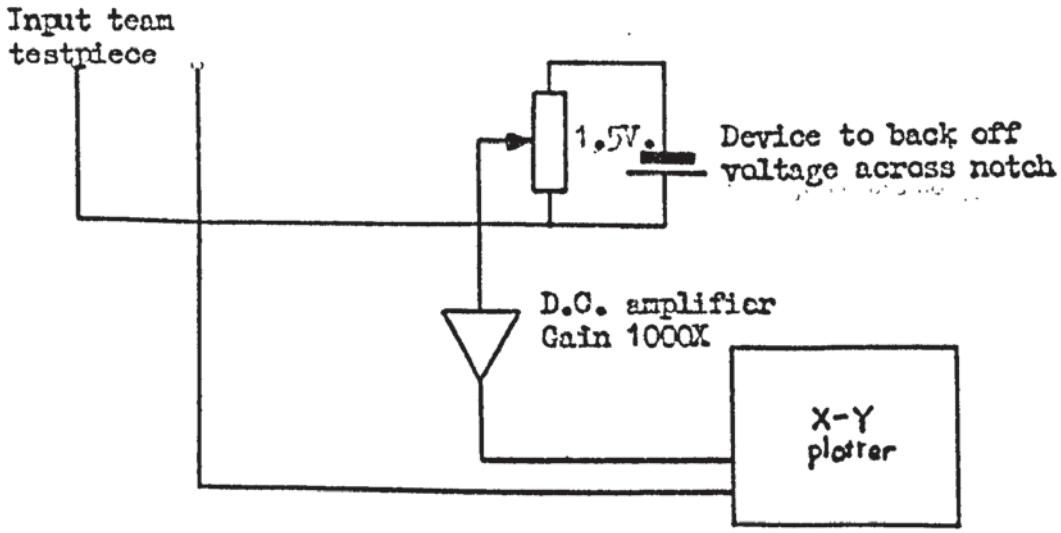

Figure (iii) Voltage measuring circuit

No.	Code	a mm	a/W	V_a μv	(V_a/WV_o) x $10^3 mm^{-1}$
1	CZ5	5.00	0.2	45.0	18.0
2	CZ6	5.25	0.21	46.0	18.4
3	CZ7	5.63	0.225	47.0	18.8
4	CZ8	6.06	0.242	48.5	19.4
5	CZ9	6.40	0.256	55.0	22.0
6	CZ10	7.00	0.28	60.0	24.0
7	CZ11	7.50	0.30	78.0	31.2
8	CZ12	7.90	0.316	87.0	34.8
9	CZ13	8.15	0.326	97.0	38.8
10	CZ14	8.30	0.332	100.0	40.0
11	CZ15	8.45	0.338	120.0	48.0
12	CZ16	8.56	0.342	133.0	53.2
13	CZ17	8.75	0.35	143.0	57.2
14	CZ18	8.80	0.352	155.0	62.0
15	CZ19	8.80	0.352	168.0	67.2

W(Specimen width) = 25.0 mm

V_o = 100 μv

TABLE 1

Material A tested at room temperature

$$a = 546.3\ V_a - 89\ V_a^2 + 4.9\ V_a^3$$

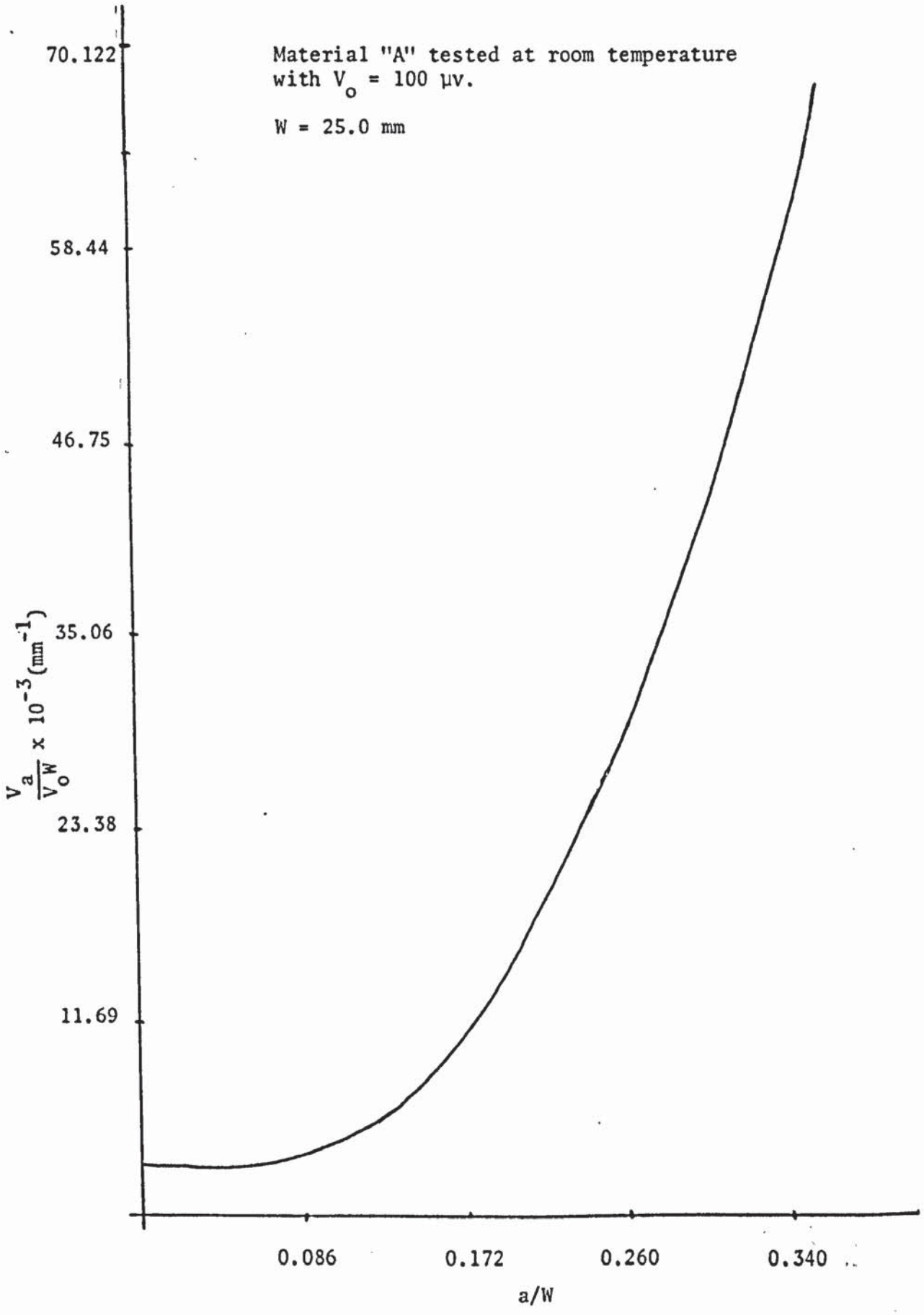

Figure (iv)

No.	Specimen Code	Crack length a(mm)	Initial voltage reading V(μv)	Voltage increase Δv (μv)	Final voltage reading V_a(μv)	Ni cycles	Test Stop N cycles	REMARKS
1	CZ1	0.000	40.0	0.000	40.00	-	-	
2	CZ2	0.490	78.50	2.50	80.00	29280	83780	-50°C
3	CZ3	1.410	65.00	5.00	70.00	48160	80250	Calibration tests.
4	CZ4	1.651	64.00	12.50	76.50	15000	60400	
5	CZ20	1.750	58.00	20.00	78.00	17000	65200	V_o = 100.8 μv
6	CZ21	2.250	42.00	27.50	69.50	9600	51940	
7	CZ22	2.112	48.00	35.00	83.00	12000	56320	
8	CZ23	2.775	54.00	40.00	94.00	7800	39660	
9	CZ24	2.810	64.00	45.00	109.00	12900	89500	
10	CZ25	2.951	76.00	52.50	128.50	12000	56930	
11	CZ26	3.110	67.50	60.00	127.50	7200	54860	
12	CZ27	3.485	62.00	67.50	129.50	9600	68710	
13	CZ28	3.540	67.00	80.00	147.00	19000	66680	
14	CZ29	3.620	55.00	100.00	155.00	21000	75400	
15	CZ30	3.650	65.00	120.00	185.00	27000	80100	

TABLE 2

1. P_{max} = 14.5 kN. P_{min} = 0.5 kN. P_{mean} = 7.0 kN.
2. Crack length (a) is the average of elevel equal-distance readings of the fractured surface.
3. Material A, specimens machined from big F.T.T. spec. after fracture.

$$a = 59.23\ V_a - 10.2\ V_a^2 + 10.2\ V_a^3$$

Material "A" tested at -50°C with V_o = 100.8 μv

W = 25 mm

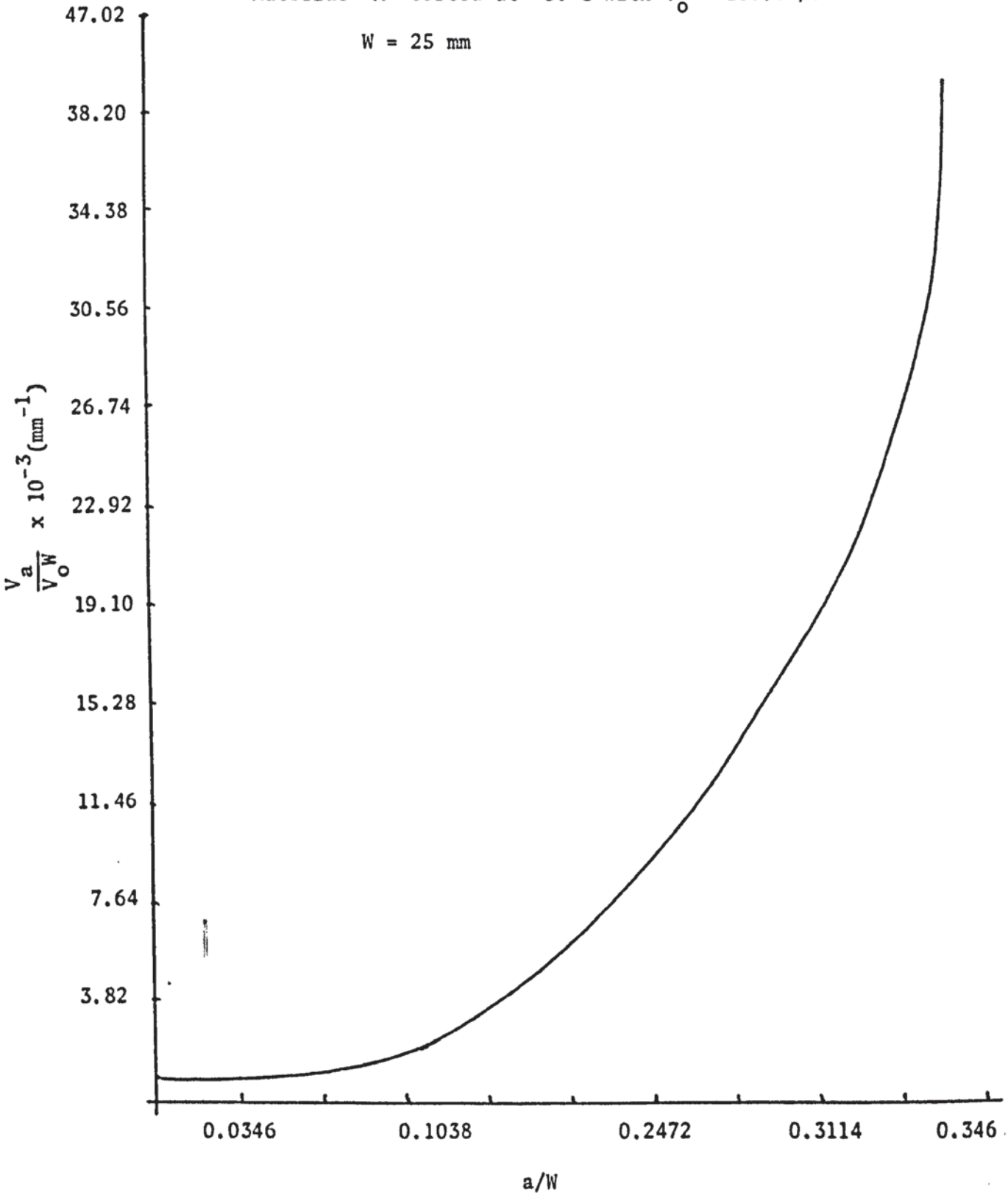

Figure (v)

NO.	Code	a mm	V_a μv	a/W	$(V_a/V_o W(mm^{-1}) \times 10^{-3}$
1	CB1	5.0	2.50	0.2	0.989
2	CB2	5.45	3.00	0.218	1.181
3	CB3	6.37	5.00	0.255	1.969
4	CB4	6.76	12.50	0.270	4.921
5	CB5	6.86	17.50	0.274	6.900
6	CB6	7.13	17.80	0.285	7.010
7	CB7	7.25	27.50	6.29	10.827
8	CB8	7.80	40.00	0.312	15.748
9	CB9	7.86	45.00	0.314	17.716
10	CB10	7.93	52.50	0.317	20.670
11	CB11	8.15	60.0	0.326	23.622
12	CB12	8.50	67.5	0.34	26.475
13	CB13	8.56	80.0	0.342	31.496
14	CB14	8.65	90.0	0.346	35.433
15	CB15	8.65	100.0	0.346	39.370

Material B (R.T.)

V_o = 101.6 μv

TABLE 3

Calibration Test Results

$$a = 124.6\ V_a - 25.12\ V_a^2 + 1.7\ V_a^3$$

Material "B" tested at room temperature with V_o = 101.6 μv

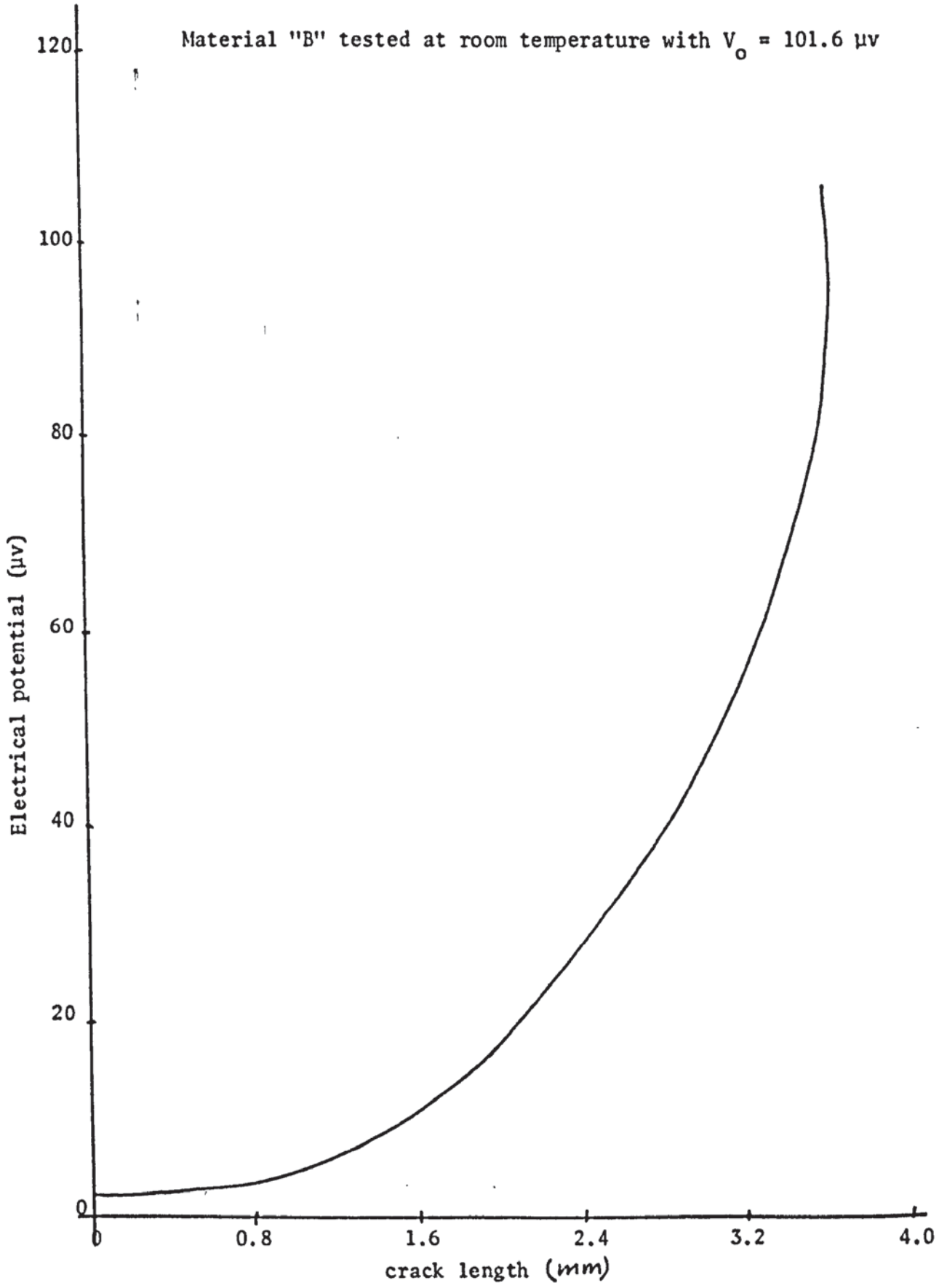

Figure (vi)

APPENDIX III

Computer programmes were written as will be shown next for the following equations, from which the plastic zone size could be compared.

1). Dugdale Model

$$S = a\left(\text{Sec}\,\frac{\pi}{2}\,\frac{\sigma}{\sigma_y} - 1\right)$$

σ - applied stress

σ_y - yield stress

S - 2ry = plastic zone size

a - Crack length

Programme

```
FORTRAN          No .....      Name .....
MASTER
REAL C,Y,S
WRITE (2,3)
3 FORMAT (11X, 11H     C     11X, 11H     Y     11X, 11Y     S   11)
DO 10 I=200,560,60
DO 10 J=1,11
C=I*0.001
Y=J*0.1
X=(90.0*3.1415)/180.0
S=C*((1/COS(X*Y))-1)
WRITE(2,180)C,Y,S
180 FORMAT(10X,F11,4,10X,F11.4,10X,F11.4,1)
10 CONTINUE
STOP
END
FINISH
****
```

2) Linear Elastic Fracture Mechanics Model

$$2r_y = \frac{1}{\pi}\left(\frac{K}{\sigma_y}\right)^2$$

Substituting for $K = \sigma_y \sqrt{\frac{CR_o}{R}}$

$$K^2 = \sigma^2 y^2 \frac{CR_o}{R}$$

C - Crack length

R_o - Critical notch root radius

R - Notch root radius

Y - Constant & it is a function of σ/W

W - Specimen width

Programme

```
JOB .....  No      Name ........ JD(JT300,M220000)
UA FORTRAN EXIT
MASTER
DIMENSION Y(120),S(129),R(3)
R(1)=0.005
R(2)=0.500
R(3)=1.000
DO 10 I=1,3
DO 100 J=10,120,10
100 Y(J)=J*0.01
WRITE(2,180)R(I),(Y(J),J=10,120,10)
180 FORMAT(1H1,50X,2HR=,F613/50X6H    1152X,1HY/5X,1HC,4X,14F6.3)
200 C=0.145
210 DC=0.005
IF (C.GT.0.365)DC=0.01
C=C+DC
IF(C.GT.1.0)GOTO 10
DO 220 J=10,120,10
Y(J)=J*0.01
S(J)=(((5.340**2.00)*0.01)/3.1416)*(C/R(I))*CY(J)**2.0)
220 CONTINUE
WRITE(2,230)C,(S(J),J= (0,120,10)
230 FORMAT(F9.3,2K,14F6.3)
GOTO 210
10 CONTINUE
STOP
END
FINISH
```

```
1 UAFORTRAN
2 MASTER
3 DIMENSION Y(800),KD(120),S(120)
4 READ KD
5 DO 100 I=10,20,10
6 DO 200J=534,739,17
7 KD(I)=I*0.01
8 200 Y(J)=J*0.01
9 WRITE(2,190)KD(I),(Y(J),J=534,798,17)
10 190 FORMAT(1H1,50X,3HKD=,F6.3/50X,6H 1152X,2HKD/5X,1HC,4X,14F6.3/)
11 210 C=0.145
12 220 DC=0.005
13 IF(C.GT.0.365)DC=0.01
14 C=C+DC
15 IF(C.GT.1.0)GOTO 100
16 DO 250 J=534,789,17
17 Y(J)=J*0.01
18 S(J)=(((Y(S)**2.00)*0.01)/3.1416)*(C/0.005)*KD(I)**2.00)
19 250 CONTINUE
20 WRITE(2,300)C,(S/J),J=534,789,17)
21 300FORMAT(F9.3,2X,14F6.3)
22 GOTO 220
23 100 CONTINUE
24 STOP
25 END
26 FINISH
27 REWRITE LINES 1 TO 26 AGAIN
   REPEAT 27 AGAIN
****
```

3) Smith's Model

$$\frac{\sigma}{\sigma_y} = \frac{(R/C)^{\frac{1}{2}}}{[1+(R/C)^{\frac{1}{2}}]}$$

$$\frac{\sigma}{\sigma_y} = \frac{(R/C)^{\frac{1}{2}}}{1+(R/C)^{\frac{1}{2}}} + \frac{2.0}{\pi(1+(R/C)^{\frac{1}{2}}]} + \cos^{-1}\left\{\frac{1 - R/C}{1+\frac{S}{C}-(\frac{R}{C})^{\frac{1}{2}}[(1+\frac{S}{C})^{2}-(1-\frac{R}{C})]^{\frac{1}{2}}}\right\}$$

Programme

```
JOB No, Name, JD(JT100,MZ,30K)
UAFORTRANLINES 10000
MASTER
REAL R,C,S,Y
DIMENSIONS R(3)
WRITE(2,3)
3 FORMAT(10X,5H C, 10X,5H   S   ,10X,5H   Y    11)
R(1)=0.005
R(2)=0.0500
DO 10 I=200,255,5
DO 10 J=1,105,5
C=I*0.001
S=J*0.0001
DO 10 K=1,2
RC=SQRT(R(K)/C)
Y=RC/(1+RC)+(2.0/3.1416*(1+RC)))*ACOS(C1-(R(K)/C))/(C1+(S/C)-RC)*SQRT((
                                    ((1+S/C)**2.0-(1-R(K)/C))))
WRITE(2,150)C,S,Y
160 FORMAT(10X,F11.4,10X,F11.4,10X,F11.4)
10 CONTINUES
R(1)=0.005
R(2)=0.500
R(3)=1.00
DO 30 I=250,550,25
DO 30 J=10,310,20
C=I*0.001
S=J*0.001
DO 30 K=1,3
Y=RC/(1+RC)+(2.0/3.1416*(1+RC)))*ACOS((1-(R(K)/C))/((1+(S/C)-RC)*SQRT
                                    ((1+S/C)**2.0-(1-R(K)/C))))
WRITE(2,170)C,S,Y
170 FORMAT(10X,F10.4,10X,F11.4,10X,F114)
30 CONTINUE
R(1)=0.005
R(2)=0.050
R(3)=0.240
DO 35I=250,550,25
DO 35 J=300,1550,50
C=I*0.001
S=J*0.001
DO 35 K=1,3
Y=RC/(1+RC)+(2.0/3.1416*(1+RC)))*ACOS((1-(R(K)/C))/((1+(S/C)-RC)*SQRT
                                    ((1+S/C)**2.0-(1-R(K)C))))
```

```
WRITE(2,180)C.S.Y
180 FORMAT(10X,F11.4,10X,F11.4,10X,F11.4)
35 CONTINUE
STOP
END
FINISH
****
```

$$s = c\left(\sec\left(\frac{\pi\sigma_a}{2\sigma_y}\right) - 1\right)$$

For $\frac{\sigma_a}{\sigma_y} = 1.08$ C = 5.08 mm

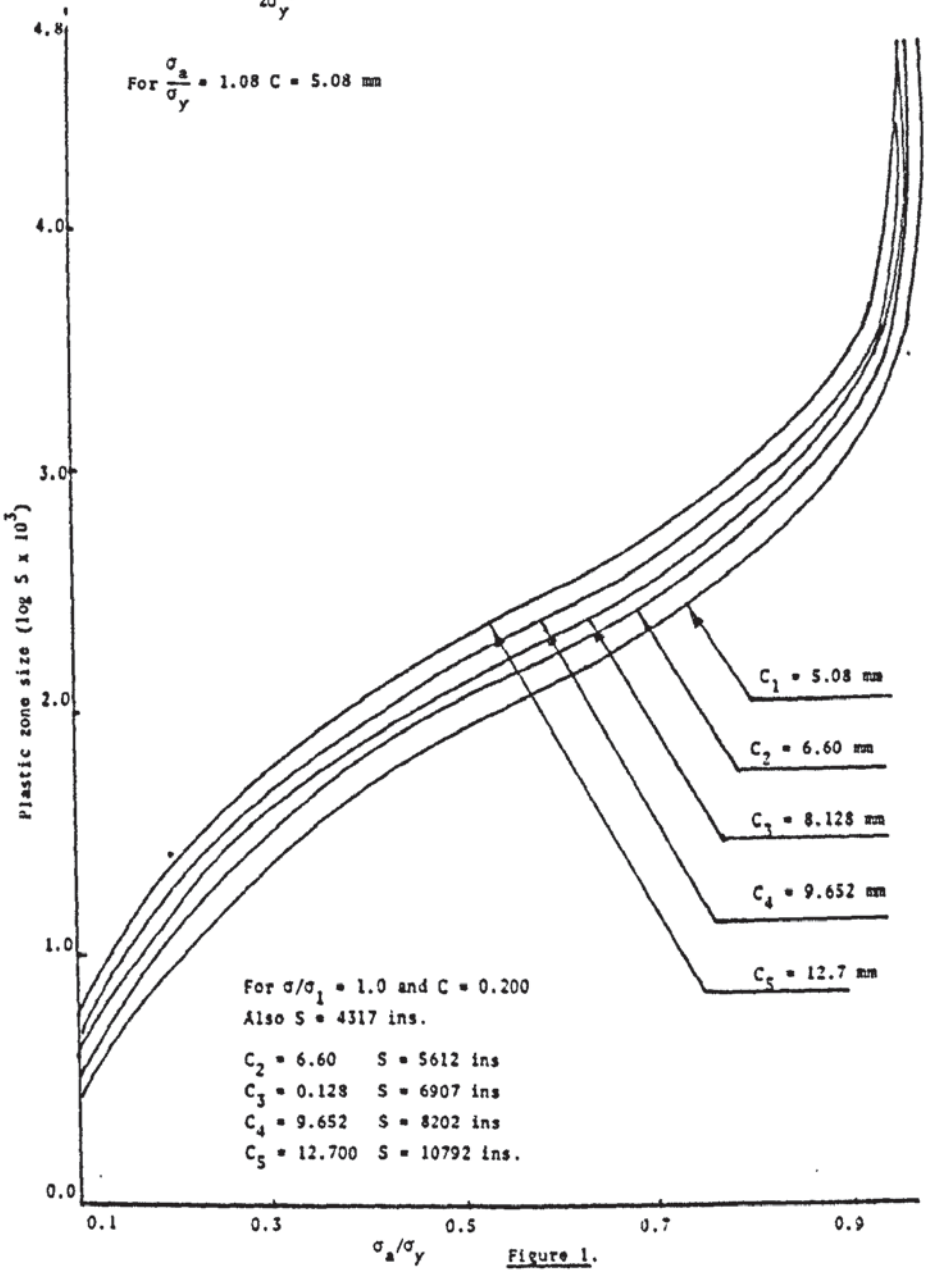

Figure 1.

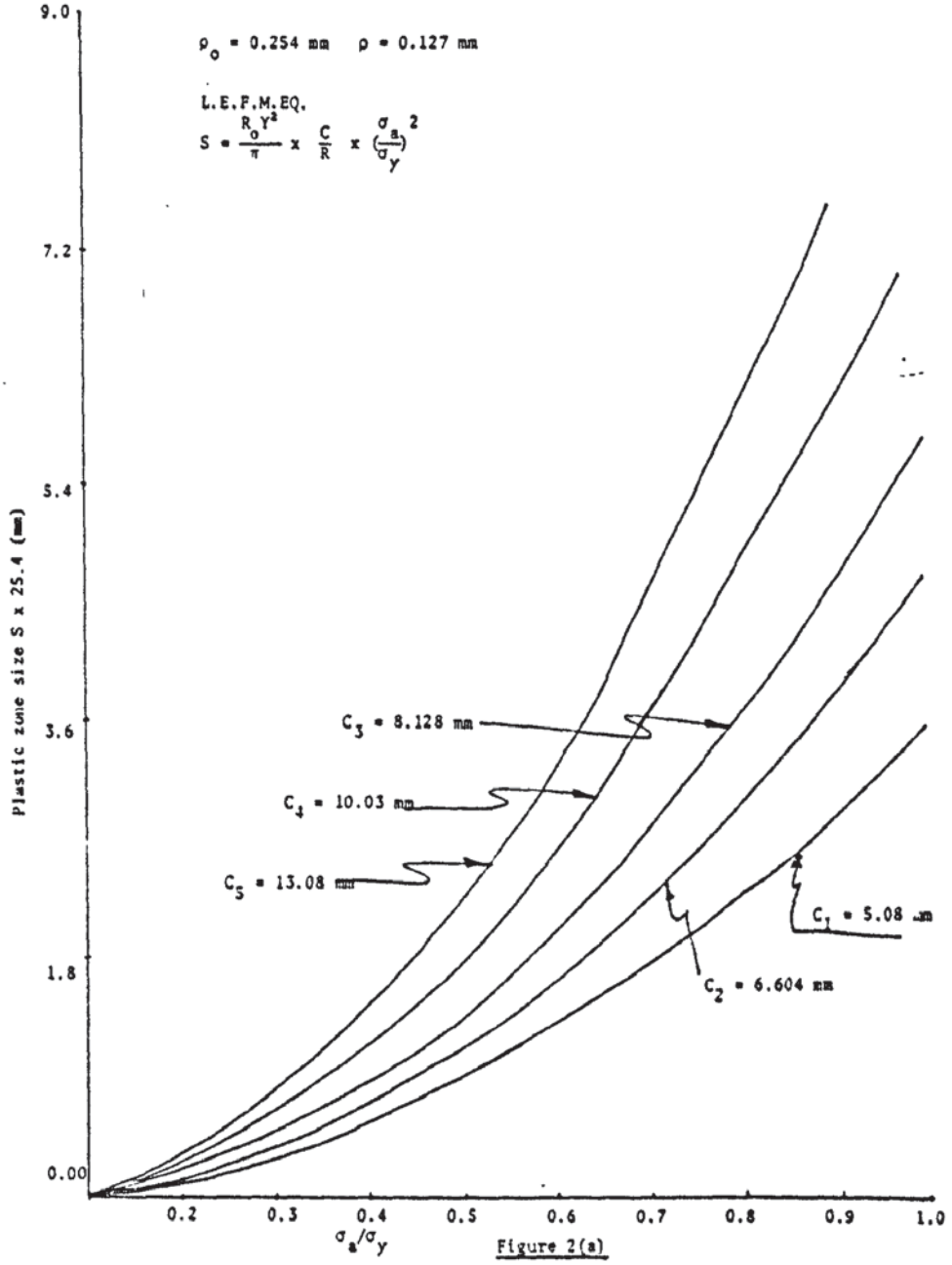
ρ_o = 0.254 mm ρ = 0.127 mm
L.E.F.M.EQ.
$S = \frac{R_o Y^2}{\pi} \times \frac{C}{R} \times \left(\frac{\sigma_a}{\sigma_y}\right)^2$
Plastic zone size S x 25.4 (mm)
9.0
7.2
5.4
3.6
1.8
0.00
0.2
0.3
0.4
0.5
0.6
0.7
0.8
0.9
1.0
σ_a/σ_y
C_3 = 8.128 mm
C_4 = 10.03 mm
C_5 = 13.08 mm
C_1 = 5.08 mm
C_2 = 6.604 mm

Figure 2(a)

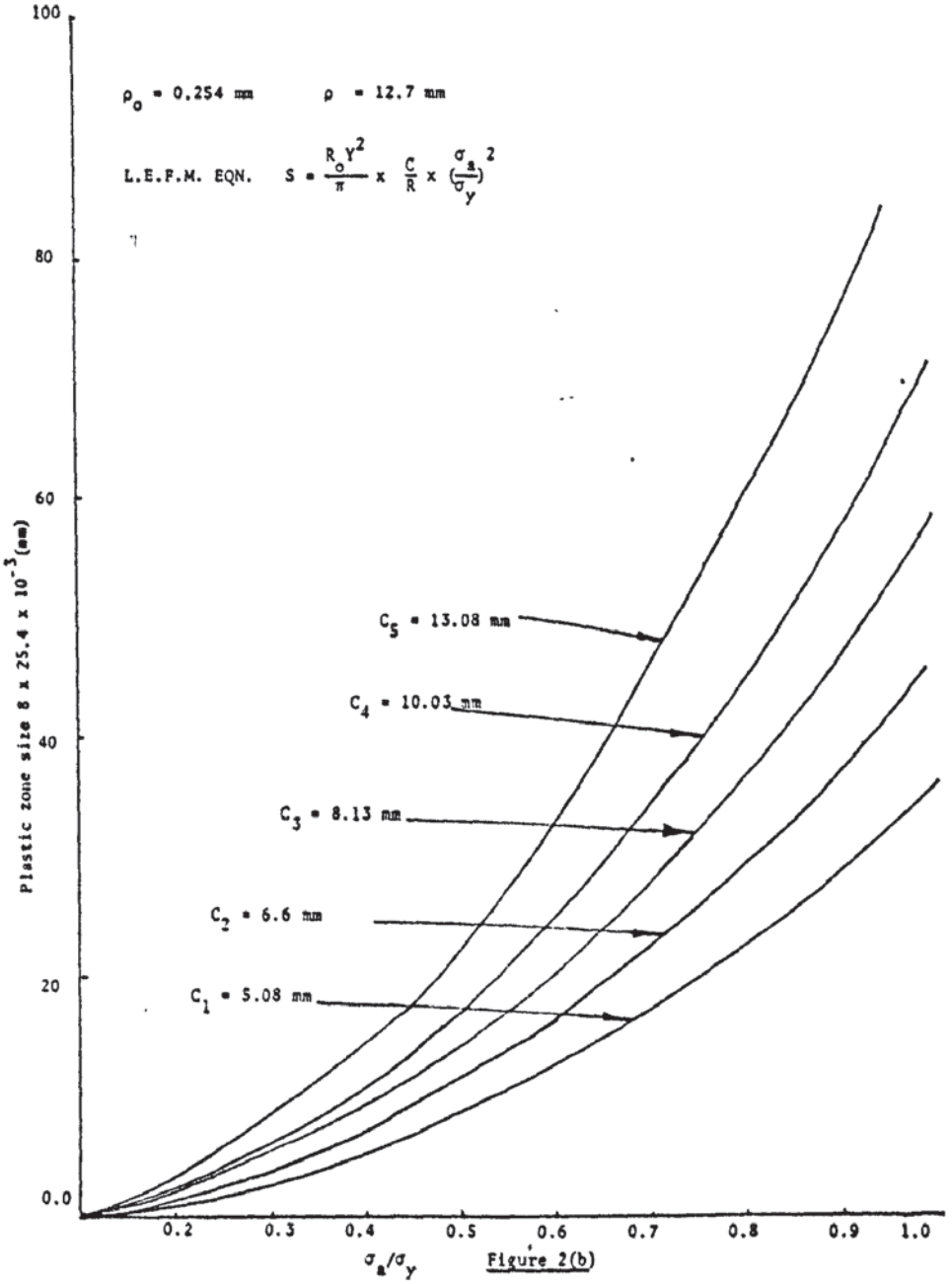
100
80
60
40
20
0.0
ρ_o = 0.254 mm
ρ = 12.7 mm
L.E.F.M. EQN. $S = \frac{R_o Y^2}{\pi} \times \frac{C}{R} \times \left(\frac{\sigma_a}{\sigma_y}\right)^2$
C_5 = 13.08 mm
C_4 = 10.03 mm
C_3 = 8.13 mm
C_2 = 6.6 mm
C_1 = 5.08 mm
Plastic zone size S x 25.4 x 10^{-3} (mm)
0.2
0.3
0.4
0.5
0.6
0.7
0.8
0.9
1.0
σ_a/σ_y

Figure 2(b)

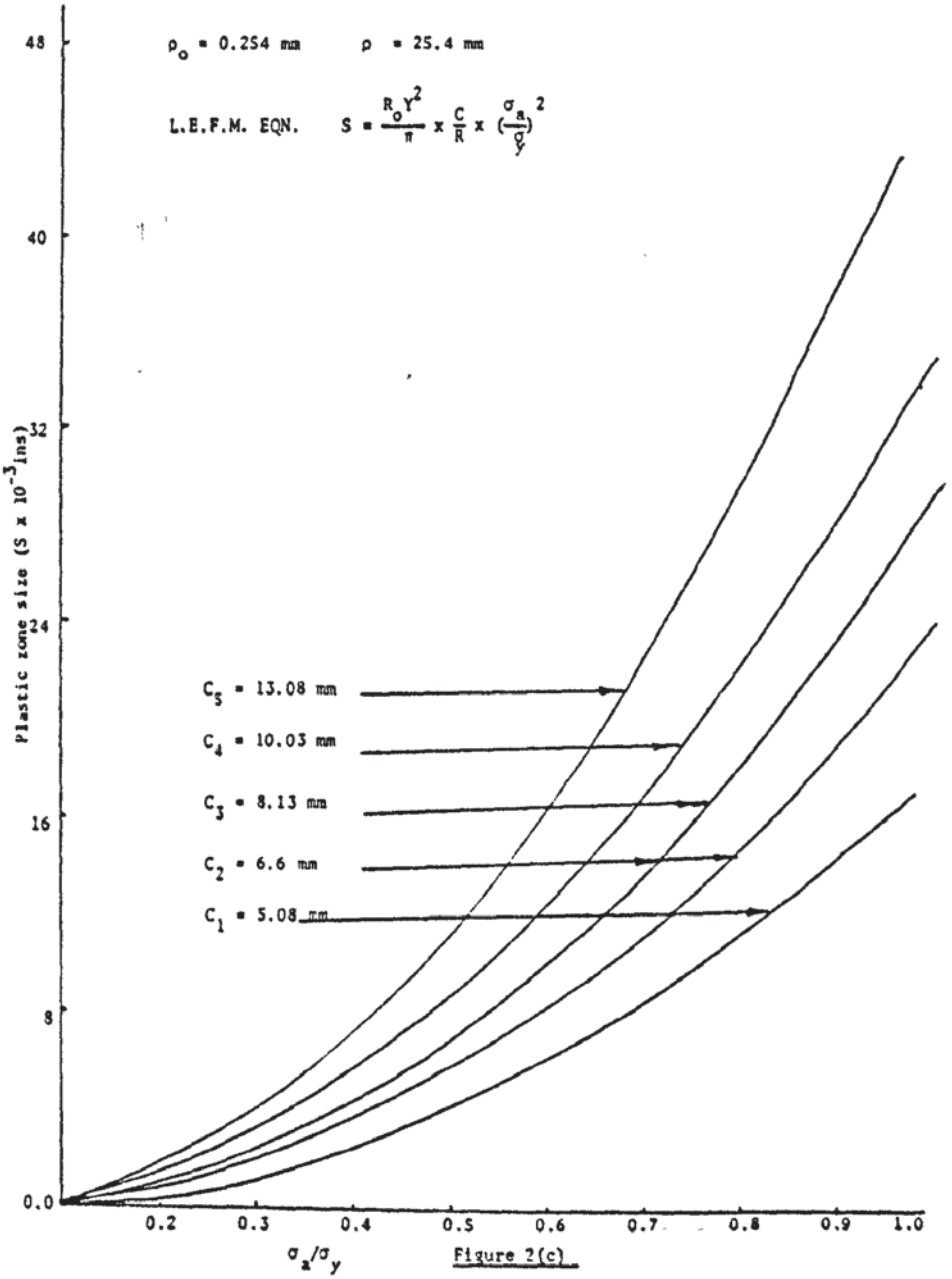
ρ_o = 0.254 mm
ρ = 25.4 mm
L.E.F.M. EQN. $S = \frac{R_o Y^2}{\pi} \times \frac{C}{R} \times \left(\frac{\sigma_a}{\sigma_y}\right)^2$
Plastic zone size (S x 10^{-3} ins)
48
40
32
24
16
8
0.0
C_5 = 13.08 mm
C_4 = 10.03 mm
C_3 = 8.13 mm
C_2 = 6.6 mm
C_1 = 5.08 mm
0.2
0.3
0.4
0.5
0.6
0.7
0.8
0.9
1.0
σ_a/σ_y

Figure 2(c)

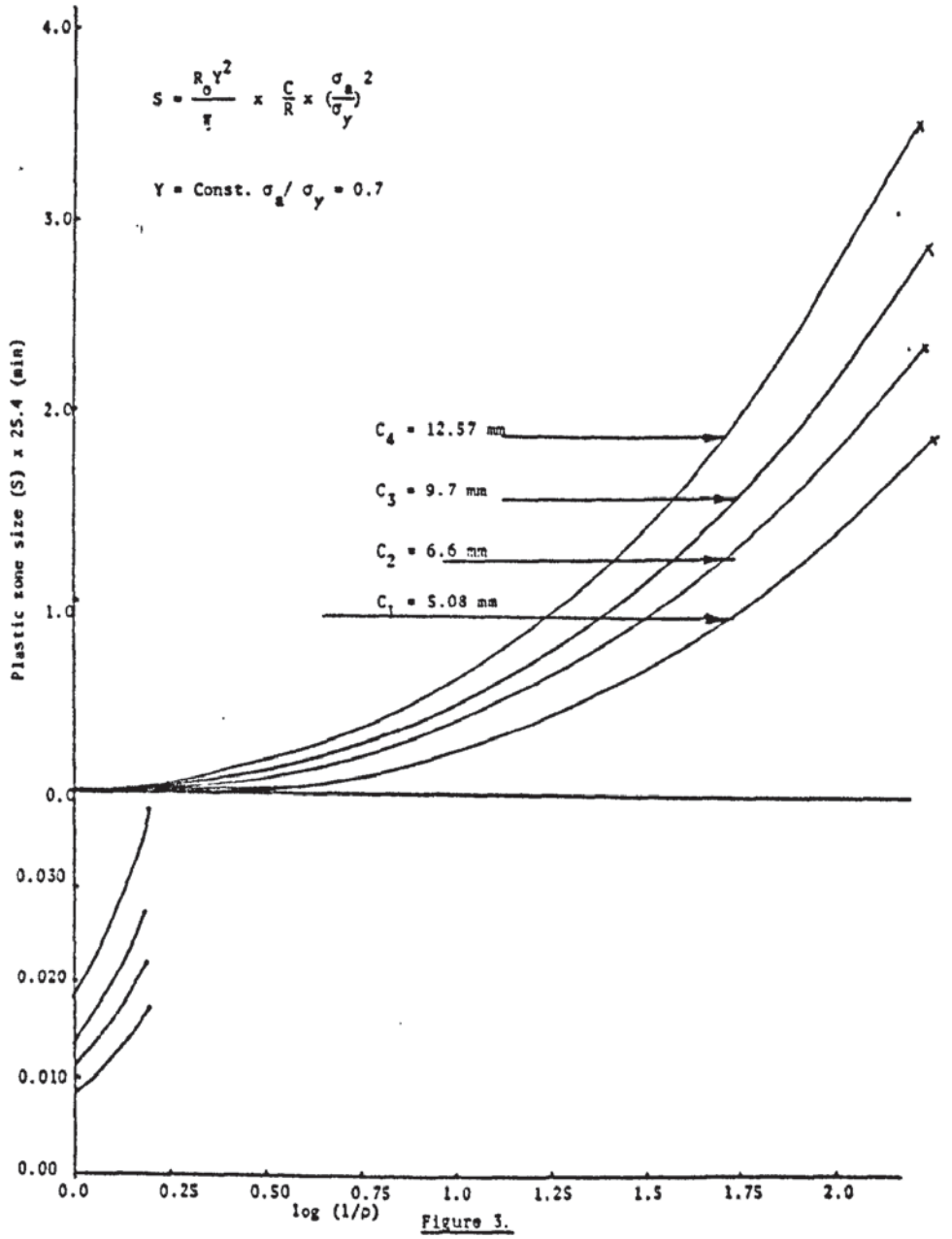
$S = \frac{R_o Y^2}{E} \times \frac{C}{R} \times \left(\frac{\sigma_a}{\sigma_y}\right)^2$
Y = Const. $\sigma_a / \sigma_y = 0.7$
C_4 = 12.57 mm
C_3 = 9.7 mm
C_2 = 6.6 mm
C_1 = 5.08 mm
Plastic zone size (S) x 25.4 (min)
log (1/ρ)
4.0
3.0
2.0
1.0
0.0
0.030
0.020
0.010
0.00
0.0
0.25
0.50
0.75
1.0
1.25
1.5
1.75
2.0

Figure 3.

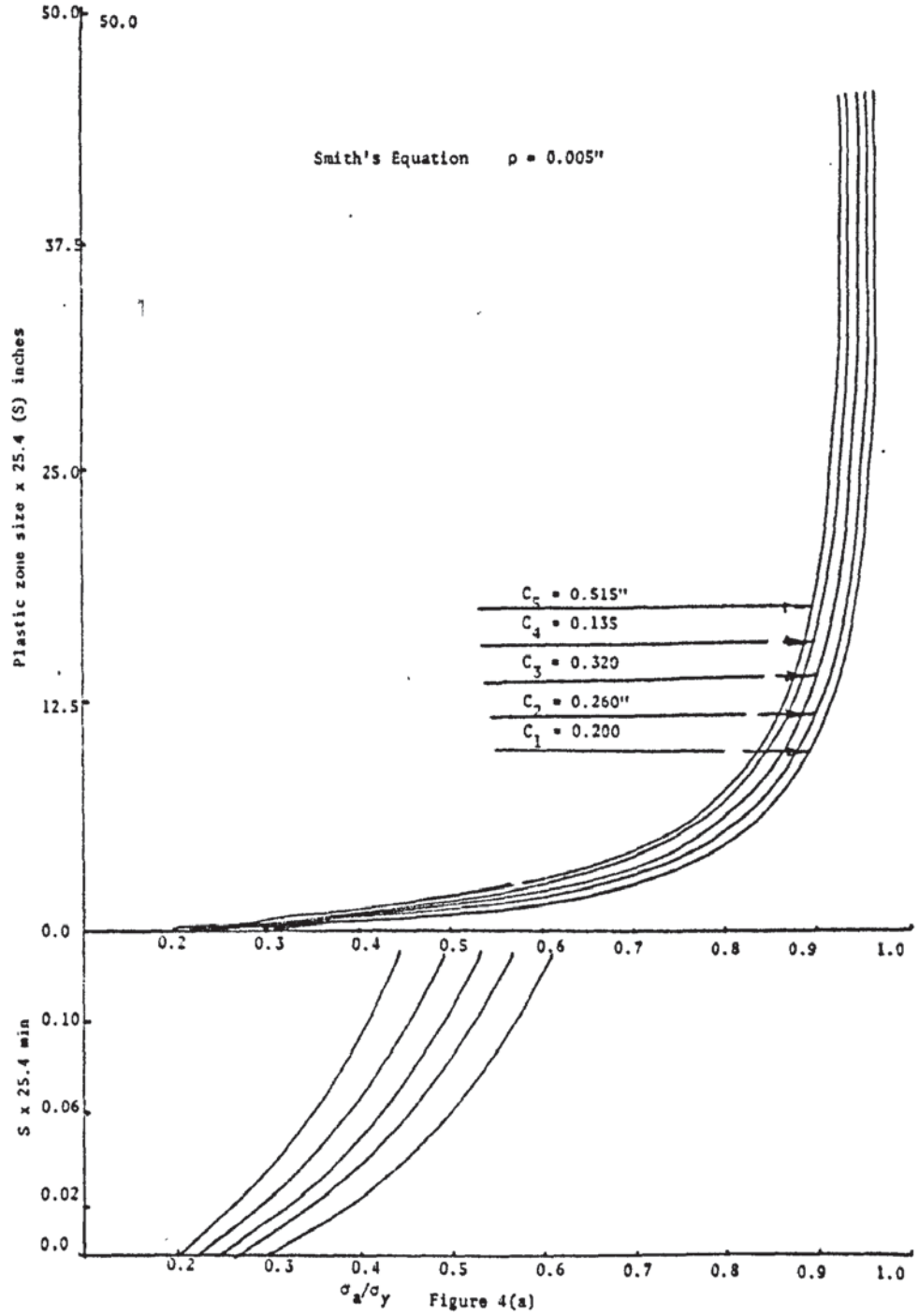
Smith's Equation ρ = 0.005"
Plastic zone size x 25.4 (S) inches
50.0
37.5
25.0
12.5
0.0
C_5 = 0.515"
C_4 = 0.135
C_3 = 0.320
C_2 = 0.260"
C_1 = 0.200
0.2
0.3
0.4
0.5
0.6
0.7
0.8
0.9
1.0
S x 25.4 min
0.10
0.06
0.02
0.0
σ_a/σ_y

Figure 4(a)

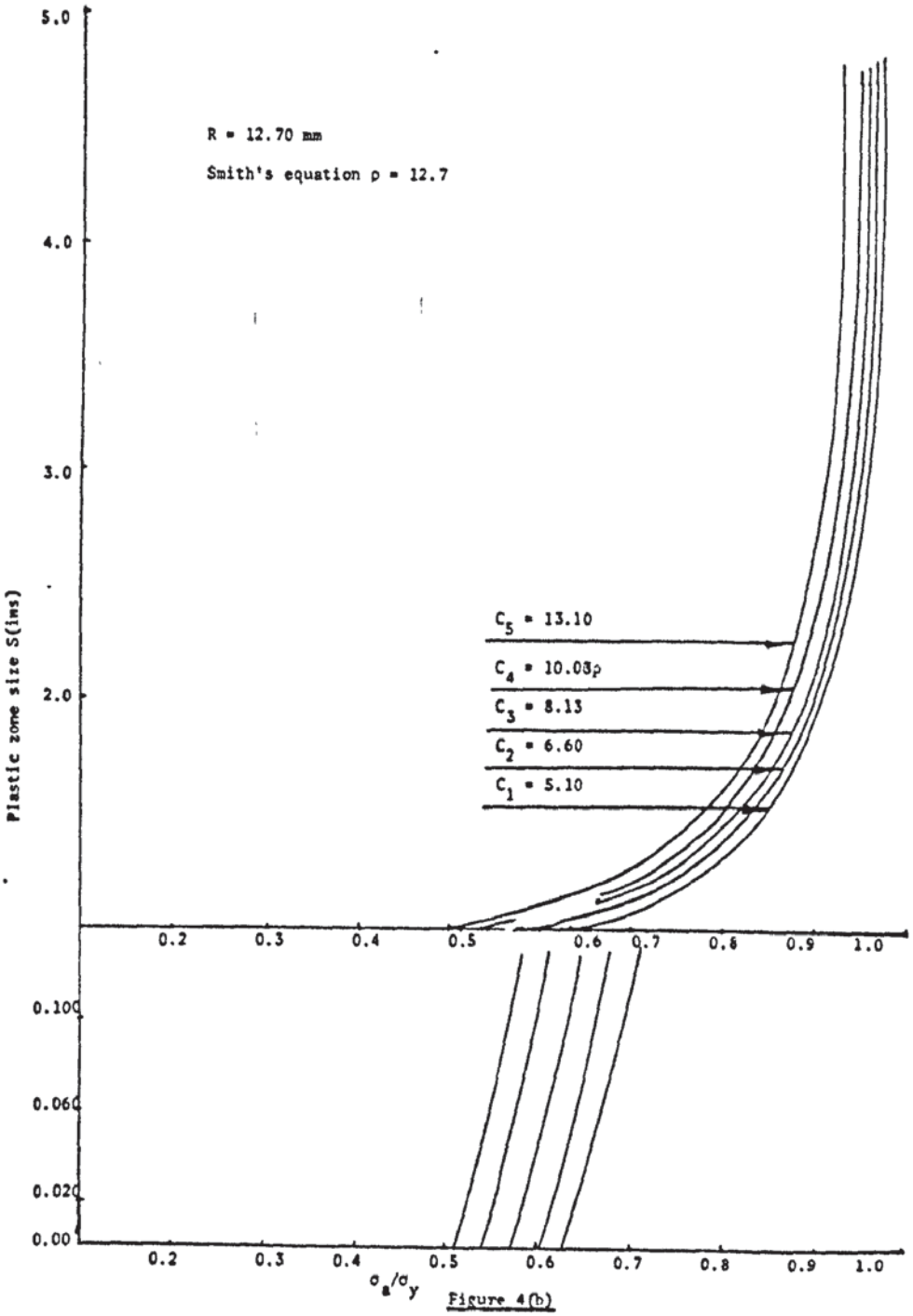
R = 12.70 mm
Smith's equation ρ = 12.7
C_5 = 13.10
C_4 = 10.03ρ
C_3 = 8.13
C_2 = 6.60
C_1 = 5.10
Plastic zone size S(ins)
5.0
4.0
3.0
2.0
0.100
0.060
0.020
0.00
0.2
0.3
0.4
0.5
0.6
0.7
0.8
0.9
1.0
σ_a/σ_y

Figure 4(b)

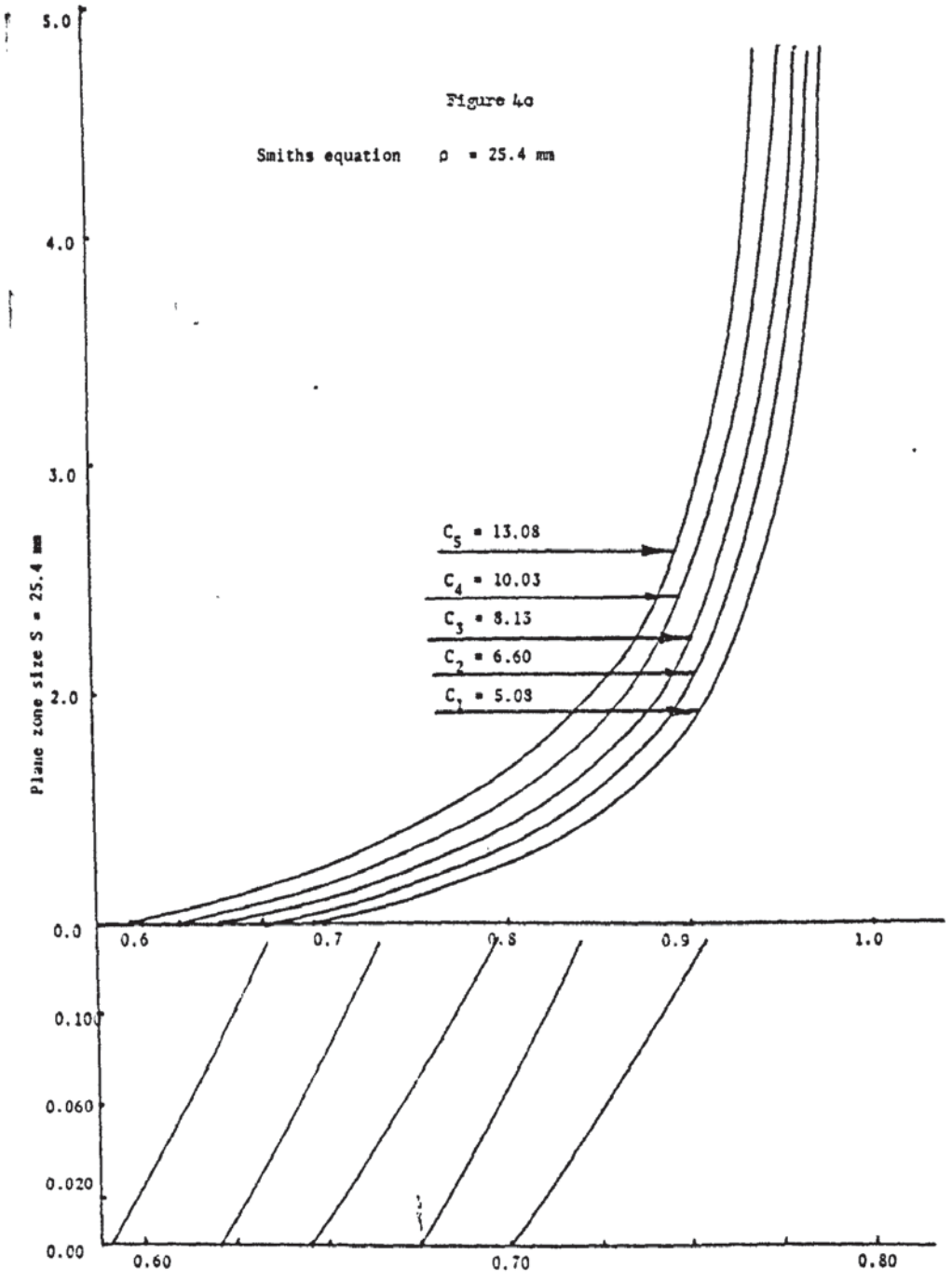
Figure 4c
Smiths equation ρ = 25.4 mm
Plane zone size S = 25.4 mm
5.0
4.0
3.0
2.0
0.0
0.6
0.7
0.8
0.9
1.0
C_5 = 13.08
C_4 = 10.03
C_3 = 8.13
C_2 = 6.60
C_1 = 5.08
0.10
0.060
0.020
0.00
0.60
0.70
0.80

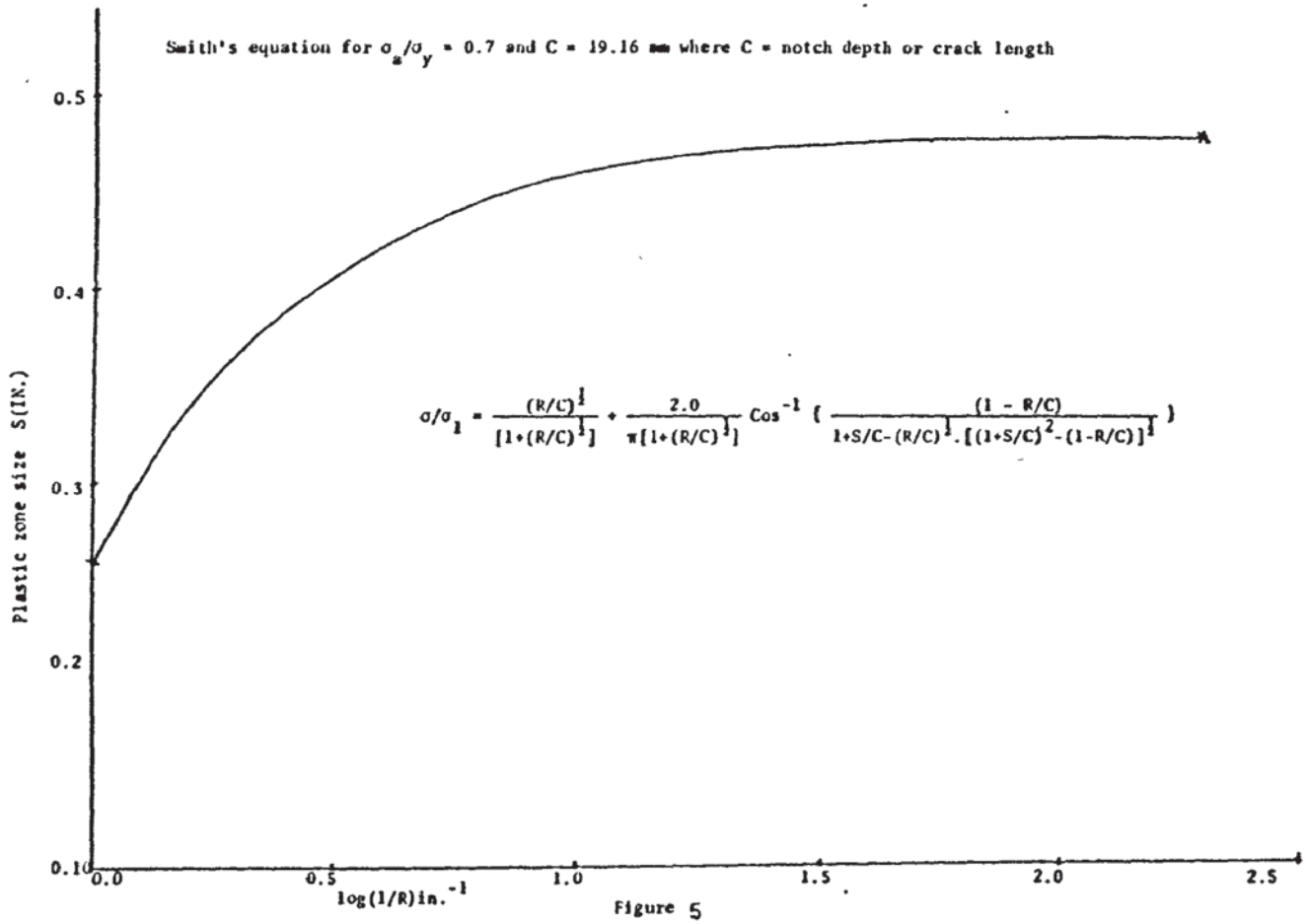
Smith's equation for σ_a/σ_y = 0.7 and C = 19.16 mm where C = notch depth or crack length
$\sigma/\sigma_1 = \frac{(R/C)^{\frac{1}{2}}}{[1+(R/C)^{\frac{1}{2}}]} + \frac{2.0}{\pi[1+(R/C)^{\frac{1}{2}}]} \cos^{-1}\left\{\frac{(1-R/C)}{1+S/C-(R/C)^{\frac{1}{2}}.[(1+S/C)^2-(1-R/C)]^{\frac{1}{2}}}\right\}$
Plastic zone size S(IN.)
0.5
0.4
0.3
0.2
0.10
0.0
0.5
1.0
1.5
2.0
2.5
log(1/R)in.$^{-1}$

Figure 5

REFERENCES

1. Afanasev N.N. J.Tech, Phys. U,S.S.R. 10, 1553,(19400).
2. Alber W.J. Arch.Miner Geognostic Berg. Huttenkunde 10, 215,(1918).
3. Allery M.B.P. and Birbeck G. J.Engng.Fract.Mech., Vol.4, p.125 (1972).
4. Ault R.T. and Spretnak J.W. Initiation Yielding and Fracture in Notched Sheet Mdy. Int.J.Mech.Sci., 7.87, 102,(1965).
5. Aurich, D. Engng.Fract.Mech. J.Vol.7, p.761-765, (1975).
6. Barnby J.T., Dinsdale K, and Holder R. Fatigue Crack Initiation, Jan. (1975).
7. Barnby J.T. and Al-Daimalani I.S. Report No. PT1/21, (1976). Assessment of the fracture toughness of cast steels (low alloy steels).
8. Barnby J.T. and Al-Daimalani I.S. Assessment of fracture toughness of cast steels (carbon and carbon manganese steels).
9. Beckfold J.H. et al. Trans. AIME, 212, 523(1958).
10. Beevers & Halliday. Progress Report 3 B'ham Univ.Contract AT/2027/095 MAT 75.
11. Bilby B.H., Cotrrell A.M. and Swinden K.N. Proc.Roy.Soc. A272, 304,1963.
12. Benham P.P. Met.Rev.3, 203,(1958).
13. Bilby B.H., Cottrell A.M., Smith E and Swinden K.H. Proc.Roy.Soc. A279.
14. Bluhm J.I. Fract.Mech. of Aircraft Structures 1974 Ed. H.Liebowitz, AGARDO Graph No. 176, pp.89.
15. Boone W.D., and Wishart H.B. Proc. ASTN 35. 147, (1935).
16. Broberg K.B. J.Mech.& Phys. Solids Vol.19, No.6, (1971),pp.407-418.
17. Broom T. and Ham R.K. Proc.Roy.Soc., A251, 186, (1959).
18. Brown W.F. and Srawley J.E., Plane Strain Crack Testing of High Strength Materials, ASTM STP 410 (1966).
19. Bucci R.J. et al. ASTM STP 514 (1972), pp.40-69.

20. Cazaud R. Fatigue of Metals, Chapman & Hull, London. (1953).

21. Charsley P. and Thompson N. Phil.Mag. 8, 77 (1963).

22. Christensen R.H. Crack Propagation Symposium, Cranfield, 326 (1961).

23. Christenson R.H. and Harmon R.B. Fatigue Crack Propagation. P.5, ASTM, STD, 415 (1967).

24. Cina B. J.Iron & Steel Inst. 194, 324 (1960).

25. Clark W.G. & Knott J.F. J.Mechanics & Physics of Solids,1975,23,265.

26. Cooker J. & Robinson J.L. Research Report. Dept. of Physical Mettalurgy Birmingham University.

27. Cottrell A.H. Trans AIME 212, 192 (1958).

28. Cottrell A.H. and Hull D. Proc.Roy.Soc. A242, 211(1957).

29. Cummings H.N. Air Development Dept. Tech.Rep. 60/42 (1960).

30. Dehlinger V.Z. Phys. 115, 625 (1940).

31. Drucker D.C. "A More Funsamental Approach to Stress-Strain Rel". Proc.1st U.S. AAT.Cong.Appl.Mech.ASME p.487-491 (1951).

32. Drucker D.C. et al. "Extended Limit Design Theorems for Continuous Media". Quarterly Appl.Mech. Vol.9, p.381 (1952).

33. Drucker D.C. at el. "Plasticity" in Structural Mechanics Proc. of 1st. Symp. on Naval Structural Mech. p.407 (1958).

34. Drucker D.C. J.of Materials. Vol.1, No.1, p.873 (1966).

35. Dugdale D.S. "Yielding of Steel Sheets Containing Slits, J.Mech.Phys. Solids, 8, (1960).

36. Discussion on Damage and Failure Mechanisms of Heavy Section Steel. Proc.Roy.Soc. A285 1-174, (1965).

37. Electron Fractography, ASTM. STP. 436 (1968).

38. Enrietto J.F. and Sinclair G.M. Dept. of Theoretical and Applied Mech. University of Illinois, Rep.No. 567 (1959).

39. Erdogan F. Engng.Fract.Mech.J. 4, 811 (1972).

40. Erdogan F. and Kibler J.J. Int.J.Fract.Mech. 5, 229, (1969).

41. Ewing J.A. and Humphrey J.C.W. Phil.Trans.A200, 241 (1903).

42. Fairbairn W. Phil.Trans.Roy.Soc. 154, 311, (1864).

43. Fegredo D.N. and Greenough G.B. J.Inst.Metals. 87, 1, (1958/9).

44. Field J.E. and Scott D. The Diagnosis of Service Failure. Instn. of Mech.Engs.Conf. on Safety and Failure of Components. Univ. of Sussex (1969).

45. Flugge W. Editor, Handbook of Engng.Mechanics, Chap.46 to 52, by Drucker D.C. et al. (1962).

46. Forman R.G. Experimental Program to Determine Effect of Crack Buckling and Spec. Dimensions on Fracture Toughness of Thin Sheet Metal. Rep. No. AFFDL TR.65-146.

47. Forrest P.G. Fatigue of Metals. Pergamon Press, Oxford (1962).

48. Forrest P.G. Metal Fatigue. Chapman and Hall. Lond.p.158 (1959).

49. Forrest P.G. and Tate A.E.L. J.Inst.Metals 93, 438 (1964-65).

50. Forsyth P.J.E. J.Inst.Metals, 80, 181 (1951-52).

51. Forsyth P.J.E. Int.Conf. on Fatigue. Inst.Mech.Eng. p.535 (1956).

52. Forsyth P.J.E. and Ryder O.A. Aircr.Engng. 32, 96 (1960).

53. Forsyth P.J.E. Proc.Crack.Prop.Symp.College of Amonaulies, Cranfield, Eng. 1 76 (1962).

54. Forsyth P.J.E. and Ryder D.A. Metallurgia, 63, 117-124 (1961).

55. Frost W.E. et al. Metal Fatigue (1974).

56. Frost, N.E. and Dixon J.R. Int.J.Fract.Mech. 3, 301 (1967).

57. Frost, J.W. and Dugdale D.S. J.Mechs.Phys.Solids, 6, 92 (1968).

58. Fujita F.E., Sci.Rep.Res.Inst. Tohoku University, 6, 565 (1954).

59. Gerberich W.W. Plastic Strain and Energy density in cracked plate experimental mechs. p.335-344 (1964).

60. Gilbey D.M. & Pearson S. Royal Aircraft Est. Tech.Report No.66402

61. Goodier J.N. and Field F.A. Plastic energy dissipation in crack propagation. Fracture of Solids, Wiley, N.Y. (1963).

62. Gough H.J. The Fracture of Metals. Scott, Greenwood & Son.Lond. (1924).

63. Griffith A.A. The Phenomena of rupture and flow in solids. Phil.Trans. Roy.Soc. A.221, 163 (1920).

64. Griffith A.A. Phil.Trans.Roy.Soc. A221, 162 (1921).

65. Grover H.J. et al. Fatigue of metals and Strustures, Bureau of Aeronautics, Dept.of U.S.Navy (1954).

66. Hardrath H.F. and McEvily A.J. CRack.Prop.Symp., Cranfield, p.231, (1961).

67. Harpur N.E. Crack propagation symposium, Cranfield, p.442, (1961).

68. Harries D.R. Ph.D. Thesis, Cambridge University, (1955).

69. Harries D.R. & Smith G.C. Colloquium on fatigue. p.89 (1956).

70. Harris D.O., Dunegan H.L. and Tetelman A.S. Tech.Rept.on prediction of fatigue lifetime by Combined fracture mechanics and acoustic emission Techniques, UCRL-7/760.

71. Harris D.O. and Dunegan H.L. Technical Report DE-73-2. Continuous monitoring of fatigue crack growth by acoustic emission techniques.

72. Head A.K. Phil.Mag.44, 925, (1953). J.Appl.Mech.,78, 407 (1956).

73. Heald P.T. and Bilby B.A. Fracture Toughness of high strength materials. Theory and Practice, p.63, ISI Pub. No.120. Iron & Steel Inst. (1970).

74. Helgeland O. J.Inst.Metals, 93, 570, (1964-1965).

75. Hertzberg R.W. and Paris P.C. Int.Conf.on Fract. Sendai, Japan (1965).

76. Hempel M. Fatigue in aircraft strictures, p.83, Acad.Press. (1956).

77. Hempel M. Int.Conf.on Fatigue. Inst.Mech.Eng. p.543, (1956).

78. Hill R. The Mathematical theory of plasticity. Oxford, Clavendon Press (1950).

79. Hodgkinson E.A. H.M.S.O. Command paper No.1123 (1849).

80. Holder R. Ph.D.Thesis, Metallurgy Dept. Aston University (1976).

81. Honda R. J.Phys.Soc. Japan. 16, 1309 (1961).

82. Huff H.W. et al. 2nd Int.Conf. on Fract. Brighton, p.83, (1969).

83. Hull D. J.Inst.Metals, 86, 425, (1957-8).

84. Hull D. Acta Met. 8, 11, (1960).

85. Irwin G.R. Fract.Dyn. Fracturing of Met. ASM Symp. p.143, (1947-8).

86. Irwin G.R. Fract.Encycl.of Physics, Vol.6, p.551, (1958).

87. Irwin G.R. et al. Fract.Strength relative to onset and arrest of crack propag. Proc.Am.Soc.Test.Mat. 58, 670 (1958).

88. Irwin G.R. J.Engng.Fract.Mech. Vol.1, 241, (1868-70).

89. Irwin G.R. "Analysis of stresses and strains near the end of a crack traversing a plate". J.Appl.Mech. 24, 361, (1957).

90. Irwin G.R. Plastic zone near a crack and fracture toughness. Proc. Sagamore Res.Ord.Materials. p.63, (1960).

91. Isitasi T. Proc.1st Japanese Cong. on testing materials. p.37 (1958).

92. Jack A.R. Ph.D.Thesis, Dept. of Metallurgy, Aston University.

93. Jacoby G.H. Exp.Mech., 5, 65, (1965).

94. Jaswan M.A. and Dove D.B. Acta.Cryst., 9, 621 (1956).

95. Johnson W. and Mellor P.B. Plasticity for Mech.Engs. (1962).

96. Kennedy A.J. Processes of Creep and Fatigue in Metals. Oliver and Boyd. Edinburgh (1962).

97. Klesnil M. and Lucas P. J.Iron & Steel Inst., 203, 1043 (1965).

98. Kuhn and Hardrath H.F. NACA TN2805 (1952).

99. Laird C and Smith G.C. Phil.Mag. 8, 1945 (1963).

100. Laird C. ASTMA Cong. of Fatigue Crack Propag. Atlantic City (1966).

101. Liebowitz H. Fract.of Metals, vol.VI, p.388.

102. Mann J.Y.J. Aust.Int.Met. 3, 222 (1958).

103. Manson S.S. NACA, TN 2933 (1954).

104. Martin D.E. Trans.ASME. J.Bas.Engng. 83, 565 (1961).

105. May M.J. and Honeycombe R.W.K. J.Inst.Met. 92, 41 (1963-4).

106. May A.N. Nature, London. 185, 303 (1960).

107. May A.N. Nature, London. 188, 573 (1960).

108. McMillan J.C. and Pelloux R.M.N. Fat.Crack.Prop. ASTM. STP, 415, p.505, (1967).

109. McCammon R.D. and Rosenberg H.M. Roy.Soc. A242, 203 (1957).

110. McClintock F.A. and Irwin G.R. Fract.Toughness Testing. ASTM STP 381, p.84 (1965).

111. McEvily A.J. and Illg W. NACA. Tech.Note 4394 (1958).

112. McEvily A.J. and Johnson T.L. Int.Conf.on Frac., Sendai, Japan (1965).

113. McEvily A.J. et al. In Fracture. M.I.T. Wiley, N.Y. p.450 (1959).

114. McGrath J.T. and Waldron B.W. H.Phil.Mag. 9, 249 (1964).

115. Mostovoy S. et al. J.Int.Mat. (U.S.) 2, 661 (1967).

116. Moore H.F. and Kommers J.B. Tha fatigue of metals. McGraw-Hill,N.Y. (1927).

117. Mott N.F. Acta Met. 6, 195 (1958).

118. Munse W.H. et al. Univ. of Illinois Report. (1965).

119. Neuber H. Kerbspannungslehre, Springer (1958).

120. Newman J.C.J.R. J.Engng.Frac.Mech. 1, 137 (1968).

121. Orowan E. Proc.Roy.Soc. D171, 79 (1939).

122. Orowan E. Report Progr.Phys. 12, 185 (1948).

123. Palmer J.G. and Heald P.T. J.Mat.Science and Enging. 11(1973)181-184.

124. Paris P.C. and Bih G.G. Symp.on fracture toughness testing and its applications. ASTM. STP. 381, p.30 (1965).

125. Paris P.C. The Mech. of Fract.Prop. and Solution to Fracture Arrestor Problems. Document D2-2195 the Boring Co. (1957).

126. Paris P.C. Ph.D.Thesis, University of Lehigh (1962).

127. Paris P.C. and Erdogen E. J.Bas.Engng.Trans. ASME, Series O, 85, 528 (1961).

128. Paxton H.W. Acta.Met. 1,141 (1953).

129. Pearson S. Roy.Aircraft Estab. Tech.Report. 69175.

130. Pelloux R.M.N. Trans.ASM. 57, 511 (1964).

131. Philips A. et al. Electron fractography handbook. (1965).

132. Prayer W. and Hodge P.G.Jnr. Theory of perfectly plastic solids. Wiley & Sons. N.Y. (1951).

133. Price A.T. and Elder W.J. J.Iron and Steel Inst. 204, 594 (1966).

134. Rankine W.J.M. Proc.Inst.Civ.Engrs. 2, 105 (1843).

135. Raynold M.H. and Coffin L.F. Trans ASME. J.Basic Engng. 85, 548(1963).

136. Reid C.N. et al. Tech.Document Rep. No.ASD TDR-63-360, pt.2. (1964).

137. Reid C.N. et al. Acta.Met. 14, 975 (1966).

138. Rice J.R. Fatigue Crack Propagation, ASTM STD.415, p.247 (1967).

139. Rooke O.P. and Cartwright D.J. A Compendium of stress intensity factors. HMSO London, to be published.

140. Rosenfield A.R. et al. Crack extension and propagation. Proc.at the Int.Conf. on fracture. Sendai, Japan (1965).

141. Shanley F.R. Colloquium on fatigue, p.251, Berlin (1955).

142. Shield R.T. and Drucker D.C. "Design of thin walled Torispherical and Toriconal pressure vessel heads". J.of Appl.Mech. vol.28, p.292 (1961).

143. Sidey D. Research Report. Cambridge University, Dept. of Enging. CUED/C-MAT/TR9 (1973).

144. Sih G.C. (Ed.) Methods of Analysis and Solution of crack problems. Noordhalf, Leydon (1973).

145. Sih G.C. Handbook of stress intensity factors, Lehigh Univ. (1973).

146. Smith E. Central Electricity Res.Lab. Leatherhead, Surrey. p.455.

147. Smith R.A. Strain (1974) Oct.183.

148. Sohijue J. Nat.Aero and Astro Res.Inst. Amsterdam. Rep.No.MP195(1960).

149. Srawley J.E. and Brown W.F. Sym.Fract.Toughness Testing and its applications. ASTM. STD 381, p.133 (1965).

150. Schlive J. et al. Nat.Devo.and Astro Res.Inst. Amsterdam. NLR TR, M.2142 (1965).

151. Stephen D. et al. Engng.Fract.Mech.J. Vol.7, 649 (1975).

152. Schwertzberg F.R. et al. Martin-Marietta Corpn. Rep.NASA CR,6329(1963).

153. Sargent G.R. and Shaw B.J. Acta Met. 14, 909 (1966).

154. Stroh A.N. Advance Phys. 6, 418 (1957).

155. Seigle L.L. and Dickinson C.D. Met.Soc.Conf. 17, 65 (1962).

156. Tada H. et al. The stress analysis of cracks handbook. Del.Res.Corp: Hellertown, Pa.(1973).

157. Tangri K, Toronchuk J.P. and Lloyd D.J. Technical Report, Acoustic emission from polycrystalline copper and iron-silicon

158. Taylor E. Private Communication. Aston University.

159. Tetelman A.S. and McEvily D.J.Jnr. "Fract. Structural Mat". (1969).

160. Thompson N. Int.Conf.on Fatigue. Inst.Mech.Engng. p.527 (1956).

161. Thompson N. and Wadsworth N. J.Phil.Mag.Suppt. 7, 72 (1958).

162. Topper T.W. et al. J.Nat. 4, 200 (1969).

163. Venn G.M. M.Sc. Thesis. Dept. of Mech.Eng. Aston University, (1972) Acoustic emission from heat treated sinc.

164. Weertman J. Proc.Int.Conf. on Fracture, Sendai, Japan (1966).

165. Walker E.F. and May M.J. BISRA Tech.Report. MG/E/307/67(1967).

166 Weibull W. SAAB Aircraft Co. Tech.Note 25, 1954, Sweden, FFA. Rep.65 (1956).

167. Weibull W. Crack propagation Symp. Cranfield, p.271 (1951).

168. Weinstein D. et al. Frans.AIME, 221, 723, 737 (1961).

169. Weisman M.H., Kaplan M.H. & others. Proc.ASTM. 50, 649 (1950).

170. Wessel E.T. J.Engng. Frac.Mech. 1, 77 (1968).

171. Wetzel R.M. J.Materials, 3, 646 (1968).

172. Witt F.J. 1st Int.Conf. in structural mechanics in Reactor tests. Tech. of European Comm., Brussels. Vol.G.P.375 (1971).

173. Wood W.A. Phil.Mag. 3, 692 (1958), Fracture, p.412, Tech.Press, Wiley (1959) N.Y.

174. Wöhler A.Z., BAUW, 8, 542 (1858), 10, 583 (1860), 13, 233 (1863), 16,67 (1866), 20,74 (1870), Engng. 11, 199 (1871).

175. Yoshikawa A. Letter to Nature, London. (1965).

176. Yoshikawa A. and Sugento T. Trans.Metall.Soc. AIME 233, 1314 (1965).

177. Zappee C.A. and Wazrden, C.O.Trans ASM 43, 958 (1961).

178. Zener C. Trans.ASM. 40, 3 (1948).

179. Metals Handbook. Vol.9.

180. Vitek V. J.Mech.Phys.Solids (1975) Vol.24, pp.67.